GEOCHEMISTRY AND PETROGENESIS OF THE OCEANIC ISLAND AND
SUBDUCTION-RELATED ASSEMBLAGES FROM THE
PALAEOTETYHAN KARAKAYA SUBDUCTION/ACCRETION COMPLEX,
CENTRAL AND NW TURKEY

A THESIS SUBMITTED TO
THE GRADUATE SCHOOL OF NATURAL AND APPLIED SCIENCES
OF
MIDDLE EAST TECHNICAL UNIVERSITY

BY

KAAN SAYIT

IN PARTIAL FULFILLMENT OF THE REQUIREMENTS
FOR
THE DEGREE OF DOCTOR OF PHILOSOPHY
IN
GEOLOGICAL ENGINEERING

JUNE 2010

Approval of the thesis:

GEOCHEMISTRY AND PETROGENESIS OF THE OCEANIC ISLAND AND SUBDUCTION-RELATED ASSEMBLAGES FROM THE PALAEOTETYHAN KARAKAYA SUBDUCTION/ACCRETION COMPLEX, CENTRAL AND NW TURKEY

submitted by **KAAN SAYIT** in partial fulfillment of the requirements for the degree of **Doctor of Philosophy in Geological Engineering Department, Middle East Technical University** by,

Prof. Dr. Canan Özgen   _____
Dean, Graduate School of **Natural and Applied Sciences**

Prof. Dr. M. Zeki Çamur   _____
Head of Department, **Geological Engineering**

Prof. Dr. M. Cemal Göncüoğlu
Supervisor, **Geological Engineering Dept., METU**   _____

Examining Committee Members:

Prof. Dr. Kadir Dirik   _____
Geological Engineering Dept., HU

Prof. Dr. M. Cemal Göncüoğlu   _____
Geological Engineering Dept., METU

Assoc. Prof. Dr. Gültekin Topuz   _____
Avrasya Institute of Geosciences, İTU

Assoc. Prof. Dr. Ercan Aldanmaz   _____
Geological Engineering Dept., KU

Assist. Prof. Dr. Fatma Toksoy-Köksal   _____
Geological Engineering Dept., METU

                              Date: 23/06/2010

I hereby declare that all information in this document has been obtained and presented in accordance with academic rules and ethical conduct. I also declare that, as required by these rules and conduct, I have fully cited and referenced all material and results that are not original to this work.

Name, Last name : Kaan SAYIT

Signature :

ABSTRACT

GEOCHEMISTRY AND PETROGENESIS OF THE OCEANIC ISLAND AND SUBDUCTION-RELATED ASSEMBLAGES FROM THE PALAEOTETHYHAN KARAKAYA SUBDUCTION/ACCRETION COMPLEX, CENTRAL AND NW TURKEY

Sayıt, Kaan

Ph.D., Department of Geological Engineering

Supervisor: Prof. Dr. M. Cemal Göncüoğlu

June 2010, 191 pages

The Nilüfer Unit of the Karakaya Complex at the pre-Liassic basement of the Sakarya Composite Terrane is composed mainly of metabasaltic lithologies with limestones, and minor cherts and mudstones. These metabasic assemblages show OIB- and E-MORB-type geochemical signatures with variable enrichment in the most incompatible elements relative to N-MORB. The Eymir Unit consists of variably deformed metaclastics, and constitutes the matrix in which the Nilüfer-type blocks are embedded. In the Ankara region, the Eymir Unit is intruded by metadiabase dikes that display intra-oceanic SSZ-type signatures with a marked negative Nb anomaly combined with a slightly depleted HFSE budget relative to N-MORB.

The wide range in trace element ratios displayed by the Nilüfer metabasic rocks can be explained by melt-mixing processes that has taken place within the spinel-garnet transition zone. Pb-Nd-Hf radiogenic isotope systematics reveal that the Nilüfer samples has been derived from enriched mantle sources, and a multi-component source mixing is required to explain their genesis. The Eymir

metadiabases, however, require contribution from a sediment component that mixes with a depleted mantle source.

The geochemical data when combined with the geological and petrographical observations suggest that the Nilüfer metabasic rocks represent ancient oceanic islands that were created by a heterogeneous mantle plume rising beneath the Palaeotethyan oceanic lithosphere. During the latest Triassic, these oceanic islands were incorporated into a subduction/accretion prism, where they mixed with the continental-derived assemblages of diverse origin, creating the Karakaya Complex. The intrusion of the SSZ-type metadiabases postdates the formation and deformation of the Complex.

Keywords: Karakaya Complex, Palaeotethys, metabasalt, mantle plume, melange

ÖZ

PALEOTETİSE AİT KARAKAYA DALMA-BATMA-EKLENME PRİZMASI'INDAKİ OKYANUS ADASI VE DALMA-BATMA-İLİŞKİLİ TOPLULUKLARIN JEOKİMYASI VE PETROJENEZİ, ORTA VE KB TÜRKİYE

Sayıt, Kaan

Doktora, Jeoloji Mühendisliği Bölümü

Tez Yöneticisi: Prof. Dr. M. Cemal Göncüoğlu

Haziran 2010, 191 sayfa

Sakarya Kompozit Birliği'nin Jura-öncesi temelindeki Karakaya Kompleksinin ana birleşenlerinden olan Nilüfer Birimi, başlıca metabazaltik litolojilerden ve bunlarla ardalanmalı kireçtaşları, ve daha az oranda çört ve çamurtaşlarından oluşur. Nilüfer Birimi içerisindeki metabazik birlikler baskın olarak OIB- ve daha az oranda E-MORB-tipi jeokimyasal özellikler sergilemekte, ve N-MORB'a göre değişken derecelerde zenginleşme göstermektedirler. Eymir Birimi ise değişken yoğunlukta deforme olmuş metaklastiklerden oluşmaktadır, ve Nilüfer Birimi bloklarının içinde yer aldığı matriksi temsil etmektedir. Eymir Birimi, Ankara civarında, okyanus-içi SSZ-karakterindeki metadiyabaz daykları tarafından kesilmektedir. Bu metabazik dayklar negatif Nb anomalileri ve N-MORB'a göre biraz daha tüketilmiş HFSE karakterleri ile göze çarparlar.

Nilüfer metabazik kayaçlarının iz element oranlarında görülen geniş aralık, spinel-garnet geçiş zonunda meydana gelen ergiyik karışması işlemleri ile açıklanabilir. Pb-Nd-Hf radyojenik izotop sistematiği, Nilüfer örneklerinin zenginleşmiş manto kaynaklarından türediğini gösterir, ve bu kayaçların jenezi çoklu kaynak karışımını gerektirir. Öte yandan, Eymir diyabazlarının jenezi, tükenmiş manto kaynağına katılan bir sediment öğesiyle açıklanabilir. Jeolojik ve

petrografik gözlemlerle ve bu çalışmada sağlanan jeokimyasal veriler, Nilüfer Birimi içerisindeki metabazik kayaçların, Paleotetis okyanusal litosferinin altından yükselen heterojen bir manto sorgucu etkisiyle oluşmuş okyanus adalarını temsil ettiğini gösterir. En geç Triyas'ta bu okyanus adaları bir dalma-batma-eklenme prizmasına katılmış, ve burada farklı kıtasal kökenli birimlerle karışarak Karakaya Kompleksi'ni meydana getirmiştir. Yay ardı basen bazaltı karakterli diyabazların intrüzyonu ise melanj oluşumu ve deformasyonundan daha sonra gerçekleşmiştir.

Anahtar Kelimeler: Karakaya Kompleksi, Paleotetis, metabazalt, manto sorgucu, melanj

To My Mother and Ayşe Peksezer

ACKNOWLEDGEMENTS

TABLE OF CONTENTS

CHAPTER 1

INTRODUCTION

1.1. Purpose and Scope

Understanding the geology of the northern margin of Turkey is of crucial importance in revealing the Tethyan events, since it bears the traces of several continental and oceanic pieces that assembled during the closure of Palaeozoic and Mesozoic oceanic realms (e.g. Şengör and Yılmaz, 1981; Okay et al., 1996; Göncüoğlu et al., 1997, 2000). From these, the Late Palaeozoic-Early Mesozoic "Tethys" had been defined differently by different authors. Şengör et al. (1984)'s ''Palaeo-Tethys'' was a wide ocean that closed prior to Early Jurassic time and is sutured in N Turkey. It was consumed by southward subduction to give rise to a marginal basin (Karakaya Rift Basin in the present study). For Stampfli et al. (2001), ''Paleo-Tethys'' is also a wide ocean that was subducted by latest Triassic time with its sutured remains now located in the Gondwanan Tauride-Anatolide Platform (e.g. Robertson, 2002). A number of Permo-Triassic back-arc type marginal basins (e.g. Meliata, Vardar and Karakaya basins) along the Eurasian southern margin were considered as related to the Paleo-Tethys (Stampfli, 2000). Ustaömer and Robertson (1994) used the name "Paleotethys" for the same entity, regardless of its exact location. It was consumed by northward subduction (Robertson et al., 2004), as it is proposed for the Permo-Triassic basins in the Caucasus (Adamia et al., 1995) giving way to a pre-Jurassic subduction complex (Karakaya Complex) with accreted seamounts, oceanic crust and pieces of a continental crust (Pickett and Robertson, 2004).

The geodynamic reconstruction of Palaeotethys is highly debated, as there is no consensus on the location of the oceanic suture zone and polarity of subduction, nor critically on the type of magmatism (see Okay and Göncüoğlu, 2004). It is commonly accepted that the Early Mesozoic Cimmeride Orogeny was product of the closure of this Palaeozoic ocean, followed by the accretion of several oceanic and continental crustal fragments (Tekeli, 1981; Şengör et al., 1984).

The relics of this subduction/accretion complex cover a substantial portion of northern Turkey as an east-west trending belt. This tectonic unit, known as the Karakaya Complex, constitutes a part of the pre-Liassic basement of the Sakarya Zone (Okay, 1989), or of the Sakarya Composite Terrane (Göncüoğlu et al., 1997) (Figure 1.1). The Karakaya Complex, however, has been greatly debated over many years (e.g. Bingöl et al., 1973; Akyürek et al., 1984; Koçyiğit, 1987; Okay et al., 1991; Altıner and Koçyiğit, 1993; Ustaömer and Robertson, 1994, 1999; Pickett and Robertson, 1996, 2004; Göncüoğlu et al., 2000; Genç, 2004; Sayıt and Göncüoglu, 2009a). Central to this debate is the degree to which similarities among disparate units have been recognized, and have consequently been interpreted as portions of a single large accretionary complex.

The term "mélange" owes his origin to Greenly (1919) when he was first used this term to characterize the chaotic rock bodies in Anglesey, Wales. Since then, lots of studies have been carried out regarding the definition and origin of mélanges, but the debate is still going on (for a detailed review and historical evolution of this concept, see Raymond, 1984 and Şengör, 2003). Although, no consensus has been reached on the exact definition of the term "mélange", it has become clear that there are two major processes responsible for formation of mélanges; fragmentation and mixing (e.g. Hsü, 1968; Closs, 1984; Raymond 1984). These processes, triggered by tectonic and/or sedimentary events, form a variety of mélange types. A common feature observed in these chaotic rock bodies is the presence of block-in-matrix structure characterized by variable sized blocks or fragments embedded in a finer-grained matrix (e.g. Raymond, 1984).
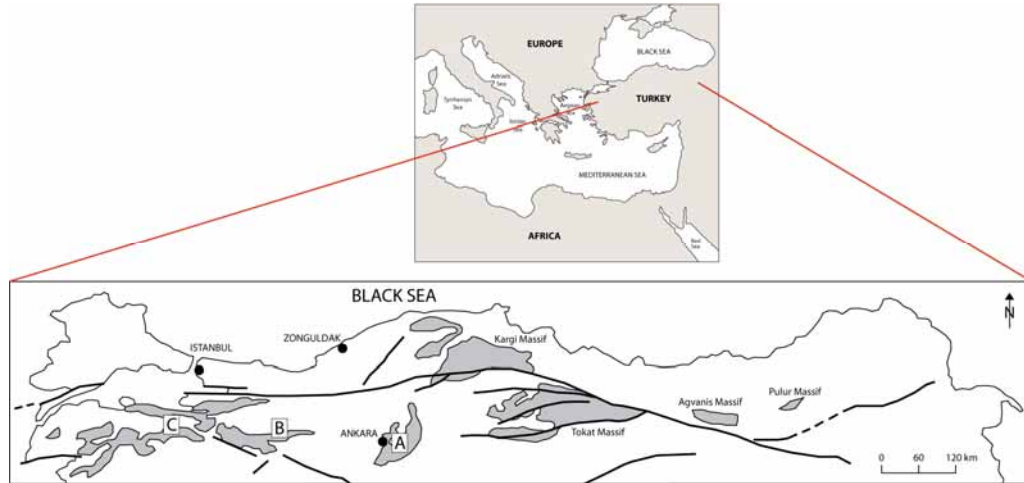
Figure 1.1. Distribution of the Karakaya Complex in northern Turkey (based on the terrane map of Göncüoglu et al., 1997) and location of the study areas. (A) Ankara region; (B) Central Sakarya Region; (C) Bursa region.

Subduction/accretion complexes are the tectonic environments where mélanges are frequently observed to develop (e.g. Raymond, 1984; Cloos, 1984). A common feature of these complexes is the ubiquitous presence of high pressure/low temperature (HP/LT) mineral assemblages which develop owing to cold burial of subducting oceanic slab with associated sediments (Coleman and Lanphere, 1971; Saha et al., 2005). Geochemical signatures of the individual magmatic suites found within ancient complexes can provide substantial insight into the origin of subduction/accretion complex worldwide. Individual magmatic suites thought to have formed in different tectonic settings could actually represent the products of the same magmatic event regardless of their metamorphic grade, if these suites have similar geochemical signatures and ages of formation.

This study aims to reconstruct the ancient pieces making up the Karakaya Complex in the light of new data from central and NW Anatolia. Taking also into account the available geochemical and paleontological information on the metabasic rocks thought to represent the relics of Cimmeride Orogeny, this study

tries to provide an insight into the geodynamics of the Palaeotethyan region during Permo-Triassic time.

1.2. Study Area

This study covers a number of areas which are mainly located in the central part of Karakaya Complex and to a lesser extent in the western part (Table 1.1 and Figure 1.2). The detailed information regarding the study areas can be found in the Appendix A.

Table 1.1. Study areas that lie along the three main regions between Central and NW Anatolia.

Central Anatolia (Ankara)	İmrahor, Üreğil, Zerdalitepe, Bayındır, Ortaköy, Gökçeyurt, Lalahan, Hacılar (Gölbaşı), Hasanoğlan, Kavaklı, Bozca, Doğanoluk, Eymir (Gölbaşı), Karataş and Hacılar (Çubuk)
Central Sakarya Region	Karaçobanpınarı, Alpagut, Laçin, Karahisarkozlu and Emremsultan
NW Anatolia (Bursa)	Sipali, Bahçecik, Subaşı and Doğancı

1.3. Methods of Study

This study was performed in two stages: a) field studies, b) laboratory studies.

Most of the fieldwork was carried out during the summers of 2005, 2006 and 2007. Approximately 400 hand specimens were collected from these locations and geological maps on 1:25000 scale topographic maps were prepared for some localities lying in the central part.
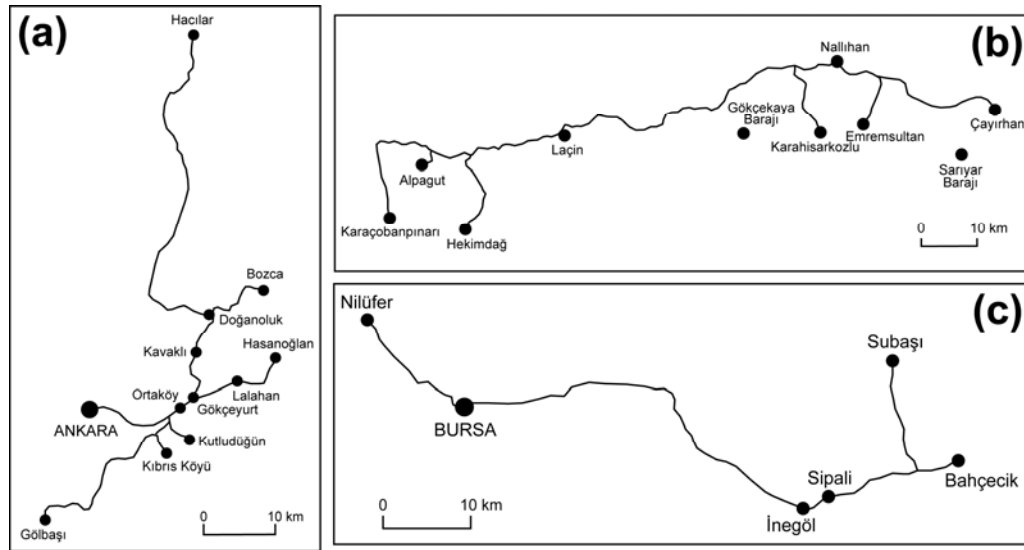
Figure 1.2. Location map of the study areas. (A) Ankara region; (B) Central Sakarya Region; (C) Bursa region.

Laboratory work included two steps; a) thin-section preparation, b) geochemical analyses. Regarding the first step of laboratory work, more than 250 thin-sections were prepared for petrographical examination under polarizer microscope in order to understand mineral assemblages and micro-textures, and to make comparison between the studied samples to reveal possible relationships or distinctions.

For petrographic examinations, Nikon, Olympus and Swift microscopes were used and photomicrographs were acquired by Nikon camera in the Department of Geosciences of the Pennsylvania State University (USA).

Geochemical analysis consisted of two parts, namely whole-rock geochemistry and isotope analyses. For the whole-rock geochemistry, 35 relatively less altered samples were analyzed for major and trace elements (including rare earth elements (REE)) in the labs of Duke University (USA) by direct current plasma spectroscopy (DCP) and inductively-coupled plasma mass spectroscopy (ICP-MS), whereas 6 samples were analyzed in the ACME labs (Canada) by inductively coupled plasma atomic-emission spectrometry (ICP-AES) and ICP-

5

MS. For the isotope chemistry, 16 samples were analyzed for Sr, Nd, Pb and Hf isotopes by multi-collector (MS) ICP-MS in the labs of San Diego State University (USA).

1.4. A Review of the Karakaya Complex and the Nilüfer-type Metabasic Assemblages in Central and NW Anatolia

1.4.1. The Karakaya Complex: Definition and Problems

The Karakaya Complex was originally defined by Bingöl et al. (1973) as the "Karakaya Formation". This term includes very low-grade metamorphosed rock assemblages of pre-Liassic age outcropping in Northwestern Anatolia. They interpret these assemblages to have formed in a continental rift setting, where Permo-Carboniferous limestone blocks were incorporated into the basin from rift shoulders owing to the extensional regime during Early Triassic. Later studies identified similar pre-Liassic assemblages in some other parts, and extended the limits of the Karakaya complex to the northeastern Turkey (Tekeli, 1981; Okay, 1989; Koçyiğit, 1991a).

In contrast to the continental rift idea of Bingöl et al. (1973), Tekeli (1981) regarded the Karakaya Complex as a Carboniferous-Triassic subduction/accretion prism which he termed the "North Anatolian Belt". He used the mélange character of the various lithologies found in this belt, and the presence of high-pressure metamorphism to infer an accretionary prism origin. There is today no consensus as to whether the Karakaya Complex developed in a rift or a subduction-accretion complex (e.g. Altıner and Koçyiğit, 1993; Genç and Yılmaz, 1995; Pickett and Robertson, 1996; Göncüoğlu et al., 2000; Okay, 2000; Sayıt and Göncüoglu, 2009a) (Figures 1.3 and 1.4).

Several studies regard the Karakaya Complex as an "ophiolitic mélange" consisting of ophiolites, blueschist facies rocks as well as limestone blocks settled in an intensely sheared matrix (Şengör et al., 1980; Şengör and Yılmaz, 1981). Tekeli (1981) also added the entire Neotethys pieces (a part of his "North

Anatolian Mélange") into the definition of the Karakaya Complex, which were later excluded (e.g. Göncüoğlu et al, 1997, Okay and Tüysüz, 1999). Actually, ophiolitic rock assemblages are rarely found within the Karakaya Complex. One of these areas, the Küre region, includes an ophiolitic suite assumed to have been generated in a supra-subduction zone (SSZ) environment (Ustaömer and Robertson, 1994; Kozur et al., 2000). Besides, there are assemblages similar to the Küre ophiolites in NW Anatolia and the Tokat region. It is not clear whether they are a part of the Karakaya Complex, though they are generally assumed to be of pre-Liassic age (Koçyiğit and Tokay, 1985; Genç, 1987; Rojay and Göncüoğlu, 1997).
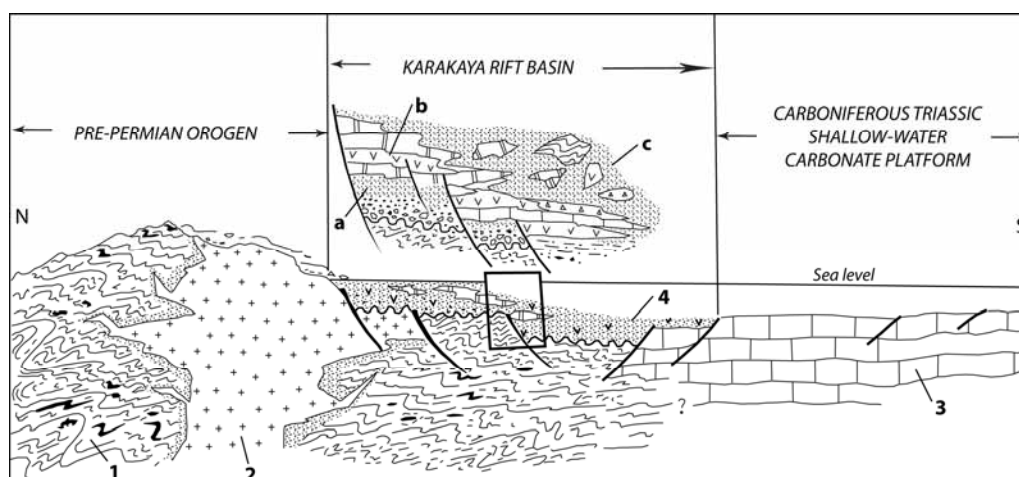
Figure 1.3. Continental- (back-arc) rift model proposed by Altıner and Kocyigit (1993) to explain the opening and development of Karakaya Rift Basin. 1. Pre-Permian low-grade metamorphic rocks, 2. Uppermost Carboniferous granitoid, 3. Carboniferous to Triassic shallow-water carbonates, and 4. Permian (?) to Triassic rift basin successions of the Karakaya Group, which includes a) Kendirli Formation, b) Bahçecik Formation, c) Olukman Formation).

Recently Sayıt and Göncüoglu (2009b) emphasized that the pre-Liassic rock assemblages represent huge mélange and/or tectonostratigraphic units which have assembled during the demise of a Palaeotethyan oceanic realm. They interpret the

Karakaya Complex as composed of a number of mélange units produced both by sedimentary and tectonic processes. These mélange units include blocks of both native and exotic origin whose dimensions range from dm-scale fragments to masses of several km scale. Some mélange units are megablocks within other mélange units.
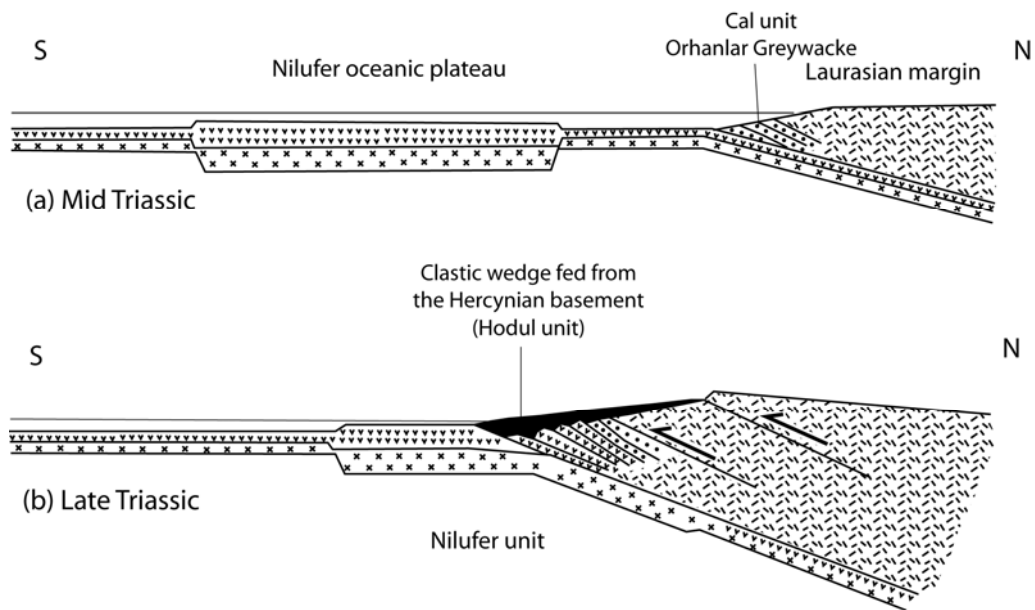
Figure 1.4. Subduction/accretion model put forward by Okay (2000), which explains the geodynamic evolution of the Karakaya Complex by a Middle Triassic-aged oceanic plateau that later have been incorporated into the Laurasian active continental margin.

This study mainly focuses on one particular mélange unit that is characterized by oceanic island basalt (OIB)- and enriched mid-ocean ridge basalt (E-MORB)-type metabasic rocks and discusses its tectonomagmatic origin on the basis of both geological and petrological features. The tectonic setting regarding these metamorphic rocks and how they have been incorporated into the Karakaya complex is a subject of controversy. Some studies suggest that they have developed in a continental-rift setting that failed to pass into ocean-floor spreading stage (e.g. Bingöl et al., 1973, Akyürek et al., 1984; Koçyiğit, 1987;

Altıner and Koçyiğit, 1993; Genç and Yılmaz, 1995; Kozur et al., 2000) or advanced into the mature oceanic stage (Şengör and Yılmaz, 1981; Şengör et al., 1984; Stampfli and Borel, 2002; Moix et al., 2008), while others argue that they are relicts of a seamount and/or oceanic island (Çapan and Floyd, 1985; Pickett and Robertson, 1996, 2004; Yalınız and Göncüoğlu, 2002), an oceanic plateau (Okay, 2000), a large igneous province (Genç, 2004) or mantle plume-related seamounts and/or oceanic islands associated with a spreading ridge (Figure 1.5; Sayıt and Göncüoglu, 2009a), based on trace element (except Okay, 2000) as well as REE geochemistry (Sayıt and Göncüoglu, 2009a). A third hypothesis is that these rock assemblages represent an intra-oceanic (ensimatic) forearc/intraarc sequence owing to their large distribution within the complex and the alkaline character of mafic rocks (Okay et al., 1996).
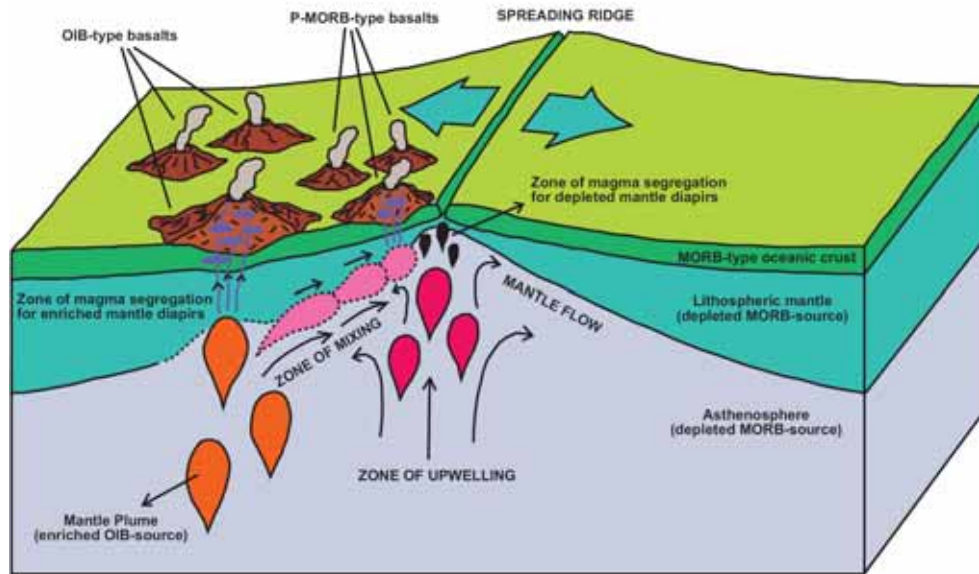
Figure 1.5. Petrological reconstruction by Sayıt and Göncüoğlu (2009a), which relates the Late-Middle alkaline-dominated magmatism to seamounts/oceanic islands fed by a mantle plume that is associated with the Palaeotethyan spreading ridge.

As seen from these diverse interpretations, therefore, resolving this question is of particular importance in order to reveal tectonomagmatic evolution of the Karakaya Complex as well as Palaeotethyan events. In the light of the new geochemical data as well as the geological and petrographical observations performed in this study, the Nilüfer Unit originally defined by Okay et al. (1991) has been redefined and reevaluated. To avoid repetition, the concepts and discussion related to the coverage and extent of the redefined Nilüfer Unit are presented in detail in Chapter 2.

CHAPTER 2

REDEFINITION OF THE NİLÜFER UNIT AND REGIONAL AND LOCAL GEOLOGICAL FEATURES

2.1. The Redefined Nilüfer Unit: Its Coverage and Extent within the Karakaya Complex on the Basis of Regional and Local Constraints

During the regional geological mapping in NW and N Anatolia, several authors (for a review see Okay and Göncüoğlu, 2004) have identified a number of mappable tectono-stratigraphic units within the Karakaya Complex. Of these units, the clastic-dominated units with metabasalt and limestones olistoliths (Çal, Hodul and Orhanlar units of Okay et al., 1991) were considered as the Upper Karakaya Complex (e.g. Okay and Göncüoğlu, 2004). The Nilüfer Unit, on the other hand, was defined as a separate tectonic unit (the Lower Karakaya Complex) characterized by a strongly deformed low-grade metamorphic assemblage consisting mainly of metabasite, phyllite and marble. The detailed fieldwork in NW Anatolia reported in this study, including the preliminary results (Sayıt and Göncüoğlu 2009a,b; Sayıt et al., 2008, 2009) are based on geochemistry and paleontological ages. By this, it is shown that these basic volcanic rocks and associated sediments are not restricted only to the Nilüfer Unit of Okay et al (1991), but may be found in all previously defined units (Çal Unit, Hodul Unit, etc.) of the Karakaya Complex as blocks or tectonic slices (Sayıt and Göncüoğlu, 2009a,b). Therefore, in this study, these rock assemblages were assembled and redefined by considering their age, lithology and geochemical characteristics rather than their structural setting and metamorphic grade.

11

The redefined Nilüfer Unit is characterized primarily by metabasaltic massive/pillow lava flows and pillow breccias, interbedded with volcaniclastics, mafic tuffs, variably recrystallized neritic and pelagic limestones, and minor brick-red cherts and mudstones (e.g. Sayıt and Göncüoğlu, 2009a). The Nilüfer-type rock assemblages are prevalent throughout N, NW and Central Anatolia (Akyürek et al., 1984; Göncüoğlu et al., 1987; Koçyiğit et al., 1991; Okay et al., 1991; Sayıt and Göncüoğlu, 2009a). The most characteristic feature of this unit is the occurrence of alkaline basalts with associated carbonate and/or cherty rocks.

In the Biga Peninsula, the newly defined Nilüfer Unit together with the pre-Karakaya units (the Kalabak Formation, the Çamlık metagranodiorite and the Kazdağ Group) constitute the pre-Liassic basement of Sakarya Composite Terrane (Göncüoğlu et al., 1997). The redefined Nilüfer Unit characterizing a Karakaya Unit in the region is found to be tectonically related to the pre-Karakaya Unit mentioned above (Bingöl et al., 1973; Okay et al., 1991) (Figure 2.1). The Kalabak Formation includes low-grade metaclastics and intruded by Devonian Çamlık metagranodiorite. Late Triassic clastics of the Eymir Unit (the Hodul Unit of Okay et al., 1991) lie unconformably over the Kalabak Formation (Okay et al., 1991).

The Kazdağ Group consisting mainly of gneiss, migmatite, amphibolite and marble (Bingöl et al., 1973) characterize the oldest rock assemblage in the Biga Peninsula. A Moscovian age (308±16 Ma) acquired from the gneisses from this unit is interpreted to represent the age of high grade metamorphism and migmatization in the Kazdağ range (Okay et al., 1996). The Kazdağ Group tectonically underlies the two Karakaya-related assemblages in the east, namely the newly defined Nilüfer Unit and the Eymir Unit (Okay et al., 1991).

In the Biga Peninsula, two major tectonostratigraphic units represent the Karakaya Complex; the redefined Nilüfer Unit and the Eymir-type clastics (the Orhanlar Greywacke and partly Hodul Unit). The Nilüfer Unit is largely found as variably deformed metabasic rocks interbedded with recrystallized limestone and
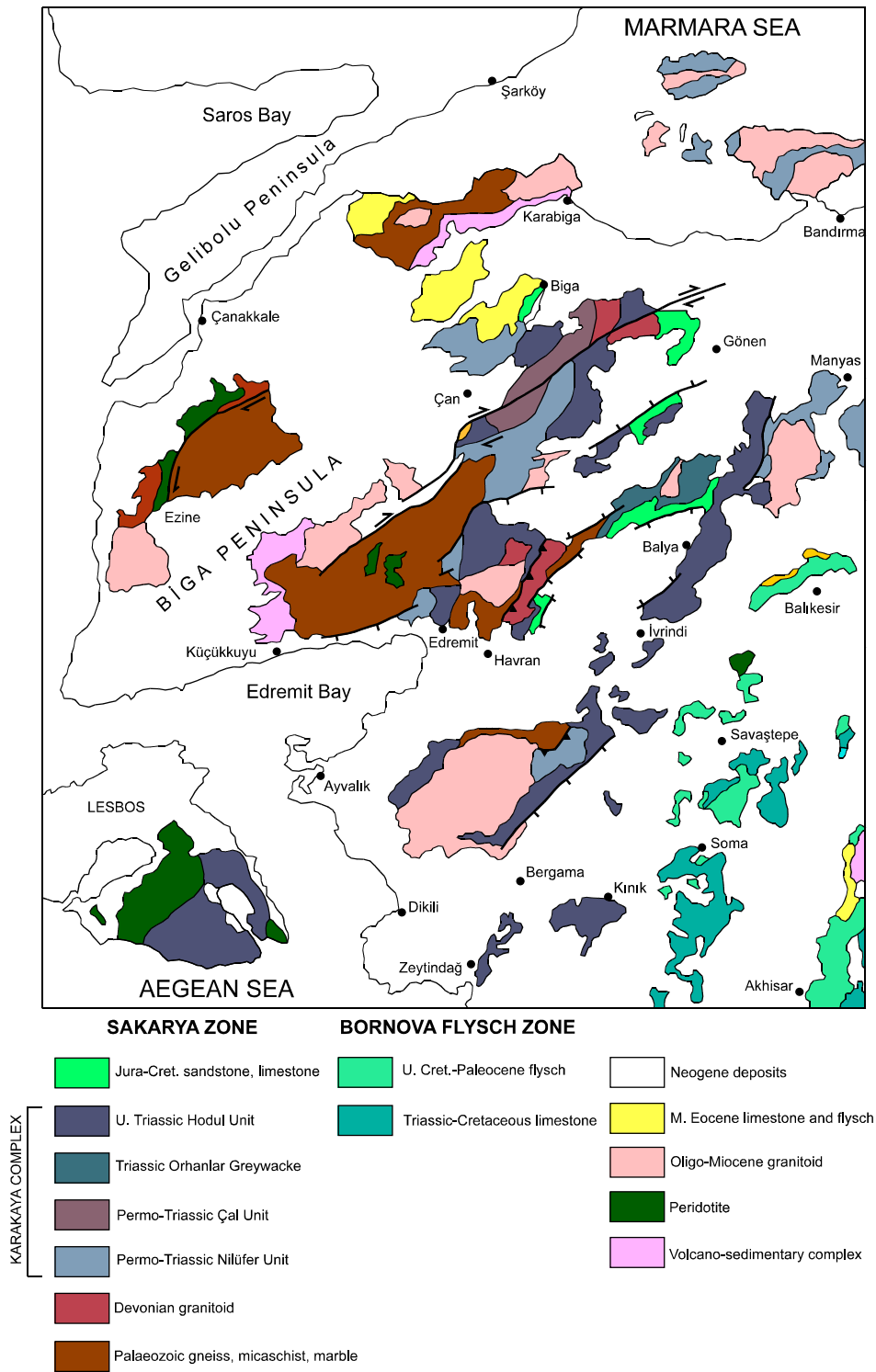
Figure 2.1. Distribution of the tectono-stratigraphic units included in the Karakaya Complex and the other units in NW Anatolia (after Okay et al., 1996). Note that this map is based on the original definition of Nilüfer Unit and given here with no changes.

13

phyllite (Okay et al., 1991). Although these metabasics appear to have been metamorphosed under greenschist facies conditions, high pressure equivalents, such as blueschists and eclogites, can also be encountered (Okay and Monie, 1997). In NW Anatolia, the redefined Nilüfer Unit comprises the originally defined Nilüfer Unit of Okay et al. (1991) and Çal Unit (Okay et al., 1991), the Bahçecik Formation (Koçyiğit et al., 1991) and a part of the Ortaoba Unit (Pickett and Robertson, 1996). The Karakaya Formation of Bingöl et al., (1973) is partially included in the unit, since the arkosic sandstones and greywackes which commonly crop out in NW and Central Anatolia are excluded from the definition given by this study. The Çavdartepe Formation (Akyürek and Soysal, 1983), the İznik Metamorphics (Göncüoğlu et al., 1987), and the Yenişehir Metamorphics (Genç and Yılmaz, 1995) are also partly included within the definition of the newly defined Nilüfer Unit.

The age of Nilüfer Unit is regarded as Early Triassic on the basis of conodont fauna found in the marbles alternating with metabasites in the south of Bursa (Kozur et al., 2000), while an Early-Middle Triassic age has been ascribed on the basis of conodont-bearing metabasalts by Genç (1987). Kaya and Mostler (1992) have assigned a Middle Triassic age to the unit based on the conodonts in the limestones interbedded with the metabasaltic rocks found in the north of Bergama. In the Edremit region, a Middle-Late Triassic age has been reported by Sayıt and Göncüoğlu (2009a) based on a conodont-bearing chert band associated with metabasalts, which places an upper age limit on these metabasaltic assemblages. Thus, in NW Anatolia, the redefined Nilüfer Unit appears to span an age-range from Early to Late Triassic.

In Central Sakarya, the Tepeköy Metamorphics of Göncüoğlu et al. (2000) lying within the lower slice of the Central Sakarya Basement are similar to the redefined Nilüfer Unit, although they include terrigenous material and metafelsic tuffs that are conspicuously absent elsewhere (Okay et al., 1996; Pickett and Robertson, 1996; Sayıt and Göncüoğlu, 2009a). However, this study reveals that the metabasaltic portion of the Tepeköy Metamorphics has the same geochemical

14

signatures with the newly defined Nilüfer Unit and these basic rocks are found as blocks within the clastic material.

In Ankara region (Central Anatolia) (Figure 2.2), the redefined Nilüfer Unit constitutes the oldest rock assemblages together with the Eymir Unit (defined by this study; see following paragraphs for a detailed discussion regarding this unit), and it is represented by variably-sized metabasic blocks associated with limestones, set in a low-grade metaclastic matrix represented by the Eymir Unit (Koçyiğit, 1987; Sayıt and Göncüoğlu, 2009a). In this region, the redefined Nilüfer Unit includes the Ortaköy Formation (Akyürek et al., 1984) and the Bahçecik Formation (Altıner and Koçyiğit, 1993; Sayıt and Göncüoğlu, 2009a). The Eymir Complex (Koçyigit, 1992) or the Emir Formation (Akyürek et al., 1984) from the same region cannot be evaluated entirely within the context of the Nilüfer-type metamorphics, though some studies regard it as a part of the Nilüfer Unit (Okay, 2000, Genç, 2004). In contrast to the metabasalt-dominant sequences seen in the Nilüfer Unit, the Eymir Complex consists largely of metaclastics (slates, phyllites, metasandstones, metaconglomerates) including minor volcaniclastics, all of which are intruded by metadiabase dikes (Sayıt and Göncüoğlu, 2009a). The Eymir Complex also includes rare variably-sized mafic and ultramafic blocks, some of which appear to have experienced elevated pressure conditions (Sayıt and Göncüoğlu, 2009a). These metaigneous blocks with/without high pressure signatures bear enriched geochemical signatures akin to OIB and E-MORB (Sayıt et al., 2008), therefore a small portion of the Eymir Complex is included in the new definition.

The age of the redefined Nilüfer Unit is constrained by paleontological findings. The paleontological ages are essentially consistent with the ones acquired from NW Anatolia. A Middle Triassic age has been obtained from the neritic limestones of the unit in the Ankara region (Akyürek et al., 1984). A tighter constraint has been provided from the Hasanoğlan (Ankara) region by Altıner and Koçyiğit (1993) which suggest a Late Anisian (Middle Triassic) age for the shallow-water limestones intercalated with pillow basalts. Another precise

15

constraint from foraminiferal fauna found in the neritic limestones of the İmrahor (Ankara) region (Sayıt and Göncüoğlu, 2009a) ascribes the age of unit to Middle Anisian (Middle Triassic). Taken together, these paleontological data imply a Middle-Late Triassic interval for the age of the redefined Nilüfer Unit.
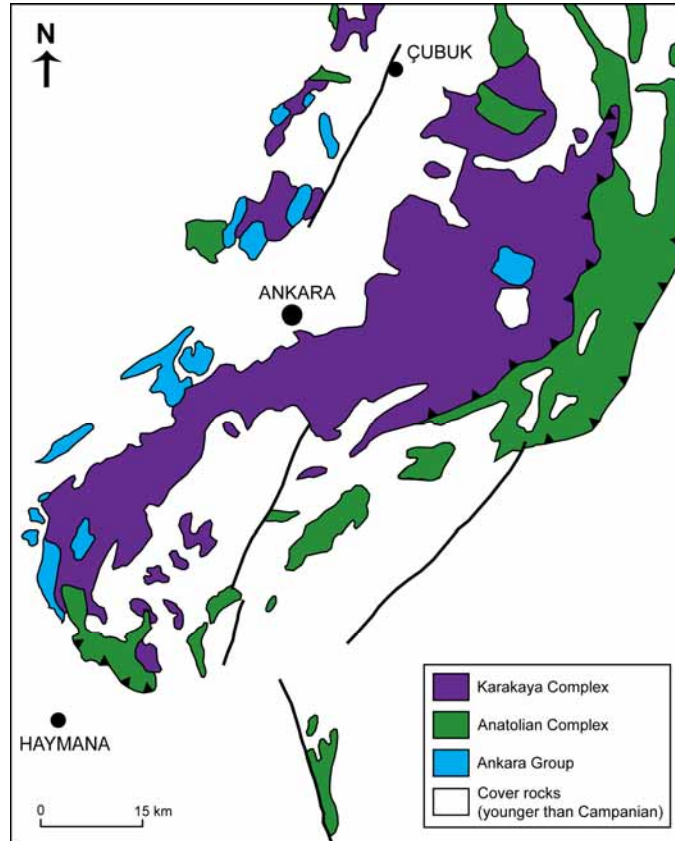
Figure 2.2. Distribution of the major tectonostratigraphic units in the Ankara region (after Koçyiğit, 1991b). Note that no change has been made on the map regarding the redefined units.

The other unit, redefined in this study, is the clastic rock assemblages outcropping all along the complex. These clastic lithologies have been previously defined under various names in different areas (e.g. Okay and Göncüoğlu et al., 2004). They are found to be variably deformed and metamorphosed just like the metabasic rocks characterizing the redefined Nilüfer Unit (e.g. Sayıt and

16

Göncüoğlu, 2009a). Some previous studies regard these clastics primarily associated with the metabasaltic lithologies that have been defined here under the context of the new Nilüfer Unit (Bingöl et al., 1973; Akyürek et al., 1984; Koçyiğit, 1987; Altıner and Koçyiğit, 1993; Genç and Yılmaz, 1995; Pickett and Robertson, 1996), whereas some others have treated them separately (e.g. Okay, 2000; Sayıt and Göncüoğlu, 2009a). This study provides a good distinction between the metabasaltic lithologies and clastics, suggesting they are not primarily associated, but incorporated during the closure of the Palaeotethys. In this study, the clastic lithologies are collectively defined as the "Eymir Unit".

In the Ankara region, the Eymir Unit partially comprises the Eymir Complex (Koçyiğit, 1992) or the Emir Formation (Akyürek et al., 1984), the Elmadağ Formation (Akyürek et al., 1984), the Elmadağ Blocky Series (Erol, 1956), the Limestone Blocky Mélange (Norman, 1973), and the Kulm Flysch Formation (Erk, 1977). The Eymir Unit differs from these previously defined units in that it does not include any metabasic rocks with E-MORB and OIB-type signatures (the Nilüfer Unit as defined here). It consists largely of metasandstones alternating with slates and phyllites. In the areas where the degree of metamorphism is very low or non-evident shales and coarser-grained clastics with no observable deformation are encountered instead. Some parts of the Eymir Unit reflect olistostromal character, containing blocks of different origins. These assemblages correspond, in NW Turkey, to the Dışkaya Formation (Kaya et al., 1986; Kaya, 1991) and the Orhanlar Greywacke (Okay et al. 1991). Although there are some other rock assemblages that also comprise arkosic sandtones, they actually differ from the Dışkaya Formation in the presence of metabasalt-chert alternations (the Hodul Unit of Okay et al., 1991, the Ortaoba Unit of Pickett and Robertson, 1996, the Kendirli Formation of Koçyiğit et al., 1991, and the Elmadağ Formation of Akyürek et al., 1984). However, as stated before, in these units the metabasalt-chert alternations are included in the redefined Nilüfer Unit. The arkosic parts as well as greywackes, on the other hand, comprise the lithologies of Eymir Unit as defined in this study. In NW Anatolia, Sayıt and

Göncüoğlu (2009a) also separated the arkosic sandstones from the Ortaoba Unit and evaluated the metabasalt-chert sequences as oceanic-derived lithologies.

The age of the Eymir Unit comes from the relatively less metamorphosed parts of the unit. The "Halobia shales" occurring as blocks within the olistromal parts of the unit indicate a Norian (Late Triassic) age (Kaya et al., 1986). Similar *Halobia* macrofauna that constrains the age of these clastics to Late Triassic has also been reported by some other studies (Okay et al., 1991; Wiedmann et al., 1992; Leven and Okay, 1996; Okay and Altıner, 2004). In constrast to these studies whose age findings are based on the halobia macrofauna, Okay and Altıner (2004) have suggested the same age (Late Triassic) on the basis of the neritic limestones that they believe to be primarily associated with the clastics. In the Ankara region, a similar age has also been obtained for the Eymir unit. Özgül (1993) assigned a Carnian-Rhaetian age (Late Triassic) on the basis of the fossil fauna in the limestones of the unit. However, Akyürek et al. (1984) have suggested a wider interval, assigning an Early-Late Triassic age. In this study, a Carnian-Norian age (Late Triassic) is suggested based on the radiolarian fauna found in the red chert band within clastics of the Eymir Unit (see the following section for the details). This finding seems very consistent with the previous works stated above which suggest a Late Triassic age for the Eymir Unit. Although it does reflect the age of unit, the finding of Carboniferous radiolarian chert block emplaced within the greywackes of the unit in NW Anatolia was also essential, since it is indicative of occurrence of a deep basin during Palaeozoic time (Okay and Mostler, 1994).

The paraautochthonous Ankara Group (Koçyiğit, 1987) unconformably overlies the pre-Liassic Nilüfer and Eymir Units. It consists of a thick, discontinuous sedimentary succession that is ascribed to late Hettengian-Campanian. The Hasanoğlan Formation (Akyürek et al., 1982) forms the bottom of this sequence, including poorly-sorted fluvial conglomerates that are followed by trangressive marine sequence. The Hasanoğlan Formation shows a lateral transition to the volcanic rocks-limestone alternation of the Günalan Formation (Akyürek et al.,

1996). The Hasanoğlan Formation is gradually replaced by the pelagic limestones of Akbayır Formation (Akyürek et al., 1982).

The Jura-Cretaceous Anatolian Complex (Koçyiğit and Lünel, 1987) is tectonically related with pre-Liassic Karakaya Units and the Ankara Group. The Anatolian Complex is tectonically overlain by the Karakaya Units, whereas it lies tectonically over the Ankara Group. The Anatolian Complex comprises three sub-units (Akyürek et al., 1996), namely Jurassic-Early Berrasian Eldivan Ophiolitic Complex (Akyürek et al., 1979b), the Early Cretaceous Dereköy Ophiolitic Mélange (Ünalan et al., 1976; Batman, 1977) and the Dereköy Ophiolitic Mélange associated with Late Cretaceous sedimentary units.

A thick flyschoidal sequence characterize Late Cretaceous-Early Tertiary interval in the Ankara region, which conformably overlies the ophiolitic mélange lying at the bottom. This sequence is unconformably overlain by younger volcano-sedimentary units.

2.2. Local Geological Features

This study mainly includes three study areas; a) Ankara region (Central Anatolia), b) Central Sakarya region, c) Bursa region (NW Anatolia). Among these study areas, the fieldwork was performed only in the Ankara and Bursa regions. It must be noted that since there are numerous localities studied in the Ankara region, the areas sharing similar geological features will be evaluated together in the following sections. Regarding the Central Sakarya region, the studied samples were collected by Dr. M.C. Göncüoğlu during the fieldwork he carried out in 1987-1988, and a detailed geological description of this region was given in the MTA report by Göncüoğlu et al. (1996). Thus, the geological features concerning this region were briefly summarized on the basis of this report.

2.2.1 Ankara Region (Central Anatolia)

2.2.1.1. Zerdalitepe, Bayındır, Ortaköy, Gökçeyurt, and Hacılar (Gölbaşı)

These study areas are represented by the Nilüfer Unit and Eymir Unit (Figures 2.3 to 2.5), and the dominancy of one unit over the other appears to be variable from one place to another. The Nilüfer Unit outcropping in these areas is mainly characterized by metabasaltic lava flows (both pillowed and massive) and metavolcaniclastics (e.g. hyaloclastic breccias, hyaloclastites), which alternates with limestone, mudstone, and minor cherts. It is important to note that the relationship between these rocks appears to be primary, thus suggesting their synchronous nature (Figures 2.6 and 2.7). This is especially well evidenced that both basalt and limestone can be observed as clasts within each other, i.e. limestone clasts can be sometimes observed within the basalts, or basalt may be found as clasts within the limestone. These metabasaltic successions are observed as variably-sized blocks embedded in a clastic matrix of terrigenous origin that is variably deformed and metamorphosed (the Eymir Unit).

Apart from the metabasalts and associated metavolcaniclastics which comprise a significant portion of the unit, there also occur minor metagabbroic rocks in the studied region. These intrusive rocks are observed either as blocks (with sizes generally not exceeding one meter) or primarily related bodies (with a cross-cut relationship) within metabasaltic sequences. One such place is the Gökdere Valley lying to the northwest of İmrahor village. In this locality, the metagabbroic blocks are found within the Nilüfer-type metavolcaniclastics. The metagabbos here are hardly differentiated from the metavolcaniclastics owing to intense shearing, and appear as highly broken and jointed bodies. Indeed, some volcaniclastic parts are observed to have been foliated, indicating the intensity of deformation.

Another locality, namely, the Ortaköy also comprises such metagabbroic occurrences. To the west of the area, approximately 1 km away from the Ortaköy village, the Nilüfer-type assemblages including mainly volcaniclastics and

silicified tuffs are observed to have been intruded by a metadiabase body. Although the contact relationship between the metadiabase dike and the surroundings is not so clear due to intense deformation within the unit, the margins of the metadiabase are found to be observed finer-grained as compared to its inner parts. Therefore, this clearly indicates the cross-cutting relationship of
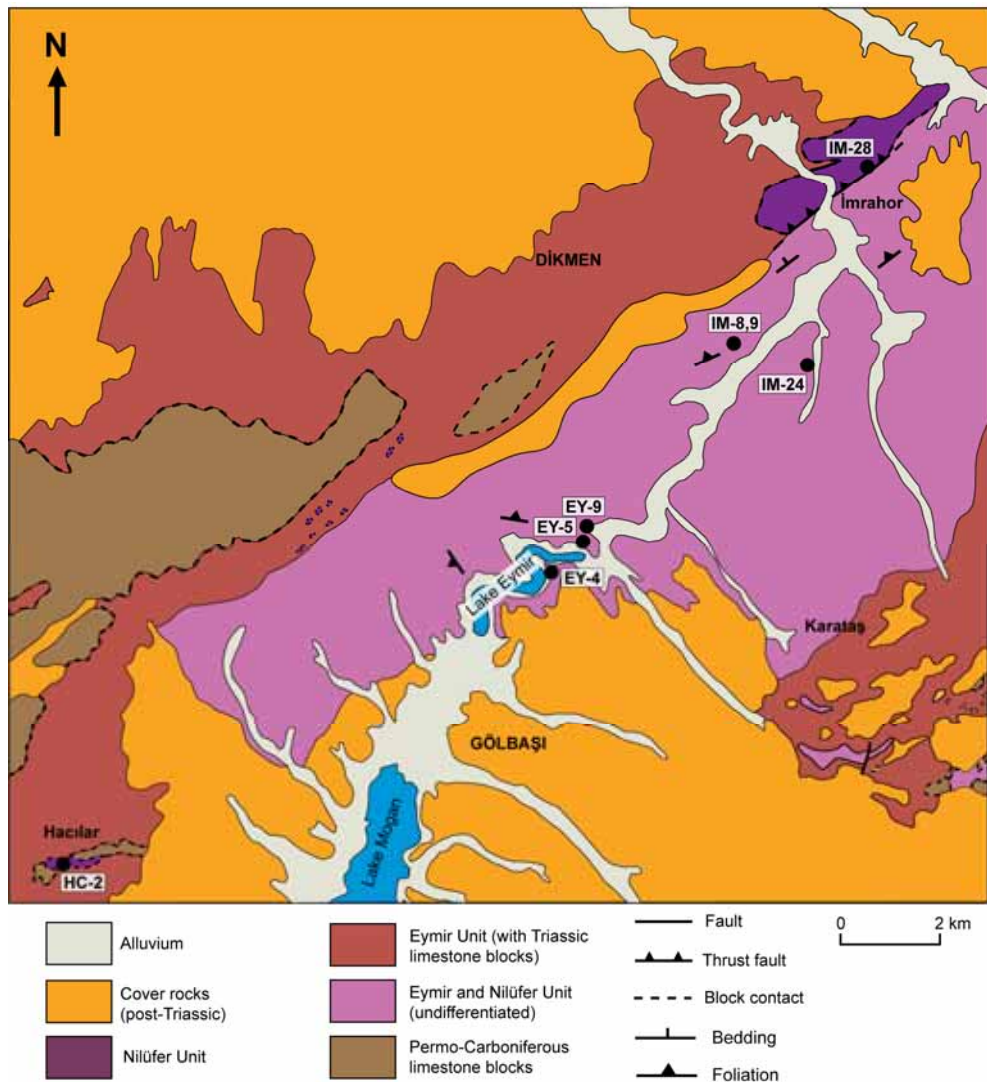
Figure 2.3. Geological map of the Ankara region including an area between Bayındır and Hacılar (modified from the 1/100000 scale MTA geological map compiled by Akyürek et al., 1997, and Sayıt and Göncüoğlu, 2009a). Locations of the geochemically analyzed samples are shown on the figure.

21
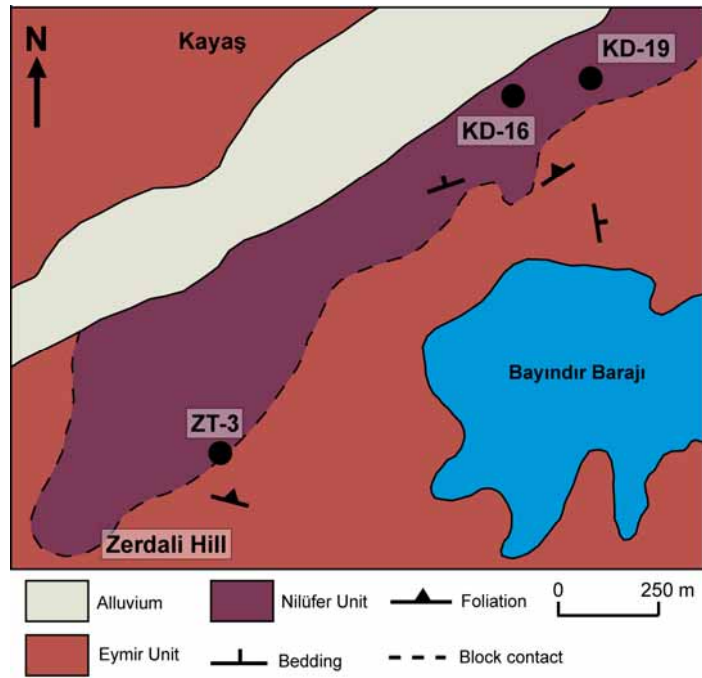
Figure 2.4. Geological map of the Zerdalitepe and Bayındır region (partially based on the 1/100000 scale MTA geological map compiled by Akyürek et al., 1997). Locations of the geochemically analyzed samples are shown on the figure.
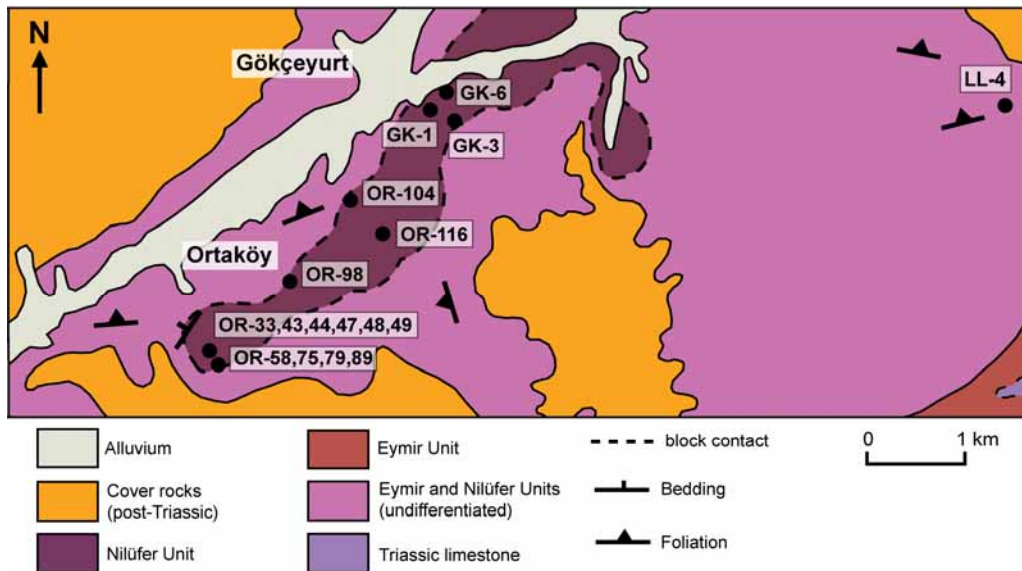
Figure 2.5. Geological map of the Ankara region including an area between Bayındır and Hasanoğlan (modified from the 1/100000 scale MTA geological map compiled by Dönmez et al., 2008). Locations of the geochemically analyzed samples are shown on the figure.

22

the metadiabase body. This metadiabase itself also appear to be sheared, and such parts can be differentiated by the presence of distinct foliation. This megascopic observation is also confirmed by microscopic examination such that even the less deformed parts that have relatively massive appearance display ductile deformation as indicated by elongated clinopyroxene phenocrysts found in a foliated matrix composed of mainly of actinolites. The metadiabase body is observed to have sheared contacts with the Eymir metaclastics.

Figure 2.6. Synchronous nature of basaltic lava flow and limestone within the Nilüfer Unit (Hacılar, Gölbaşı).

Another similar occurrence is found to the south of İmrahor along the Ankara peripheral highway. Here, the Nilüfer-type assemblages are observed as a relatively small block which is cross-cut by a metadiabase body which is of OIB-type geochemical character. It is noteworthy, however, that these metagabbroic bodies (either blocks or intruding bodies) are the products of the same magmatism that has generated the metabasalts (i.e. E-MORB- and OIB-type

magmatism). The other type, namely, the Eymir metadiabases are considerably different, both in terms of mineralogical assemblage and geochemistry and should not be confused with each other.

Figure 2.7. The primary relationship between pelagic limestones and metabasalts within the Nilüfer Unit (Zerdalitepe).

The metabasalts studied in this area are represented by both pillowed and massive lava flows, though an exact characterization is generally difficult in many cases, owing to the deformation they have undergone. The pillowed basalts can be especially well observed in the parts dominated by pillow breccias in Ortaköy area. These pillowed lava fragments are seen as variably-sized ellipsoidal bodies (sometimes exceeding 50 cm) which are set in a basaltic matrix. They generally appear highly amygdaloidal, indicating formation in relatively shallow levels. There also occur hyaloclastites composed of abundant glass fragments (glass shards) now entirely turned into secondary minerals, such as chlorite and smectite? The influence of low-grade metamorphism on the metabasalts studied

in the area is evidenced by their greenish colors. Rarely, also observed are high-MgO varieties of these metabasalts, and they can be differentiated in the field by the presence of abundant large pseudomorphosed olivine phenocrysts (see Chapter 3). The gabbroic rocks in the study area range from fine-grained diabasic varieties to coarser medium-grained ones. The high-MgO metagabbros, like the extrusive counterparts, are characterized by various olivine phenocrysts now replaced entirely by secondary mineral phases. These rocks are also observed as greenish colored, indicative of low grade alteration/metamorphism.

The volcanoclastic lithologies that represent the products of basaltic volcanic activity, such as pillow breccias, hyaloclastites, are widespread in the study area. In the places where the deformation has not been so effective, it is possible to observe these clastic assemblages as regular layered bodies on top of each other. The clast-size ranges in a wide spectrum, so resulting in varieties that range from tuff to breccias. In the coarse-grained lithologies, the presence of numerous lava fragments of variable size can be observed very well, which are embedded in a weakly foliated matrix composed dominantly of chlorite and calcite. Carbonate rock fragments (i.e. limestone, dolostone) also occur within these clastic lithologies. In Ortaköy and Bayındır, the volcaniclastics are seen primarily with limestones, where the latter can be found as lens-shaped bodies within basaltic matrix of pillow breccias, or sometimes thick limestone bodies are observed alternating with mafic tuffs (Figure 2.8). In these localities, namely Ortaköy and Bayındır, these tuffaceous rocks are found to be silicified, probably indicating the deposition of silica in the quiescence of magmatism. These silicified assemblages can be seen as well-bedded bodies within the basaltic-volcaniclastic succession (Figure 2.9). In Ortaköy and Gökçeyurt, these tufficeous rocks are found to have been affected by high pressure metamorphism, and can be easily identified by their bluish colors. These metatuffs bearing Na-amphibole are observed as primary related with limestone (Figure 2.10).

Figure 2.8. Primary relationship observed between mafic tuff and limestone within the Nilüfer Unit (Bayındır).

Figure 2.9. Silicified tuff layers interbedded with volcaniclastics within the Nilüfer Unit (Ortaköy).

Figure 2.10. Synchronous relationship between bluish HP-metatuffs and pinkish pelagic limestone within the Nilüfer Unit (Ortaköy).

The limestones in the study area are characterized by grayish and pinkish colors, and they are observed to have experienced varying degrees of recrystallization. They are sometimes found as small lenses in mm scale, or sometimes observed as large, bedded bodies that can be defined in meter scale. In the Hacılar area, the primary relationship between limestone and metabasalt is observed very well, where an almost 7 meter-thick lava flow is interbedded with thick limestone layers (Figure 2.6). This succession is observed to pass into mudstone-limestone alternation, which is followed upwards by volcaniclastic sequences interlayered with limestone. In this area, several neritic and pelagic limestones interbedded with metabasalts were found to include some foraminiferal fauna to yield the following ages (unpublished data of N. Turhan): a) Ladinian-Carnian: *Glomospirella aff. densa* (PANTIC), *Glomospirella* sp., *Endothyranella* sp.; b) Anisian: *Involutina* sp., *Meandrospira* sp., *Ammobaculites* sp., *Lagenidae*; c) Middle-Late Triassic: *Tubiphytes* sp., *Endothyra* sp., *Trochammina* sp., *Meandospira* sp., *Lagenidae*. In some parts, limestones include basaltic

27

fragments, suggesting that the basaltic pieces should have been integrated into limestone while it was still unconsolidated (Figure 2.11). Or, in a similar manner, the basalt can include limestone fragments in it (Figure 2.12).

Figure 2.11. Basaltic fragments within limestone, indicating that they have been incorporated into limestone while it was not entirely consolidated (Bayındır).

Mudstones are represented by reddish colors, and generally observed as thin-bedded bodies within limestone or basaltic assemblages (Figure 2.13). In the study area, there also occur, to a lesser extent, cherts found to alternate with basaltic lithologies or the metaclastics that forms the matrix on which the basaltic assemblages are embedded. In the Ortaköy area, within the Eymir Unit, a pinkish chert band interbedded with mudstones and metaclastics has been found to be of Carnian age (Late Triassic; det. by Dr. U.K. Tekin) on the basis of the following radiolarians (Figure 2.14): *Triassocrucella* sp., *Paronaella claviformis* (KOZUR & MOSTLER,1978), *Paratriassoastrum* sp., *Canoptum cucurbita* (SUGIYAMA, 1997), *Canoptum inornatum* TEKIN, 1999, *Canoptum levis* TEKIN, 1999, ?

Corum sp., *Annulotriassocampe* sp. cf. *A. baldii* KOZUR, 1994, *Annulotriassocampe* sp. cf. *A. sulovensis* (KOZUR & MOCK, 1981). The importance of this finding is given in Chapter 5.

Figure 2.12. Limestone fragments observed inside altered basalt within the Nilüfer Unit (Hacılar, Gölbaşı).

Apart from the metabasaltic assemblages (including also limestone, mudstone and chert) which represent the Nilüfer Unit, there also occur metaclastic assemblages, namely the Eymir Unit, which forms the matrix material in which the Nilüfer Unit is embedded (Figures 2.15). Thus, the Nilüfer Unit is found to be as variable-sized blocks within the Eymir Unit. It is important to note that the clastic lithologies within the Nilüfer Unit (i.e. volcaniclastics, hyaloclastic breccias) are all ocean-derived, however, the Eymir Unit comprises clastics of terrigenous origin.

Figure 2.13. Alternation of reddish thin-bedded mudstone with limestone, observed within the Nilüfer Unit (Bayındır).

The clastic lithologies of the Eymir Unit (Figure 2.16) are characterized largely by brownish and grayish colors, and include slates, phyllites, metagreywackes and metaconglomerates. The intensity of deformation and metamorphism on these rocks is highly variable; sometimes these clastic rocks display no observable foliation and deformation, but sometimes they are found to be intensely deformed and have well-developed schistosity planes. The influence of deformation can also be observed in macro-scale, where the primary bedding planes are no longer observable, instead they are seen folded and sheared. A weak foliation development can also be observed on metaconglomerates, resulting in elongated clasts. Metasandstones in the study area are represented by greywackes and arkosic varieties, and in some places mica-rich sandstones are also identified with their shiny appearances. On the basis of the clasts making up the Eymir metaclastics are considered, it can be suggested that the clasts have been derived from a number of sources. This polygenetic nature is especially well observed on the conglomeratic varieties.
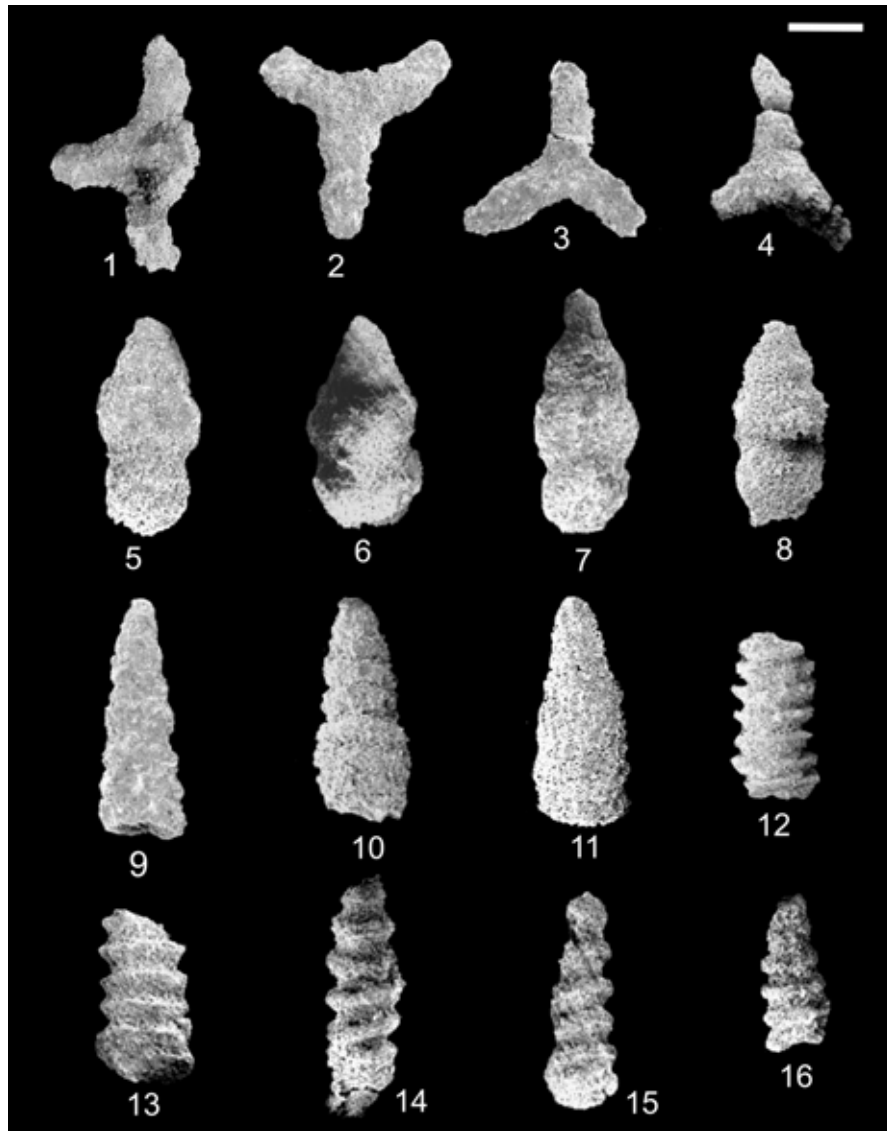
Figure 2.14. Scanning electron micrographs of early to middle Carnian (Late Triassic) Spumellaria (Radiolaria) from the Karakaya Complex near city of Ankara. Scale = number of microns for each figure. 1. *Triassocrucella* sp., sample no. 08-Orta-1, scale bar = 250μm, 2-3. *Paronaella claviformis* (KOZUR & MOSTLER,1978), both samples are from sample no. 08-Orta-1, scale bar for both figures= 225μm, 4. *Paratriassoastrum* sp., sample no. 08-Orta-1, scale bar = 170μm, 5-8. *Canoptum cucurbita* (SUGIYAMA, 1997), all samples are from sample no. 08-Orta-1, scale bar for all figures= 100μm, 9. *Canoptum inornatum* TEKIN, 1999, sample no. 08-Orta-1, scale bar = 100μm, 10. *Canoptum levis* TEKIN, 1999, sample no. 08-Orta-2, scale bar = 80μm, 11. ? *Corum* sp., sample no. 08-Orta-1, scale bar = 110μm, 12-13. *Annulotriassocampe* sp. cf. *A. baldii* KOZUR, 1994 Group, 12. Sample no. 08-Orta-1, 13. Sample no. 08-Orta-2, scale bar for both figures = 130μm, 14-16. *Annulotriassocampe* sp. cf. *A. sulovensis* (KOZUR & MOCK, 1981), 14. Sample no. 08-Orta-1, 15-16. Sample no. 08-Orta-2, scale bar for all figures = 120μm.
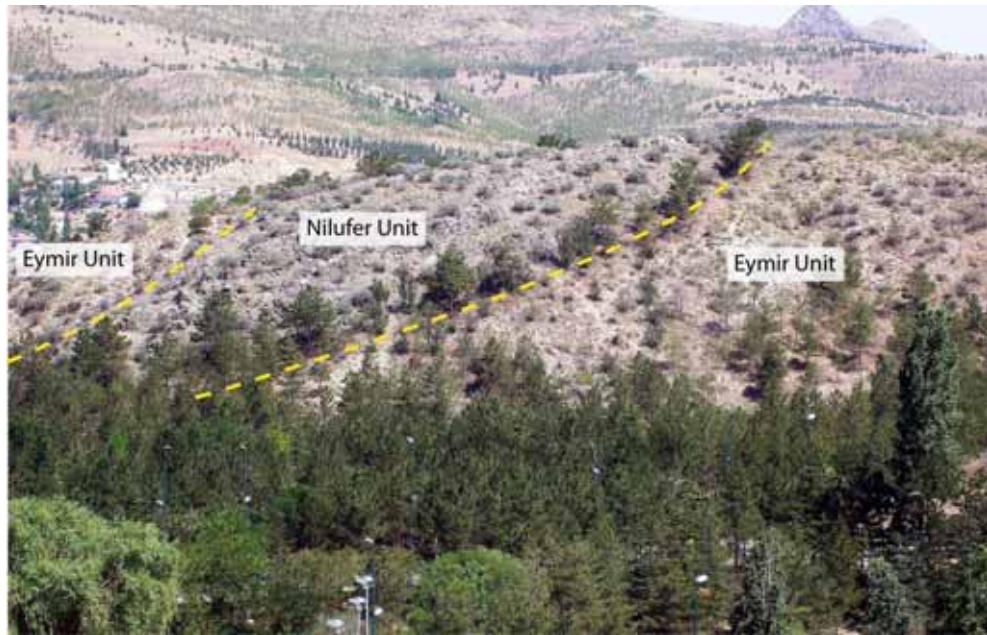
Figure 2.15. Block-matrix relationship observed between the Nilüfer Unit (here observed as megablock) and the Eymir Unit (the matrix material) (Bayındır). The boundary between these two units is highlighted with yellow.

Figure 2.16. The metaclastics of the Eymir Unit (Bayındır).

2.2.1.2. İmrahor

A part of this area was previously studied in general terms by Sayıt (2005) and Sayıt and Göncüoğlu (2009a). Here the metabasic rocks in the southern sector of this area will be described detail.

The metabasic rocks are characterized by purplish, bluish and greenish colors, and they are observed as variable-sized blocks within the metaclastics of the Eymir Unit (Figure 2.17). The block-contact boundaries of these lithologies are sometimes identified as sheared probably owing to a later tectonic event after their mixing. The metabasaltic rocks display varying degrees of schistosity, and on the basis of their original protoliths, they have been interpreted to represent largely mafic tuffs and volcaniclastics (Figure 2.18).
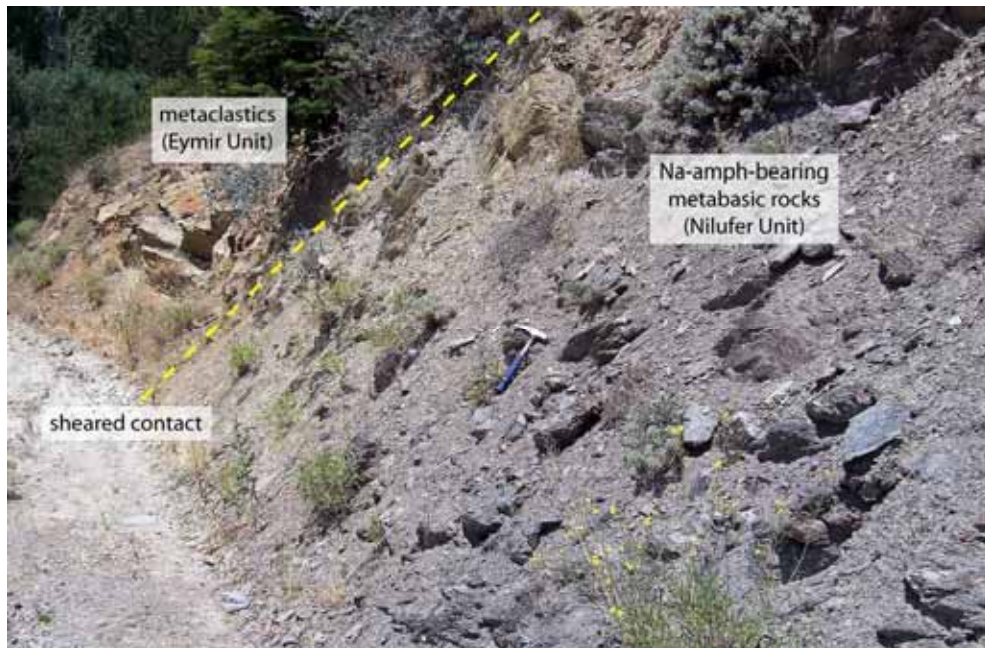
Figure 2.17. The HP/LT metabasic rocks of the Nilüfer Unit (blue-purple) in contact with the metaclastics of the Eymir Unit (brownish) (İmrahor).

Figure 2.18. Coarse-grained mafic metavolcaniclastics within the Nilüfer Unit (İmrahor). Note the elongation of basalt fragments and foliation in the matrix, which defines the schistosity. The matrix is largely composed of chlorite and calcite.

The basalt clasts within the coarse-grained volcaniclastics are observed to have gas vesicles some of which have been filled by secondary minerals, showing amydaloidal appearance. The original layering between coarse-grained volcaniclastics (e.g. hyaloclastic breccias) and fine-grained ones (e.g. metatuffs) can be still recognized in spite of deformation and metamorphism (Figure 2.19). Both varieties, however, appear to have been strongly overprinted by high pressure metamorphism as indicated by the presence of numerous Na-amphibole crystals.

In some cases, the intense carbonate influx that has probably developed at the same time with these mafic volcanic products formed is reflected by the presence of numerous calcite crystals. This process is sometimes so intense that some of these metamorphic rocks appear to contain calcite constituting more than 50% of the entire mineral assemblage. These carbonate-rich rocks are observed to have been experienced intense ductile deformation; however, the presence of

amygdaloidal basalt clasts can be still identified in spite of the deformation. The greenish portions seen in these carbonate-rich metamorphic rocks probably represent the basaltic matrix material in which the basaltic fragments are embedded or the tuffaceous levels interlayered with the basalt flows. In some parts of the area, it is also possible to observe greenish metabasalts without any high pressure imprint. These metamorphic rocks, however, are found to have been severely altered by carbonate minerals. They show amygdale-like structures, probably indicating that their protoliths have formed in shallow levels in a submarine environment. Sometimes, it is observed that the metabasaltic assemblages are embedded in well-bedded silicified tuff layers.

Figure 2.19. Primary layering between coarse- (at the top) and fine-grained (at the bottom) mafic metavolcaniclastics within the Nilüfer Unit (İmrahor).

The metaclastics representing the Eymir Unit in the İmrahor area are found to be very similar to those in the other study areas. The deformation in the area is observed to have been very intense in some places so that crenulation cleavage

can also be identified in addition to the primary foliation planes (Figure 2.20). These metaclastics are cross-cut by numerous metadiabase dikes. These dikes, in most places, appear to have been intensely altered by surface weathering, and they generally appear in reddish brown colors. Indeed, they can be easily misinterpreted as metasandstones if a close-up examination is not performed.

Figure 2.20. Intensely deformed phyllitic metamorphics of the Eymir Unit. Note the development of crenulation cleavage (İmrahor).

2.2.1.3. Hasanoğlan, Kavaklı, Doğanoluk, Bozca, Hacılar (Çubuk)

Of these localities, some parts of Hasanoğlan that were previously examined by Sayıt (2005) and Sayıt and Göncüoğlu (2009a) were restudied, and the studies were extended towards the north in the extent of this study (Figure 2.21).

In the southeastern parts of Hasaoğlan, the relationship reflected by metabasalts (generally pillowed) and limestones is very similar to what is observed in the Ortaköy, Hacılar, Bayındır, Zerdalitepe and Gökçeyurt areas. The basalts are

characterized by reddish brown-black colors with amygdaloidal textures, and their pillow structures are well identified (Figure 2.22). The presence of abundant gas vesicles filled by secondary minerals can be attributed to formation in a shallow submarine environment.
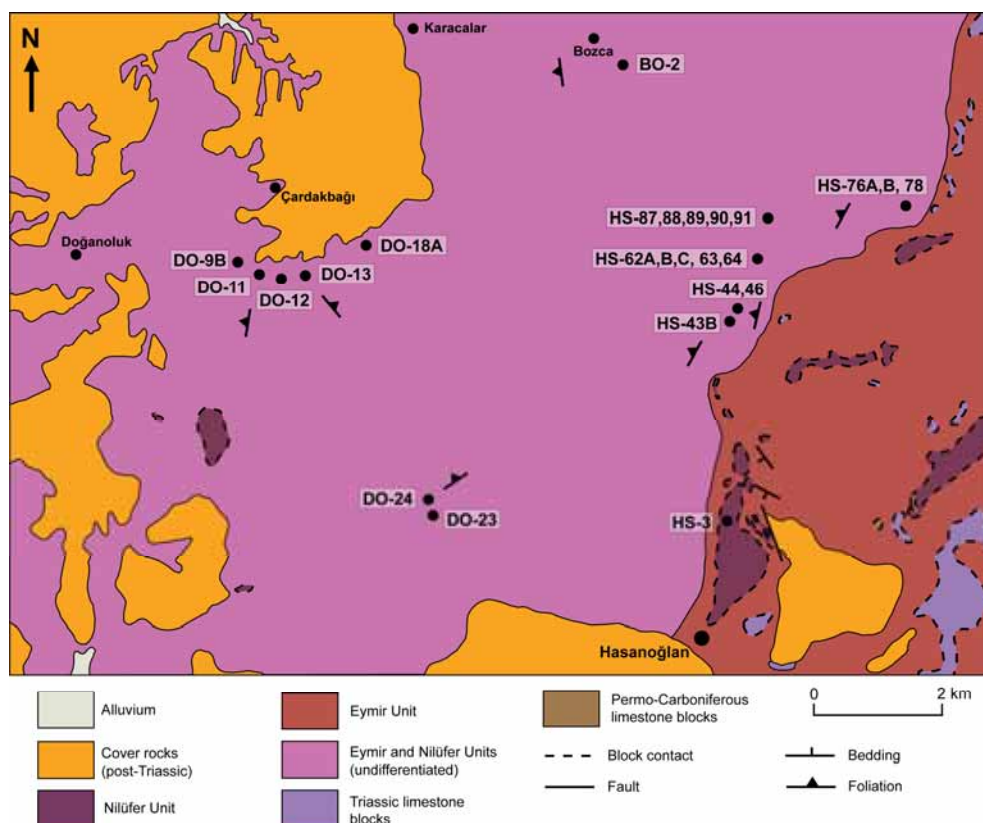
Figure 2.21. Geological map of the Ankara region including the area between Hasanoğlan and Bozca (modified from Akyürek et al., 1982). Locations of the geochemically analyzed metabasic samples are shown on the figure.

While the matrix is represented by shaly material in some places, it is characterized by sand- and gravel-size olistostromal clastics in the others. The fine-grained clastics are sometimes found to have converted to slates and phyllites in response to metamorphism. The synchronous nature of basalts and limestones is well observed; sometimes limestone clasts are found embedded in a basaltic matrix, or sometimes basalt clasts are observed within a carbonate matrix

(Figures 2.23 and 2.24). In some cases, the metabasaltic assemblages display an olistostromal appearance with variable-sized limestone and greenish metabasalt fragments (mostly amgydaloidal) set in aphanitic metabasaltic matrix. In some parts, limestones appear to alternate with thin cherty layers, probably related to silica saturation caused by synchronous basaltic volcanism (Figure 2.25). In this area, there also occur, to a lesser extent, volcaniclastics and silicified tuffs that represent products of the same basaltic system.

Figure 2.22. Pillow basalts in the Nilüfer Unit (Hasanoğlan).

In the northern and northwestern sectors of the area, the intensity of deformation and shearing are observed to increase as indicated by the development schistosity planes and folding in variety of rock types. These parts actually appear very similar to what is observed in İmrahor. The presence of metabasaltic rocks is very apparent with their bluish and greenish colors. These metabasic lithologies display well-developed schistosity and varying degrees of crenulation cleavage.

Figure 2.23. The synchronous relationship observed between basalt and limestone within the Nilüfer Unit (Hasanoğlan).

Figure 2.24. The same phenomena observed as in Fig 2.23. However, in this case, basalt clasts are found within a carbonate matrix (Hasanoğlan). Note that the basalt fragments display vesicular and amygdaloidal textures.

Sometimes, the tufficious members are found to have distinct banding with alternation of bluish and white layers. The bluish layers include Na-amphibole together with mostly chlorite, while the white layers are composed largely of calcite. Thus, this type of metamorphics probably represents an alternation of tuff and carbonate. In these sectors of the study area, silicified metatuffs are characterized by light greenish-white colors, and found to be entirely recrystallized. This can be understood by well-developed idiomorphic quartz crystals within these rocks. The influence of metamorphism on the thin muddy portions interbedded with these silicified layers, however, is revealed by the development of white mica (phengitic?) and chlorite. Sometimes, the tuffaceous rocks are found to have experienced intense ductile deformation as indicated by formation of crenulation cleavages.
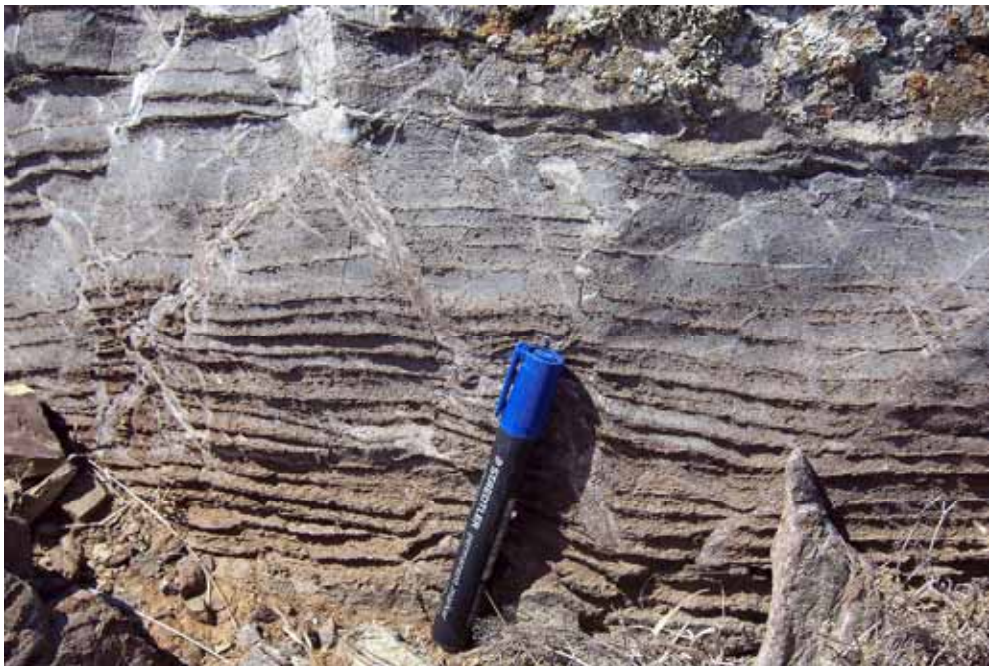
Figure 2.25. Limestone with chert laminations within the Nilüfer Unit (Hasanoğlan).

In these parts of the study area, it is also possible to observe the metabasalts, though they are not so widespread. These metabasalts are light-greenish in color, and in the places where the effect of regional metamorphism has been more dominant, foliation planes are observed to have developed on these rocks, resulting in typical "greenschist" appearance. In some parts, however, cataclastic deformation appears to be more dominant, and no foliation is found to have developed on the basaltic rocks in these areas, instead there occur brecciated textures and fractured/crushed phenocrysts.

Apart from these rock types, there also occur also high-MgO metagabbros and metabasalts which have undergone low-grade metamorphism. They are characterized in the field by light/dark greenish colors, and their big phenocrysts in can be easily recognized by naked eye. The metabasalts, picritic in composition according to petrographic investigation, are sometimes found to have been experienced some degree of deformation as revealed by elongated pseudomorphed olivine phenocrysts and foliated matrix, which together defines the schistosity. The metagabbros, on the other hand, are rather found to have been affected by brittle deformation. In these parts of the study area, there also occur carbonate rocks, however they are observed entirely recrystallized, thus no fossil evidence could have been obtained.

Towards the northwestern parts, namely Doğanoluk, Kavaklı and Bozca, the metaclastic rocks dominate, and metabasaltic rocks representing the Nilüfer Unit diminish. In these parts, metaclastics are largely represented by grayish and greenish colors, and they appear to have been experienced multiple deformation. The first two deformation phases are observed to be ductile, whereas the last phase appears to have been brittle. In some parts, metavolcaniclastics can be observed within the Eymir Unit as greenish, foliated rocks. Instead of the metabasaltic assemblages of the Nilüfer Unit, in these sectors of the study, there appear metadiabase bodies which mostly cross-cut the metaclastic lithologies of the Eymir Unit (Figure 2.26).

These metadiabase dikes are characterized by dark-greenish colors, though their surface colors are largely observed to be in tones of brown owing to weathering. It is important to note that in contrast to the metaclastics which are foliated in most cases, no foliation plane have developed on the metadiabase dikes. However, brittle deformation is sometimes observed to have affected these dikes. The cross-cutting relationship can be well observed in the east of Doğanoluk, where well-foliated metaclastics of the Eymir Unit are cut by a non-foliated metadiabase body (Figure 2.27).

Figure 2.26. Metadiabase dikes intruding into metaclastics of the Eymir Unit (west of Hasanoğlan). The metadiabases can be differentiated easily by their dark colors and steep morphologies.

2.2.1.4. Eymir and Karataş (Gölbaşı)

This area is very similar to the southern parts of İmrahor and northwestern parts of Hasanoğlan (namely Doğanoluk and Kavaklı). The metaclastics ranging from slates to metaconglomerates dominate the region. They are generally characterized by grayish colors with silvery (phyllitic) appearances. These

variably metamorphosed and deformed metaclastic successions are intruded by metadiabase dikes. The cross-cutting relationship is well observed in several locations (Figure 2.28). The Hacılar (Çubuk) area shares very similar characteristics to these study areas, so it will not be repeated here. The geological map of this region, however, is given in Figure 2.29.

Figure 2.27. The cross-cutting relationship observed between metadiabase (dark brownish) and metaclastics (light grayish) of the Eymir Unit. Note the well-developed foliation shown by metaclastics, whereas no foliation is observed on the metadiabase dike (Doğanoluk). The contact is roughly indicated by yellow dashed lines.

2.2.2. Central Sakarya Region

The low-grade metamorphic rocks that are observed as a tectonic slice between the Söğüt Metamorphics and the Dağküplü Complex (Göncüoğlu et al., 1996) represent the newly defined Nilüfer Unit in the Central Sakarya area (Figure 2.30). The geological characteristics of the Nilüfer Unit in this region appear very similar to what is observed in Ankara and Bursa; the metabasaltic assemblages are found as blocks within metaclastics of terrigenous origin that form the matrix material.

Figure 2.28. The cross-cutting relationship between metadiabase (to the left) and phyllite (to the right) (Lake Eymir). Note that no foliation is observed on the metadiabase dike, while the phyllite is clearly foliated and displays folding in response to ductile deformation.
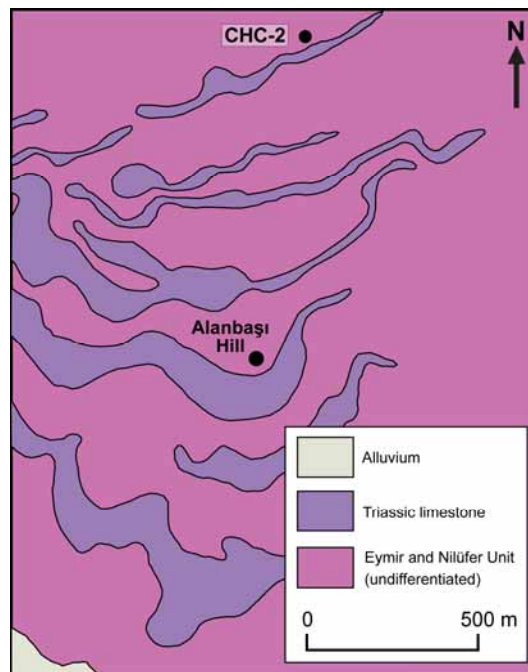
Figure 2.29. Geological map of the Hacılar (Çubuk) region (modified from Akyürek et al., 1979a). Location of the geochemically analyzed sample is shown on the figure.
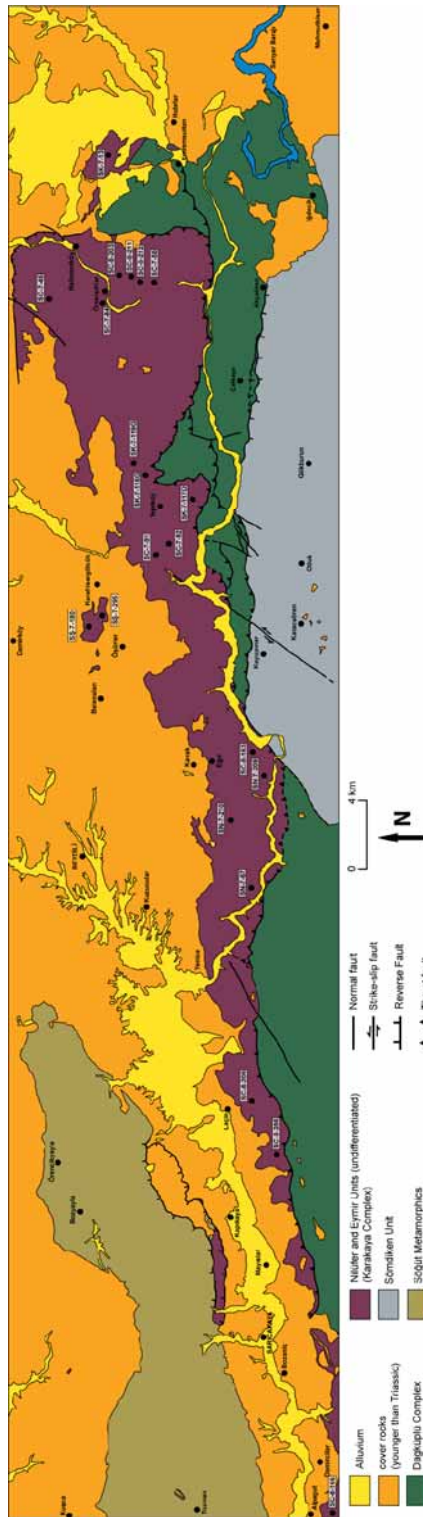
Figure 2.30. Geological map of the Central Sakarya region (modified from Göncüoğlu et al., 1996). Locations of the geochemically analyzed samples are shown on the figure.

The metabasic rocks in the study area are represented by metabasalts, metagabbros, and metatuffs. The metabasalts are observed primarily associated with metavolcaniclastics, limestones and cherts. Compared to the other rock types in the study area, the development of foliation on the metabasalts are found to be more apparent. In some parts of the area, there also occur picritic varieties of metabasalts. These highly magnesian metabasaltic rocks are observed as lenses within the metabasalts or olistostromal parts. The metagabbros are characterized by dark greenish colors, and distinguished by the presence of relatively large hornblende and albite crystals. Sometimes, a weak foliation can be observed to develop on these intrusive bodies.

2.2.3. İnegöl-Nilüfer (Bursa)

In the Bursa region (Figures 2.31 and 2.32), similar to what is observed in Ankara, the rock lithologies are found to be variably deformed and sheared. Owing to this change in the intensity of deformation, in some areas there occur mafic schists with well-developed schistosity planes, while in the others massive and pillowed lava flows with no observable foliation planes. However, even in such areas where no foliation has been developed, several shear zones within these basaltic successions were observed. The metabasalts are again primarily related with the limestones, suggesting their synchronous nature (Figure 2.33).

The limestones in the area are observed in the gray and pinkish colors, and generally thin bedded. They are sometimes found as small lenses within basalts. In some parts of the area, there also occur some ultramafic bodies, however, they are entirely serpentinized. Locally, there are mafic schists that bear Na-amphibole, thus indicating the influence of high pressure metamorphism.
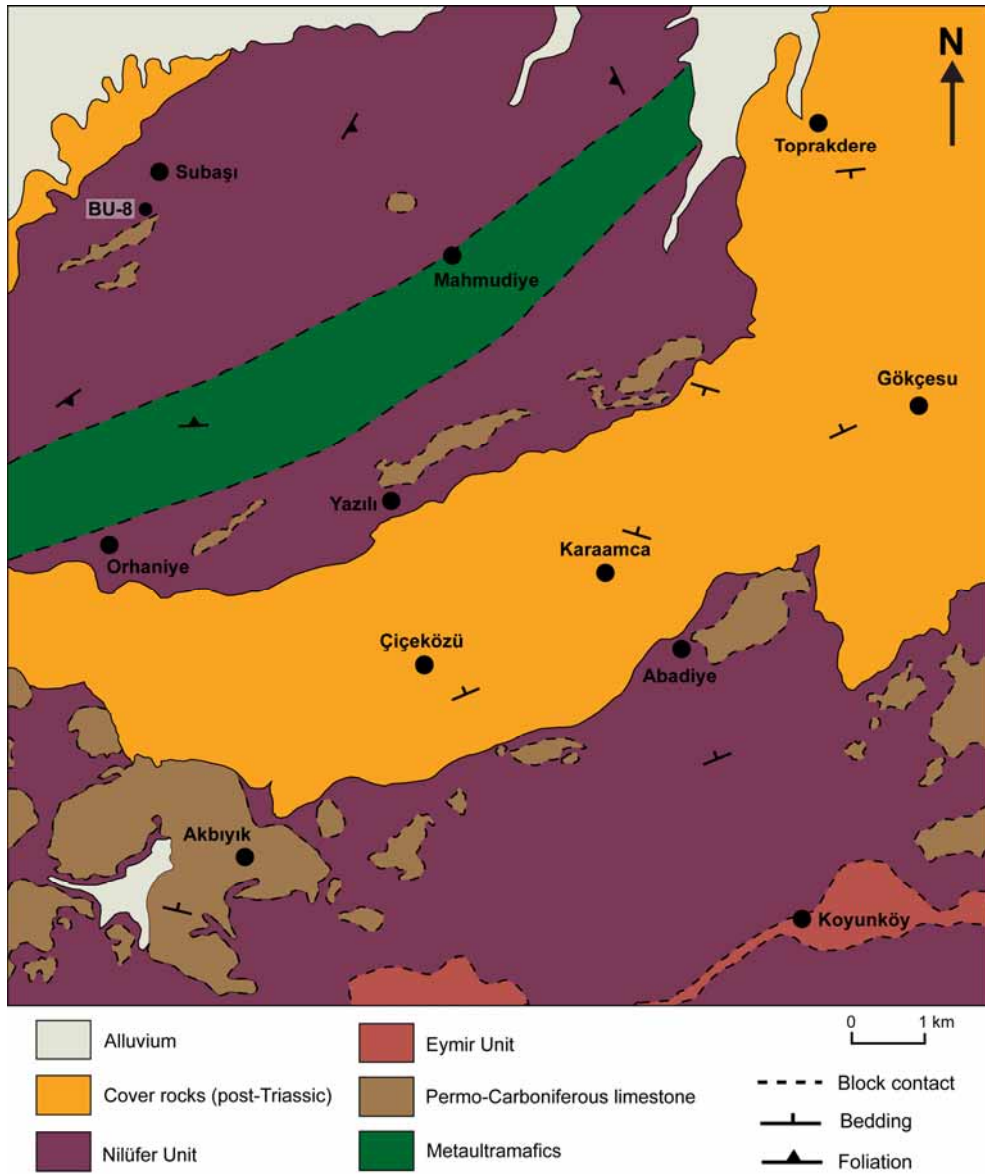
Figure 2.31. Geological map of the Bursa region including the area between İnegöl and Yenişehir (modified from Genç, 1987). Location of the geochemically analyzed sample is shown on the figure.
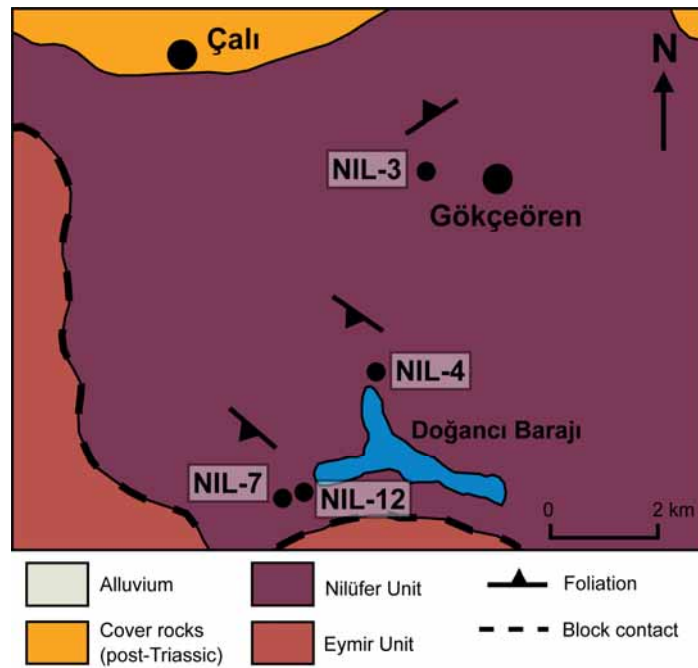
Figure 2.32. Geological map of the Bursa region including the area around the Nilüfer River and the Doğancı Dam (modified from the İstanbul sheet of 1/500000 scale MTA geological maps compiled by Türkecan and Yurtsever, 2002). The location of geochemically analyzed sample is shown on the figure.

Figure 2.33. The synchronous relationship between metabasaltic rocks and limestone within the Nilüfer Unit (Nilüfer Valley). Note that the whole succession is deformed.

CHAPTER 3

PETROGRAPHY

3.1. Introduction

This chapter concerns the petrographical features of samples collected from various localities assumed to represent the Nilüfer-type metabasic rocks and the Eymir metadiabases. For this purpose, more than 250 thin-sections were prepared and examined under the microscope. All rock samples have been metamorphosed to some degree as indicated by various secondary assemblages. All samples have also been variably sheared and deformed. For the sake of simplicity, the metabasalts and metagabbros of the Nilüfer Unit were treated separately from mafic schists and metavolcaniclastics of the same unit and they were divided into two groups on the basis of their dominant phenocryst phase as "augite-phyric" and "olivine-phyric". These sub-types may also show distinct textural relationships in response to their degree of cooling rate and/or extent of deformation.

Overall, augite-phyric samples consist of titaniferous augite; also include kaersutitic amphibole in some cases. The Eymir metadiabase samples, on the other hand, comprise diopsidic augite, thus contrast with the previous groups. The compositional differences between sub-types are also reflected by their modal mineralogy, especially olivine content (on the basis of pseudomorphs after olivine).

3.2. Metabasalts

3.2.1. Augite-phyric Metabasalts

Most of these metabasalts are generally aphanitic, though some of them are medium- to coarse-grained, reflecting microphaneritic texture (Figure 3.1a). Some of the aphanitic varieties are characterized by distinctly thin, elongated crystals; somewhat like spinifex texture (Figure 3.1b). Some of the phenocrysts are large, visible to naked eye, and they are embedded in a fine-grained groundmass (Figures 3.2 and 3.3a). In some cases, groundmass plagioclase tends to be relatively larger (Figure 3.3b).
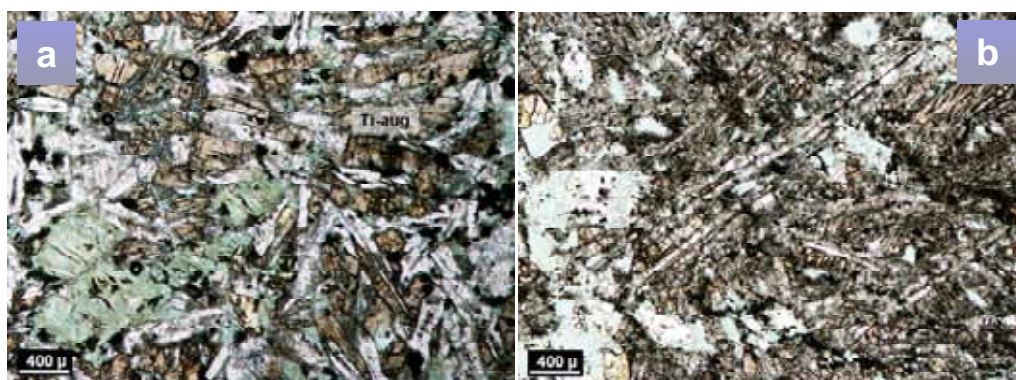
Figure 3.1. a) Typical view of a coarse-grained (diabasic) augite-phyric metabasalt. Ti-augite is apparent with its distinctive pinkish colors. Light-colored parts are mostly represented by plagioclase laths. There is a pseudomorph after olivine (green colored part, oriented from center to the lower left), now represented by serpentine and chlorite. Epidote is distinguished by yellowish colors (Sample OR-116, PPL); b) Spinifex-like texture displayed by augite-phyric metabasalts. Pinkish-brown grains are Ti-augite. Note the considerably long, acicular plagioclase crystal just above the center. Yellowish grains are epidote. Pale green parts are mostly composed of chlorite and minor amont of serpentine (Sample OR-33, PPL) (Ti-aug: Ti-augite).

Most of these metabasalts are characterized by porphyritic texture; although there are samples with aphyric appearance as well. Some of the augite-phyric metabasalts are composed of variably-sized phenocrysts and microcrysts,

resulting in seriate textures. Some samples contain considerable amount of degassing structures filled with various secondary minerals displaying amygdaloidal texture (Figures 3.4a,b). However, in some cases the secondary mineral-filled features are phenocrysts and/or crystal aggregates which have undergone intense alteration and present definite crystallographic shapes with subhedral appearance (Figure 3.4c). Rarely, some samples appear to have experienced some degree of brittle and/or ductile deformation (Figure 3.5a).
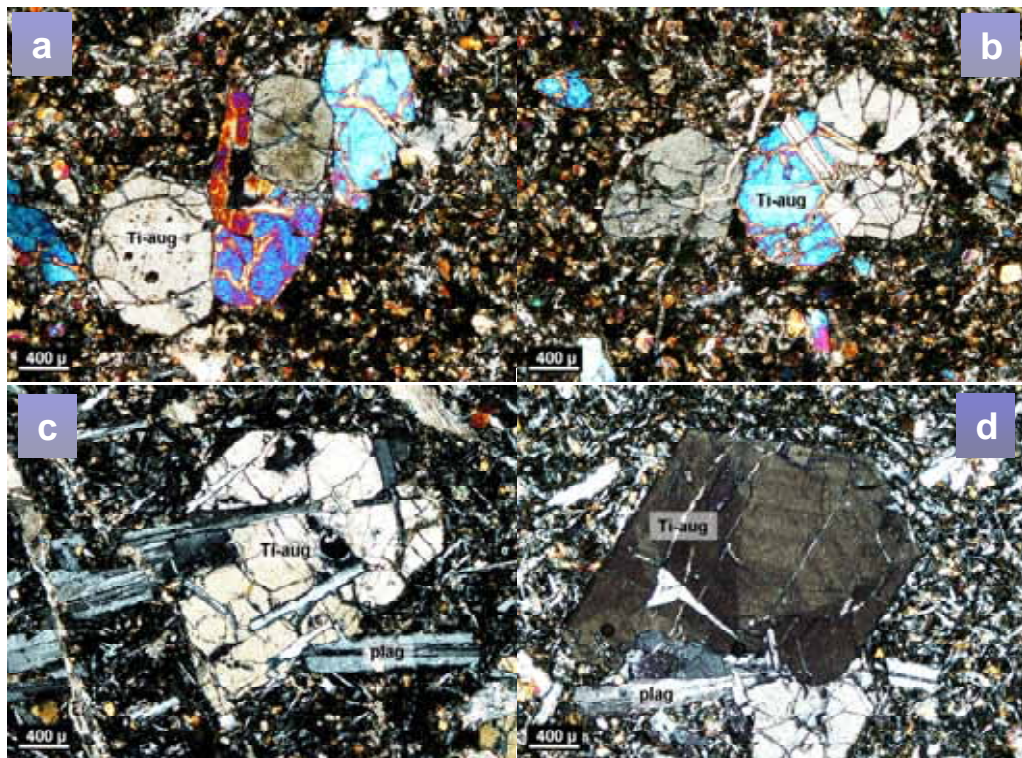
Figure 3.2. a and b) Glomeroporphyritic aggregate of Ti-augite embedded in a fine-grained groundmass. Note multiple twinning displayed by three of the crystals (b) (Sample OR-28, XPL); c) Large Ti-augite grain associated with several plagioclase crystals; together they display a sub-ophitic relationship. Note the size difference between grains (Sample OR-29, XPL); d) Ti-augite grain characterized by combined sector and concentric zoning (Sample OR-29, XPL) (Ti-aug: Ti-augite, plag: plagioclase).

Figure 3.3. a) Serpentine pseudomorphs after olivine. Note that the pseudomorph at the left hand side has been largely resorbed by groundmass. Minerals with higher interference colors in the groundmass are Ti-augite. (Sample GK-1, XPL); b) Augite-phyric metabasalt with relatively larger groundmass plagioclase. The interstices between plagioclase crystals are occupied by Ti-augite, which is distinguished by higher interference colors (Sample OR-41, XPL) (serp-ol: serpentinized olivine; Ti-aug: Ti-augite).

Primary minerals in these basalts are Ti-augite and to a lesser extent plagioclase. No olivine has survived; it is present mostly as serpentine pseudomorphs and to a lesser extent epidote, chlorite and calcite (Figure 3.3a). Ti-augite appears to be very fresh compared to plagioclase and olivine, and is characterized by brownish, pinkish-brown crystals with generally subhedral outlines and showing poorly-developed cleavage traces (Figures 3.2a-d). In fact, they appear to be rather fractured (Figures 3.1a and 3.2). In the parts where these metabasalts have experienced brittle deformation, variably-sized fragmented Ti-augite crystals are set in a very-fine grained dark matrix (Figure 3.5a). The parts that reflect ductile deformation, on the other hand, are characterized by Ti-augite associated with dynamically recrystallized albite. Ti-augite can be found both as phenocrysts and microcrysts. Ti-augite crystals sometimes form glomeroporphyritic clusters with other Ti-augite and/or plagioclase and/or serpentinized olivine (Figures 3.2a,b). Sub-ophitic texture is displayed by large Ti-augite grains together with several plagioclase laths (Figure 3.2c). Poikilitic Ti-augite crystals, though very rare, are also found. In addition, Ti-augite microcrysts occupy the interstices between

52
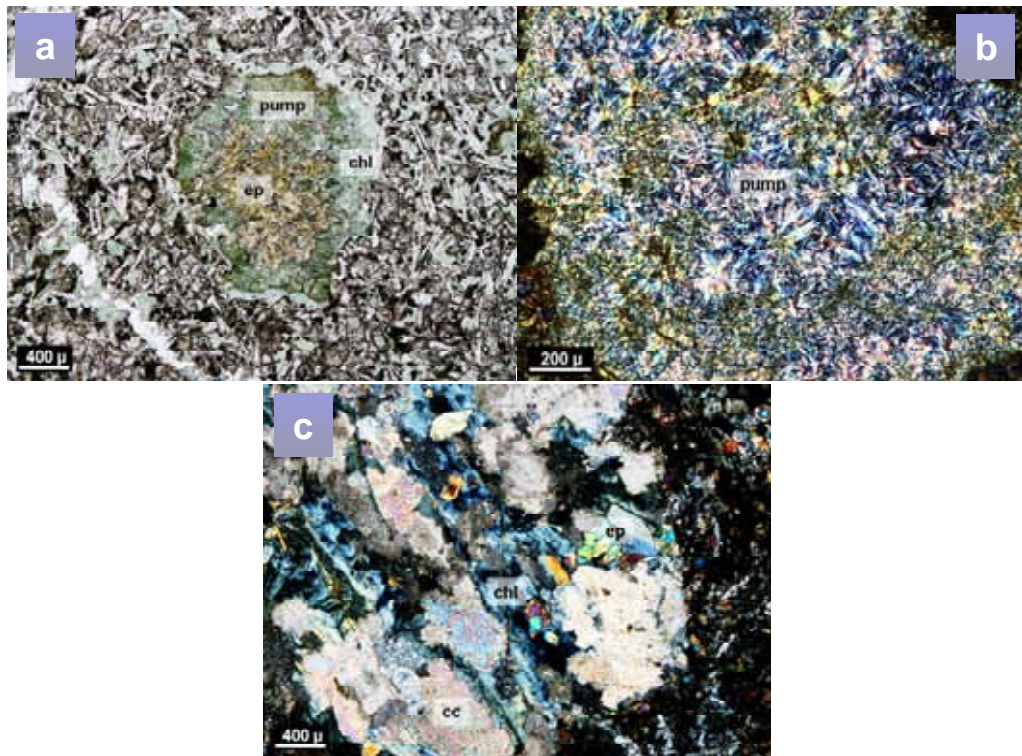
Figure 3.4. a) Amygdule filled with epidote in the core, which is surrounded mostly by pumpellyite. Note chlorite to the right part of amydule (Sample OR-67, PPL); b) Amygdule filled with pumpellyite; note the anomalous 1st order interference colors (Sample GK-1, XPL); c) A large olivine (?) phenocryst now entirely replaced by a number of secondary phases. Note the two perfect crystal faces of this grain. The mineral with extreme interference colors is calcite. Chlorite displays anomalous 1st order bluish-grey colors. Epidote is also present as mainly identified by high interference colors (Sample OR-28, XPL) (chl: chlorite, ep: epidote, cc: calcite, pump: pumpellyite).

plagioclase laths, showing intergranular texture. Compositional zoning, generally of sector type, can be identified in most of Ti-augite crystals. Some grains show combined concentric- and sector-type zoning (Figure 3.2d). In addition, some are twinned in either simple or multiple (polysynthetic) fashion (Figure 3.2b). In one sample, Ti-augite appears to have corroded cores (Figure 3.5b). Rarely, exsolution lamellae developing on Ti-augite can also be observed.

53
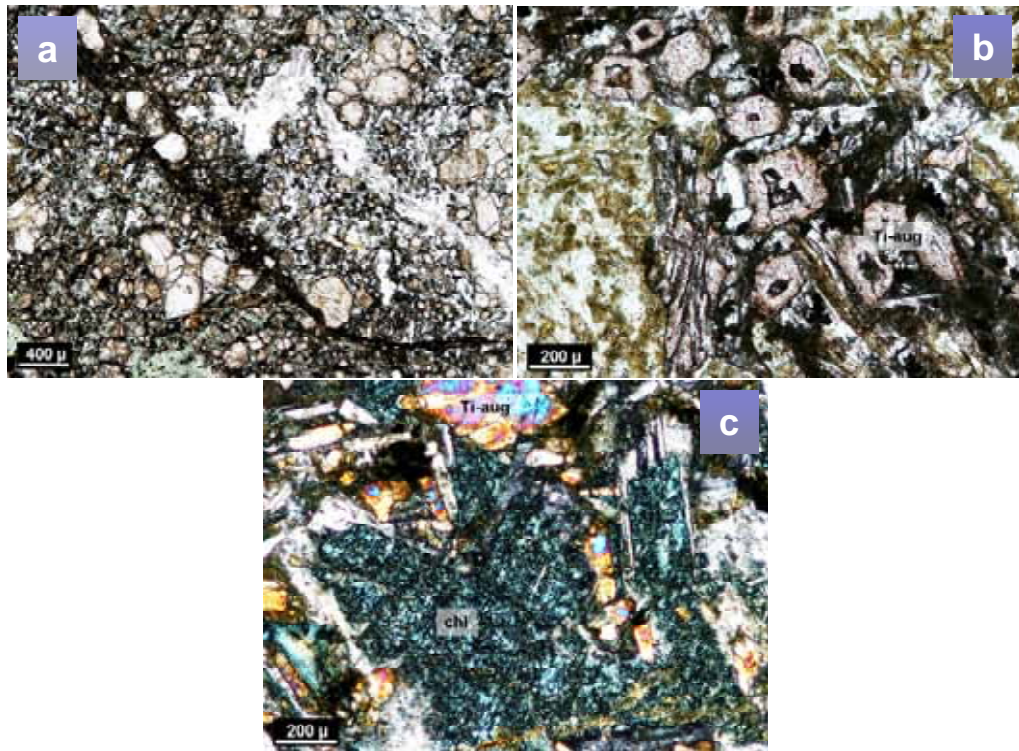
Figure 3.5. a) Type-1 metabasalt that has experienced brittle and ductile deformation. The dark colored part extending from NW to SE represents a brittle fault (Sample HS-88, PPL); b) Pinkish, corroded Ti-augite crystals in the groundmass. They are surrounded by amygdules on both sides, which are filled by secondary minerals, including largely chlorite and pumpellyite (Sample GK-1, PPL); c) Severe alteration of plagioclase laths by chlorite. Note multiple twinning displayed by a plagioclase to the upper right (Sample OR-41, XPL) (Ti-aug: Ti-augite, chl: chlorite).

Plagioclase is less abundant than Ti-augite and appears to be altered, though some relatively fresh crystals are still observable. Multiple twinning can be identified, where the primary nature is relatively preserved. Plagioclase sometimes forms glomeroporphyritic aggregates, either by themselves or the other type of phenocrysts. Sometimes, groundmass plagioclase display intergranular texture in association with Ti-augite. It is often the case that they are rather albitic (Na-rich) having lost their Ca-rich nature during low-grade metamorphism. They are seen to be replaced by several secondary phases, such as epidote, chlorite and sericite. In some cases, they are intensely replaced by

54

chlorite such that only the outer parts have survived (Figure 3.5c), and sometimes total replacement of plagioclase by sericite can be observed. Calcite also replaces plagioclase; however it is much less common than the others.

3.2.2. Olivine-phyric (High-Mg) Metabasalts

These metabasalts are mostly aphanitic and porphyritic, with large serpentinized phenocrysts sometimes exceeding 1 cm. More rarely, microphaneritic samples have also been found, and these coarse-grained basalts show equigranular texture. The Mg-rich nature of these basalts is evident from abundant pseudomorphs after olivine (Figure 3.6). They sometimes display elongated serpentinized olivine and sheared Ti-augite phenocrysts owing to intense strain rate.
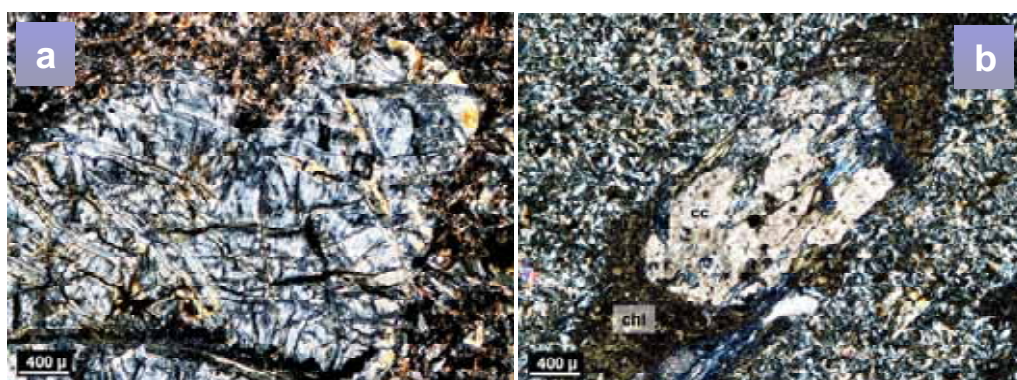
Figure 3.6. a) Serpentine pseudomorph after olivine showing mesh-texture, surrounded by numerous Ti-augite and opaque phases (Sample HS-62B, XPL); b) Large pseudomorph after olivine embedded in a fine-grained matrix. Note the euhedral shape of pseudomorph. Calcite is identified by its extremely high interference colors and it is associated with minor serpentine (1st order bluish grey). Chlorite displays its typical 1st order anomalous brown color (Sample OR-43, PPL) (chl: chlorite, cc: calcite).

The primary mineral phases recognized in these high magnesian metabasalts are Ti-augite and kaersutite. Ti-augite is found in brown, pinkish-brown generally subhedral crystals with fractured appearance and barely visible cleavage (Figure

55

3.7). It is present as both phenocryst and microcryst phases. Ti-augite has been totally destroyed by severe alteration in some cases. Sector zoning can occasionally be observed. Rarely, kaersutite is found replacing large Ti-augite phenocrysts (Fig. 3.7d).
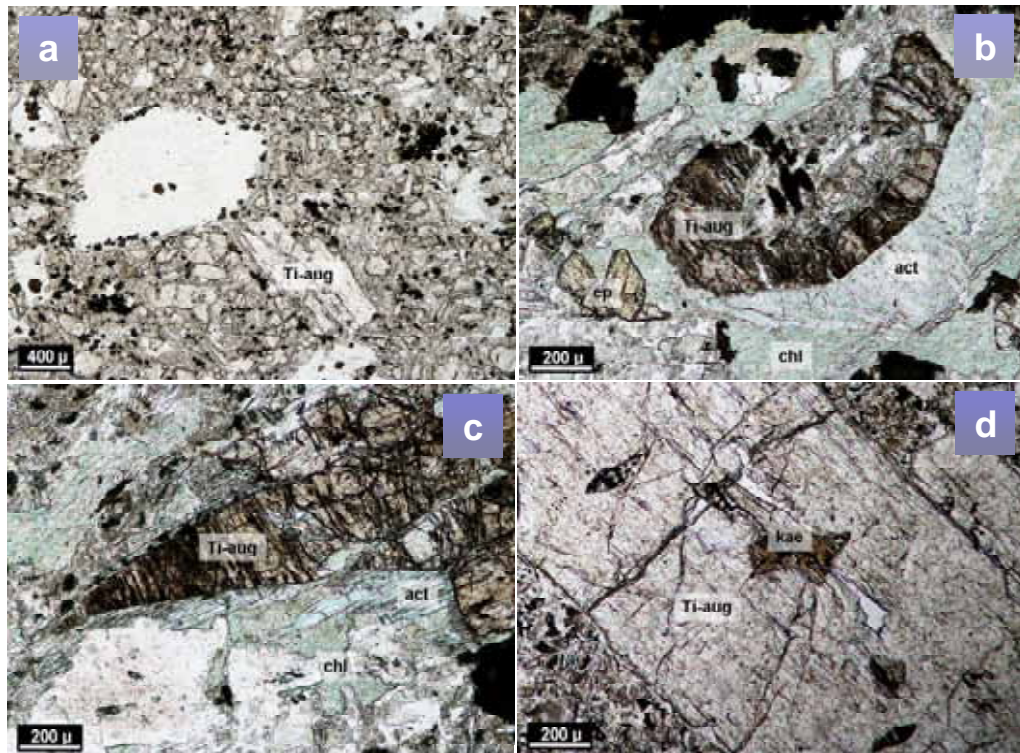
Figure 3.7. a) Olivine-phyric metabasalt with relatively large groundmass Ti-augite. Note that lots of Ti-augite grains dominate the sample both as phenocryst and microcryst (Sample OR-48, PPL); b) Subhedral Ti-augite grain which has been affected by alteration (Sample ZT-3, PPL); c) Another example depicting effects of low-grade metamorphism on the olivine-phyric metabasalts. Note needle-like actinolite crystals emerging from Ti-augite (Sample ZT-3, PPL); d) Kaersutite developing on a Ti-augite phenocryst (Sample HS-62A, PPL) (Ti-aug: Ti-augite, act: actinolite, chl: chlorite, kae: kaersutite).

No original plagioclase appears to have survived following low-grade metamorphism. Olivine appears to have been an important constituent of the oli-phyric metabasalts as indicated by numerous pseudomorphs some of which have

euhedral outlines (Figure 3.6). Some olivine crystals are completely serpentinized with well-developed mesh-texture; others appear to have been subsequently altered by chlorite and actinolite as well as calcite (Figure 3.6).

Some of the oli-phyric metabasalts seem to have experienced some degree of ductile deformation, as evidenced by a number of elongated pseudomorphs after olivine, which are aligned in a sub-parallel manner. It is also possible to observe microfaults transecting some of the Ti-augite phenocrysts.

3.3. Metagabbros

3.3.1. Augite-Phyric Metagabbros

The augite-phyric metagabbros are variably-sized, ranging from fine- to coarse-grained, and they are characterized by porphyritic texture, where Ti-augite crystals and pseudomorphs after olivine are set in a matrix mostly composed of Ti-augite and plagioclase. The finer-grained varieties have somewhat larger plagioclase crystals, but smaller Ti-augite. These metagabbros appear to have variably influenced by ductile deformation. Sometimes, relict igneous textures appear to be preserved and there is no signature of brittle or ductile deformation.

Primary mineral assemblage consists mainly of Ti-rich augite and to a lesser extent plagioclase and kaersutite. Ti-augite appears to be most abundant primary phase. In some of the samples, no relict plagioclase has survived. Ti-augite is seen as brown to pinkish-brown crystals with generally subhedral outlines. Poor- to well-developed cleavage is recognizable in some cases (Figures 3.8a). Both simple and multiple twinning can be seen (Figures 3.8a,b). In addition, sector- and concentric-type zoning are frequently observed on Ti-augite (Figure 3.8c). It is possible to see the effects of shearing on Ti-augite in some samples, where they display undulatory extinction, sub-grain development and boudin-like structures (Figures 3.9a,b). Sub-parallel fracture development related to ductile deformation is also recognized (Figure 3.9a). Furthermore, small-scale faulting appears to

have affected some of Ti-augite crystals, as indicated by the displacement of their twin-lamellae (Figures 3.8a,b). Ti-augite is sometimes associated with plagioclase in a sub-ophitic manner (Figure 3.10a).
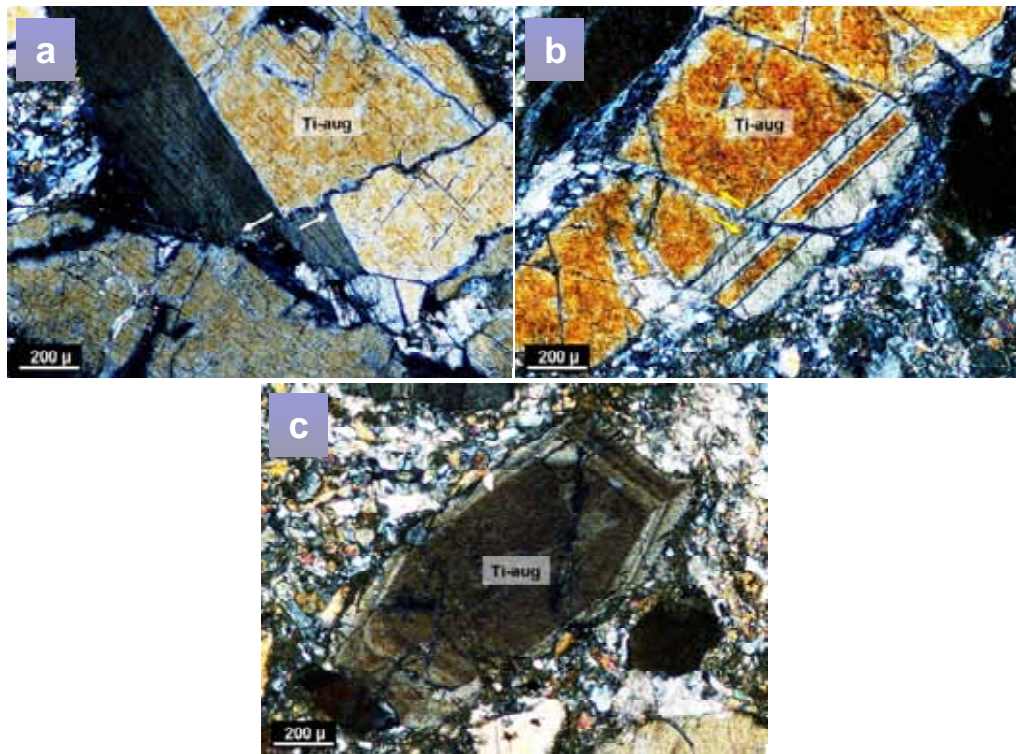
Figure 3.8. a) Ti-augite crystal displaced by a small-scale fault. The grain is characterized by moderately-developed cleavages and simple twinning. Note also that the fault does not affect the other Ti-augite grain (Sample HS-90, XPL); b) Another example depicting the affect of shearing on the augite-phyric metagabbros. Note also multiple twinning on the Ti-augite crystal (Sample HS-90, XPL); c) Concentric zoning displayed by a euhedral Ti-augite. Note the anomalous interference colors of the crystal (Sample HS-90, XPL) (Ti-aug: Ti-augite).

Plagioclase is rarely identified as a primary phase in these metagabbros. Unlike Ti-augite, it appears to have suffered pervasive alteration. Thus, it is not unusual to see albitic plagioclase in these metagabbros. They generally appear to have undergone dynamic recrystallization due to deformation, becoming recrystallized

albite. Simple and multiple twinning are sometimes observable. Although vary rare, pericline twinning is also recognized. However, in the samples that have experienced relatively less deformation, plagioclase seems rather preserved. In some cases, plagioclase is replaced by prehnite and sericite.
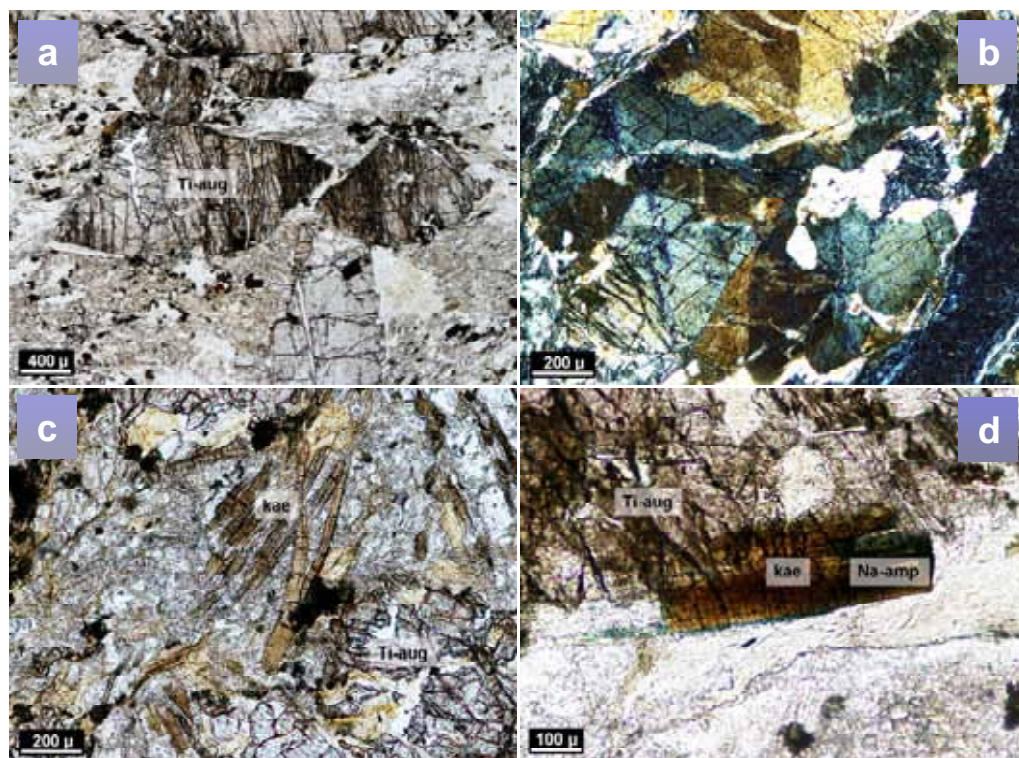
Figure 3.9. a) Augite-phyric metagabbro including abundant Ti-augite crystals as a primary phase. Note the effect of shearing and sub-parallel fractures developed on Ti-augite at the center. No plagioclase has survived in this sample (Sample OR-98, PPL); b) Ti-augite crystal which has experienced some degree of strain, which leads to undolatory extinction and sub-grain development. Note also the presence of moderately developed cleavages (Sample OR-98, XPL); c) Acicular kaersutite crystals growing after Ti-augite (Sample IM-23, PPL); d) Development of late-stage primary kaersutite after Ti-augite, which is in turn replaced by metamorphic Na-amphibole in response to elevated pressures (Sample IM-24, PPL) (Ti-aug: Ti-augite, kae: kaersutite; Na-amp: Na-amphibole).

Kaersutite is the other primary mineral characterizing these metagabbros, though it is absent in some of them. They are largely observed replacing Ti-augite and

rarely as individual crystals (Figure 3.9d). Development of kaersutite is mostly identified at the rims of Ti-augite.

3.3.2. Oli-phyric (High-Mg) Metagabbros

These coarse-grained metagabbros are characterized by porphyritic texture; large Ti-rich augite crystals are observed to be embedded in intensely metamorphosed matrix. Ductile deformation appears to have been predominant on these metagabbros leading to schistosity on groundmass. All olivine have been totally replaced by serpentine minerals, thus represented by pseudomorphs.

Primary mineral assemblage characterizing these metagabbros, very similar to the previous types, mainly consists of Ti-rich augite and kaersutitic amphibole. Plagioclase appears to have lost its original identity and now it is present as of albitic composition. Ti-rich augite is found in brown crystals with mostly subhedral appearance. Poor- to well-developed cleavage can generally be observed (Figure 3.11a,b). Owing to deformation, Ti-augite grains are observed to have been re-aligned and become sub-parallel relative to foliation. Microfaults can also be recognizable as reflected by the displaced clinopyroxene phenocrysts (Figure 3.11a).

Kaersutite is the other primary mineral characterizing these metagabbros. It is largely observed as individual crystals in the matrix, otherwise seen replacing Ti-augite (Figures 3.11b-c). Some of kaersutite grains display nearly euhedral crystal faces with two-directional basal cleavages intersecting at an angle of 124°-56° (Figure 3.12d).

3.3.3. Eymir Metadiabases

The Eymir metadiabases are considerably different relative to the rest, since they do not include a Ti-rich clinopyroxene phase as well as having a more evolved composition with the occurrence of hornblende. These metagabbros can generally

be regarded as fine-grained gabbros with a few medium-grained members. They display equigranular texture.
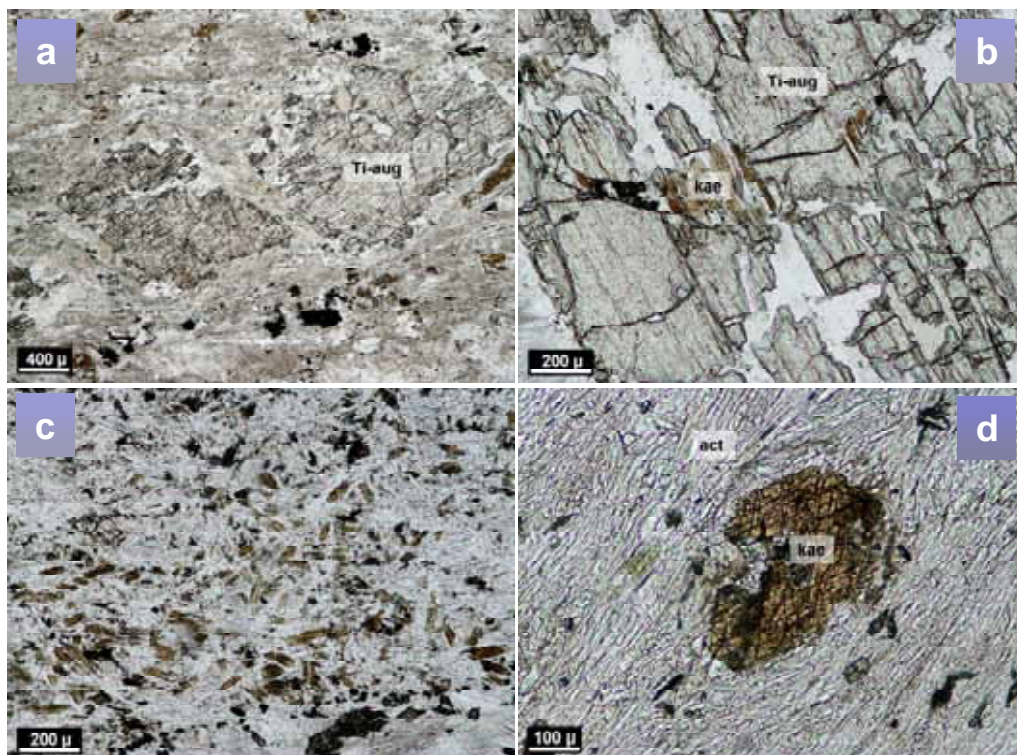
Figure 3.11. a) Large Ti-rich clinopyroxene displaced by a microfault. Note the alignment of the clinopyroxene grain compared to foliated groundmass (Sample HS-89, PPL); b) Kaersutite development on a fractured Ti-augite phenocryst (Sample HS-87, PPL); c) Numerous prismatic kaersutite grains developed on the groundmass of a olivine-phyric metagabbro (Sample HS-87, PPL); d) Kaersutite crystal with well-developed basal cleavages. The grain is partly corroded by groundmass which have replaced by actinolite (Sample HS-89, PPL) (Ti-aug: Ti-augite, kae: kaersutite, act: actinolite).

Hornblende and plagioclase together with/without a Ti-poor clinopyroxene phase make up the major primary assemblage of the SSZ-type metagabbros. Interestingly, these microgabbros sometimes consist of minor amount of quartz, which has probably crystallized at the last stages of their magmatic evolution. As mentioned above, these metagabbros do not comprise any Ti-rich augite as

clinopyroxene phase, instead they include diopsidic augite. It must be noted, however, that some samples do not include any clinopyroxene at all. Thus, the presence of clinopyroxene is not so common in the SSZ-type gabbros, being restricted to more primitive samples. Where it is present, diopsidic augite is represented by rather colorless to pale brown crystals. Since they have been replaced by primary hornblende, no crystal face appears to have survived against this magmatic replacement (Figures 3.12a,b), thus clinopyroxene is characterized by anhedral crystals. Cleavage traces are hardly recognizable; only a poorly-developed cleavage can be identified if present.

Hornblende, together with plagioclase, is the most common primary phase observed in these microgabbros. Hornblende is found as greenish to more rarely brownish crystals with generally subhedral outlines. It is also not unusual to see euhedral crystals of hornblende. Two-directional cleavages are often recognizable (Figure 3.12a). They are mostly found as individual crystals, otherwise associated with diopsidic augite. It is sometimes the case that their strong body colors mask the interference colors so that they somewhat look like chlorite.

Plagioclase constitutes the other important primary phase of the SSZ-type metagabbros. It is generally unaltered when compared with those found in the other types. Thus, it is generally possible to recognize multiple-twinned crystals, though simple- and combined-twinned crystals are also found. They rarely display a symplectic relationship with quartz, producing graphic-like structures.

3.4. Secondary Mineral Assemblages of the Metabasalts and Metagabbros

Based on secondary mineral assemblage, it can be inferred that the metabasalts and metagabbros have been largely metamorphosed under greenschist facies conditions, comprising typical greenschist paragenesis with actinolite+chlorite+epidote+albite. Few of them, though, reflect sub-greenschist conditions.
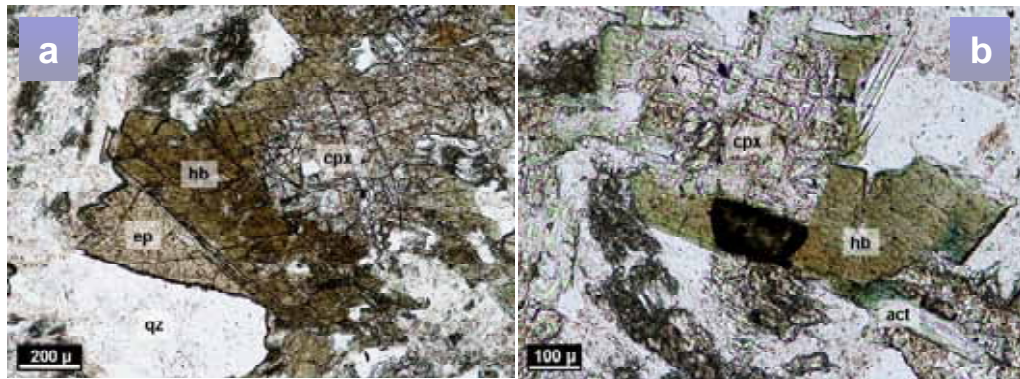
Figure 3.12. a) Replacement of diopsidic augite by hornblende. Note two-directional cleavage displayed by hornblende. Quartz seems very fresh compared to part just above it, where the cloudy appearance is due to alteration of plagioclase (Sample BO-2, PPL); b) Another example illustrating the replacement of diopsidic augite by hornblende. In this case, however, metamorphic amphibole (actinolite) overgrows hornblende. The mineral characterized by high relief just below the center is sphene (Sample DO-13, PPL) (cpx: diopsidic augite, hb: hornblende, ep: epidote, qz: quartz, act: actinolite).

Actinolite is seen variably replacing Ti-augite grains; overgrowing as needle-like crystals (Figures 3.7b,c, 3.12b, 3.13a). In some cases, actinolite is observed to have developed in the matrix probably after plagioclase together with Ti-augite Actinolite is sometimes associated with chlorite and these two secondary minerals together form pseudomorphs after large olivine crystals (Figure 3.13b). Actinolite also variably replaces hornblende. There are also some phenocrysts that have been entirely replaced by actinolitic amphibole, which may have been originally Ti-augite crystals.

Chlorite is generally seen next to serpentine and/or actinolite, and can be observed, replacing Ti-augite to varying degrees. It is possible to observe chlorite pseudomorphs after entire replacement of Ti-augite grains. Chlorite is also seen as a secondary mineral replacing hornblende. Epidote generally contributes to alteration of plagioclase grains, benefiting from their Ca content. It is largely found as yellowish anhedral, and more rarely brownish crystals. In some cases, it is observed as fan-shaped crystals, displaying radial extinction. It is quite

common to see epidote together with abundant sericite when replacing plagioclase.
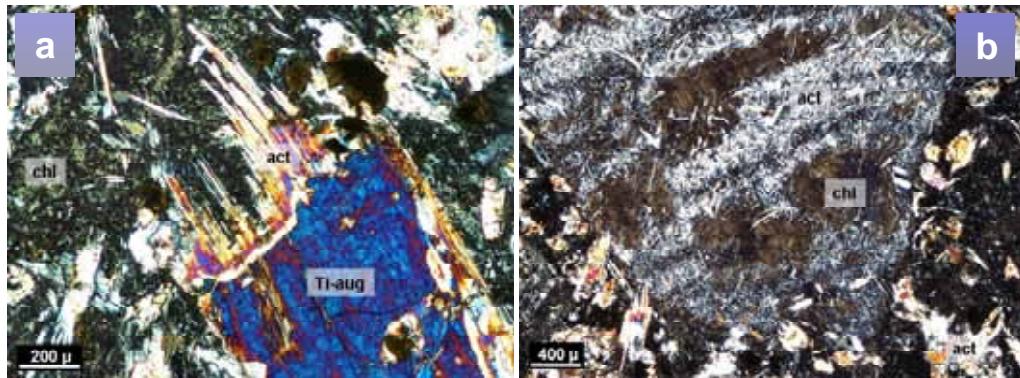
Figure 3.13. a) Replacement of Ti-augite by needle-like actinolite crystals in response to low-grade metamorphism; b) Large olivine phenocryst totally replaced by actinolite and chlorite. Note the lower interference colors of actinolite needles replacing the olivine compared to those in the groundmass; c) A thick vein filled by epidote. Note undolatory extinction on epidote grains indicating influence of deformation (OR-51, XPL). (Ti-aug: Ti-augite, act: actinolite, chl: chlorite).

Green biotite, though very rare, can also be observed. This green mica is strongly pleochroic, ranging in tones of brownish green. It appears to have grown locally rather than pervasively. Some of these metabasalts appear to have been severely altered as indicated by abundant veins of varying thicknesses and vesicles filled by several minerals. Calcite is the most abundant vein/vesicle-filling mineral in these basalts, however, quartz veins are also observed in association with calcite, pumpellyite and epidote. Pumpellyite is also of considerable importance in terms of vesicle-filling minerals in some of the samples (Figures 3.4a,b). It can also be noticed in some parts associated with minor prehnite, probably using Ca that left the structure of calcic plagioclase during albitization. In some places, pumpellyite can be seen as green, fibrous, radiating crystals. Prehnite is sometimes present as fibrous crystals like the former; otherwise it shows leaf-shaped appearance. Calcite is not as common as in the previous type, and largely observed as vein-

filling mineral. This mineral together with epidote constitutes additional secondary minerals found in the amygdules. Calcite is also seen to have replaced olivine.

Na-amphibole is rarely found, indicating elevated pressure conditions. Therefore some samples appear to be relatively transitional to HP-greenschist facies field. It is seen that Na-amphibole development usually takes place as result of replacement of kaersutite (Figure 3.9d). It is mostly the case that the three minerals, namely Ti-augite, kaersutite and Na-amphibole display a close relationship with each other.

3.5. Mafic Schists

3.5.1. Type-1 Mafic Schists

This type of metamorphics represents mafic schists, which have been probably derived from a basaltic protolith as indicated by substantial content of kaersutite relicts. In some samples, however, no relict kaersutite is observed; they appear to have been entirely replaced by secondary sphene and Fe-Ti oxides. The schistosity is defined by lepidoblastic white mica in addition to relatively elongated recrystallized albite and chlorite.

Kaersutite is observed as brown prismatic and/or tabular crystals which have most likely developed after Ti-augite (Figures 3.14a,b). Poor- to moderately-developed cleavage can be observed. Actinolitic amphibole together with chlorite appears to have developed on kaersutite. Apart from kaersutite and actinolite, there is also a third type of amphibole present in the sample, namely Na-amphibole. This bluish metamorphic mineral seems to replace kaersutite (Figure 3.14b). Therefore, the Type-1 mafic schists bear the evidence of elevated pressure during its metamorphic evolution.

White mica occurs next to recrystallized albite. In some parts, the replacement relationship can be observed such that white mica is present as patches inside
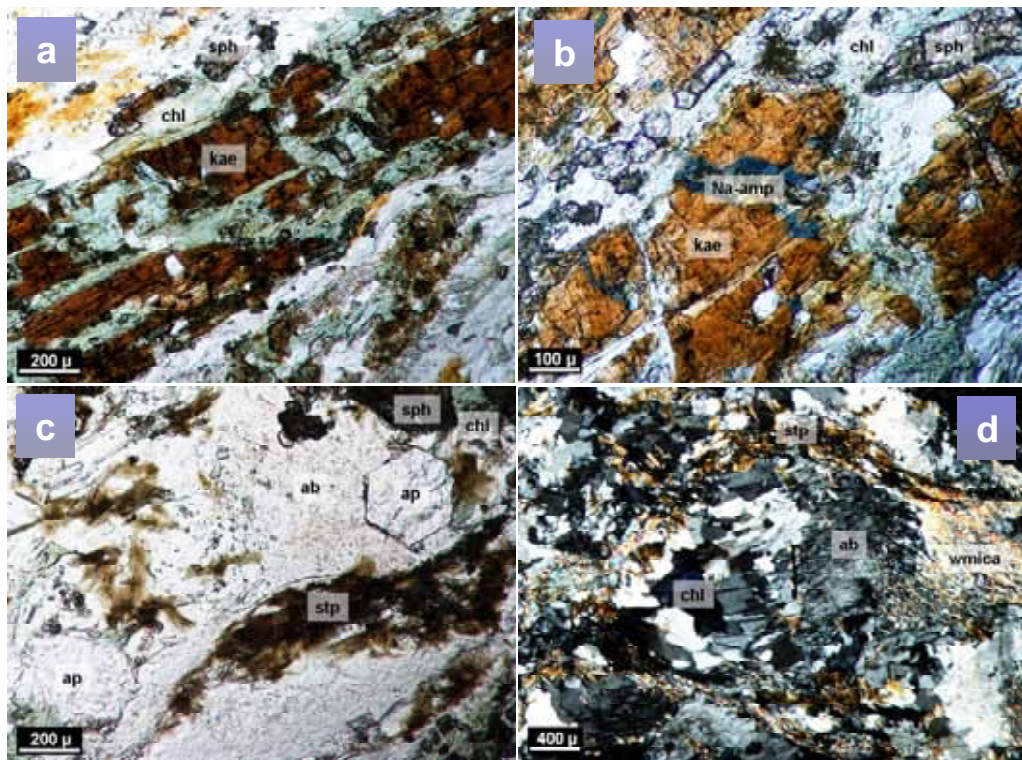
Figure 3.14. a) Relict kaersutite crystal replaced by secondary mineral phases. Note that actinolite also exists in this view, however, not labeled due to its similar body color with chlorite (Sample NIL-1, PPL); b) Development of sodic amphibole after kaersutite (Sample NIL-1, PPL); c) Development of stilpnomelane in the Type-1 mafic schists. Note euhedral apatite crystal to the upper right of view (Sample NIL-2, PPL); d) Albite porphyroblast undergone dynamic recrystallization, giving way to numerous smaller albite crystals. Note also the development of stilpnomelane (Sample NIL-2, XPL) (Na-amp: sodic amphibole, kae: kaersutite, chl: chlorite, sph; sphene ab: albite, stp: stilpnomelane, ap: apatite, wmica: white mica).

albite. Otherwise, they occur in distinct clusters representing pressure shadows in association with albite. The pale yellowish color can be noticed, suggesting its phengitic composition. Albite is an important constituent of this rock, occurring as recrystallized crystals probably after porphyroblastic albite. Multiple (polysynthetic) twinning is remarkable in some of the crystals. The effect of dynamic recrystallization is evidenced by sub-grain development, undolatory extinction, and sutured boundaries between recrystallized crystals. Albite porphyroblasts are frequently observed in association with smaller recrystallized

counterparts (Figure 3.14d). Sometimes relatively large apatite crystals can be observed in these schists, some of which display basal sections with typical hexagonal outlines (Figure 3.14c). In some samples, stilpnomelane is also present (Figure 3.14c,d).

3.5.2. Type-2 Mafic Schists

Compared to the Type-1, schistosity is more remarkable in Type-2 mafic schists. Some parts of these metamorphics are characterized by continuous cleavage (schistosity). The other portions, however, display disjunctive cleavage, where cleavage domains are composed of nematoblastic actinolite together with porphyroblastic albite, while the microlithons consist largely of zoisite/clinozoisite crystals with lesser actinolite. No relict mineral is found in these mafic schists.

These metamorphics are characterized by a mineral assemblage of actinolite, zoisite/clinozosite, albite, chlorite, white mica and calcite. It appears that the dominant mineral is actinolitic amphibole. They are observed as light green acicular minerals, and form sub-horizontal arrangements defining the schistosity (Figure 3.15a-c). In some cases, bluish-green actinolite crystals also occur (Figure 3.15a). The epidote group minerals are frequently observed, following actinolite. They are differentiated by their higher relief and brownish appearances. Epidote is recognized anhedral most of the time, though subhedral crystals also occur. Anamolous blue (berlin-blue) colors suggest that it is represented by zoisite/clinozoisite rather than pistacite (Figure 3.15c).

Albite is generally observed as porphyroblasts in close relationship with epidote and actinolite (Figure 3.15b-c). Twinning planes of albite are observable in some of the porphyroblasts and they sometimes display undolatory extinction and distinct crystal domains, probably in response to deformation which gives way to dislocations through the crystal and/or recrystallization. The albite porphyroblasts

67

seems synkinematic due to deformation of internal foliation (D_i) and external foliation (D_e) at the same time (Figure 3.15b).

White mica is observed as colorless, flaky minerals with high interference colors (Figure 3.15d). Their cleavage planes are visible and they are generally aligned parallel, sub-parallel to each other forming lepidoblastic texture. Calcite is observed in some portions of the samples. Sphene is also recognized frequently in these mafic schists.
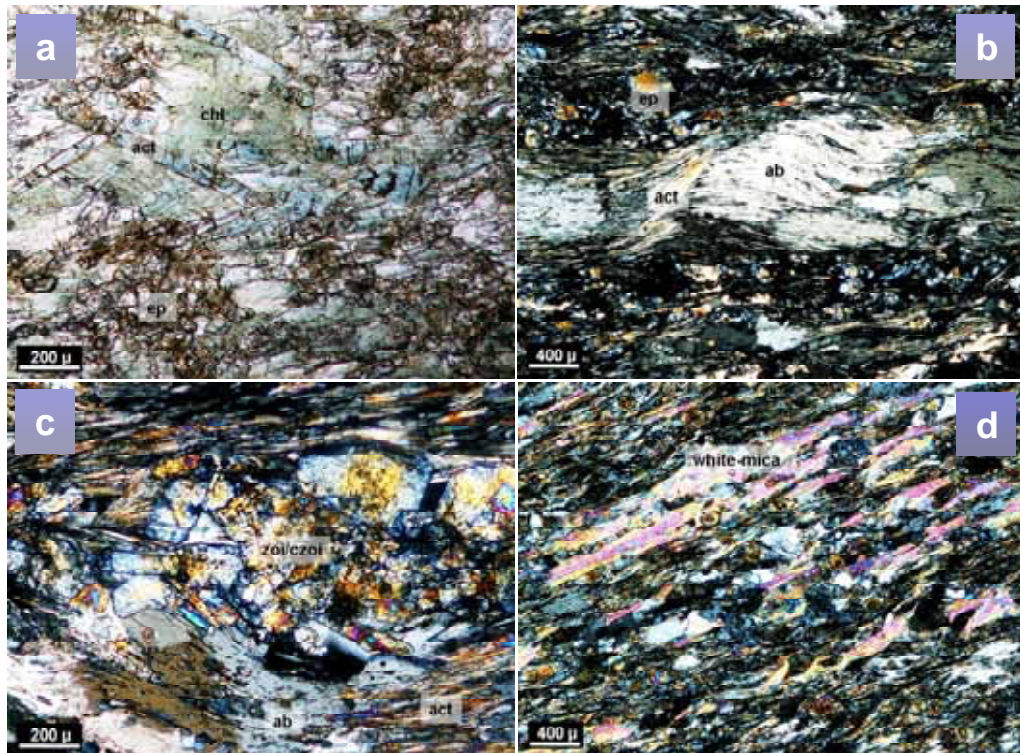
Figure 3.15. a) Development of bluish acicular actinolitic amphibole (Sample BU-7, PPL); b) Synkinematic albite porphyroblast as suggested by the simultaneous deformation of both S_i and S_e (Sample BU-8, XPL); c) Zoisite/Clinozoisite group epidote in association with actinolite and porphyroblastic albite. Note that albite displays imprints of recrystallization as indicated by distinct domains (Sample BU-8, XPL); d) Lepidoblastic white mica displaying high order interference colors (Sample BU-8, XPL) (act: actinolite, chl: chlorite, ep: epidote group, zoi/clizoi: zoisite/clinozoisite, ab: albite).

3.5.3. Type-3 Mafic Schists

In these metamorphics, foliation planes are well-developed, which are mainly characterized by nematoblastic actinolite crystals. It must be noted that these schists are variably deformed and crenulation cleavage is a typical feature for these metamorphics.

Some of these schists contain relict Ti-augite with kaersutite. Ti-augite is characterized by light brown crystals with poor- to well-developed cleavages. However, fracture planes are also observed. Sometimes, bluish green actinolite appears to develop fractures of Ti-augite (Figure 3.16a). It is also seen that Ti-augite is rimmed by actinolite in some parts (Figure 3.16b). Kaersutite, the other relict mineral in these metamorphics, is observed only where Ti-augite is present. This Ti-rich amphibole appears to have overgrown after Ti-augite. Actinolite is also seen to replace kaersutite.
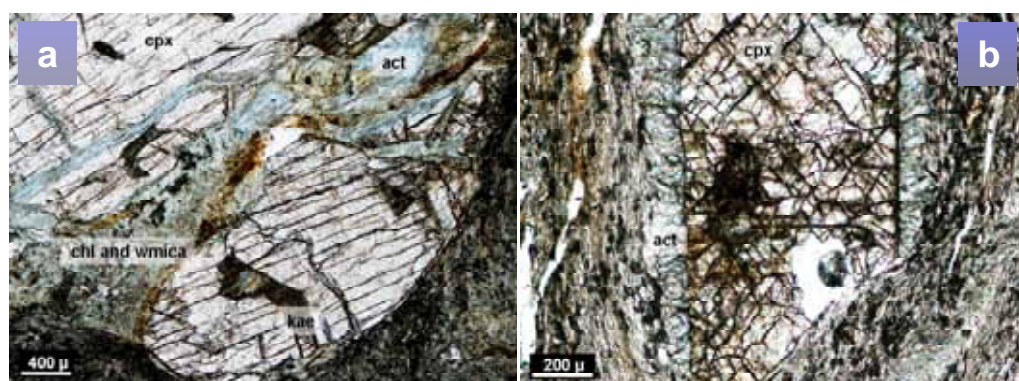
Figure 3.16. a) Large relict Ti-augite grain in the Type-3 mafic schists. Note that two fragments of Ti-augite were originally representing the same, single grain. Actinolitic amphibole develops on fractures and/or fragmented parts. (Sample HS-43A, PPL); b) Actinolitic rim overgrowing Ti-augite. Note the grain-size difference between rimming actinolite and those defining foliation (Sample HS-43A, PPL) (Ti-aug: Ti-augite, act: actinolite, kae: kaersutite, chl: chlorite, wmica: white mica).

Actinolite is the most abundant metamorphic mineral characterizing these mafic schists. They sometimes appear bluish green (Figure 3.16), otherwise typical pale green color is observed. Although it occurs mostly as tiny, needle like crystals, relatively larger acicular and prismatic crystals also recognized. This metamorphic amphibole reflects a close relationship with white mica; together they define foliation planes. White mica seems to be rather phengitic owing to their pale green colors.

3.5.4. Type-4 Mafic Schist

This type of mafic schists are distinct in terms of the development of lots of Na-amphibole needles (Figure 3.17). The sub-parallel arrangement of the metamorphic amphibole also defines schistosity. The protolith of these mafic schists was probably basalt and they most likely represent basalt clasts within metahyaloclastic breccias or the breccia itself.
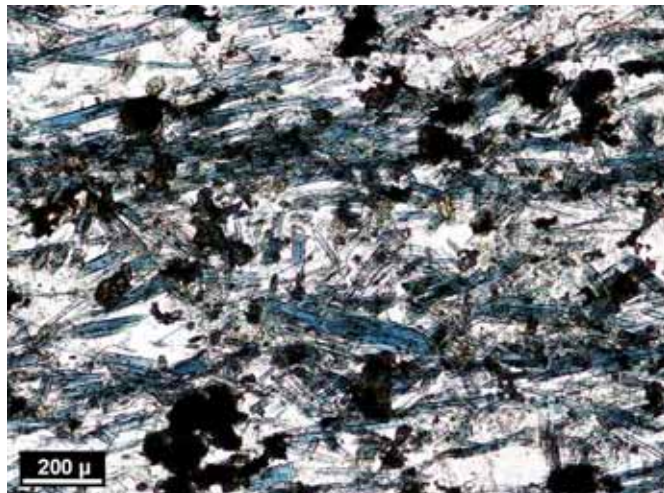
Figure 3.17. Nematoblastic Na-amphibole (blue minerals) characterizing the Type-4 mafic schists. Minerals with very high relief are sphene (Sample IM-9B, PPL).

Type-4 mafic schists comprise no relict minerals. As mentioned above, these metamorphics contain lots of tiny Na-amphibole needles which are arranged mostly in a sub-parallel manner (Figure 3.17). They are strongly pleochroic in tones of deep blue and purple (lavender blue). Another abundant mineral is albite which is observed as small recrystallized minerals. Calcite is found in substantial amounts; it has probably replaced former relicts and/or filled gas vesicles in the original rock owing to severe carbonatization.

3.6. Metavolcaniclastics

The clastic nature of these samples is apparent as evidenced by many crystal and rock fragments. However, they are also metamorphic like the others. It must be noted that metamorphism seems to have no effect on the texture of these rocks, while the mineralogy has been affected.

The mineral fragments are represented by brownish Ti-augite, which can be seen as well-preserved fresh crystals. The rock fragments, on the other hand, comprise various basalt fragments most of which are intensely oxidized. The clasts are binded by a carbonate-dominated matrix. Relatively less oxidized fragments reveals the presence of several metabasalts with different relict igneous textures. Development of sodic amphibole on Ti-augite can be observed (Figure 3.18), suggesting elevated pressure conditions.

3.7. Metamorphism of the Mafic Schists and Volcaniclastics

Metamorphic mineral assemblages observed in mafic schists and volcaniclastics indicate that these rocks have experienced HP-greenschist facies conditions as indicated by the occurrence of Na-amphibole, actinolite, albite, chlorite and epidote.
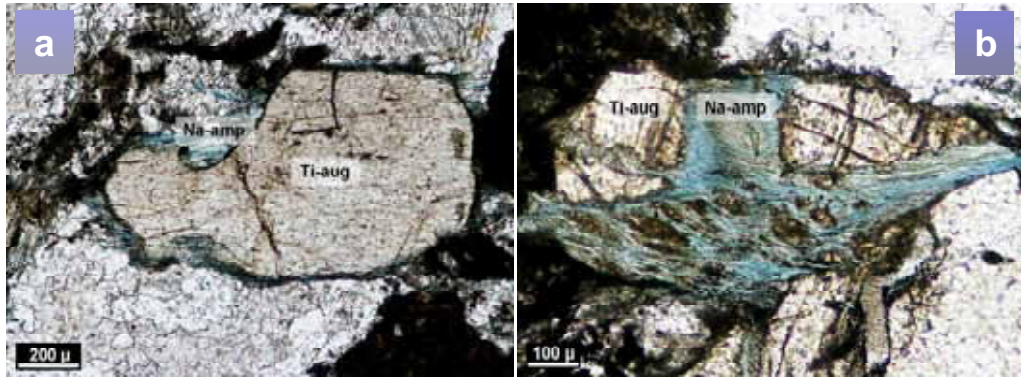
Figure 3.18. a) Development of needle-like Na-amphibole crystals on Ti-augite. The fragment on the lower left is oxidized basalt clast (Sample KD-16, PPL, 20X; Na-amp, Ti-aug: Ti-augite); b) Another picture depicting the replacement of Ti-augite by Na-amphibole (Sample GK-6, PPL, 20X; Na-amp, Ti-aug: Ti-augite).

CHAPTER 4

GEOCHEMISTRY

4.1. Major and Trace Element Geochemistry

In order to examine major and trace element characteristics of the newly defined Nilüfer Unit and the Eymir metadiabases, 89 representative samples were selected for analysis after detailed petrographic examination (see Appendix C). The samples represent metabasalts (including metapicrites), metagabbros (including metadiabases), mafic schists and metavolcaniclastics. All major oxide values measured in the ACME labs were recalculated on a volatile-free basis for the graphical purposes and elemental comparisons.

4.1.1. Method

The studied rock samples were initially cut into slabs, removing altered parts and veins. Slabs were reduced to chips by a jaw crusher, and selected fresh chips were powdered using a tungsten carbide disc mill.

Of the 89 analyses, 35 analyses were performed at Duke University (North Carolina, USA), while the remaining 54 analyses were carried out at ACME Analytical Labs. (Vancouver, Canada). In the Duke labs, major element and high abundance trace element concentrations were determined by direct current plasma spectroscopy (DCP) based on techniques modified after Klein et al. (1991). The analyses of solutions were performed using a Fisons SpecterSpan 7 DCP equipped with a multi-element cassette. Si, Al, Ca, Fe, Mg, Na and Ti were analyzed in a 1:4750 dilution, whereas 1:250 dilution were applied for Zn, Co,

Cu, Ni, V, Sc, Cr, Zr, Y and P. Abundances of Ba, Sr, Mn and K were analyzed in both solutions. The standards used in the procedure were NBS-688, AII92-29-1 and K1919. Analysis for each sample was run twice. Low-abundance trace element concentrations were determined by inductively-coupled plasma mass spectroscopy (ICP-MS) using a VG-Elemental PlasmaQuad3 applying modified techniques of Cheatham et al. (1993). The standards used were BHVO-1, BIR-1, DNC, and W2-1. Each sample was analyzed twice within a run.

In the ACME labs, the major elements as well as Ba and Sc were determined by inductively coupled plasma atomic-emission spectrometry (ICP-AES) with $LiBO_2$ fusion. Trace elements (including REE) were determined by ICP-MS after acid decomposition with 5% HNO_3.

4.1.2. Effect of Post-Magmatic Processes

The studied samples bear imprints of low-grade alteration/metamorphism as indicated by loss on ignition (LOI) values between 1.3 and 13.7 weight (wt.) %. The metadiabase dikes from the Eymir Unit display somewhat lower LOI values (1.3-3.4 wt %). The negative correlation observed between SiO_2 and LOI suggests that some SiO_2 has been mobilized during post-magmatic processes (Figure 4.1). Large-ion lithophile elements (LILE) are assumed to be mobile during post-magmatic alteration processes (e.g. Wood et al., 1976; Pearce, 1975), whereas rare earth elements (REE) and high-field strength elements (HFSE) are relatively immobile during such secondary events (e.g. Pearce and Cann, 1973; Pearce and Norry, 1979). The plots of mobile incompatible elements (e.g. Rb, Ba and Sr) against an immobile incompatible element (like Zr) yield scattered results (not shown), reflecting mobilization of these elements, whereas HFSE and REE reflect well-defined trends against Zr, indicating they have remained relatively immobile. Parallel/sub-parallel patterns observed in REE and HFSE indicate that the original immobile trace element systematics have not been significantly modified. Therefore, petrogenetic interpretation will be mainly based on

immobile elements which are not significantly modified by secondary processes (e.g. Floyd and Winchester, 1978).

4.1.3. Major and Compatible Element Variations

Some samples have compositions characterized by Mg numbers (Mg#) between 65-84 (Mg# calculated as 100 x atomic $Mg^{2+}/(Mg^{2+} + Fe^{2+})$; assuming that $Fe^{3+}/Fe^{2+} = 0.15$), suggesting primitive and/or primary compositions (e.g. Frey et al., 1978; Hart and Davis, 1978), whereas the others are of lower Mg# (30-65), characterizing more evolved magmas.
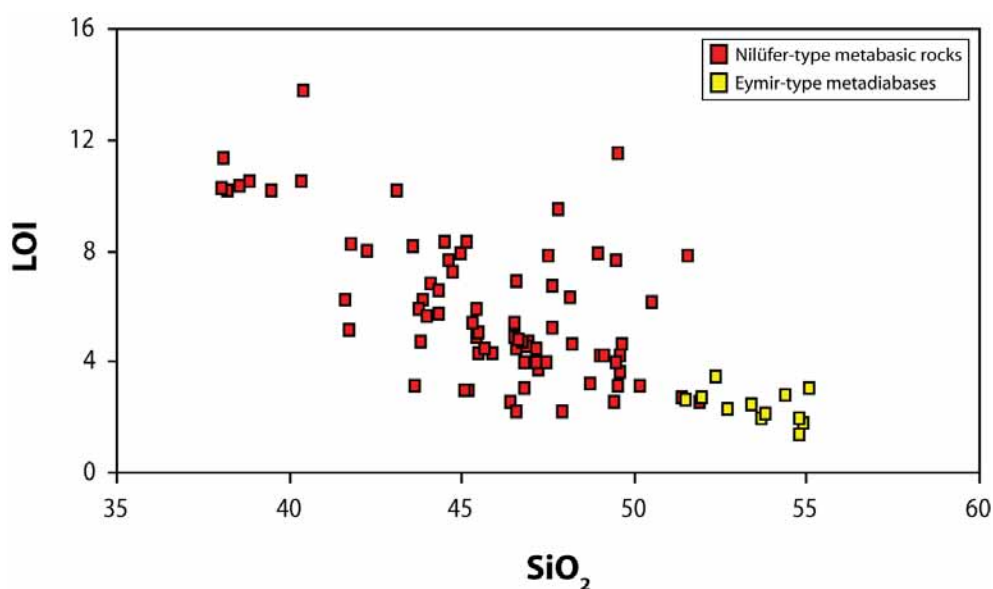
Figure 4.1. Variation of SiO_2 against LOI, displaying loss of SiO_2 in the studied samples

Samples with high Mg# are also coupled with high Ni (avg = 642 ppm) and Cr (avg = 1266 ppm) concentrations. In contrast, more evolved compositions represented by lower Mg# have lower Ni (avg = 96 ppm) and Cr (avg = 238 ppm) values. MgO (wt %) contents of the studied samples range in a significantly wide interval between 3.9 and 32.1, spanning both evolved and primitive compositions.

75

This is also indicated by extensively varying Mg numbers. Similarly, SiO_2 also appear to change in a highly varying interval (42.8-56.0 wt %). Fe_2O_3 contents are observed to vary between 8.4 and 18.3 wt. %. CaO compositions of the samples are highly variable, changing between 2.0 and 19.7 wt %. This remarkable range in CaO can be attributed to the post-magmatic processes to some extent, which result in mobilization of this element. Na_2O contents, like the other ones, show a substantial variability between 0.02 and 6.47 wt %. Although this may have partially resulted from mobilization of Na_2O, this element is known to be more stable than CaO during post-magmatic events (e.g. Pearce, 1975), thus the effect of some magmatic processes (e.g. fractional crystallization) cannot be excluded (see the discussion part). TiO_2 contents also display a large range between 0.6 and 4.6 wt %. The stable behavior of this element as also reflected by Figure 4.2, however, reflects the work of magmatic processes rather than post-magmatic events. Another immobile element, P_2O_5, spans a compositional spectrum between 0.06-0.64 wt %.

4.1.4. Incompatible Trace Element Variations

When the samples are plotted on the multi-element variation diagrams, it appears that they can be divided mainly into three distinct groups. The first of these (Group 1) shows variable enrichment in most incompatible elements relative to normal MORB (N-MORB), resulting in "humped" patterns (Fig 4.2) characteristic of OIB-type magmas from intra-plate settings (e.g. Weaver, 1987; Sun and McDonough, 1989; Furman et al., 2004). The second type of samples (Group 2) is relatively depleted compared to Group 1, but still enriched relative to N-MORB, thus they are more comparable to E-MORB rather than typical OIB (e.g. Sun and McDonough, 1989) (Fig. 4.2).
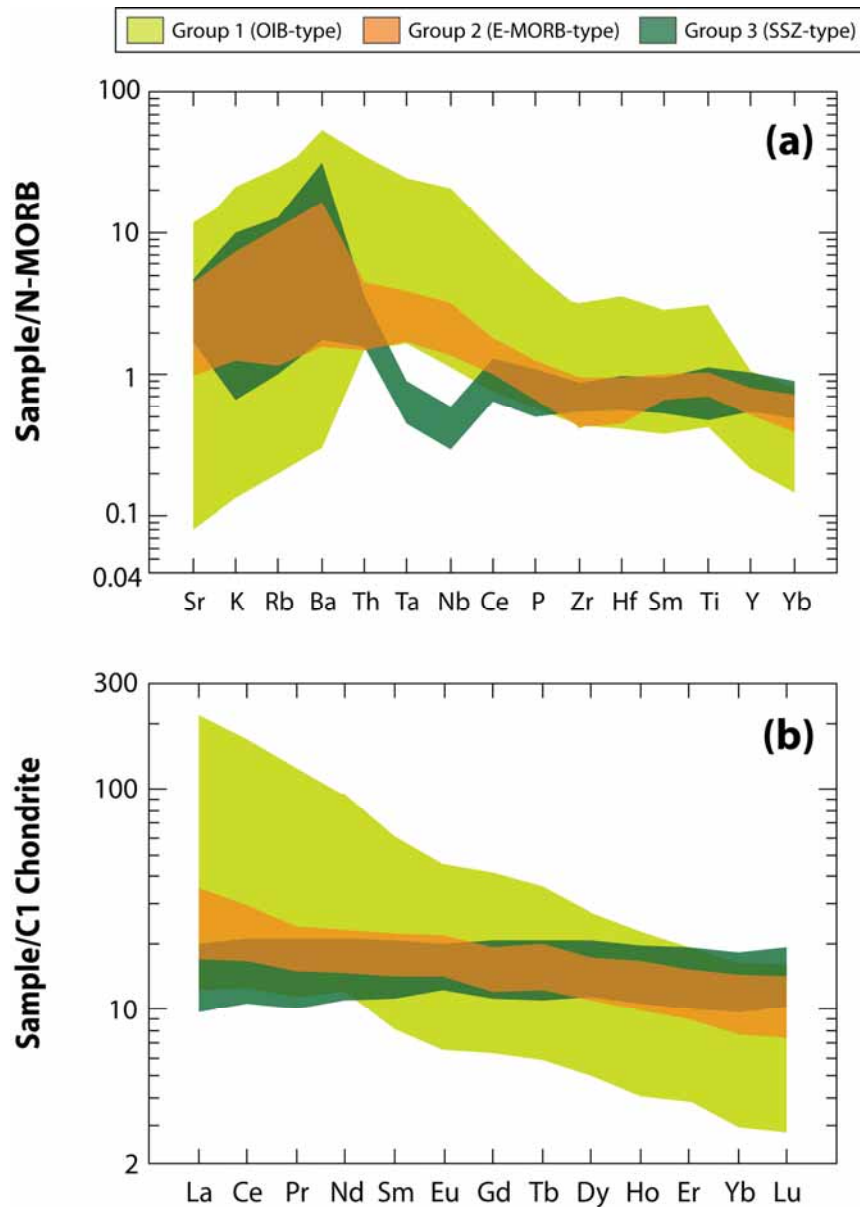
Figure 4.2. Multi-element and REE variation patterns of the studied samples. Normalization values for N-MORB and C1-Chondrite from Pearce et al. (1983) and Sun and McDonough (1989), respectively.

The last group (Group 3) is characterized by variable enrichment in Th associated with negative Ta-Nb anomalies, followed by slightly depleted HFSE patterns relative to N-MORB (Figure 4.2). Among these groups, Group 1 and Group 2 suites characterize the Nilüfer Unit, whereas Group 3 samples are representative

of the Eymir Unit. OIB-like Group 1 samples are quite enriched in LREE ($[Ce/Sm]_N$ = 1.06-3.34) and display fractionated HREE patterns ($[Ce/Yb]_N$ = 3.4-19.4), while E-MORB-like Group 2 samples show moderate enrichment in LREE ($[Ce/Sm]_N$ = 1.06-2.11) together with a slight depletion in HREE ($[Ce/Yb]_N$ = 1.6-3.3) (Figure 4.2). The SSZ-like Group 3 samples show relatively unfractionated REE patterns ($[Ce/Yb]_N$ = 0.96-1.33) which contrast with variably fractionated nature of Groups 1 and 2.

A detailed examination reveals that the Group 1 suite can be further subdivided into two subgroups on the basis of Zr-Nb systematics; one subgroup having noticeably higher Nb at a given Zr. Thus, this relationship reveals two different subgroups with different Zr/Nb ratios, probably reflecting some processes inherited from source region and/or during partial melting events (Figure 4.4). In the remainder of this work, I refer to the one with lower Zr/Nb as "subgroup-1", and the other as "subgroup-2" (see the discussion section and Figure 4.12 for the details).

When plotted on a classification diagram based on immobile elements (Winchester and Floyd, 1977), the studied samples range from variably tholeiitic to alkaline (Figure 4.3); the latter being dominant over the former compositional series. Group 2 and Group 3 samples are mainly characterized by sub-alkaline (tholeiitic) composition, whereas Group 1 appears to have dominantly alkaline signatures. It must be noted that although both Group 2 and 3 are of tholeiitic composition, the latter have distinctly lower Nb/Y values relative to the former. In addition, some Group 3 samples reflect more evolved compositions, plotting on the andesitic-basalt field.

Group 1 suite shows the highest Nb concentrations (avg = 35.0) between the studied groups, together with largely varying Zr abundances (37.4-287.7) (Figure 4.4), while Group 2 samples are observed to have lower Nb concentrations (avg = 7.2). Group 3 samples show the lowest Nb concentrations (avg = 1.7). However, both Group 2 and Group 3 suites show somewhat similar and limited variation in

Zr (Zr_{SSZ} = 49.7-78.3; Zr_{E-MORB} = 38.0-85.3). Group 1 samples are characterized by high TiO_2 values (wt.%) varying in a large interval (0.63-4.59) (Fig. 4.4). Group 2 and Group 3 suites display much lower and overlapping TiO_2 contents (Group 2 TiO_2 = 1.05-1.56; Group 3 TiO_2 = 0.68-1.67).
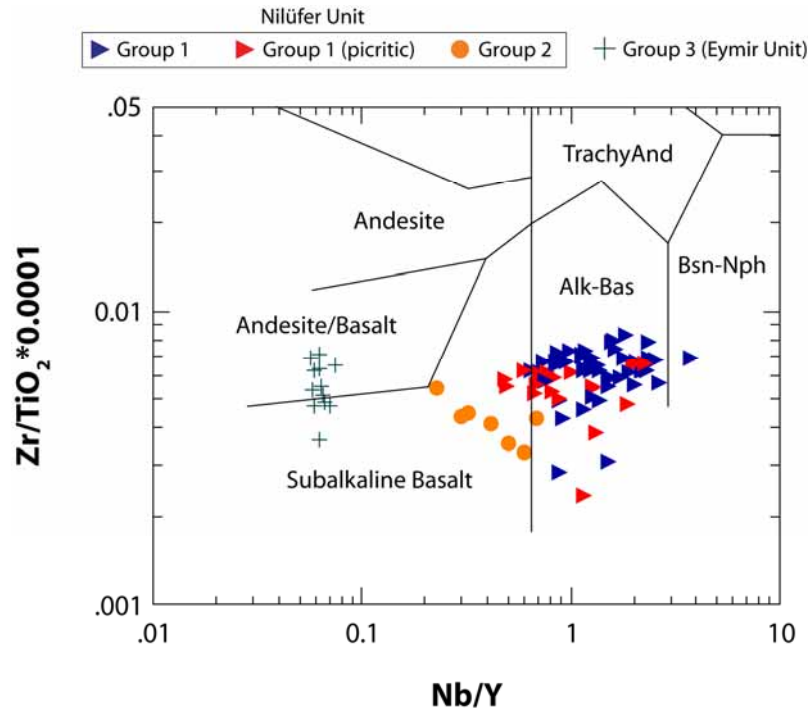
Figure 4.3. Chemical classification of the studied samples based on relatively immobile elements under conditions of low-grade alteration/metamorphism (after Winchester and Floyd, 1977).

In terms of Y/Nb ratios, Group 1 samples display the lowest values (0.4-2.1), while this ratio tends to be a bit higher for Group 2 (1.5-4.4). Group 3 suite has Y/Nb ratios (13.4-17.6) significantly higher than these two groups. It must be noted that Group 1 suite and to a lesser extent Group 2 display a large range in Ce/Sm ratio at a given MgO ([Ce/Sm]$_{OIB}$ = 4.2-13.4, [Ce/Sm]$_{E-MORB}$ = 4.2-8.4), while this ratio tends to change in a limited interval in the case of Group 3 samples ([Ce/Sm]$_{SSZ}$ = 1.2-1.6).
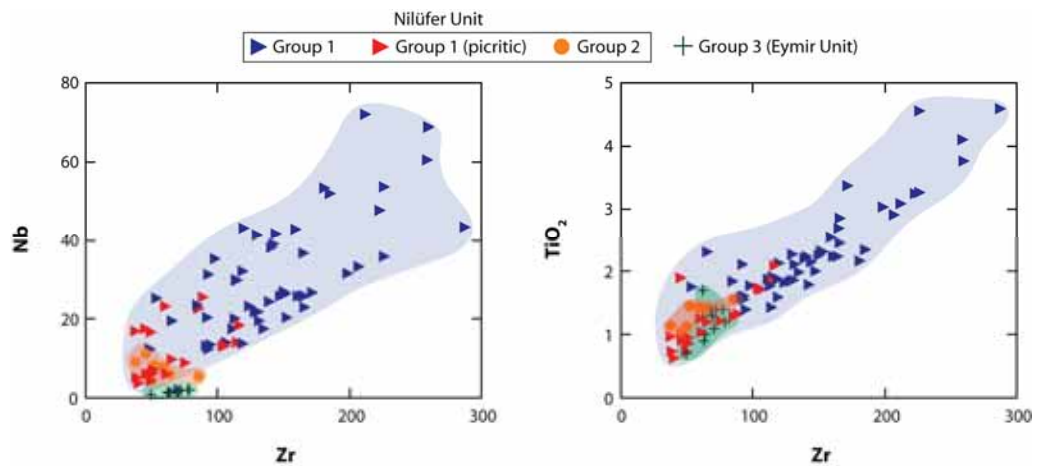
Figure 4.4. Variations of Nb and TiO$_2$ against Zr for the studied sample groups. Note the highly variable concentrations observed in Group 1 relative to the other suites.

4.2. Isotope Geochemistry

For the assessment of Sr, Nd, Pb and Hf radiogenic isotope characteristics of the newly defined Nilüfer Unit and the Eymir metadiabases, 16 samples were selected on the basis of trace element geochemistry. Among these, 9 samples are representative of Group 1 (OIB-type), 4 samples characterize Group 2 (E-MORB-type), and the remaining 3 samples represent Group 3 (SSZ-type group) suite. Isotopic compositions of all the studied samples suites were calculated back to 240 Ma that represents Middle Anisian time.

As indicated by numerous isotopic studies performed on oceanic basalts as well as mantle xenoliths, it has long been recognized that the mantle is heterogeneous both on small scales and very large scales (e.g. Dupre and Allegre, 1983; Hart, 1984; Zindler and Hart, 1986). The differences in isotopic characteristics of oceanic basalts define several distinct arrays or trends which extend towards the "end-member" mantle components. The isotopic space as inferred from oceanic basalts can be defined by at least four end-member components (Zindler and Hart, 1986); DMM (depleted MORB mantle), HIMU (high μ) and two enriched mantle reservoirs (EMI and EMII). Of these, DMM is represented by MORB

derived from the depleted mantle or the MORB mantle itself and characterized by unradiogenic $^{87}Sr/^{86}Sr$ and $^{143}Nd/^{144}Nd$ ratios. HIMU represents high time-integrated U/Pb and reflects extremely radiogenic Pb isotopic compositions coupled with unradiogenic $^{87}Sr/^{86}Sr$ and intermediate $^{143}Nd/^{144}Nd$. The enriched end-members EMI and EMII reflect isotopic evolutions indicative of high time-integrated Rb/Sr but low Sm/Nd. EMI is characterized by low $^{206}Pb/^{204}Pb$ and highly unradiogenic $^{143}Nd/^{144}Nd$, whereas EMII shows very high $^{87}Sr/^{86}Sr$ ratios along with relatively low $^{143}Nd/^{144}Nd$ and intermediate $^{206}Pb/^{204}Pb$. A fifth end-member may be regarded as FOZO (Focus Zone; Hart et al., 1992) that may represent a common mantle component. Aside from the DMM component which is commonly believed to have derived from depleted upper mantle, the origin of isotopic signatures of the other components has been largely attributed to recycled oceanic crust with/without terrigenous/pelagic sediments, ancient metasomatised oceanic lithosphere and recycled subcontinental lithosphere (e.g. Weaver et al., 1986; Salters and Hart, 1991; Chauvel et al., 1992; Hart et al., 1992; Workman et al., 2004).

4.2.1. Method

Bulk rock isotopic analyses were carried out at San Diego State University (USA). Nd-Pb-Hf isotopic data were measured using multi-collector inductively coupled plasma mass spectrometry (MC-ICP-MS) on a Nu Plasma system following the methods of Schilling et al. (1994), Hanan and Schilling (1989) and Blichert-Toft et al. (1997), while Sr isotopic data were collected using a VG Sector 54 thermal ionization mass spectrometer (TIMS) using the methods of Schilling et al. (1994). Pb values were corrected using the Tl-doping technique (White et al., 2000; Thirlwall, 2000; Albarede et al., 2004). Fractionation was checked by using standard-sample-standard bracketing using a solution of NBS 981 (30 ppb) and NBS 997 Tl (3 ppb). Data were corrected using a delta correction and values of Todt et al. (1996).

4.2.2. Sr-Nd-Pb-Hf Isotope Variations

All the studied groups display an extensive range in $^{87}Sr/^{86}Sr$ ratios, probably related to post-magmatic processes, such as hydrothermal alteration/ metamorphism (Figure 4.5). Since seawater is characterized by a particularly high $^{87}Sr/^{86}Sr$ ratio (0.70916; e.g. Faure, 2001) compared to oceanic mantle, basalts that have experienced hydrothermal alteration may display elevated Sr isotopic compositions. Some of the OIB-type samples and especially SSZ-type samples are also markedly higher than age-corrected Bulk Silicate Earth (BSE). The OIB-type samples reflect the widest $^{87}Sr/^{86}Sr$ range among the sample groups, varying from 0.703832 to 0.705852. The E-MORB-type suite, however, appears to have more consistent $^{87}Sr/^{86}Sr$ ratios between 0.703954 and 0.704930. The SSZ-type samples reflect particularly high values compared with the OIB- and E-MORB-type suite, ranging from 0.705639 to 0.707177.

Owing to the highly variable values that may be indicative of significant seawater alteration and metamorphism, Sr isotope ratios will not be considered further for the evaluation of isotopic characterization and source features of the investigated samples. However, although post-magmatic processes appear to have largely influenced the Sr isotopic compositions of the studied samples, there is also a possibility that the radiogenic Sr isotope signatures, to some extent, may have been inherited from an EM-II component, since it is known to have highly radiogenic $^{87}Sr/^{86}Sr$ ratios coupled with relatively unradiogenic $^{143}Nd/^{144}Nd$ (e.g. Hart et al., 1988).

In contrast to the wide range of $^{87}Sr/^{86}Sr$ ratios, $^{143}Nd/^{144}Nd$ values seem much more coherent, indicating the stable behaviour of Nd during post-magmatic processes (Figure 4.5). The relative immobility of Nd during post-magmatic processes makes it a reliable indicator to trace ancient mantle source characteristics (e.g. Staudigel et al., 1995; Pearce et al., 1999). All the studied samples are characterized by Nd isotopic compositions higher than that of BSE.
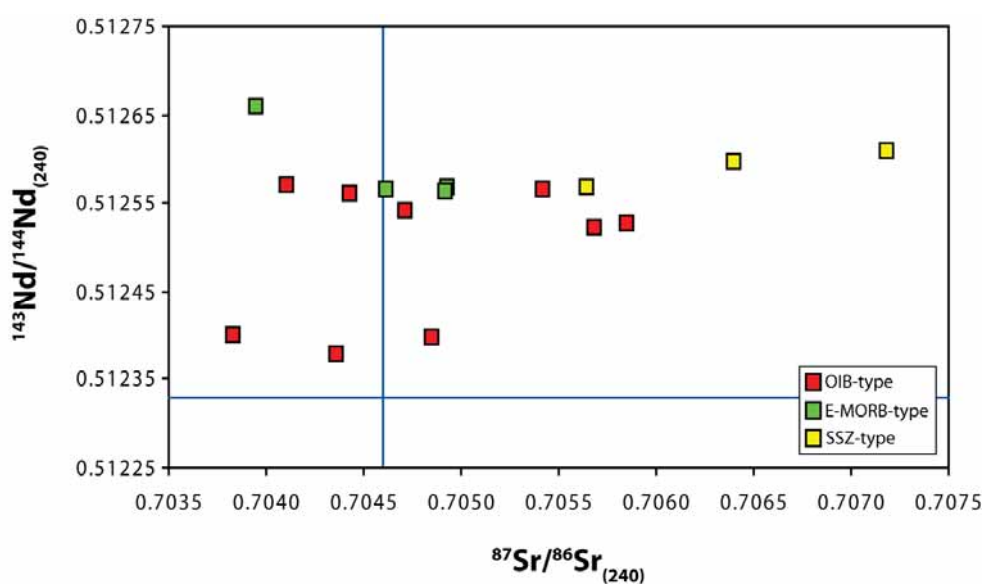
Figure 4.5. Age-corrected $^{87}Sr/^{86}Sr$ vs $^{143}Nd/^{144}Nd$ variation diagram of the studied samples. Blue lines indicates the composition of BSE. BSE was corrected, assuming $^{143}Sm/^{144}Nd = 0.1967$; $^{87}Rb/^{86}Sr = 0.031$ and a present day isotopic composition of 0.7047 for Sr, and 0.512638 for Nd (Jacobsen and Wasserburg, 1984).

The OIB-type samples display the largest variation among the studied groups, with time-corrected Nd isotopic compositions between 0.512378 and 0.512570 (Figure 4.5). When examined in detail, it appears that the OIB-type samples actually comprise two groups on the basis of Nd isotope compositions. The first of these groups ("less radiogenic OIB-type") is characterized by lower Nd isotopic ratios between 0.512378 and 0.512398. The other group ("more radiogenic OIB-type") has higher $^{143}Nd/^{144}Nd$ ratios that range from 0.512523 to 0.512570. Therefore, although the OIB-type suite spans a large in terms of Nd isotopic ratios in overall, the subgroups are observed to change within a limited interval. The E-MORB-type suite has limited Nd compositions compared with the OIB-type, ranging between 0.512563 and 0.512658. The SSZ-type samples show the smallest variation in $^{143}Nd/^{144}Nd$ ratios with values between 0.512568-0.512608.

The OIB-type suite has the most heterogeneous Pb isotopic compositions ($^{206}Pb/^{204}Pb$ = 18.58-21.14; $^{207}Pb/^{204}Pb$ = 15.59-15.72; $^{208}Pb/^{204}Pb$ = 38.40-40.98) (Figure 4.6). Two samples from this group have highly radiogenic Pb isotopic values ($^{206}Pb/^{204}Pb$ = 20.68-21.14), reflecting strong HIMU characteristics. The E-MORB-type suite, on the other hand, reflect relatively more homogeneous compositions ($^{206}Pb/^{204}Pb$ = 18.55-19.09; $^{207}Pb/^{204}Pb$ = 15.54-15.61; $^{208}Pb/^{204}Pb$ = 38.53-39.16). The Pb isotope compositions of the SSZ-type samples vary within a very narrow interval, similar to what is observed in Nd ratios ($^{206}Pb/^{204}Pb$ = 18.33-18.42; $^{207}Pb/^{204}Pb$ = 15.59-15.60; $^{208}Pb/^{204}Pb$ = 38.29-39.34).

Hf isotope systematics shows behavior similar to that of Nd, so the combination of these two systems is powerful for tracking mantle sources and processes (e.g. Patchett and Tatsumoto, 1980; Patchett, 1983; Salters and White, 1998). A particular advantage of the Lu-Hf and Sm-Nd isotope systems is the relatively immobile behavior of parent and daughter elements during post-magmatic processes (e.g. low-grade metamorphism) therefore making Hf-Nd isotope system a reliable indicator in most cases (e.g. Pearce et al., 2007).

The OIB-type samples have initial $^{176}Hf/^{177}Hf$ ratios reflecting a marked heterogeneity, between 0.282698 and 0.282836 (Figure 4.7). The E-MORB-type suite shows $^{176}Hf/^{177}Hf$ ratios between 0.282820-0.282891. The SSZ-type suite once again appears to be very homogeneous, with Hf compositions between 0.282943-0.282958. All the studied samples are plotted above the BSE, indicating their time-integrated depletion.

4.3. Discussion of the Results Inferred from Major and Trace Element Geochemistry

4.3.1. Fractional Crystallization

Compared with Group 1 and Group 2 suites that have relatively high Mg# (avg = 65), Group 3 samples are characterized by lower Mg# (avg = 48). This is also confirmed by the very low Ni values of the latter, varying between 2.1 to 49.4

ppm. Such evolved compositions suggest extensive olivine + clinopyroxene ± spinel fractionation before ponding in high-level magma reservoirs. On the other hand, the presence of numerous pseudomorphs after olivine phenocrysts suggests that significantly high Mg numbers observed in some samples may have resulted from olivine accumulation, and therefore they may not represent primary magma compositions.
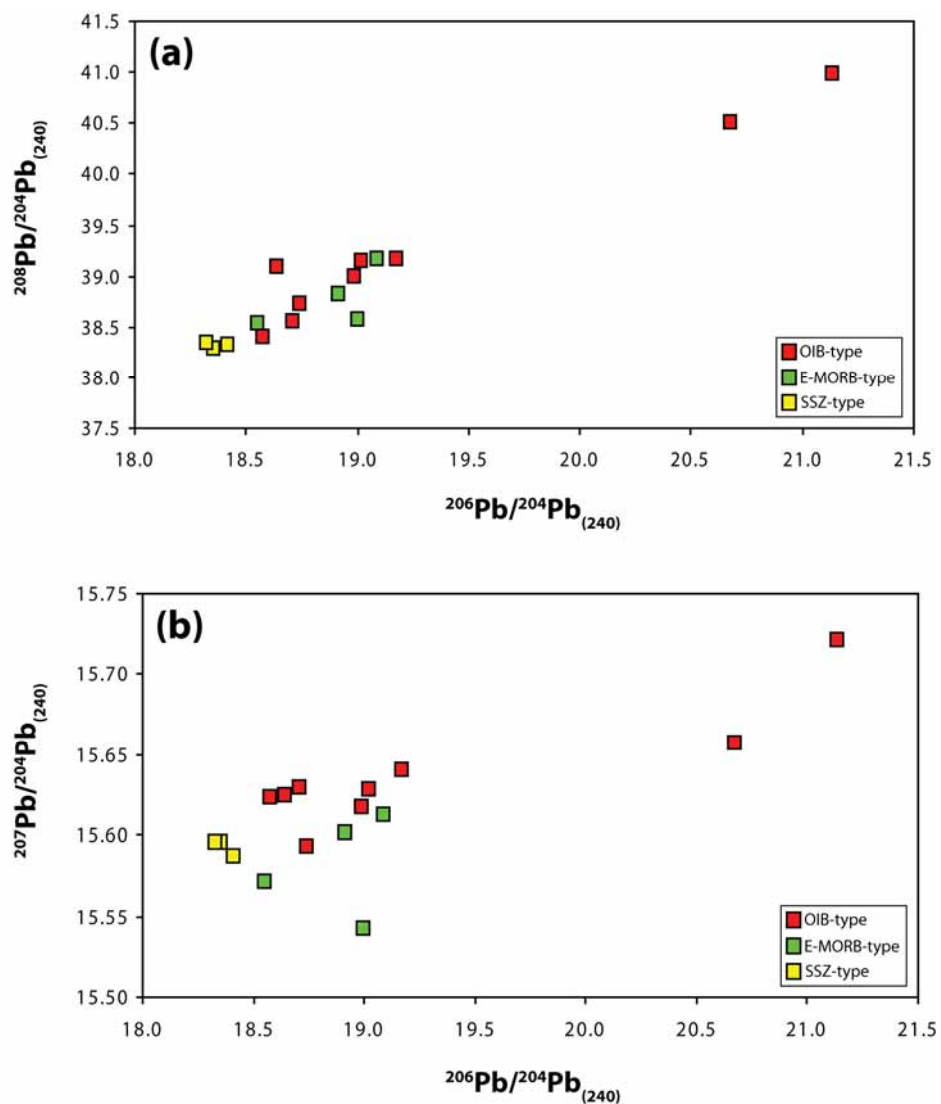
Figure 4.6. Variation of the studied samples in age-corrected Pb isotopic space. Data sources and correction procedure are the same as in Figure 4.4.
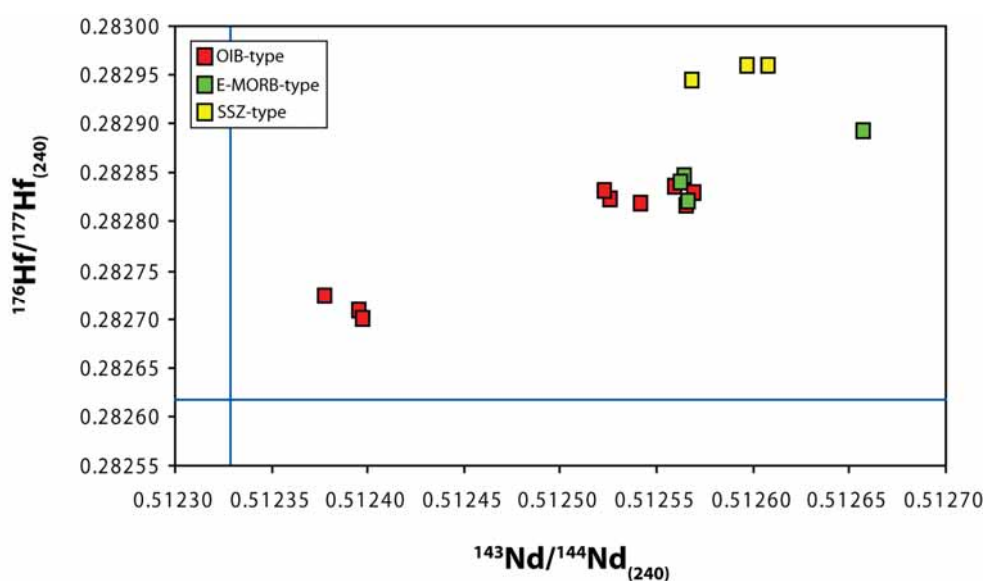
Figure 4.7. Age-corrected $^{143}Nd/^{144}Nd$ vs $^{176}Hf/^{177}Hf$ variation diagram of the studied samples. Blue lines indicates the composition of BSE. BSE was corrected, assuming $^{143}Sm/^{144}Nd$ = 0.1967; $^{176}Lu/^{177}Hf$ = 0.0332, and a present day isotopic composition of 0.512638 for Nd, and 0.282772 for Hf (Jacobsen and Wasserburg, 1984; Blichert-Toft and Albarede, 1997).

Most of the major elements as well as some trace elements show well-defined trends against MgO, suggesting that fractional crystallization and/or crystal accumulation have played an important role during differentiation (Figures 4.8 to 4.11). The Group 2 suite, however, has MgO contents that vary over only a very narrow interval (8.1-9.1 wt.%, excluding the sample BU-8), thus making very difficult to infer about their fractionation histories. Thus, they were excluded from the discussion regarding fractional crystallization.

When an incompatible element is plotted against a compatible element at log-scale, the differences in compositions resulting from fractional crystallization or accumulation can be identified (e.g. Rhodes, 1995; Norman and Garcia, 1999). A log-log plots of MgO-Al_2O_3 and MgO-Na_2O for the Group 1 samples show that the compositions with approximately <15% MgO tend to follow a different trend than their more magnesian (picritic) counterparts (Figure 4.8). MgO contents of the more magnesian samples may be attributed to olivine accumulation, whereas

the lower MgO compositions may reflect control by fractionation process. The inflection point between fractionation and olivine accumulation processes may roughly imply a parental magma composition, namely ~15 % MgO, ~11 % Al_2O_3, ~2% Na_2O, and ~450 ppm Ni.
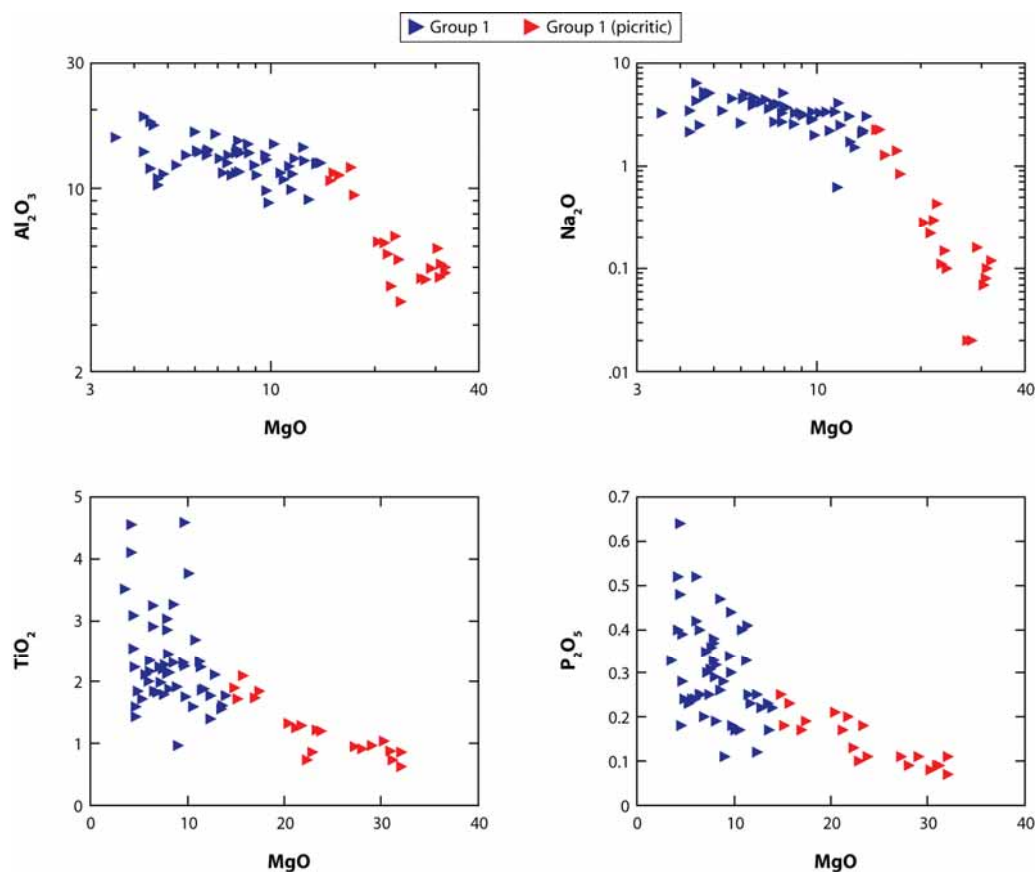
Figure 4.8. Variation of selected major elements (wt.%) against MgO (wt.%) within Group 1 suite.

The decrease in Ni concentration with decreasing MgO indicates that olivine fractionation was important in creating the observed trends for Group 1 and Group 3 suites (Figures 4.9 and 4.11). Note that some Group 1 samples tend to have higher Ni abundances at a given MgO, which may suggest influence of olivine accumulation on these samples. Similarly, for the Group 3 suite, Ni
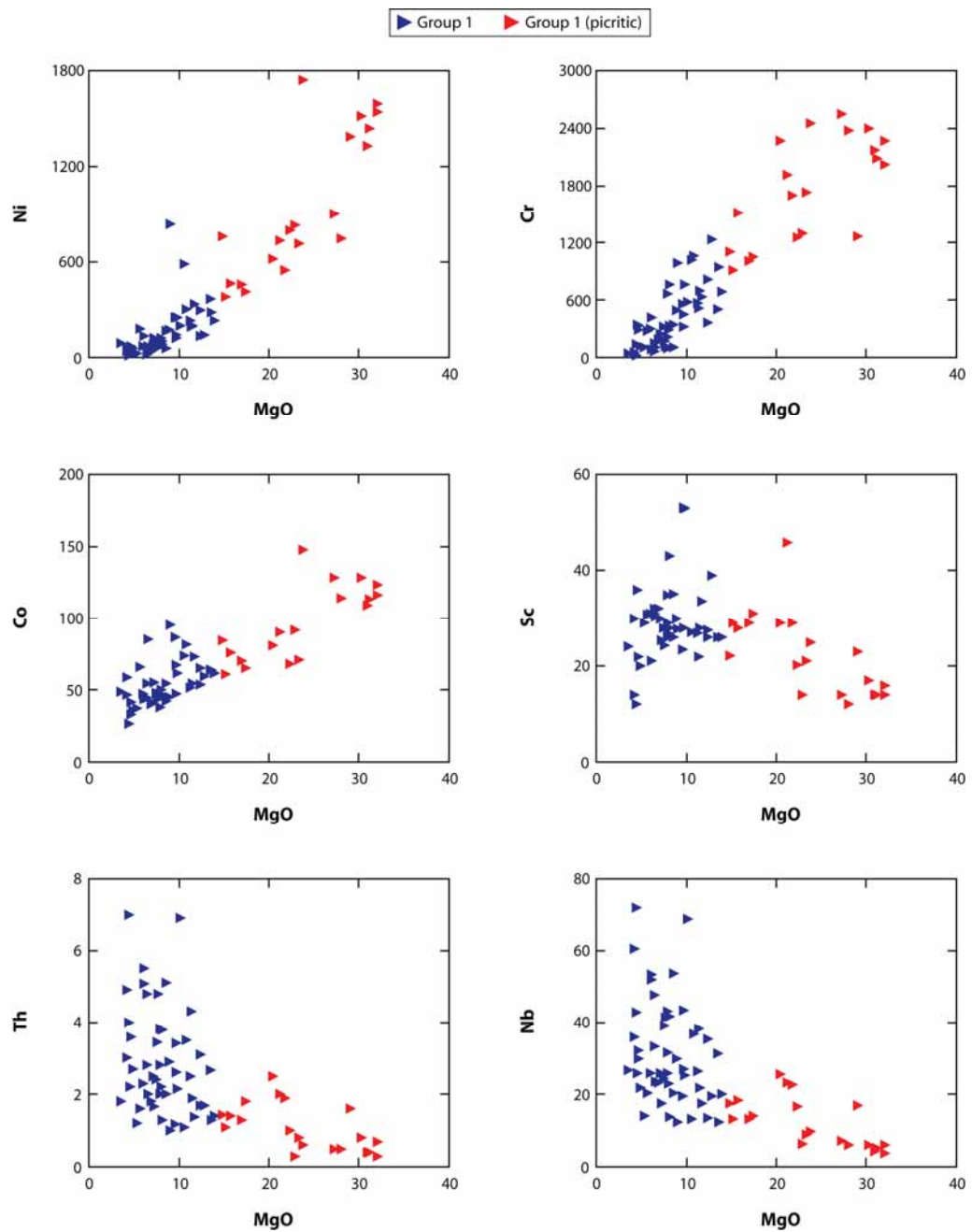
Figure 4.9. Variation of selected trace elements (ppm) against MgO (wt.%) within Group 1 suite.

appears to stop its sharp decrease and get down to very low concentration levels at about 4.5-5% MgO (wt.%), suggesting that olivine has been removed

and/or a new mineral phase(s) has been added to the fractionating assemblage at that interval (Figure 4.9).

In both suites, Cr abundances decrease with decreasing MgO, supporting olivine fractionation in addition to clinopyroxene and/or Cr-spinel (Figures 4.9 and 4.11). Co also shows a linear correlation with decreasing MgO, consistent with the overall crystallization of these mineral phases. Among Group 1 samples, Sc contents decrease with decreasing MgO after falling down to about 8.5 wt.%, as expected for removal of clinopyroxene, while in some cases high Sc contents (over ~35 ppm) are likely indicative of clinopyroxene accumulation. For Group 3, Sc/Y ratios also decrease until MgO gets down to ~4.5 wt.%, hence consistent with extensive clinopyroxene fractionation up to a certain level (Figure 4.11).

CaO variations against MgO appear scattered in the Group 1 suite, perhaps owing to intensive alteration and metamorphism (not shown). This relationship, however, seems more coherent in Group 3 samples, and the decline in CaO contents with decreasing MgO (until it reaches ~4.5%) may suggest fractionation of plagioclase in addition to clinopyroxene (Figure 4.10). Therefore, covariations of CaO and Sc with MgO observed within Group 3 samples show that both plagioclase and clinopyroxene have been significant fractionating phases for this suite. In contrast, Al_2O_3 reflects an inverse relationship with MgO for Group 1 suite (Figure 4.8), suggesting that plagioclase fractionation was negligible for this group.

TiO_2 increases with decreasing MgO in Group 1 samples, consistent with fractionation of olivine and clinopyroxene (Figure 4.8). The higher TiO_2 concentrations of some samples at a given MgO, however, may reflect accumulation of amphibole and/or Fe-Ti oxides, or alternatively can be partly attributed to the partial melting. Increasing TiO_2 contents may also imply that fractionation of Fe-Ti oxide phases (e.g. ilmenite, magnetite and titanomagnetite) were insignificant for Group 1 suite. Within Group 3 suite, TiO_2 tends to increase until ~4.5 wt.% MgO, but then it declines rapidly at lower MgO contents (Figure
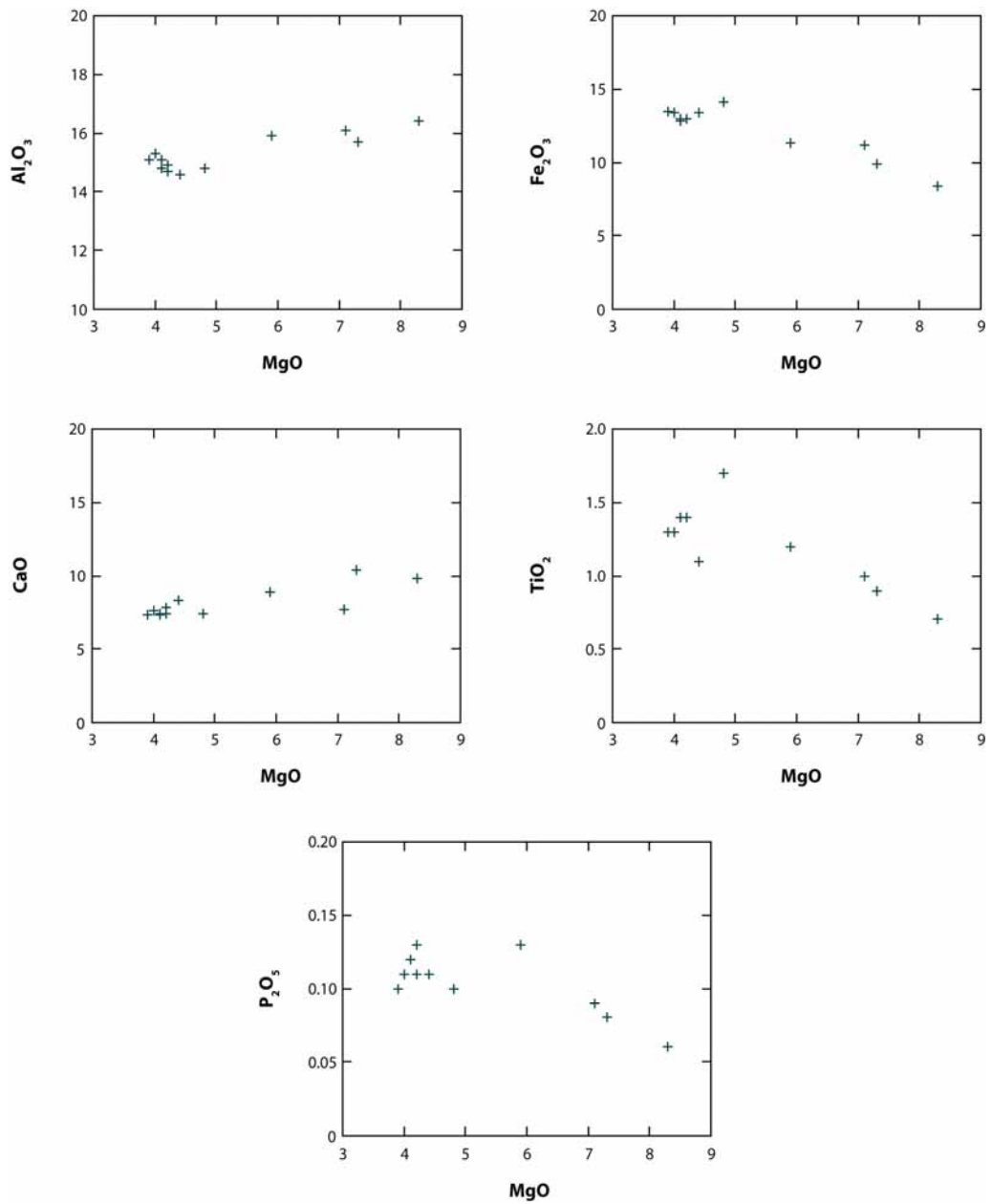
Figure 4.10. Variation of selected major elements (wt.%) against MgO (wt.%) for Group 3 suite.

4.10). This noticeable decrease can be attributed to amphibole and/or Fe-oxide phase fractionation. Similarly, V and Nb concentrations correlate inversely with MgO >~4.5 for this group, below which there appears a well-defined decreasing trend. Fractionation of Fe-Ti oxides, especially ilmenite, can be very effective in

decreasing both V and Nb (e.g. Bedard, 1994). Amphibole can also partition V very effectively as ilmenite, but not Nb. Therefore, the marked decreases in TiO_2 and V may have been controlled by fractionation of both Fe-oxides (possibly ilmenite) and amphibole, whereas Nb has been greatly fractionated by ilmenite. The sharp decreases in Nd, Gd, Sm (not shown) and to a lesser extent Sc, however, should have probably resulted from amphibole rather than Fe-Ti oxides. Therefore, the resulting picture is that both Fe-Ti oxides and amphibole have played an important role during the late-stage fractionation of Group 3 suite.

For Group 3 samples, P_2O_5 starts to decrease below 4.5% MgO (wt.%), indicating fractionation of apatite (Figure 4.10), whereas no sign regarding fractionation of this phase has been found in Group 1 suite (Figure 4.5). High P_2O_5 concentrations seen in Group 1 suite can be attributed to apatite accumulation and/or generation under small degrees of partial melting. However, since the former idea is not supported by petrographical observations, formation by small degrees of partial melting seems a more plausible reason, which results in high P_2O_5 contents.

If the geochemical implications stated above are taken into account with petrographical observations, it can be suggested that Group 1 samples with greater than ~15% MgO (wt.%) represent olivine cumulates and not primary compositions. Fractionation process appears to have been effective for MgO concentrations lower than ~15% MgO (wt.%). In the Group 1 suite, ~15% MgO and 450 ppm Ni may characterize primary magma compositions. Olivine + clinopyroxene ± spinel are the major mineral phases dominating the fractionation history of Group 1 samples. Some of the samples within the suite have been also influenced by clinopyroxene accumulation, consistent with their clinopyroxene-rich petrography. Within Group 3 suite, none of the samples appear to have compositions representative of primary magmas. Early stages of fractionation are controlled by olivine + plagioclase + clinopyroxene, however in later stages Fe-Ti oxides together with hb dominates the fractionation trends. Crystallization of hornblende as a late-stage crystallizing phase in the fractionation sequence of the

metadiabases is supported by clinopyroxene crystals rimmed/overgrown by hornblende.
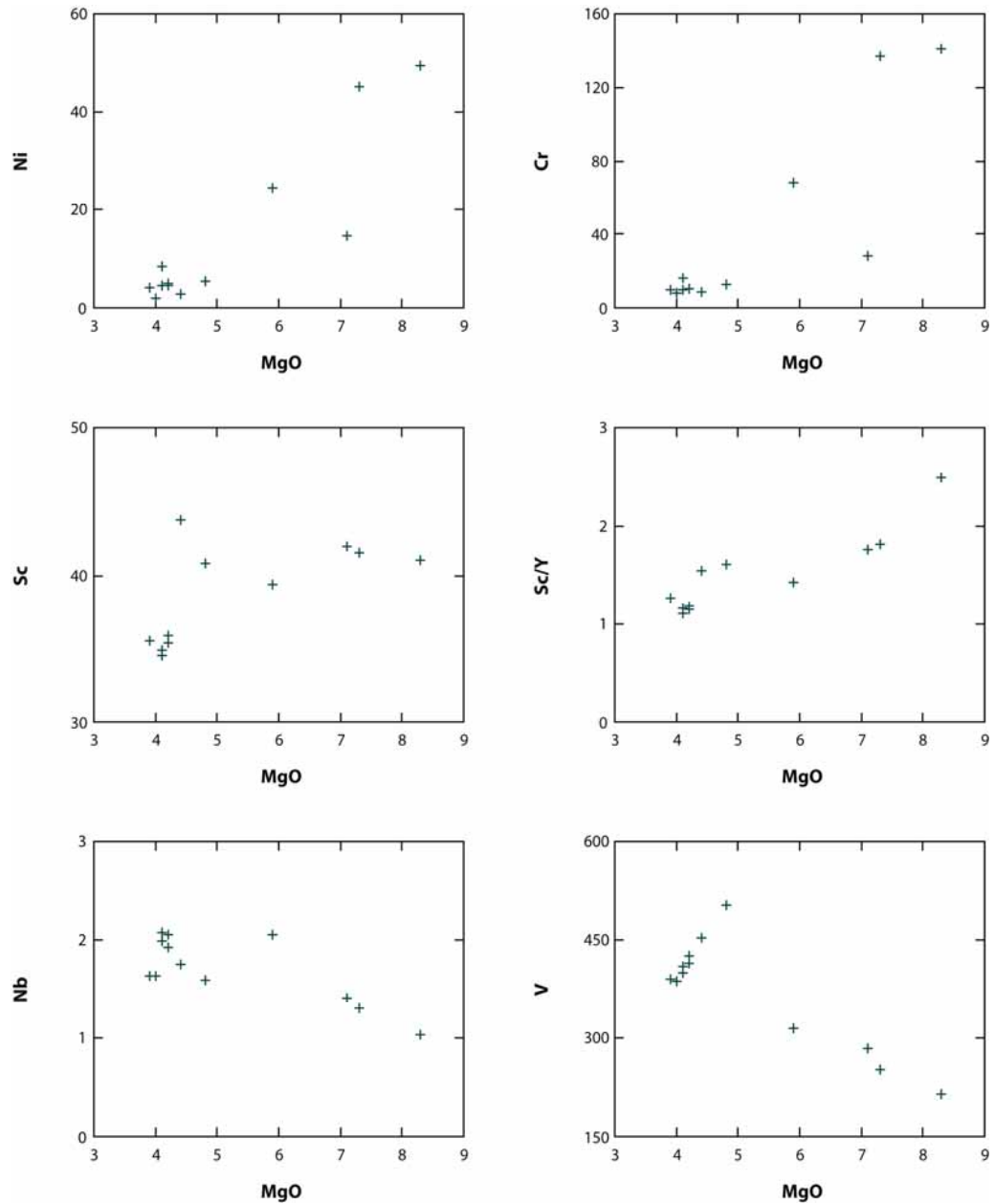
Fig. 4.11. Variation of trace elements (ppm) against MgO (wt.%) for the SSZ-type suite.

4.3.2. Nature of the Source Region

Group 1 and Group 2 samples are characterized by low Zr/Nb ratios (2.1-11.1 and 4.1-15.5, respectively), reflecting significant enrichment of Nb in these samples. The low ratios observed in these suites may imply involvement of enriched source(s) and/or relatively small degrees of partial melting during their genesis. Zr/Nb ratios appear to be extremely high in Group 3 suite (32.2-48.2; ave = 40.07); a result of their Nb-depleted compositions, suggesting derivation from depleted source such as N-MORB (Zr/Nb = 31.8; Sun and McDonough, 1989). This interpretation is further supported by the Y/Nb ratios (13.4-17.6) of Group 3, which are significantly higher than those of Groups 1 and 2, therefore consistent with origin from a depleted source. The observed variability and high concentrations in Nb and TiO_2 values reflected by Group 1 suite clearly imply involvement of different type of sources and/or source heterogeneity coupled with varying degrees of melting. In contrast, the limited variation of Nb and TiO_2 in Group 2 and Group 3 samples suggests that they have been probably derived from relatively homogeneous source regions.

Fractional crystallization cannot account for the large Zr/Nb variations observed within Group 1 and Group 2 suites. High Ce/Y ratios may have resulted from crustal contamination, however this would lead high Zr/Nb at the same time. Such a relationship is not observed (Figure 4.12). Indeed, within Group 1 suite, there appears no meaningful relationship between Zr/Nb and MgO, which can be interpreted as the result of fractional crystallization, and more importantly the same significant Zr/Nb range is observed throughout the entire MgO spectrum. Therefore, the observed variations in Group 1 and Group 2 suites should have largely originated from source-related processes (e.g. partial melting, source heterogeneity). As Group 2 samples display very limited variation in MgO, their widely varying Zr/Nb ratios have not resulted from fractional crystallization. Similarly, the large Zr/Nb spectrum varying in a limited Ce/Y interval in Group 3 suite appears to be largely result of source-related processes (e.g. source depletion). Since this group is mainly composed of relatively evolved samples,

the effect of fractional crystallization on Zr/Nb ratio cannot be entirely excluded. The remarkably high values of Ce/Y observed in Group 1 suite compared to Groups 2 and 3 may indicate generation under smaller degrees of partial melting and/or derivation from relatively a more enriched source region (Figure 4.12).
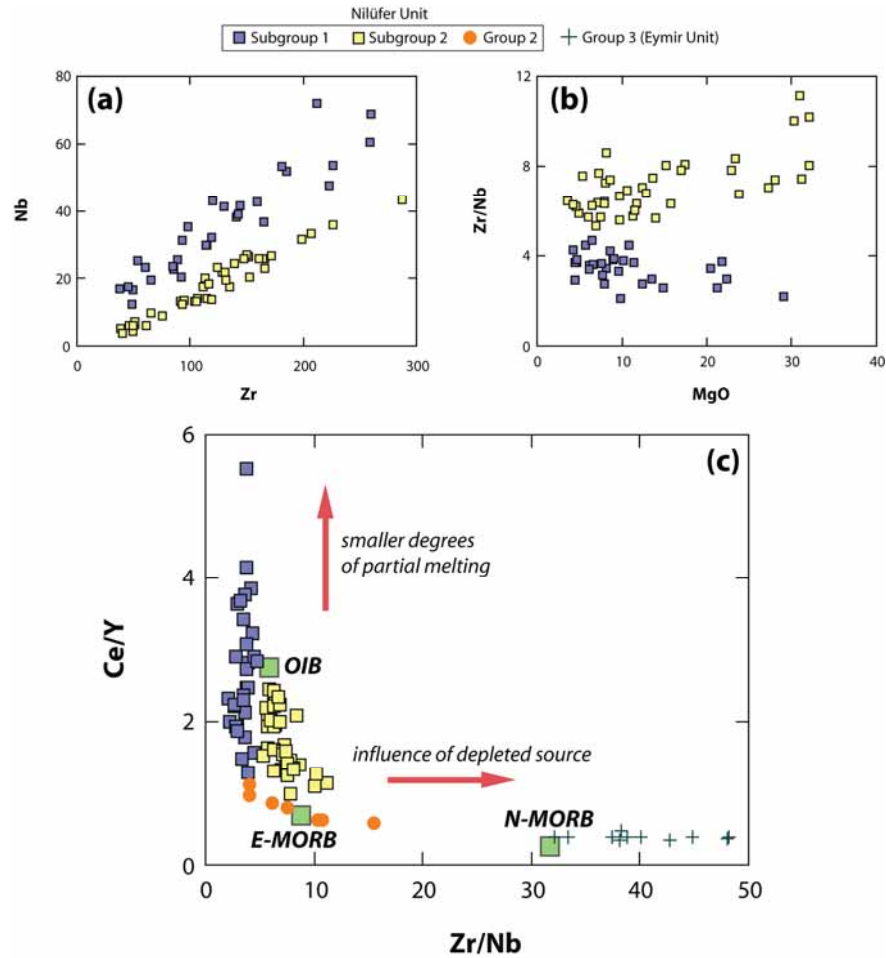
Figure 4.12. a) Zr-Nb variations observed within Group 1 suite, revealing two distinct subgroups with different Zr/Nb signatures. b) MgO-Zr/Nb plot, indicating the distinct Zr/Nb signatures shown by the subgroups are largely related to source processes. c) Zr/Nb-Ce/Y plot, indicating that the Zr/Nb and Ce/Y variations have been originated from source-related features rather than fractional crystallization or crustal contamination. N-MORB, E-MORB and OIB values from Sun and McDonough (1989).

It must be noted that Group 1 suite and to a lesser extent Group 2 display a large range in Ce/Sm ratio at a given MgO ($[Ce/Sm]_{OIB}$ = 4.2-13.4, $[Ce/Sm]_{E-MORB}$ = 4.2-8.4), while this ratio tends to change in a limited interval in the case of Group 3 samples ($[Ce/Sm]_{SSZ}$ = 1.2-1.6) (Figure 4.13). This wide range especially shown by Group 1 suite cannot be explained solely by fractional crystallization. Instead, differences in degree of partial melting and/or source-related features should account for such large variations. Ce/Sm ratio is not sensitive to fractionation of olivine and plagioclase as well as Fe-Ti oxides, whereas clinopyroxene can be effective in fractionating this ratio relative to the other phases (D_{Sm}/D_{La} = 4.19; Johnson 1998). However, even substantial crystallization of clinopyroxene (i.e. 90%) cannot account for the variations observed in Group 1 suite; even within subgroups. It appears, therefore, that the variations in Ce/Sm ratios should have been largely inherited from varying degrees of partial melting and/or the mantle source heterogeneities.
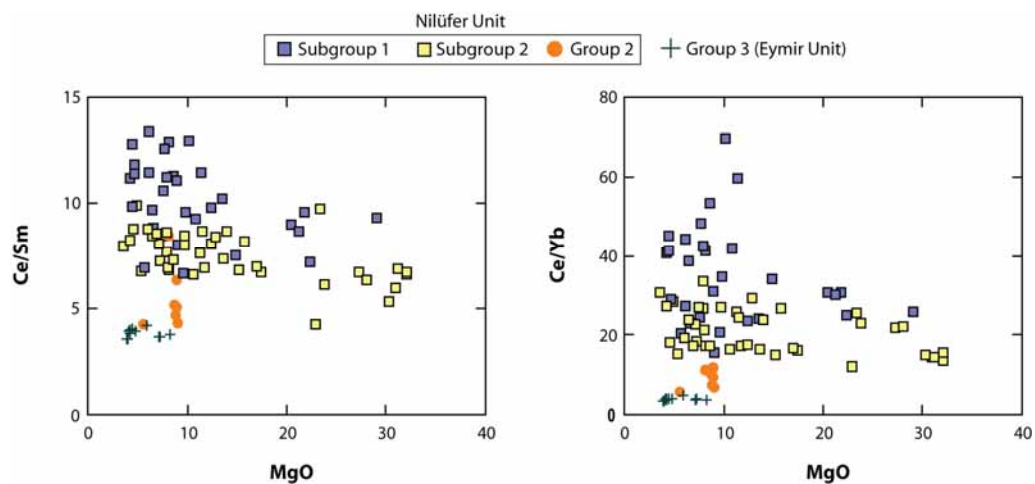
Figure 4.13. Ce/Yb and Ce/Sm variations against MgO (wt.%), highlighting the influence of source-related processes on creating the wide range shown by Group 1 suite.

Supporting this argument is the Ce/Yb ratios that span an extensive range in Group 1 suite (Figure 4.13). During fractional crystallization, the residual melt would become gradually more enriched in terms of both Ce and Yb with the increasing degree of crystallization owing to their tendency to go to the liquid phase. Thus, such a process should create relatively unfractionated Ce/Yb distributions with respect to the primary melt. Therefore, the significant increase in Ce/Yb with increasing Ce observed in Group 1 samples is consistent with the influence of different degrees of melting and/or source processes rather than fractional crystallization.

High Ce/Yb ratios of the OIB-type group may indicate the presence of residual garnet in their mantle source(s). The lower Ce/Yb ratios observed in E-MORB-type samples, however, likely reflect generation under somewhat large degrees of partial melting that eventually lead to total exhaustion of garnet in the mantle source. Another alternative explanation is that melting occurs across the garnet-spinel transition, thus obscuring the effect of garnet alone.

The presence of marked Nb anomalies coupled with depletion in HFSE relative to N-MORB observed in Group 3 suite are typical features of SSZ-type basalts and suggests that the mantle wedge may have suffered melt extraction before magma generation (e.g. Woodhead et al., 1993; Pearce et al., 1995; Sinton et al., 2003). It has been argued that LILE (like Rb, Sr, Ba, U) and LREE are transported into mantle wedge from the slab by aqueous fluids, whereas Th is transferred by silicate melts (e.g. Brenan et al., 1995; Elliott et al., 1997). Therefore, significant enrichment in LILE (except Th) with respect to N-MORB observed within Group 3 suite can be attributed to the role of slab fluids in addition to low-grade alteration/metamorphism, while the depletions in these elements have probably resulted from the latter processes that have led to remobilization of these elements.

As noted above, SSZ-type Group 3 samples display typical LILE enrichment with negative Nb-Ta signatures, leading to high Th/Ta (3.0-5.3) and Th/Nb (0.3-0.4)

values. In contrast, Group 1 and Group 2 suites show no negative Nb-Ta anomalies, hence resulting in low Th/Ta (0.6-2.3 and 0.8-1.3, respectively) and Th/Nb (0.05-0.13 and 0.05-0.09, respectively) ratios. Negative Nb-Ta anomalies can be seen in some continental within-plate settings if the partial melting takes place in the subcontinental lithospheric mantle that has been previously modified by subduction components and/or they have been contaminated by continental crust on their way to the surface (e.g. Hawkesworth et al., 1992; Ellam and Cox, 1989; Peate et al., 1992). Oceanic within-plate magmas, however, seem to be devoid of such Nb-Ta anomalies caused by subduction- and continental crust-related processes (e.g. Chaffey et al., 1989; Floyd, 1989; Sun and McDonough, 1989).

Negative Nb-Ta anomalies are also commonly associated with subduction zones where metasomatic modification of mantle wedge occurs, leading to enrichment of large ion lithophile elements (LILE) and light rare earth elements (LREE) via fluids and melts generated by dehydration of the subducting oceanic slab (e.g. Gill, 1981; Hawkesworth et al., 1993; Woodhead et al., 1993). However, Nb and Ta are retained in the slab and/or in depleted mantle; which is assumed to be linked to the presence of a residual phase(s), such as rutile and amphibole (e.g. Green, 1995; Ionov and Hofmann, 1995) and this leads to negative Nb-Ta anomalies in the magmas forming in subduction zones.

Group 1 and Group 2 suites have high Zr/Y and Nb/Y ratios, suggesting that garnet may have been a residual phase (in varying amounts) in the source of these samples (especially for Group 1 suite that displays higher fractionation of LREE/HREE). Group 3 samples, however, have markedly lower Nb/Y ratios coupled with low Zr/Y. As seen from Figure 4.14, all Group 1 and Group 2 samples plot above (or on) the ΔNb line of Fitton et al. (1997), suggesting their derivation from enriched source(s), whereas all Group 3 samples are plotted below the line, indicating that they have been derived from depleted source (N-MORB-type source). It is significant that both Group 1 and Group 2 suites appear to derive from similar type of sources, suggesting that the OIB-type Group 1

samples have been generated in response to low degrees of partial melting, while the E-MORB-type Group 2 samples reflect higher degrees of partial melting. Note also that the subgroups of the OIB-type suite clearly plot in distinct areas that reflect the decoupling of Zr-Nb systematics related to melt-mixing processes.
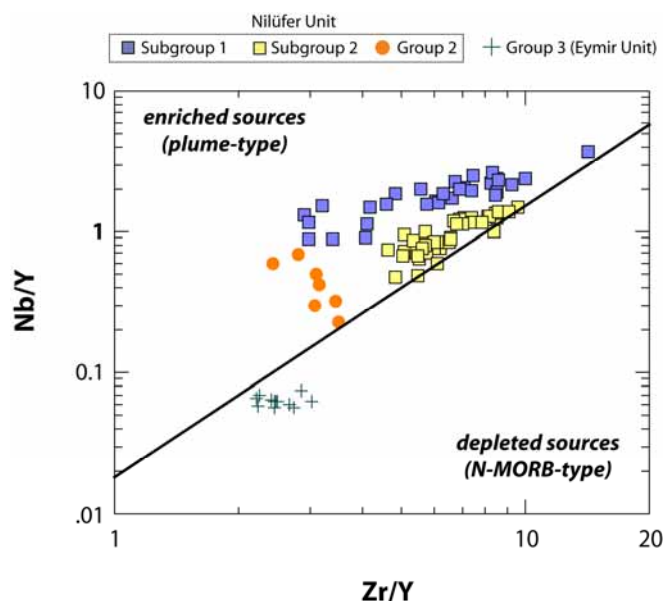
Figure 4.14. Zr/Y-Nb/Y plot of the studied samples, indicating generation of Group 1 and Group 2 suites from enriched sources. The low ratios observed in Group 3 suite, however, imply derivation from depleted sources. The dividing ΔNb line (indicated as thick black line) is from Fitton et al. (1997).

Nb/Yb-Th/Yb plot is also particularly useful in differentiating between mantle and subduction components (Figure 4.15). Within-plate processes leads to simultaneous enrichment of Nb (Ta) and Th, while subduction events have a significant effect on Th but not on Nb (e.g. Pearce, 1983; Pearce and Peate, 1995). Thus, basalts derived from mid-oceanic ridges (MORB) and within-plate settings (OIB-like) will define a linear array (MORB array) where Th/Yb increases with increasing Nb/Yb, whereas basalts generated in subduction zones show increasing Th/Yb trends at nearly constant Nb/Yb. It is observed that OIB- and E-MORB-type samples (Groups 1 and 2) plot along the MORB array. Note

that OIB-type samples are displaced towards higher Th/Yb and Nb/Yb values compared to E-MORB-type, indicating the influence of degree of partial melting and source-related features. SSZ-type samples, on the other hand, are characterized by low Nb/Yb ratios because of their Nb-depleted nature. It must be noted that Nb/Yb ratio is a good indicator of partial melting and it is not influenced by contributions from subducting slab during subduction magmatism (e.g. Pearce and Parkinson, 1993; Fretzdorff et al., 2002). Low Nb/Yb ratios similar to that of N-MORB shown by SSZ-type samples are indicative of relatively high degrees of partial melting of a depleted source, whereas the high Nb/Yb values of E-MORB and OIB-type samples are consistent with their derivation by lower degrees of partial melting of enriched source(s) as indicated by Zr/Y-Nb/Y plot (Figure 4.14).
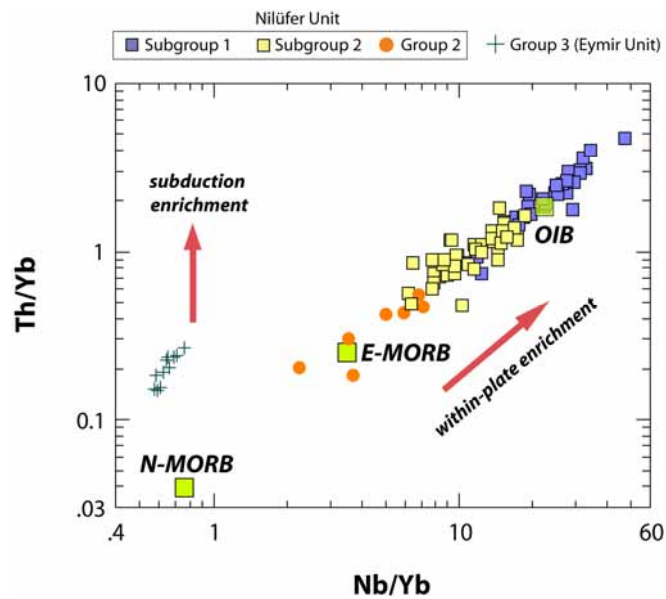
Figure 4.15. Th/Yb vs Nb/Yb plot (based on Pearce, 1983; Pearce and Peate, 1995), showing the influence of within-plate enrichment on Group 1 and Group 2, whereas Group 3 suite appears to have experienced subduction-related processes that make them shift upwards relative to the MORB array. N-MORB, E-MORB and OIB values from Sun and McDonough (1989).

4.3.3. Crustal Contamination

Low Ce/Nb and Th/Nb ratios mainly characterize the magmas unaffected by crustal contamination (e.g. Pearce, 1983; Hart et al., 1989). Group 1 and Group 2 samples have low Ce/Nb (0.9-2.3 and 1.6-2.6, respectively) and Th/Nb ratios (0.05-0.13 and 0.05-0.09, respectively), providing no evidence for crustal contamination (Figure 4.16). In contrast, the Group 3 suite displays notably higher ratios, which may be indicative of crustal involvement (Ce/Nb = 5.7-6.7; Th/Nb = 0.25-0.37).
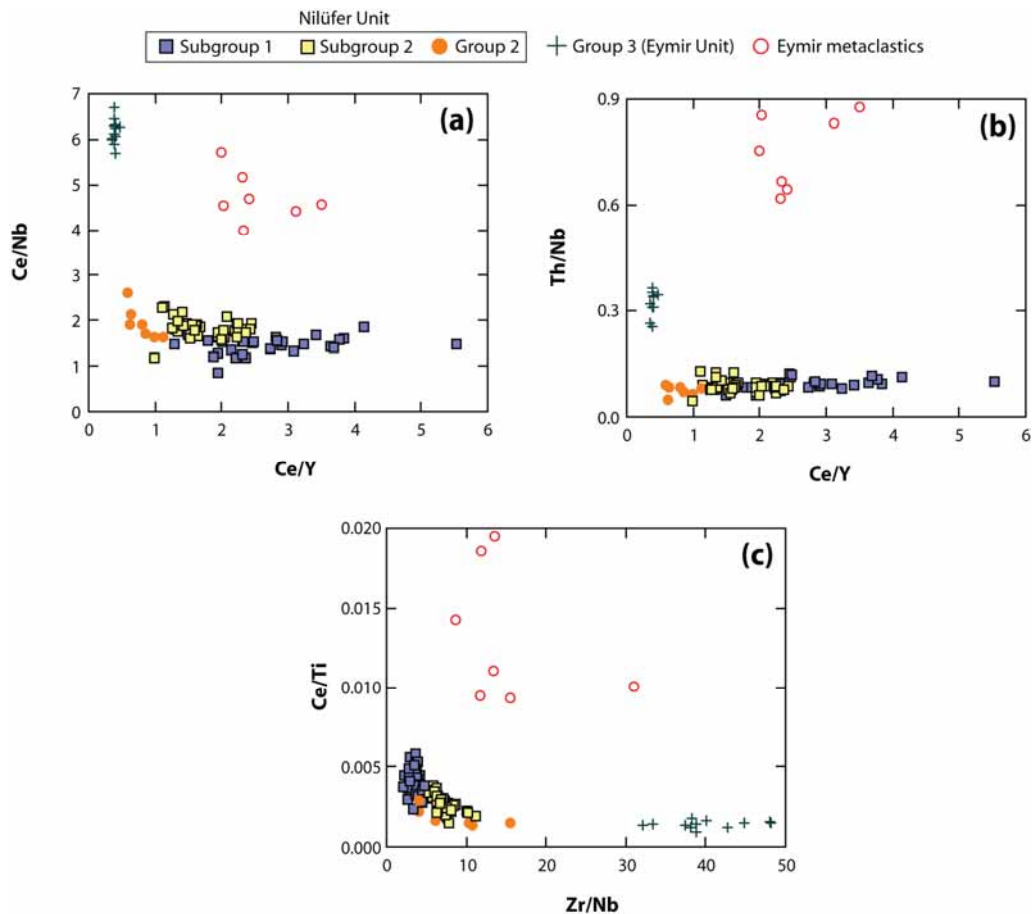
Figure 4.16. The sample suites studied here show no evidence of crustal contamination. (a) Variation of Ce/Nb and Th/Nb against Ce/Y; (b) Ce/Ti against Zr/Nb, Data for the Eymir metaclastics are taken from the unpublished data of Dr. M.C. Göncüoğlu.

HFSE-depleted patterns (relative to N-MORB) with negative Nb anomalies and high Zr/Nb values shown by the Group 3 suite are suggestive of intra-oceanic trace element signatures, indicating the influence of subduction zone processes rather than crustal events (e.g. Pearce et al. 1995; De Astis et al., 1997; Elliott et al., 1997; Peate and Pearce, 1998; Gribble et al., 1998; Woodhead et al., 1998; Stern et al., 2006).

Since continental crust is enriched in LREE and Th, but depleted in Nb and Y (e.g. Taylor and McLennan, 1995), crustally contaminated magmas are characterized by high and positively correlated La/Nb, Th/Nb and Ce/Y signatures. As seen from Figure 4.16, the studied suites do not show such a relationship, indicating that continental crust has not been involved during their genesis. Instead, the low Ce/Y, high Ce/Nb and Th/Nb ratios of Group 3, suggest that these signatures should have been acquired from subduction-zone processes (subduction enrichment) rather than crustal contamination. The absence of any crustal input is also supported by the fact that none of the investigated suites have tendency towards the composition of the Eymir metaclastics which are the potential contaminants in the studied region (Figure 4.16). These clastics, as mentioned before, represent the matrix material for Group 1 and Group 2 suites, whereas Group 3 samples intrude into these metaclastics. Therefore, this result clearly suggests that the samples have not experienced any influence from continental crust.

4.3.4. Petrogenesis of the Nilüfer and Eymir Metabasic Rock Suites

In this section, the role of partial melting in generating the diversity of studied rocks will be evaluated through geochemical modeling. Such a numerical approach may provide a better understanding of the mantle source region and the related processes (e.g. partial melting), thus they are of particular importance to put some constraints on the petrogenesis of a magmatic suite. Through geochemical modeling, one can explore the profound influence of residual garnet on melt compositions, if the considered rock types are of enriched trace element

compositions, such as OIB- and E-MORB-type. The depleted-type samples (e.g. SSZ- or N-MORB-type), on the other hand, would not reflect an elemental impact that has been inherited from residual garnet. Instead, such compositions, bear the traces of a spinel-dominated mantle, and in some cases, they may reflect previous melt extraction events. Therefore, in order to track the influence of the residual mantle minerals better, I treated the OIB- and E-MORB-type samples (Groups 1 and 2) separately from the SSZ-type suite (Group 3). Furthermore, specific elements or elemental pairs were chosen to perform the partial melting models, which may give the best picture about their mantle sources and melting systematics. All chemical groups were modeled by non-modal batch melting, using the equations of Shaw (1970). The distribution coefficients used in the calculations are compiled from McKenzie and O'Nions (1991), Kelemen (1993), and Bedard (1994).

4.3.4.1. OIB- and E-MORB-type (Groups 1 and 2) samples

Geochemical modeling of the OIB- and E-MORB-type samples was carried out with the goal of evaluating the role of garnet in the source region. Garnet can fractionate LREE/HREE and MREE/HREE ratios as long as it remains as a residual phase in the mantle source because the HREE are highly compatible in this mineral (e.g. McKenzie and O'Nions, 1991; Johnson, 1998). If garnet is totally consumed during partial melting or the source does not bear any garnet (like spinel-lherzolite), then the change in LREE/HREE and MREE/HREE ratios will be very small. Thus, the element pairs used for the modeling are Zr/Nb-Ce/Yb, Ce/Yb-Lu/Hf, and Ce/Sm-Sm/Yb (Figure 4.17). Note that only garnet-lherzolite partial melting curves are plotted because the melting curve of a spinel lherzolite varies over a very limited interval compared to that of garnet-lherzolite. Thus, for the partial melts derived from spinel-facies mantle, a representative melt composition obtained by 7.5% melting of spinel-lherzolite source was used in the plots instead. My aim in performing this modeling is to reproduce the observed trace element concentrations in the sample groups by aggregating the
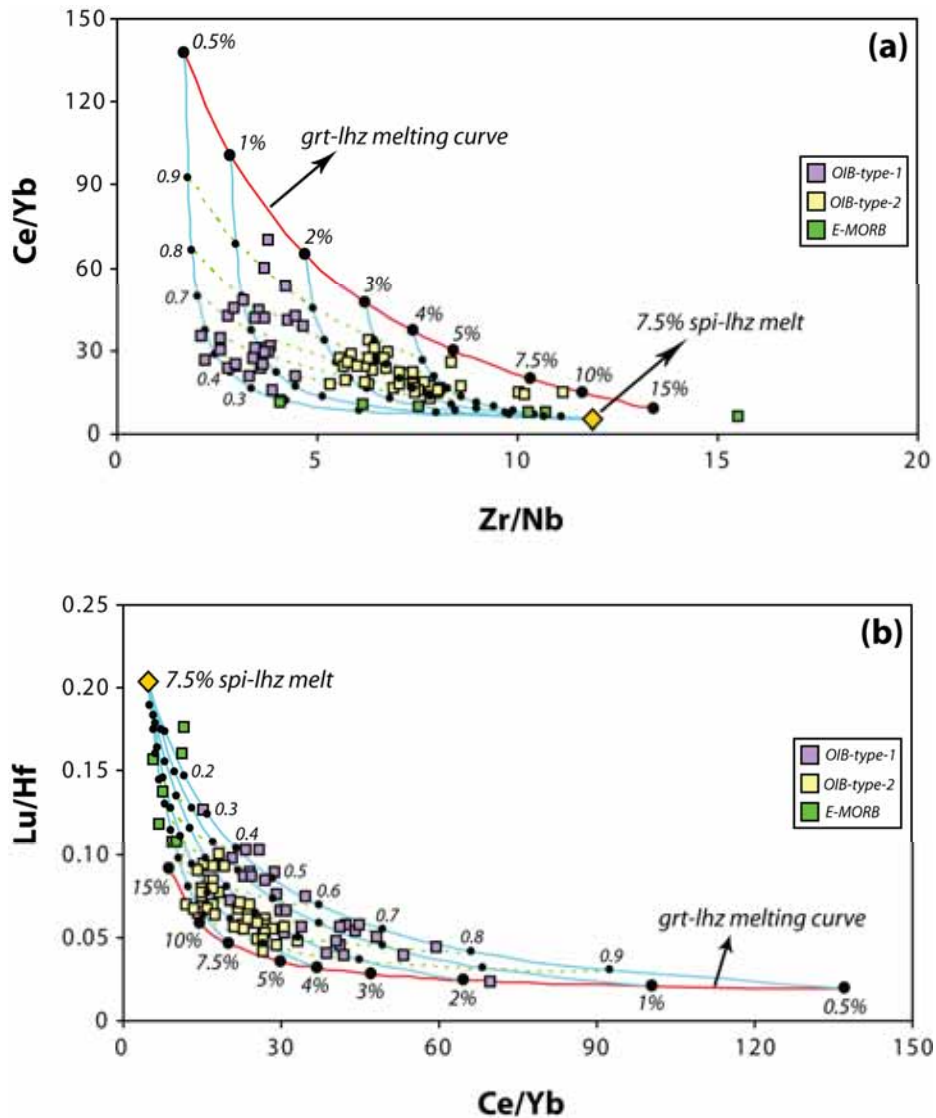
Figure 4.17. Geochemical modeling of the OIB- and E-MORB-type Nilüfer metabasic rocks using non-modal batch melting. Both mantle sources were assumed to have primitive mantle (PM) composition given by McKenzie and O'Nions (1991), except for Zr and Nb which are from Hofmann (1988). Numbers on the garnet-lherzolite curve indicate the percentage of degree of partial melting. 7.5% spinel-facies melt is indicated by a light-orange colored diamond. Aqua-colored solid lines represent melt-mixing lines and the corresponding numbers indicate the percentage of melt fraction contributed by garnet-facies mantle (e.g. 0.2 corresponds to 20%). The dashed lines represent melting curves which joins the melt compositions of equal melt-mixing mode.
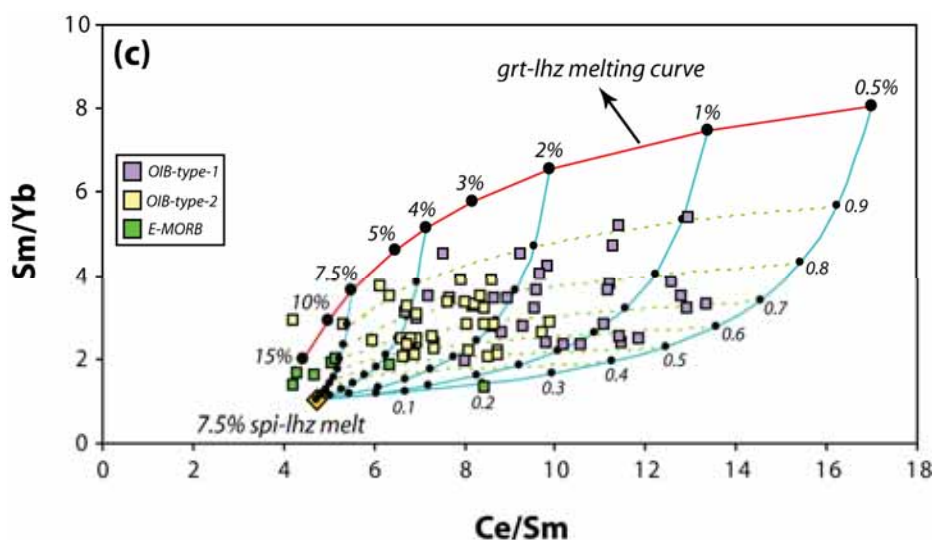
Figure 4.17 (continued).

partial melts generated at different depths. Therefore, in all three plots, I
constructed some mixing lines that were calculated on the basis of the end-
members represented by garnet-facies melts varying between 1% and 5% at the
one end, while 7.5% spinel-facies melt at the other. Both garnet-lherzolite and
spinel-lherzolite sources were assumed to be of PM compositions compiled from
McKenzie and O'Nions (1991) and Hofmann (1988). Regarding the garnet-
lherzolite melting curves, the source mode is taken from McKenzie and O'Nions
(1991), while the melt mode is from Haase et al. (1997). For the calculation of
spinel-lherzolite melt, both source and melt modes are taken from Haase et al.
(1997).

Neither pure spinel lherzolite nor pure garnet lherzolite is capable of creating the
partial melt compositions representative of most of the studied samples (Figure
4.17). The scattered distribution of the samples, however, can be explained by
melt-mixing involving variable contributions from both garnet- and spinel-facies
melts. The OIB-type group melts require the largest contribution from garnet-
lherzolite, with greater than 50% garnet-facies melt in most cases. In contrast, E-

MORB-type melts appear to be dominated by contributions from spinel-facies melts, with involvement of garnet-facies melt smaller than 50%.

Another important result is that although the OIB-type subgroups require approximately the same mixing proportions for their genesis, Subgroup 1 largely represents smaller melt fractions. The subgroup 2 melts are characterized by garnet-facies melts formed by 2-5% partial melting. The geochemical modeling presented here also may shed light onto the different Zr-Nb behaviors shown by OIB-type subgroups. It is apparent that increasing Ce/Yb at nearly constant Zr/Nb can be explained by melt-mixing involving small degree melt fractions (1-3%) of garnet-lherzolite (where the contribution of garnet-facies melt is between 40-90%) with spinel-facies melts (Fig. 4.17). This result supports earlier inferences that the distinct Zr/Nb behaviors observed in OIB-type group resulted from source-related processes, rather than from fractional crystallization or crustal contamination.

The ratio-based geochemical modeling presented above provides a good approximation on the degree of partial melting and melt-mixing phenomena for the E-MORB- and OIB-type metabasic samples. However, although the elemental ratios are good indicators to monitor the degree of partial melting, REE variations based on absolute abundances (i.e. REE variation patterns) may provide better constraints on this process. Since absolute abundances of trace elements (including REE) will be affected by fractionation/accumulation processes after partial melting, using primary or near primary melts is the best way to quantify the degree of melting and related mixing events.

Samples with MgO (wt.%) contents between 11% and 17% were selected to represent primary or near primary melts. Although these primary melt candidates may not reflect the entire primary REE variation spectrum observed in the dataset, they are representative of the majority of samples. Not all the variation patterns of the assumed primary melts are parallel (not shown); they clearly appear to be variably fractionated, suggesting different degrees of melt generation

and amount of mixing between garnet and spinel stability fields. To model the primary melts, non-modal batch melting equation of Shaw (1970) was used and the same procedure as in the previous section was applied. The calculation was performed on the 6 representative samples which best reflect the variability among the REE patterns.

As seen from Fig 4.18, the calculated melts appear to match very well with the observed melts (the compositions represented by samples), therefore they can provide a valuable insight for the melting systematics of the OIB-type suite. The results indicate that the OIB-type primary melts can be modeled by 1-4% melting of a garnet-lherzolite source with PM composition, which mixes at a ratio between 60-100% garnet-facies melt, and they are in good agreement with those obtained from the trace element modeling. Sample NIL-12 has a remarkable HREE depletion compared to the other primary samples, thus reflecting strong contribution from garnet-facies mantle. Indeed, the modeled melt suggests a 100% contribution from the garnet-bearing source which has undergone 3% partial melting.

To perform REE-based melt modeling of the Group 2 E-MORB-type melts, two samples were chosen with MgO contents greater than 8.5 wt.%. The E-MORB-type samples are not typical of primary melts like their OIB-type counterparts, as reflected by their somewhat low MgO contents varying between 8.7 and 9.0. Thus, in order to get more realistic results, the REE contents of the samples to be used in the modeling need to be corrected for fractionation. For this purpose, olivine with 88% Fo content (Fo_{88}) was added to the samples until their MgO reached 13.5 wt.%. This MgO composition was chosen to be consistent with the values used for the OIB-type samples.

The low REE concentrations of the E-MORB-type samples compared to OIB-type group requires either generation under relatively high degrees of melting, especially for sample GK-3 (~14%), or melting of a source that has experienced a previous melt extraction. The latter alternative is preferred as it requires lower

106
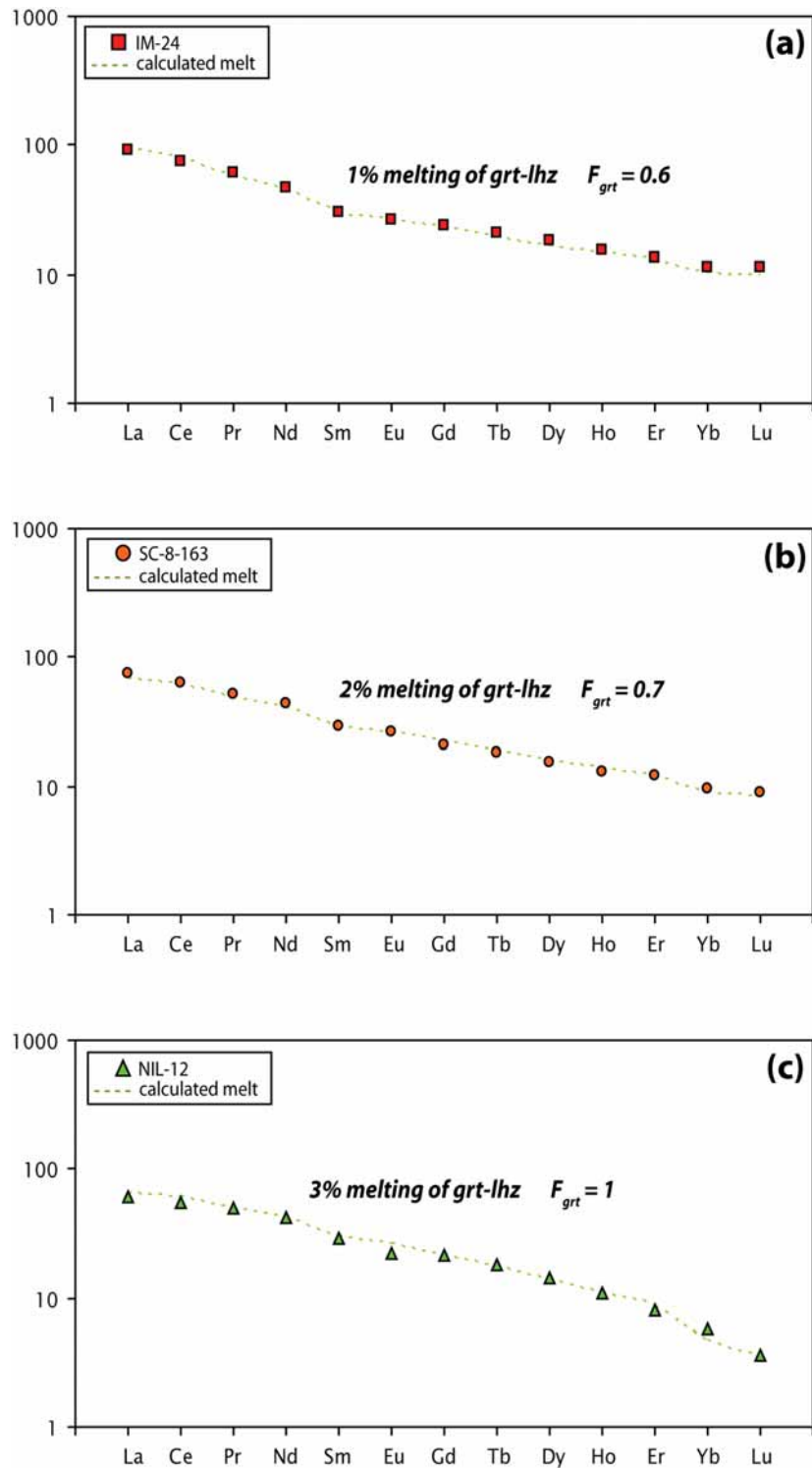
Figure 4.18. REE modeling (chondrite-normalized) of the selected primary OIB-type samples. "F_{grt}" corresponds to the percentage of melt contributed by garnet-facies mantle as in Figure 4.17. Normalization values from Sun and McDonough (1989).

107
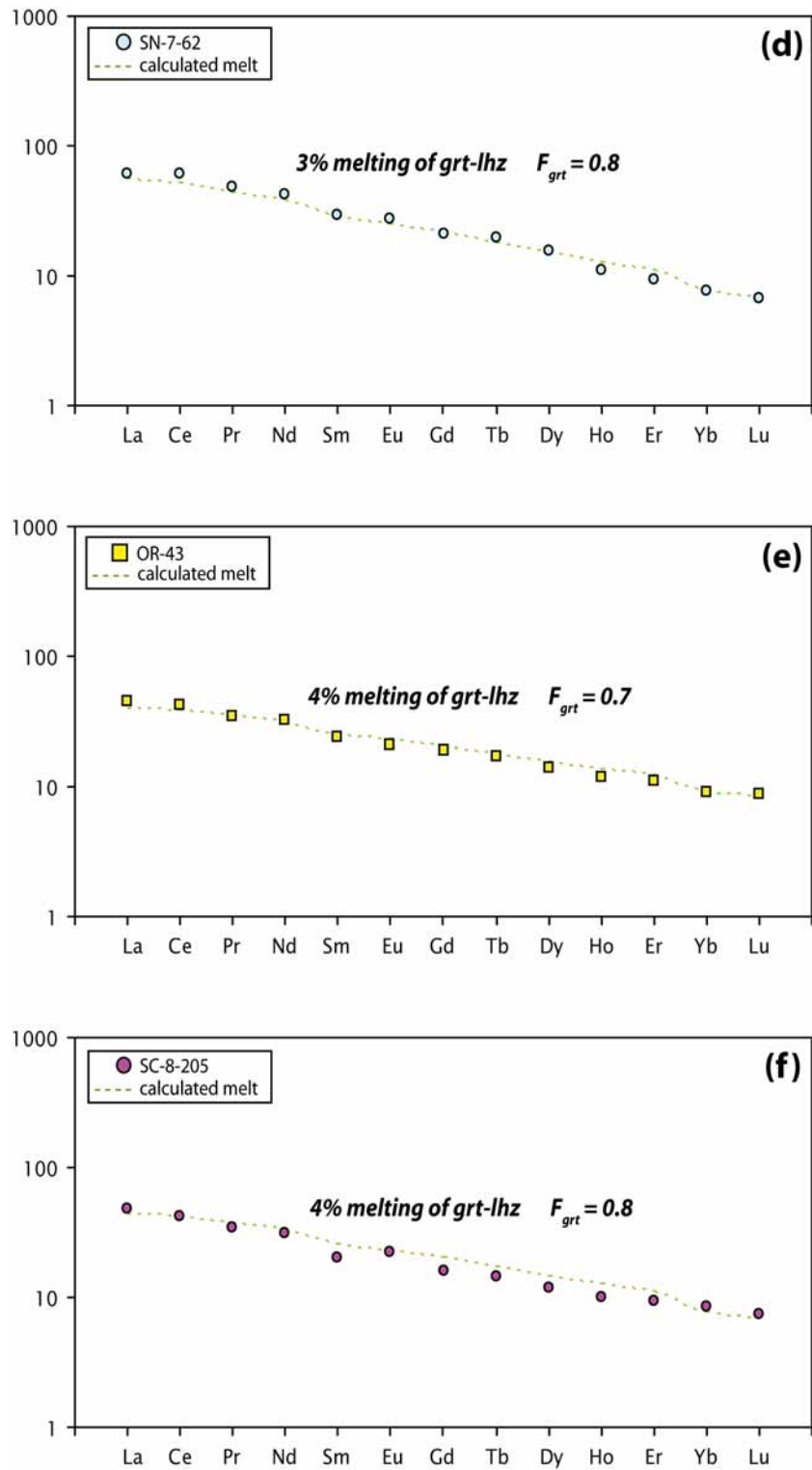
Figure 4.18 (cont'd).

degrees of melting that are more consistent with results obtained for OIB-type melts, and more importantly yields a better match between the calculated melts and the observed melts.

To model this physical scenario, I first removed 6.5% melt from garnet-lherzolite with PM composition (Source 1). Then, the residue was remelted at a fraction of 8%, and subsequently mixed with the varying degrees melts deriving from another garnet lherzolite source with again PM composition (Source 2). For both calculated melts, the contribution of the melts from Source 1 (previously melt-extracted source) was 80% (Figure 4.19). It must be noted a different modal mineralogy was used for the Source 1 relative to the Source 2 that includes the same modal assemblage used for the OIB-type melt modelling (see Figure 4.19 for the details). The calculated melts appears to fit quite well with the observed abundances for both samples. As seen from Figure 4.19, a smaller melt fraction (1.5%) is required from Source 2 to reproduce the sample OR-104, while GK-3 requires 3% garnet-facies melt from the second source, consistent with its less fractionated nature (i.e. low La/Yb).

4.3.4.2. SSZ-type (Group 3) samples

Assessment of influence of partial melting on the SSZ-type Eymir diabases was performed by two methods. The first method used is based on elemental ratios, very similar to that applied to the E-MORB- and OIB-type samples. The second method, on the other hand, uses absolute abundances of Nb and Yb that were corrected for fractionation to 9% MgO (wt.%). The reason for applying this MgO value is that the modeling curves were directly taken from Pearce and Parkinson (1993). These authors, in their work, constructed the partial melting curves on the basis of the values that had been corrected for 9% MgO to minimize the effects of fractional crystallization, thus providing a better estimation on melting conditions in SSZ-type systems.
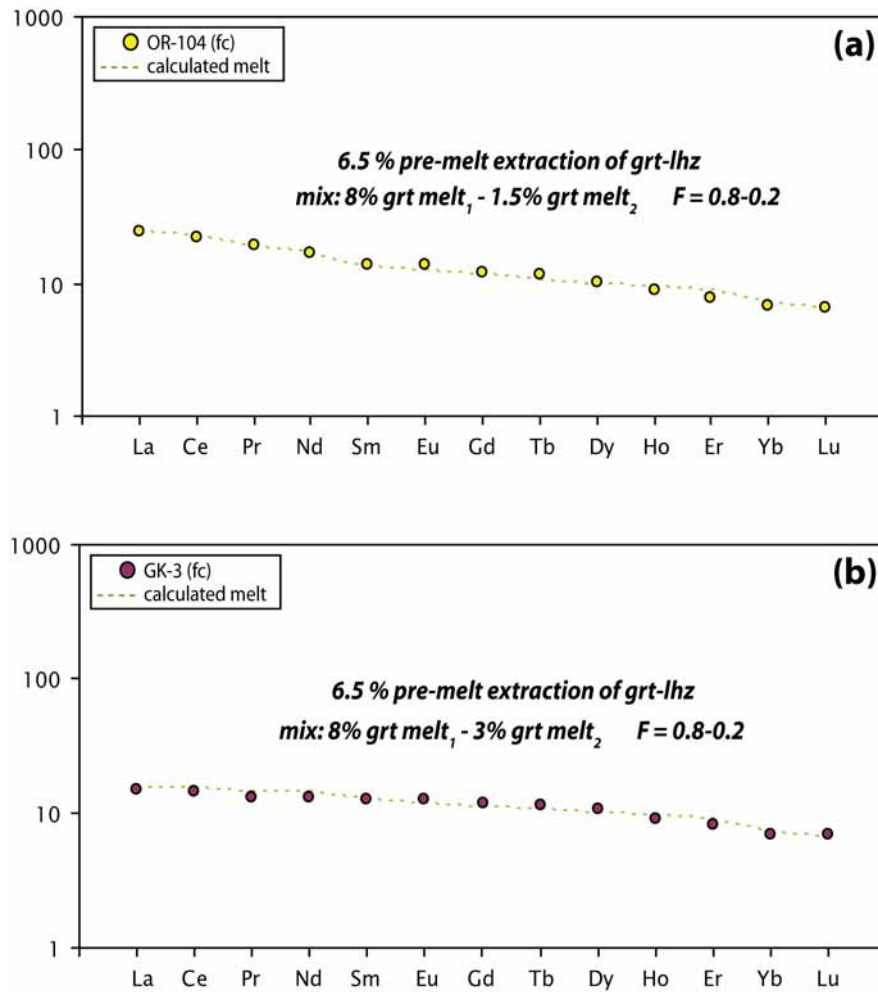
Figure 4.19. Modelling of the E-MORB-type samples. "FC" means the samples were corrected for fractionation before performing melt modeling. The subscripts "1" and "2" refer to the different garnet-lherzolite sources, namely Source 1 and Source 2. Regarding Source 1, the source and melt modes were presumed to have not changed after melt-extraction, and the source mode was assumed to be 0.595 ol + 0.195 opx + 0.150 cpx + 0.06 grt, which melts in the proportions given by Johnson et al. (1990). The source and melt modes of the Source 2 was assumed to be the same as that of garnet-lherzolite source in Figure 4.17.

For the elemental ratio modeling, Lu/Hf and Nb/Yb pairs were selected owing to their relatively immobile nature in hydrous conditions of the subduction zone systems as well as in post-magmatic processes (e.g. alteration, metamorphism) (e.g. Pearce and Peate, 1995). Furthermore, these elements do not partition into sediment melt as Th does (e.g. Elliot et al., 1997; Pearce and Stern, 2006), thus

110

they can provide good constraints on the degree of partial melting of the mantle source. The modeling was performed using non-modal batch melting equation of Shaw (1970). The mantle source were assumed to be of DMM composition and compiled from Hofmann (1988).

The ratio-ratio modeling indicates that the Eymir melts cannot be obtained by melting of a fertile DMM source (Fig. 4.20). However, ~5-7.5% melting of a fertile DMM source that has previously experienced a 2.5% degree of melt extraction can reproduce the observed composition of the Group 3 samples. Thus, this may further explain the reason of depletion in HFSE relative to N-MORB within this suite.
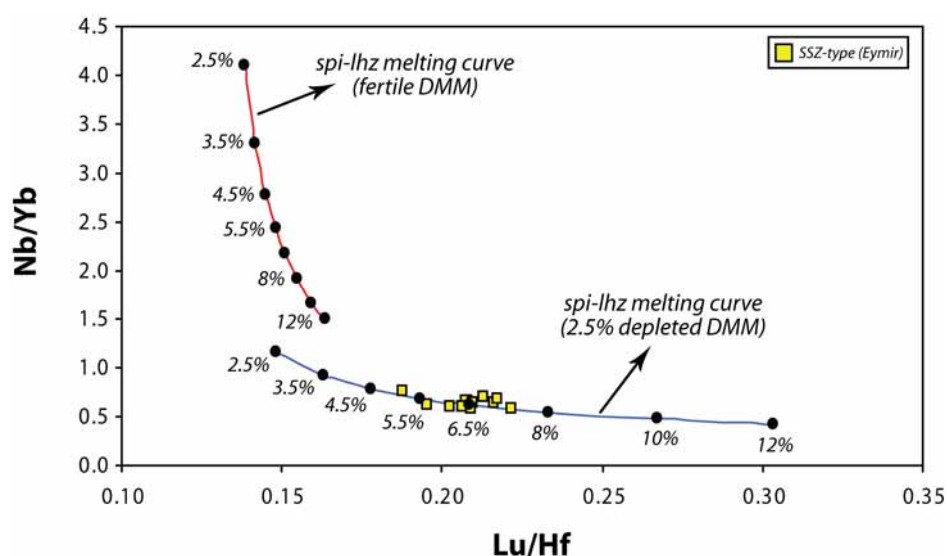
Fig 4.20. Ratio-ratio modeling of the Eymir diabases. DMM composition was taken as 1/10 of the MORB composition proposed by Hofmann (1988). The source mode for fertile DMM and the melt mode are from Kostopoulos (1991). After 2.5% melt extraction, the source mode was assumed to be 0.5813 ol + 0.2585 opx + 0.1376 cpx + 0.0226 spi on the basis of melting residues given by Kostopoulos (1991). The same melt mode was applied to the depleted DMM.

The second method, in constrast, uses absolute abundances of Nb and Yb, instead of using elemental ratios (Figure 4.21). To perform this modeling, first the samples with MgO greater than 5% were selected to obtain relatively primitive compositions as much as possible. Second, to further remove the effects of fractional crystallization on the studied samples, all the samples were corrected using least-squares best-fit lines to give a final MgO content of 9% (wt.%). It must be noted that in order to increase the sample resolution, two Eymir-type samples from the dataset of Sayit and Göncüoglu (2009) were also added and used for the fractionation correction and the modeling.
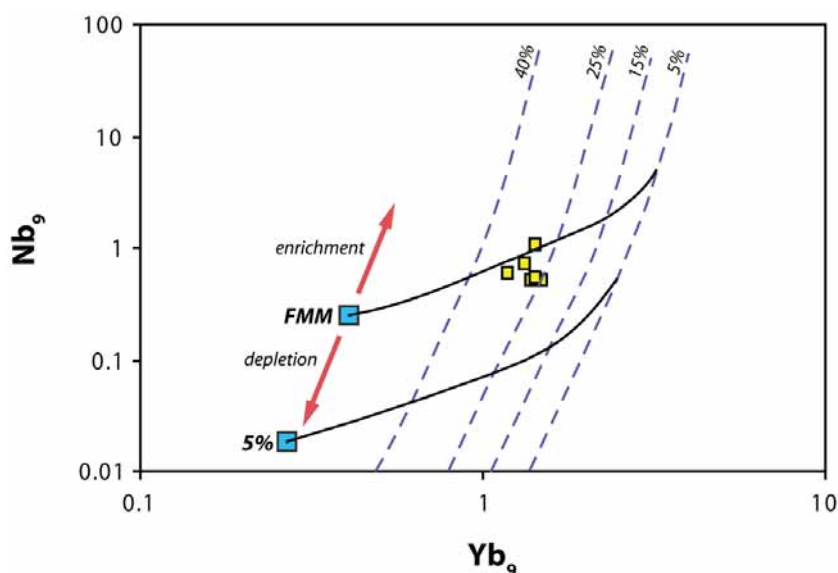
Figure 4.21. Nb-Yb modeling of the SSZ-type samples. The subscript "9" denotes the fractionation corrected abundance of that element. Modelling curves are from Pearce and Parkinson (1993). The solid black lines indicate the melting curves produced by melting of FMM and 5% depleted FMM sources. The dashed blue lines represent melting lines which joins the melt fractions that has experienced an equal amount of melting. For further details about the melting scheme used in the modeling, see Pearce and Parkinson (1993).

The modeling curves were adopted from Pearce and Parkinson (1993), which is based on non-modal melting of fertile and depleted FMM sources. This

modeling, however, differ markedly from the previous one in the sense that Pearce and Parkinson (1993) used different melting systematics, different distribution coefficients as well as different mantle source compositions. Although these clear differences, the resulting picture is consistent with the previous result that requires a previous melt extraction (smaller than 5%). However, the melting range appears to be different between these two models (~5.-7.5% vs. ~25-30%). Considering that the Eymir metadiabases reflect BABB-like character (see Chapter 5 for the details) on the basis their transitional character between N-MORB and IAT, the melting range recorded by the first model seems more realistic, since 25-30% degree of melting is rather high for the melting regimes observed in the oceanic back-arc systems. Gribble et al. (1998) suggest a total range of 6-24% for their "Spread BABB" from the Northern Mariana Trough. Stolper and Newman (1994) also report a similar range between 5-19% for the basaltic glasses from the same region. Similarly, Kelley et al. (2006) suggest a range of 5-15% for the melting of BABB. Pearce and Stern (2006) also propose a maximum of 25% melting for the generation of the BABB magmas. Therefore, of the two geochemical models presented here, the first one (ratio-modeling) with a total melting range of ~5-7.5% appears to be more appropriate for the genesis of the Eymir metadiabase dikes.

4.4. Discussion of the Geochemical Data Inferred from Nd-Pb-Hf Systematics.

The relatively large isotopic range of the OIB-type group as inferred from Nd-Pb-Hf isotope systematics may suggest derivation from a heterogeneous mantle source region. The limited Nd compositions of the E-MORB-type suite compared to the OIB-type imply a more homogeneous source region for their petrogenesis. The highly restricted isotopic variations displayed by the SSZ-type samples strongly implicate generation from a relatively homogeneous source. There appears to be no clear distinction between subgroups of the OIB-type group in terms of Pb isotope ratios. All the sample suites display Nd and Hf isotopic compositions higher than that of BSE, suggesting time-averaged incompatible

element depletion. Three OIB-type samples, however, have $^{143}Nd/^{144}Nd$ and $^{176}Hf/^{177}Hf$ values close to that of the BSE, thus indicating derivation from a less depleted mantle source relative to the others. Sample IM-28 of the E-MORB group, however, appears to have the lowest $^{143}Nd/^{144}Nd$ and $^{176}Hf/^{177}Hf$ ratios compared to the other E-MORB and OIB-type samples, suggesting its more depleted character. This indicates DMM reservoir may have provided an important contribution during the genesis of this sample. It must be noted that all E-MORB-type samples except for IM-28 exhibit similar Nd isotopic characteristics with that of the more radiogenic group of the OIB-type suite. This may suggest that the mantle sources of these two suites were very similar.

It is observed that some of the E-MORB and OIB-type samples with similar $^{143}Nd/^{144}Nd$ have distinct Ce/Sm ratios, indicating recent fractionation of incompatible elements during partial melting (Figure 4.22). Two of the OIB-type samples (IM-24, OR-98), however, appear to trend towards slightly lower $^{143}Nd/^{144}Nd$ with high Ce/Sm values; suggesting that this slight negative trend can be linked to time-integrated evolution of Sm/Nd in the mantle source. It is noteworthy that sample IM-28, with relatively radiogenic $^{143}Nd/^{144}Nd$, also shows low Ce/Sm values that may indicate the involvement of a depleted component with high time-integrated Sm/Nd (i.e. DMM), thus in agreement with the previous interpretation. The less radiogenic OIB-type subgroup shows slightly lower Ce/Sm values, but markedly lower Nd isotope ratios than samples IM-24 and OR-98, indicating that the differences between the subgroups of the OIB-type suite has been inherited from their mantle sources with distinct isotopic compositions.

The Nd isotopic composition of the SSZ-type suite is somewhat close to some samples from the OIB- and E-MORB-type suites, and distinctly lower than sample IM-28. They also have distinctly higher $^{176}Hf/^{177}Hf$ than the E-MORB and OIB-type samples. These features may suggest involvement of a distinct component(s) (other than DMM) to explain the source characteristics of the SSZ-

type suite. A potential candidate would be a sediment component (e.g. sediment-derived melt) that has transported into the source region from the subducting slab.
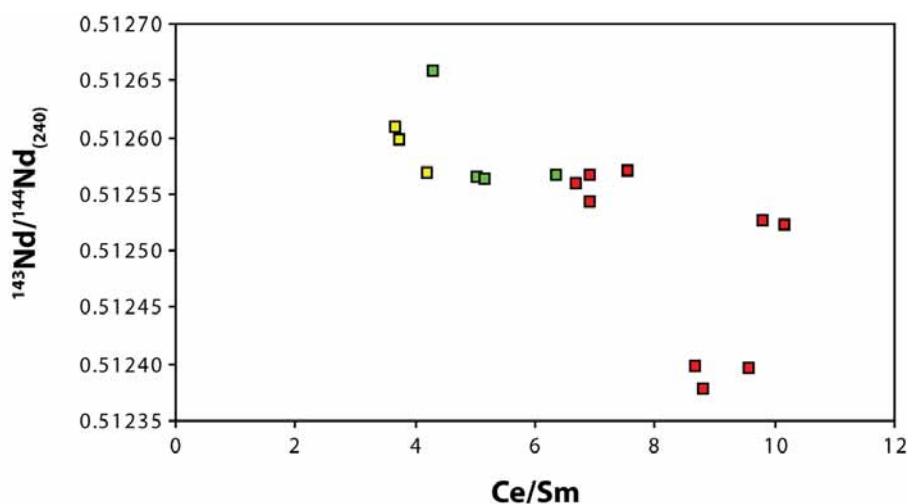
Fig 4.22. Ce/Sm vs ^{143}Nd/^{144}Nd plot, illustrating the close relationship between most of the E-MORB-type samples and OIB-type samples. The variation in Ce/Sm ratio at a given ^{143}Nd/^{144}Nd value, however, implies recent fractionation of the incompatible elements in response to partial melting.

As seen from Figure 4.6, the OIB- and E-MORB-type samples are dispersed in a way that they extend to higher Pb isotopic compositions. This trend may suggest the presence of HIMU as a potential end-member in the source region of OIB- and E-MORB-type suites. However, the particularly high Pb isotopic values of the two OIB-type samples appear to have resulted from post-magmatic processes. The Nb/U, Ce/Pb and Nb/Pb ratios of these samples were evaluated to gain insight into this question. These two samples have Nb/U ratios (47.0-59.8) which lie within scatter of oceanic basalts worldwide (47 ± 10; Hofmann et al., 1986) and uniform Nb/Th values (11.5-12.2). In contrast, Ce/Pb and Nb/Pb ratios are significantly higher (Ce/Pb = 50.4-52.1; Nb/Pb = 26.0-44.0) than average oceanic basalt values (Ce/Pb = 25 ± 5; Nb/Pb ~ 15; Hofmann et al., 1986; Sun and McDonough, 1989). This observation may indicate that the extremely radiogenic Pb isotopic characteristics of these samples have resulted from Pb loss during

post-magmatic processes, which seems to have extensively affected the Pb isotope systematics. Since the HIMU nature of these samples does not appear to be real (i.e. not a source feature), the Pb isotope ratios for these samples will not be considered any further.

4.4.1. Characterization of Mantle source(s) of the OIB- and E-MORB-type Suites

As noted in the previous section, the OIB- and E-MORB-type magmatic suites show striking similarity except for sample IM-28 from the former and the "less radiogenic subgroup" of the latter group. Although both groups display enrichment in the more incompatible trace elements relative to N-MORB, the OIB-type suite is clearly more enriched than E-MORB-type suite, and dominantly of alkaline character. The geochemical modeling results suggest that both suites require some melt-mixing processes to reproduce their observed compositions; however their mixing systematics appear to be quite different from each other. While the OIB-type group calls for a mixing scheme where end-members are represented by garnet-facies and spinel-facies melts, the E-MORB-type suite shows necessity for a mixing process where both end-members are of garnet-facies-derived. Furthermore, the latter group requires a previous melt extraction to recreate its relatively depleted composition.

The isotopic subgroups of the OIB-type suite are observed not to be consistent with the Zr/Nb systematics. Apart from one sample (OR-48), all the isotopically analyzed samples belong to "OIB-type 1" subgroup. Therefore, there are some samples that reflect the same Zr/Nb behaviour, but different isotopic characteristics (the first case). And, there is a sample that display distinct Zr/Nb behavior, but the same isotopic signatures with some samples (the second case). Such a result apparently suggests that the distinct Zr/Nb ratios of the OIB-type subgroups is not a source feature, but due to a recent process (i.e. melt mixing). The first case can be explained if the there are source regions (we can consider a mantle plume as the source due to the oceanic character of volcanism as reflected

by no crustal contamination and geological constraints) with distinct isotopic domains (a heterogeneous plume) that have experienced similar melt-mixing scheme. In the second case, however, similar isotopic domains will undergo melting with distinct mixing schemes.

Now, I will characterize the source region of the OIB- and E-MORB-type suites and discuss the potential mantle end-members involved in the genesis of these suites, leading to the observed heterogeneities.

To evaluate the possible mantle source domains involved in genesis of the OIB- and E-MORB-type samples, mixing curves were constructed using $^{143}Nd/^{144}Nd$, $^{176}Hf/^{177}Hf$, $^{206}Pb/^{204}Pb$ and $^{208}Pb/^{204}Pb$ ratios. FOZO was assumed as the common end-member (Hart et al. 1992), and the HIMU end-member was 2 Ga recycled oceanic crust based on the compositions given by Chauvel et al. (1992). EM II was assumed to represent recycled ancient oceanic lithosphere as suggested by Workman et al. (2004).

The calculated mixing arrays clearly indicate that the OIB- and E-MORB suites require multi-component mixing involving the FOZO, EM II and HIMU end-member in varying amounts (Figure 4.23). This observation suggests that the mantle source regions of these magmatic suites were heterogeneous. The contribution of FOZO is greatest in the case of the E-MORB-type samples, generally >50% overall, whereas OIB-type samples requires rather strong contributions from HIMU and EM II components. Based on the robust Nd-Hf isotopic space, it is observed that E-MORB-type sample OR-104 may reflect mixing only between FOZO and HIMU without needing a third component. In order to explain the compositions of the other samples, however, a third component (EM-II) is needed. To illustrate the effect of EM-II on for the origin of the other samples, a fourth mixing array was drawn, which emerges from FOZO towards the mixture between EM-II and HIMU. The composition of this mixture was selected as to comprise 90% EM-II and 10% HIMU. As seen from the Hf-Nd plot, those samples lie on or very close to the fourth mixing line,
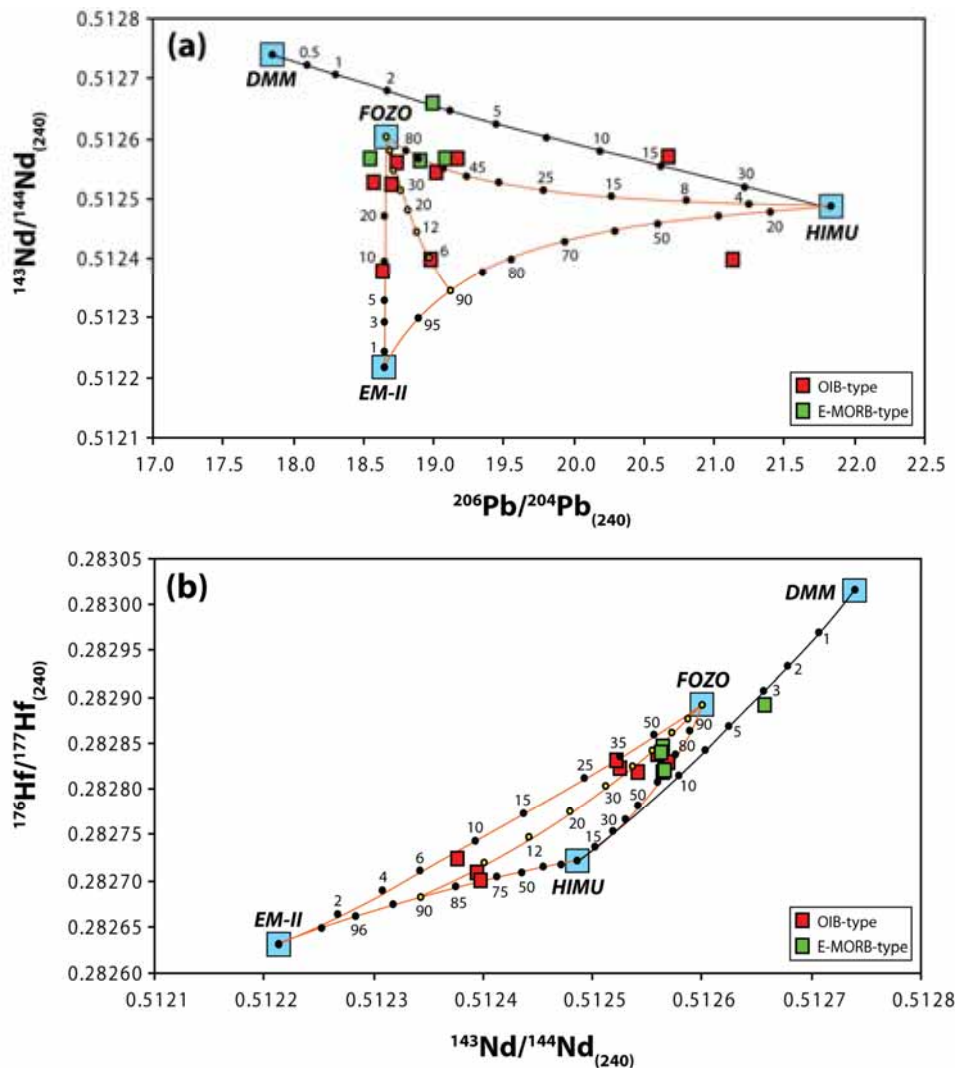
Figure 4.23. Mixing modeling on the basis of Pb-Nd, Hf-Nd and Pb-Pb systematics, explaining the possible origin of mantle source components of the E-MORB- and OIB-type suites. All the end-members were calculated back to 240 Ma based on the following compositions and assumptions. The present day isotopic composition of DMM is from Su and Langmuir (2003), while its trace element composition taken from Workman and Hart (2005). The present day isotopic composition of FOZO were assumed based on values given by Gibson et al. (2005) and Stracke et al. (2005). For the trace element composition, the least-enriched Walvis Ridge basalt (flow unit 3 of DSDP 527) analyzed by Gibson et al. (2005) was used; similar to their approach, but here the composition of that sample was used for the source not for the melt. The HIMU source were assumed as a 2Ga recycled oceanic crust, and its present day isotopic composition along with trace element composition and parent/daughter ratios required for its evolution are from Chauvel et al. (1992). The present day isotopic compositions of EM-II compiled from Workman et al. (2004) and Salters and Hart (1991). Its trace element composition from Workman et al. (2004).
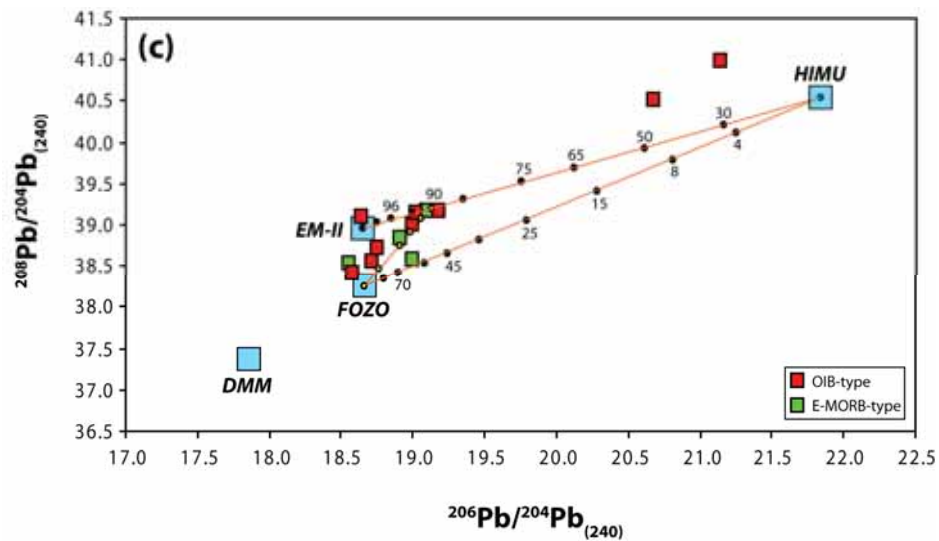
Figure 4.23 (continued).

contributed by 50% FOZO and 50% the mixture of HIMU-EM-II. Therefore, this indicates the necessity of multi-component mixing and that EM-II component has been also involved in the mantle source of the E-MORB-type suite.

In contrast to the E-MORB-type samples that can be explained by the involvement of FOZO, HIMU and EM-II, sample IM-28 with relatively radiogenic isotopic Nd probably requires a different mixing systematics. The radiogenic nature of this sample as compared with the others may suggest DMM as a potential source component. Indeed, as seen from Fig 4.23, it is obvious that this sample cannot be obtained by simply mixing FOZO with DMM. The relatively radiogenic $^{143}Nd/^{144}Nd$ nature coupled with somewhat radiogenic Pb isotopic compositions lead this sample to appear in a place that is bounded by DMM, FOZO and HIMU. The mixing calculations suggest that this sample reflects a mixture only between DMM and HIMU, and there is no requirement for FOZO to be involved in the mixing. It must be noted the contribution of DMM for the origin of IM-28 is really strong, being about 97%.

The origin of the OIB-type samples can also be explained in a similar manner, with multi-component mixing, though the contribution of the end-members is

119

quite different in some cases. Two samples from the OIB-type suite can be explained in terms of mixing largely between FOZO with HIMU, and possibly a small contribution from EM-II. In this case, the contribution of FOZO is rather dominant being more than 50%. Another two samples from this suite also requires mixing where again FOZO is involved, but EM-II being involved at this time. The influence of FOZO for these samples seems a bit weak, being smaller than ~35%. Another two samples from the suite are observed to require different mixing systematics relative to the formers. These samples appear to reflect mixing mainly between HIMU and EM-II, with probable small contribution from FOZO.

Therefore, the mixing arrays constructed on the basis of age-corrected end-member components indicate that both OIB- and E-MORB-type samples (Group 1 and Group 2) require multi-component mixing to explain their isotope systematics of their mantle sources. It must be noted, however, that the mixing models presented are strictly based on both trace element and isotopic composition of the end-members, which, in turn based on the published values. So, they are highly sensitive to the values applied.

4.4.2. Characterization of Mantle source(s) of the SSZ-type Suite

For the generation of subduction-zone magmas, there are mainly two components that originate from the slab and contribute to the overlying mantle wedge: slab-derived fluids, and sediments or sediment melts (e.g., Gill, 1981; Hawkesworth et al., 1993; Plank and Langmuir, 1993; Elliott et al., 1997). The efficiency of these components on modifying the mantle wedge is variable; however, one of these components is generally seen to dominate over the other (e.g. Woodhead et al., 2001). Therefore, at this stage, it is important to decide what type of slab-component could have been more effective for the genesis of SSZ-type suite. To figure out this, several elemental ratios including Ba/Yb, Nb/Yb, Ba/Nb and Th/Nb were first used before proceeding with isotope ratios (Figure 4.24).
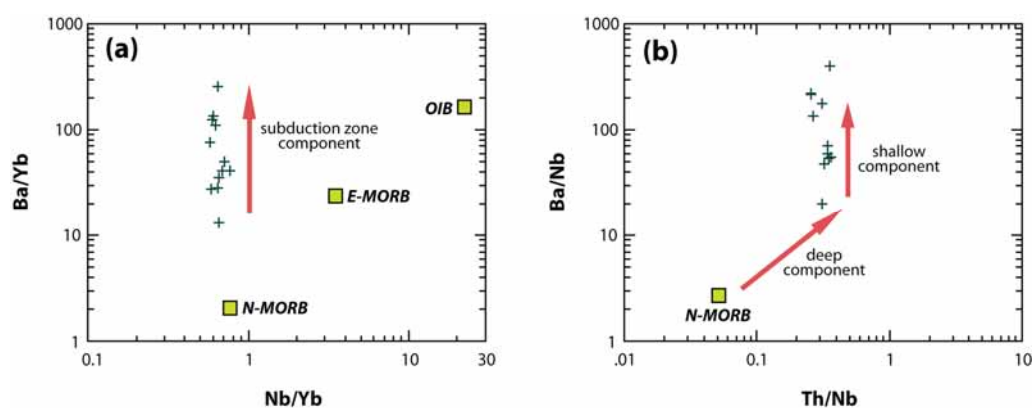
Fig 4.24. Ba/Yb-Nb/Yb and Ba/Nb-Th/Nb plots (based on Pearce et al. 2005), indicating the influence of subduction zone components on the SSZ-type Group 3 samples. It is also apparent from the diagram that DMM is a potential mantle end member for the origin of SSZ-type suite. Average N-MORB, E-MORB and OIB are from Sun and McDonough (1989).

The altered nature of the SSZ samples makes conventional assessments of trace element distributions in slab-derived fluids difficult. The LIL elements (except Th) are known to be fluid mobile, thus they can be transported to the mantle wedge region by aqueous fluids released at low temperatures (e.g. Pearce and Peate, 1995; Pearce and Stern, 2006). In contrast, subduction-mobile elements (e.g. LILE, LREE, Th, U, Pb) characterizes the behavior of sediment melt (or bulk sediment) generated at high temperatures (e.g. Elliot et al., 1997; Woodhead et al., 2001; Pearce and Stern, 2006). As a result, Ba/Th values can be considered a proxy for shallow subduction component related to low temperature aqueous fluids, whereas Th/Nb characterizes a deep subduction component related to high temperature sediment melts. Thus, Ba/Nb is an appropriate proxy for the total subduction component. In contrast, Nb/Yb is a stable indicator of mantle fertility and melting degree, since these elements cannot be modified by subduction processes (e.g. Pearce, 1983; Pearce and Parkinson, 1993; Gribble et al., 1998).

The SSZ-type samples have higher Ba/Yb ratios than average N-MORB (Fig. 4.24), thus this may reflect variable influence of subduction component related to mobility of Ba. However, since the samples have undergone low-grade

121

metamorphism, there is also a strong possibility that Ba has been remobilized. Indeed, when the samples with greater than 50 ppm Ba (sample DO-11 excluded) are plotted against LOI, there appears a positive trend, suggesting that the Ba contents of these samples have been partly controlled by post-magmatic processes, whereas there is no meaningful relationship obtained for the rest of samples (not shown). It is likely that sample DO-11B has been similarly affected given its very high Ba content (631 ppm). Although some samples appear to have been influenced by post-magmatic processes, the rest still have high Ba/Yb ratios (relative to N-MORB) indicative of a subduction component related to aqueous fluids.

A plot of Ba/Nb against Th/Nb (Fig 4.24) indicates that SSZ samples are displaced towards markedly higher Th/Nb and Ba/Nb than N-MORB. This observation clearly indicates that a deep subduction component has been involved during the genesis of these samples. This plot further supports the influence of slab-derived fluids as characterized by shallow subduction component.

Another important question is whether or not the Palaeotethyan plume mantle (as possibly represented by the OIB- and E-MORB-type Nilüfer samples based on this study) has influenced the compositions of the SSZ-type samples. Such a problem can be best revealed by trace element ratios, since isotope ratios can mislead owing to variable involvement of sediments into the mantle region. In the previously given Th/Yb-Nb/Yb plot (Figure 4.15), none of the SSZ-type samples (Group 3) appear to be directed towards the OIB compositions represented by Group 1 suite. Instead, they are displaced towards higher Th/Yb contents due to the presence of a sediment component, and follow a sub-parallel path with respect to MORB array in response to variations in degree melting. Another evidence comes from the Th/Nb-Nb/Sm variation (Figure 4.25), where the Group 3 samples clearly trend towards the sediment compositions represented by global subducting sediment (GLOSS; Plank and Langmuir, 1998) and the sediment melt (Hochstaedter et al., 2001).
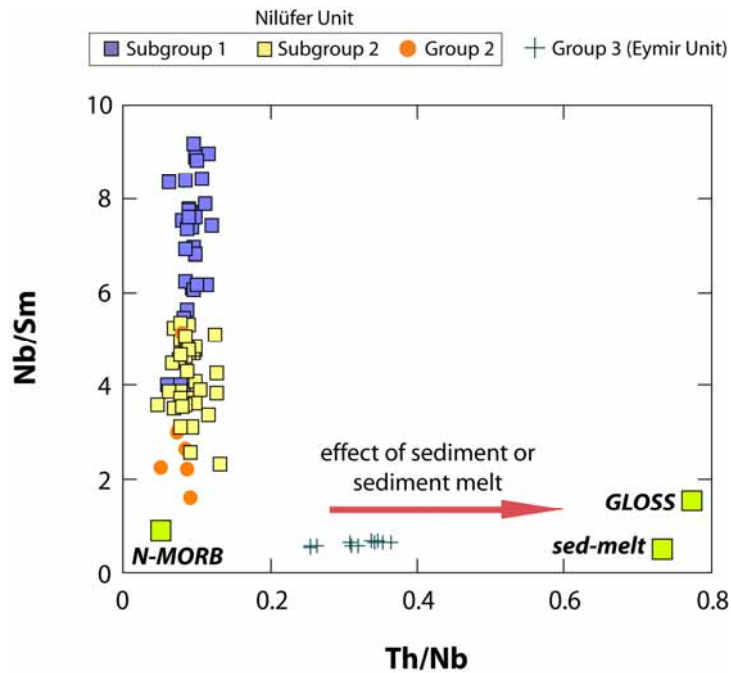
Figure 4.25. Nb/Sm vs Th/Nb plot, indicating that the SSZ-type samples have not been affected by enriched-type (plume) component displayed by OIB-type samples. Instead, they appear to have involved a strong sediment component as indicated by relatively high Th/Nb ratios. GLOSS from Plank and Langmuir (1998). Sediment melt from Hochstaedter et al. (2001). N-MORB from Sun and McDonough (1989).

For the isotopic characterization of possible source components involved in the genesis of the Group 3 suite, three end-members were used to construct the mixing arrays (Figure 4.26). The isotopic composition of the mantle wedge was assumed to have DMM composition, while the sediment melt and sediment fluid are assumed to have isotopic ratios 18.45 for $^{206}Pb/^{204}Pb$, and 0.5122 for $^{143}Nd/^{144}Nd$. This assumption was made, since the isotopic compositions of the sediments are known to be highly variable within subduction zones (e.g. Plank and Langmuir, 1998; Woodhead et al., 2001), thus the exact characterization of this component is very difficult to constraint.

To perform the mixing modeling, first an isotopic mixing array between DMM and sediment melt was constructed. Then, two specific compositions on this

DMM-sediment melt mixture were chosen, and subsequently were mixed with a sediment fluid component with the same isotopic composition as the sediment melt was used to create two additional mixing arrays. As seen from Figure 4.26, the calculated arrays fit very well with the compositions of the samples. Therefore, the observed compositions can be reproduced by mixing of a MORB-source mantle (DMM) with the 0.3-0.5% sediment melt, which, in turn, mixes with a ~0.1-1% sediment fluid. It must be noted that the effect of sediment (either as melt or fluid) on the mixing arrays is quite strong; only an amount of sediment melt/fluid smaller than 1% can considerably change the composition of DMM.
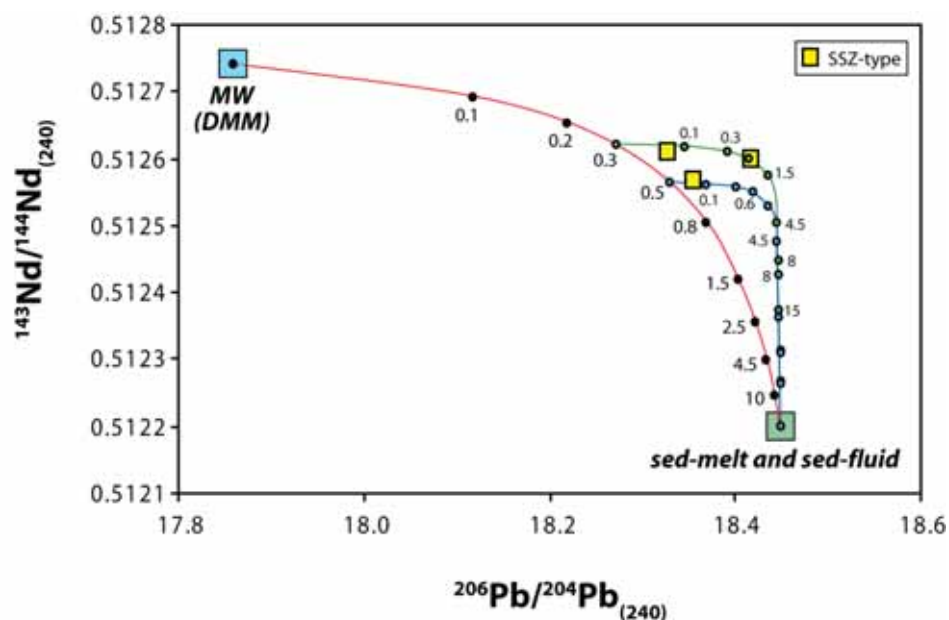
Figure 4.26. Isotopic mixing modeling of the SSZ-type samples on the basis of Pb-Nd systematics, highlighting strong influence of sediment components on the isotopic composition of the studied samples. Isotopic composition of DMM was taken from Su and Langmuir (2003), while trace element composition from Workman and Hart (2005). Isotopic compositions of sediment melt and sediment fluid were assumed as 0.5122 for $^{143}Nd/^{144}Nd$, 18.45 for $^{206}Pb/^{204}Pb$. Trace element composition of the sediment melt from Hochstaedter et al. (2001), whereas the sediment fluid from Class et al. (2000). Numbers on the curves indicate the contribution of the end-member on the mixture.

4.5. Overall Geochemical Evaluation

The geochemical examination of the studied metabasic suites reveals 3 distinct tectonomagmatic groups on the basis of immobile trace element chemistry. Two of these groups are of enriched trace element chemistry relative to N-MORB, namely OIB- and E-MORB-types, the latter of which being more depleted with respect to the former. The third group has a depleted chemistry as reflected by negative Nb anomaly coupled with HFSE abundances slightly lower than N-MORB. The OIB-type group is further divided into 2 groups according to differences in the Zr/Nb ratio.

The geochemical modeling highlights that the trace element compositions OIB- and E-MORB-type magmas have been controlled principally by melt-mixing processes involving spinel- and/or garnet-facies melt components. Unlike OIB-type suite, the E-MORB melts require a previous melt extraction event for their petrogenesis. The chemistry of depleted SSZ-type samples shows that garnet has not been a residual mantle phase during their genesis, and they have been formed by melting of a spinel-lherzolite source that has experienced a previous melt-extraction event. The isotope chemistry suggests that the OIB- and E-MORB-type samples have been derived from enriched mantle sources, and their isotope systematics reflect multi-component mixing for their origin. The SSZ-type suite, however, requires a different source mixing systematics, including a sediment component.

CHAPTER 5

DISCUSSION

5.1. General Evaluation

This study examines a huge metabasaltic mélange unit, named the Nilüfer Unit, within the Karakaya Complex, and its relation with variably metamorphosed and deformed clastics called the Eymir Unit, and the metadiabase dikes which intrude into the latter unit. In the extent of this study, these rock assemblages were studied in a wide region including the Ankara region (Central Anatolia), the Central Sakarya region and Bursa region (NW Anatolia). In the following, I combine the geochemical data with field data and petrography, and discuss the geological implications of these findings to shed light into the origin of the metabasic rocks, and also to highlight the geodynamical evolution of the Karakaya Complex and the Palaeotethys.

In brief, the Karakaya Complex has been a highly debated issue in spite of lots of works performed in this regard (e.g. Bingöl et al., 1973; Genç and Yılmaz, 1995; Okay et al., 1996; Göncüoğlu et al., 2000; Okay et al., 2000; Pickett and Robertson, 1996; Sayıt and Göncüoğlu, 2009a). Geochemistry-based studies, however, is not much; and most of them does not include a detailed examination and comparison on the geochemical nature of the metabasic rocks in question. In this respect, excluding the preliminary work of Sayıt and Göncüoğlu (2009a), this thesis presents a detailed geochemical and petrological interpretation based on a wide spectrum of trace elements including also REE. Furthermore, the new paleontological age findings introduced by this study provide better constraints on the time-space relationship to understand the geodynamic evolution of the

126

Karakaya Complex. This study is of particular importance in terms of geochemical grounds owing to the presence of isotopic data acquired from metabasic samples. Apart from these detailed geochemical examination and paleontological age findings, the large extent of the studied region in this study allows making a wide correlation between the rock assemblages. Below, all the findings acquired from this study will be discussed in detail in an order starting from geology, which is followed by petrography and geochemistry. And then, combining all of these data, a final geodynamic discussion concerning the tectonomagmatic evolution of the Karakaya Complex will be presented, and the significance of this huge subduction/accretion complex in terms of the Palaeotethyan realm will be discussed.

5.2. Reevaluation, Redefinition and Correlation of the Karakaya Units

The important point emphasized in this study is that the Karakaya Complex can largely be considered as a tectonic mélange that comprises several tectonostratigraphic units. In some places, these units reflect a clear block-matrix relationship, where the block size ranges from m- to km- scale. In this study, the key criterion for differentiating units is their tectonic setting, not the degree of metamorphism. Since in a subduction/accretion prism, a rock package that have derived from the same tectonic setting may experience different degrees of metamorphism depending on how deep the burial is, it is inevitable to encounter the rock assemblages with different type of metamorphism, but bearing the same geochemical signatures. Therefore, the type of metamorphism should not be taken as a constraint to differentiate between or correlate the mélange units.

One of these mélange units, which this study is mainly centered around, is the Nilüfer Unit of Okay et al. (1991). In this study, this unit was redefined mainly in the light of geochemical and geological constraints. The redefined Nilüfer Unit is mainly composed of metabasaltic rocks that are primarily associated with limestones, muds, and minor cherts (Figures 2.6 to 2.12). The metabasaltic lithologies are largely characterized by metabasaltic flows and their direct

derivatives, such as metavolcaniclastics and metavolcanic breccias. The important point about these metabasaltic rocks is that they reflect E-MORB and OIB-type geochemical signatures as also supported by many other works (Çapan and Floyd, 1985; Pickett and Robertson, 1996, 2004; Genç, 2004; Sayıt and Göncüoğlu, 2009a). Thus, these enriched-type geochemical features (relative to N-MORB) hold the major constraint in defining the new Nilüfer Unit. With this study, the widespread occurrence of the metabasic rocks with E-MORB- and OIB-type geochemical signatures has been clearly shown in a region extending from central to western part of the Karakaya Complex.

By the redefinition proposed by this study, any geochemical signature other than E-MORB and OIB is excluded from the context of the Nilüfer Unit. The other important point to note that the terrigenous metaclastic assemblages defined as the Eymir Unit here forms the matrix material in which the Nilüfer Unit is embedded. Therefore, the relationship between these two mélange units is not primary, but may have been incorporated during some later events following their formation. A similar view is also suggested by Sayıt and Göncüoğlu (2009a) which regards the Bahçecik metabasaltic assemblages (now included in the Nilüfer Unit) as megablocks within the Olukman-type metaclastics (now included in the Eymir Unit). According to Akyürek et al. (1984), however, these units (their Ortaköy and Elmadağ Formations) are primarily related, and represent the lithologies of the same tectonic environment, namely a continental rift. They further mention that their Ortaköy and Elmadağ Formations are transitional with each other. Koçyiğit (1987), on the other hand, accepts the mélange character of these units, but he suggests that these units were originally found together in a continental rift setting. This idea is also shared by Koçyiğit et al., (1991) which suggest that their Karakaya Group composed of the Kendirli Formation (arkosic sandstones), the Bahçecik Formation (volcanosedimentary succession) and the Olukman Formation (sedimentary mélange) display a transitional relationship. In this study, the primary relationship between the metabasaltic assemblages and metaclastics is not supported by this study owing to two reasons. First, there is no

continent- derived detritus found within the Nilüfer Unit as also supported by a number of studies (Pickett and Robertson, 1996, 2004; Okay et al. 1996; Sayıt and Göncüoğlu, 2009a). Second, the Nilüfer metabasaltic rocks reflect no continental contamination in terms of geochemical character. Third, the presence of some HP/LT varieties (HP-greenschists bearing Na-amphibole) within the Nilüfer metabasic rocks (e.g. Okay et al., 1991) suggests their cold burial into deep levels in a subduction zone. Such conditions can only be achieved by the subduction of an oceanic slab (e.g. Thompson and Ridley 1987; Bucher and Frey, 1994). Therefore, this may also indicate that the metabasic rocks of the Nilüfer Unit have been generated in an oceanic setting. The presence of high pressure metamorphism is not restricted only to the parts including schistose metabasics, but also found in the areas consisting of the non-deformed varieties. It is important to note that both schistose and non-schistose Nilüfer-type metabasic rocks display the same geochemical signatures, i.e. E-MORB and OIB, and thus they are of the same tectonic origin.

Concerning the Ankara region, the redefined Nilüfer Units covers the Bahçecik and Ortaköy Formations (Akyürek et al., 1984; Altıner and Koçyiğit, 1993; Sayıt and Göncüoğlu, 2009a). In this study, the geochemical characteristics of the pre-Liassic metabasic rocks were examined in a large region. The results show that, the metabasaltic blocks are invariably of enriched trace element signatures (with respect to N-MORB) and these metabasic assemblages of oceanic origin here redefined as the Nilüfer Unit can be traced towards the Biga Peninsula. Furthermore, the metabasic rocks which are evaluated within the context of the Emir Formation (Akyürek et al., 1984), the Upper Karakaya Nappe (Koçyiğit, 1987), or the Eymir Complex (Koçyiğit, 1992) are actually the blocks of Nilüfer Unit, Thus, the Emir Formation (Akyürek et al., 1984) or the Eymir Complex (Koçyiğit, 1992) can only be partially included in the definition of the new Nilüfer Unit, since this unit is made up largely of metaclastic lithologies. The most powerful evidence regarding this issue comes from the isotopic data acquired. The isotopic evaluation has shown that all the samples studied

(including previously named Ortaköy, Bahçecik, Eymir, Emir, Lower and Upper Karakaya Nappes) bear isotopic signatures inherited from involvement of enriched reservoirs (see Chapter 4 and the later discussion for details). Thus, the similarities of trace element characteristics and especially the isotopic signatures strengthen the idea that the metabasaltic blocks found inside the Eymir Complex also belong to the Nilüfer Unit.

In the Central Sakarya region, the Nilüfer Unit consists of the Tepeköy Metamorphics of Göncüoğlu et al. (1996), and a part of the Soğukkuyu Metamorphics. The new geochemical data from the metabasic rocks in this region is very similar to Ankara region; the metabasaltic assemblages again display enriched trace element signatures (OIB- and E-MORB-type). Moreover the Tepeköy Metamorphics (now included in the redefined Nilüfer Unit) which is believed to be of pre-Permian age (Göncüoğlu et al., 2000) may actually be Triassic in age. Although no fossil data has been found regarding the age of the Tepeköy Metamorphics, the similarities in terms of petrography and geochemistry between these metabasic assemblages and those from the Ankara region, and their similar association with limestones, mudstones and cherts may indicate that the Tepeköy Metamorphics constitute a continuum of the metabasic succession in the Ankara region. Another point worthy to mention is the presence and striking similarities between metapicritic rocks cropping out in the Ankara region (especially in the north of Hasanoğlan) and those found in the Central Sakarya region. These highly magnesian metabasaltic and metagabbroic rocks are found to be of OIB-type- and E-MORB-type signatures, and indicate a seamount/oceanic island setting as will be discussed in the subsequent paragraphs. This result is of particular importance, since these metamorphics were previously interpreted by Göncüoğlu et al. (2000) to have been formed in an intra-oceanic forearc setting.

Towards NW Anatolia, the newly Nilüfer Unit includes the Bahçecik Formation (Koçyiğit et al., 1991) and the Abadiye Formation (Genç and Yılmaz, 1995). In the Biga Peninsula, it covers the originally defined Nilüfer Unit of Okay et al.

(1991), the Çal Unit (Okay et al., 1991) and a part of Ortaoba Unit (Pickett and Robertson 1996). The main difference between the redefined and originally defined Nilüfer Units comes from the fact that the newly defined one covers some additional units that do not belong to the originally defined one. The similarity of Çal Unit with the Nilüfer Unit is inferred on the basis of the geochemical data reported by Pickett and Robertson (1996). Their data indicate that the Çal extrusives are of OIB-type signatures, thus consistent with the other metabasic rocks defined under the name of the redefined Nilüfer Unit. The Ortaoba Unit of Pickett and Robertson (1996) in Kazdağ area is also partially included within the context of the Nilüfer Unit as the geochemical nature of the metabasalts within this unit is also E-MORB and not N-MORB as originally suggested by these authors.

Towards the eastern parts of the Karakaya Complex, the metabasic rocks with N-NORB-like geochemical signatures from the Pulur Complex (Topuz et al., 2004) cannot be regarded as a part of the redefined Nilüfer Unit. However, a more detailed work is needed to discover the geochemical nature of the metabasic rocks in this area. The Tokat Massif is another place, where the geochemical identification of the metabasic rocks is unknown, but the geological relationships are studied in detail. Yılmaz et al. (1997) suggest that the Yeşilırmak Group comprises two main units that are related to each other with an unconformity; namely the Triassic upper unit and the Permo-Carboniferous lower unit. Based on the lithological observations reported by Yılmaz et al. (1997), it appears that only some part of Triassic portion of the Yeşilırmak Group can be regarded within the context of the redefined Nilüfer Unit. These authors, however, regard the entire Triassic Yeşilırmak units as a part of a single tectonic setting, i.e. continental rift. The age of the upper unit, however, seems a bit controversial. On the basis of their age findings within the Laçin Formation, which is the lowermost unit of the Triassic assemblage, they ascribe this unit to the Middle to Late Triassic interval. However, the authors place this unit to the Early Triassic period in their columnar section. At this point, it is probable that the lithologies from which they have

131

obtained the age (limestones alternating with clastics) are no older than Middle Triassic, similar to what is seen in the Ankara region. Furthermore, the clastic lithologies that they believe to be primarily related with metavolcanics may actually represent the matrix material in which the metabasic rocks are embedded.

There is no distinction between the metaclastics of the Olukman Formation (Koçyiğit et al., 1991; Sayıt and Göncüoğlu, 2009a) and the Eymir Complex. Thus, this study regards both units as parts of the Eymir Unit as previously mentioned. This interpretation is actually somewhat different then that of Akyürek et al. (1984), who suggests that these two units (corresponding to their Elmadağ and Emir Formations) are transitional. Koçyiğit (1987) and Sayıt and Göncüoğlu (2009a), however, propose that these units are related to each other by a tectonic contact. In this study, however, no distinct tectonic contact has been found between these metaclastic units. Furthermore, the degree of metamorphism and deformation of these metaclastic assemblages appear to be highly variable, thus it is not possible to make a distinction like the less- or non-metamorphosed Olukman (or Elmadağ) Formation and the more metamorphosed Eymir Complex (or Emir Formation). In this study, it was clearly observed that the intensity of metamorphism and deformation can change in a short interval. It is therefore suggested that these two metaclastic-dominated units, previously mapped under different names and regarded as separate units were actually the same, and named here as "the Eymir Unit". There is no thrust contact that can be traced for long distances found within the study area, which may show a clear evidence for their separation.

It is not true to separate the mélange units outcropping in the Ankara region as "less metamorphic" or "more metamorphic". This study clearly indicates that the part of the mélange previously interpreted as "less-metamorphic" (Koçyiğit, 1987) or "limestone blocky mélange" (Norman, 1973) bear imprints of elevated pressures as indicated by the presence of Na-amphibole within the Nilüfer-type metabasic blocks, very similar to what is observed in the other part named

"metamorphic blocky mélange" (Norman, 1973) that is interpreted as more metamorphic (Koçyiğit, 1987). It is very evident that both parts have been variably influenced by HP/LT metamorphism, and therefore it is not appropriate to make a distinction in terms of differences in the degree of metamorphism in the Ankara region and in the other parts of the Karakaya Complex. The main reason that has led to this problem seems to lie in the fact the mélange character of the Karakaya assemblages were obscured in many places. Consequently, this has resulted in the misinterpretation that the Karakaya assemblages are represented by individual allochthonous bodies (i.e. nappes) which display distinct metamorphic features compared to one another. However, as noted above, this study shows that there is no such distinction between the Karakaya assemblages, neither in the matrix lithologies, nor in the blocks.

5.3. Age Constraints

This study presents the first age finding acquired from the cherts primarily associated with metaclastics of the Eymir Unit in the Ankara region. This paleontological age finding is of considerable importance due to two main reasons: First, there is no age data ever found regarding the clastics of the rock assemblages previously known as "the Eymir Complex" or "the Emir Formation". Second, for the first time a radiolaria-based age has been reported from the metaclastics in the Ankara region. Third, this is the first age finding acquired from a chert layer primarily associated with metaclastics in the Ankara region. The Late Triassic age finding obtained from this study is consistent with the previous works (Akyürek et al., 1984; Özgül, 1993) that suggest a similar interval regarding the age of clastics in the Ankara region. Based on the foraminiferal fauna acquired from limestones, Akyürek et al. (1984) suggested a relatively wide interval, namely Early-Middle-Late Triassic, for the age of the Eymir Unit (their Elmadağ Formation). It must be noted, however, that the former age findings acquired thus far (from syn-sedimentary layers, not from the olistoliths) are all based on foraminiferal fauna found in neritic limestones apart

133

from that of Göncüoğlu et al. (2004). The in-situ Carnian (Late Triassic) radiolaria finding obtained in this study, therefore, is of crucial importance in the respect that it reflects installation of a relatively deep basin during Late Triassic. Although, the age finding of Göncüoğlu and his coworkers are also based on syn-sedimentary chert layer within metaclastics, they reported a Chanxingian (Late Permian) age. This large difference may imply some important insights regarding the geodynamic framework of the Karakaya Complex. If the Late Permian arkosic sandstone succession is indeed overlain unconformably by Triassic units as suggested by Göncüoğlu et al. (2004), then there appears a clear distinction between these clastics and those from the Ankara region.

The presence of the Gondwanan-type shallow water Permian limestones in both areas is more consistent with the previous idea which suggests that the Late Permian metaclastics have developed in a rift basin. The Late Triassic metaclastics, on the other hand, should have developed in a different tectonic environment. Such an idea is consistent with the Rhaetian-Norian neritic limestone (the Kaşal Limestone) within the Hodul Unit (now defined as the Eymir Unit) that is interpreted to represent in situ carbonate deposition with the clastics (Okay and Altıner, 2004). The Late Triassic conodont finding of Önder and Göncüoğlu (1989) from the recrystallized limestone found within the İznik Metamorphics further supports this result. At this point, it is also important to mention that this recrystallized limestone interbedded with chert and mud is bounded at its top and bottom by the terrigenous clastics which comprise metabasic lithologies (Göncüoğlu et al., 1986). These clastics, in fact, may be associated with these metabasic rocks with a block-matrix relationship, analogous to the situation seen in the Ankara region. Therefore, the clastic assemblages evaluated under the term "İznik Metamorphics" can be regarded as the equivalent of the Eymir Unit redefined in this study. The metaclastic assemblages alternating with carbonates found to the NW of Domaniç may also be considered within the context of Eymir Unit. The carbonates interbedded with these clastics have yielded a Late Norian age (Kaya et al., 2001), in agreement with the other age

findings noted above. Therefore, there are several lines of evidence that constraint the age of the Eymir-type clastics to a Late Triassic age. For example, the Kaşal limestone of Okay and Altıner (2004) characterize a shallow-marine deposition as compared to the deep-sea sediments (e.g. radiolarian cherts) of the same age from the Ankara region (this study) as well as the micritic limestones in the Armutlu Peninsula (Önder and Göncüoğlu, 1989). It can be inferred that both shallow and deep-marine environments have been developed probably in small basins during Late Triassic time. Another alternative may be to consider the Late Triassic limestone as a part of a Palaeotethyan oceanic island. However, if the relationship between the limestone and continental clastics is primary as suggested, then it seems not probable that the Kaşal limestone has been developed on the top of a seamount owing to continental nature of the associated clastics. Taking into account the fact that the formation of the Karakaya subduction/accretion complex took place in the latest Triassic, it may be possible that the Late Triassic deep-sea record found in the Ortaköy area characterizes small-scale piggy-back-type basins that were formed on the accretionary prism during the closure of the Palaeotethys.

Another age finding acquired from pelagic sediments comes from the work of Okay and Mostler (1994). However, in their study, they report ages acquired from pelagic limestone-chert blocks embedded in the redefined Nilüfer Unit (Çal Unit of Okay et al., 1991). On the basis of conodont and radiolaria fauna found in these blocks, they suggest Middle Carboniferous and Early Permian ages. The latter age, however, has been reevaluated as Late Permian by Kozur (1997). Although their age data do not come from a syn-sedimentary carbonate layer which would give a direct age of the unit, these pelagic "block" or "olistolith" ages are still of crucial importance, since they are indicators of a deep sea environment as old as Carboniferous. The Late Permian age is actually consistent with the Chanxingian age reported by Göncüoğlu et al. (2004), and both studies may indicate a similar deepened rift basin during Late Permian. The Middle Carboniferous chert block of Okay and Mostler (1994), however, should

definitely indicate a distinct pre-Karakaya environment, at least compared to the rift succession in the Geyve area.

5.4. Origin of the Post-Accretionary Metadiabase Dikes

Although the presence of diabase dikes cutting across the Eymir metaclastics was previously reported by Akyürek et al. (1982), petrological features of these dikes in İmrahor (Ankara) has been presented by Sayıt and Göncüoğlu (2009a). In this study, these metadiabases were sampled in a much wider region. Their geochemical characteristics indicate an intra-oceanic SSZ-signature and show striking similarities with those discussed in Sayıt and Göncüoğlu (2009a), Therefore, the Eymir metadiabase dikes probably represent the products of the same volcanic activity, and their subduction-related characteristics make them entirely different compared to the Nilüfer metabasics that reflect E-MORB- and OIB-type signatures. This result is especially important, because Akyürek et al. (1984) regard these dikes as the feeders of the Nilüfer-type volcanics (their Ortaköy Formation). This study together with the work of Sayıt and Göncüoğlu (2009a), however, draws a clear distinction between the geochemical nature of the Eymir metadibases and the Nilüfer metabasics, indicating that the Eymir metadiabase dikes cannot be feeders of the Nilüfer metavolcanics.

A detailed discussion and comparison regarding the geochemical characteristics of the studied metabasic rocks can be found in the later paragraphs. The age of these dikes is a matter of debate. There is no relative or absolute age that has been reported so far. Sayıt and Göncüoğlu (2009a) interpreted these metadiabase bodies as syn- or post-accretionary, and regard that they are pre-Liassic in age, thus suggesting they are the last magmatic products related to the Karakaya Complex.

5.5. Metamorphism

Petrographically, both Nilüfer- and Eymir-type samples appear to have been variably metamorphosed mostly under greenschist conditions. This is evidenced by the development of albite+actinolite+epidote+chlorite paragenesis. The lower temperature (sub-greenschist facies) conditions are also encountered with the presence of Ca-Al silicates, such as, prehnite and pumpellyite. Locally, the OIB-type Nilüfer metabasic rocks also bear sodic amphibole as indicative of elevated pressure conditions. However, no lawsonite has been observed. Therefore, in terms of the uppermost pressure limits, the Nilüfer samples have remained within the boundaries of HP-greenschist facies conditions. The Eymir metadiabases, on the other hand, has been found to bear no sodic amphibole.

5.6. Petrographical Evaluation

For both the Nilüfer and Eymir metabasic samples, the most stable primary phase that has survived the metamorphism appears to be clinopyroxene. Kaersutite, observed as a late-stage primary phase in the Nilüfer metabasic rocks, is also observed to have preserved its original identity. The brownish and to a lesser extent pinkish colors of the clinopyroxene crystals found in the Nilüfer samples show their Ti-rich character (Ti-augite). In the Eymir metadiabases, on the other hand, the clinopyroxene phase is found to be rather diopsidic as indicated by their colorless nature. The presence of kaersutite in the alkaline Nilüfer-type rocks, confirms the high Ti-contents of these samples. In constrast to this Ti-rich amphibole found in the Nilüfer-type samples, the Eymir metadiabases include green hornblende as a primary amphibole phase. This hornblende is observed to replace diopsidic augite in most cases. This magmatic replacement is reflected by the clinopyroxene crystals rimmed by the hornblende. Regarding both Nilüfer and Eymir samples, plagioclase is mostly found to have lost its original composition, and observed as replaced by albite. In the Nilüfer metabasic rocks, olivine has been totally replaced by secondary minerals, including serpentine, chlorite and actinolite. The higher Mg contents of the Nilüfer-type samples,

137

compared to the Eymir samples, in general are indicated by the presence of abundant pseudomorphs after olivine.

5.7. Geochemical Evaluation

The geochemical investigation reveals that both evolved and primitive members are present within studied metabasic samples. The effect of post-magmatic processes is evident by the highly variable abundances of the fluid-mobile elements as well as LOI values. However, HFSE and REE have mostly remained undisturbed as reflected by their consistency in the multi-element patterns and well-defined trends against Zr. The studied samples are divided into 3 groups; OIB-type, E-MORB and SSZ-type. The OIB-type is characterized by the enrichment in the most incompatible elements with respect to N-MORB, and display highly fractionated REE patterns. The E-MORB-type group show enriched patterns relative to N-MORB, similar to the first group, but it appears to be more depleted. The last group, namely SSZ-type, is quite different than the other groups in that it displays a marked Nb anomaly coupled with Th enrichment, and has HFSE abundances similar, but slightly lower than N-MORB.

Apart from the E-MORB-type group which shows a very limited MgO variation, all the studied suites show the effect of fractional crystallization as indicated by the observed differentiation trends when plotted against MgO. Regarding the OIB-type suite, fractionation of olivine + clinopyroxene ± spinel has played an important role; however some samples reflect the effects of accumulation, mostly olivine. In the SSZ-type suite, oli + plag + clinopyroxene represent the early fractionation history; however in later stages Fe-Ti oxides together with hornblende join the fractionating assemblage. In the OIB-type group, ~15% MgO may represent the composition of the primary melts, whereas no sample representative of a primary magma found within the E-MORB- or SSZ-type suite.

The OIB- and E-MORB-type display lower Zr/Nb and Y/Nb ratios when compared with the SSZ-type, suggesting derivation from more enriched sources

and/or lower degrees of partial melting. The considerably high Zr/Nb of the latter group coupled with HFSE abundances lower than N-MORB, however, strongly imply that the mantle source of these samples was of a depleted composition (DMM or N-NORB source), and may have experienced higher degrees of melting. The plot of Zr/Y-Nb/Y, where all the OIB- and E-MORB-type samples plot on/above the ΔNb line, also confirms the previous interpretation, indicating a more enriched source region for this two groups with respect to the SSZ-type group which stays below the line. More importantly, this plot suggests a similar source region (enriched type) for the genesis of the OIB- and E-MORB-type groups. This result is supported by the isotope systematics of the studied samples, indicating that the OIB- and E-MORB-type groups have been derived from enriched sources (i.e. FOZO, HIMU, EMII), while the SSZ-group requires a depleted component (DMM) therefore, consistent with the interpretation inferred from trace element ratios.

The investigated samples all are away from any continent-derived effects. The absence of such an input in the OIB- and E-MORB-type samples is evidenced by their distribution along the MORB array in a Th/Yb-Nb/Yb plot as well as their low ratios of Th/Nb and Ce/Nb. Although the latter ratios appear to be high for the SSZ-type samples, the low HFSE abundances combined with very high Zr/Nb is indicative of an intra-oceanic origin, thus ruling out the effect of crustal contamination for this group. That all the studied samples do not bear any contamination signatures introduced by continental crust is clearly reflected by the fact that none of the studied suites displays a tendency towards the metaclastics of the Eymir unit.

The geochemical modeling shows that partial melting of neither pure garnet-lherzolite nor spinel-lherzolite can account for most of the variations observed within the OIB-type and E-MORB-type suites. Instead, their melting systematics can be explained in terms of melt-mixing requiring variable contribution from garnet- and spinel-facies melts. The OIB-type melts appear to have been generated by mixing of ~1-5% garnet-facies melt with 7.5% spinel-facies melt,

where the contribution of the former is generally greater than 50%. Although the petrogenesis of the OIB-type samples are attributed to mixing of melts derived from garnet- and spinel facies lherzolite, the origin of the E-MORB-type melts cannot be explained in the same way. Their REE modeling reveals that these samples requires melt-mixing, where a garnet-lherzolite source have undergone a 6.5% previous melt-extraction event, subsequently re-melted at a ratio of 8%, then mixed with ~1.5-3% garnet-facies partial melts derived from a fertile garnet-lherzolite source.

The genesis of the SSZ-type samples can be attributed to ~5-7.5% partial melting of a DMM source which has experienced a 2.5% previous melt extraction event. This result may further explain the reason of the depletion in HFSE in this magmatic suite.

The isotopic chemistry shows that the OIB-type suite reflects the greatest heterogeneity among the studied suites, while the SSZ-type group appears to be the most homogeneous. The more radiogenic subgroup of OIB-type suite display similar isotopic characteristics with the E-MORB-type suite, suggesting that they have been derived from similar source regions. The less radiogenic group, however, is of very dissimilar isotopic ratios, indicating a distinct source region for its genesis. The similar Nd-Hf isotopic compositions, but different Ce/Sm ratios shown by some OIB- and E-MORB-type samples imply a recent fractionation event (e.g. partial melting). The isotopic ratios clearly indicate that the distinct Zr/Nb ratios observed in the OIB-type group have been caused by a recent process.

The isotopic modeling using age-corrected end-members suggests that a multi-component mixing of FOZO, HIMU and EMII can explain the isotope systematics of the OIB- and E-MORB-type basalts. One sample (IM-28), however, requires somewhat a different mixing systematics relative to rest; including some DMM component for its origin. Therefore, on the basis of the mixing arrays, it is very evident that the source region of the OIB- and E-MORB-

type suites has comprised enriched isotopic domains. If the robust Nd-Hf isotopic space is considered, there are 3 such distinct domains within these suites. First of these groups is largely dominated by EMII component with minor FOZO and HIMU. The second group mostly requires FOZO and to a lesser extent EMII and HIMU. The last group is represented by sample IM-28, and calls largely for DMM and HIMU components.

The somewhat similar $^{143}Nd/^{144}Nd$ but markedly different $^{176}Hf/^{177}Hf$ ratios of the SSZ-type samples strongly indicate that a distinct component is needed to explain the petrogenesis of this suite. The geochemical nature of the SSZ-type group requires a depleted mantle wedge source (DMM) which has been modified by of slab-derived fluids and sediment melts. The involvement of these shallow- and deep-subduction zone components is well monitored by the trace element ratios, such as Ba/Yb, Nb/Yb, Th/Nb and Ba/Nb. The isotopic mixing modeling is also in good aggrement with this interpretation, indicating that both sediment melt and sediment fluid have been involved component. The that the SSZ-type suite can be attributed to a DMM component which first mixes with a 0.3-0.5% sediment melt, and then subsequently mixed by ~0.1-1% sediment fluid.

The presence of enriched isotopic domains with variable composition within the OIB- and E-MORB-type suites suggests a heterogeneous mantle plume source for the origin of the Nilüfer-type magmatism. The enriched nature of the samples excludes depleted asthenospheric source (DMM) as a source for this magmatism. Even if the asthenosphere may comprise some small-scale heterogeneities to give slightly radiogenic isotopic compositions (e.g. Haase and Devey, 1993), it is not enough to match with the degree of isotopic enrichment and heterogeneity observed within the OIB- and E-MORB-type suites. Furthermore, the asthenosphere-related magmatism would create a tholeiite-dominated magmatism, which contrasts with the alkaline-dominated nature the Nilüfer Unit. The presence of picritic metabasalts and metagabbros found throughout the study area constitutes another evidence supporting the plume origin for the genesis of the Nilüfer Unit comes from. The picritic or high-Mg magmas require mantle

potential temperatures higher than ambient upper mantle for their generation (e.g. Campbell and Griffiths, 1989; McKenzie and Bickle, 1988). Such anomalously hot conditions can be achieved only by involvement of a mantle plume. Therefore, the existence of the picritic samples further supports the plume origin of the Nilüfer Unit samples. Another constraint arguing for the plume-related genesis of these samples is the occurrence of Nilüfer magmatism over a relatively large time period. If the well-constrained Anisian-Carnian paleontological age (Middle-Upper Triassic) is taken into account, then this would correspond to a time interval of some 20 My for the occurrence of magmatism. Such a long-term magmatic event appears to be very consistent with the plume hypothesis to explain the Nilüfer magmatism.

The intermediate character of the SSZ-type Eymir diabases between N-MORB and IAB suggests that this group may represent a back-arc system rather than an arc environment. Magmas erupted on intra-oceanic back-arc settings are of highly variable compositions, displaying geochemical signatures between IAB and N-MORB (e.g. Gribble et al., 1998; Sinton et al., 2003). Although sometimes it is impossible to distinguish BAB basalts from IAT or MORB, BAB basalts are generally found to have influenced by a subduction component, reflecting the effect of subducting slab for their petrogenesis (e.g. Pearce et al., 1994; Gribble et al., 1996; Fretzdorff et al., 2002). A transitional nature intermediate between N-MORB and IAB can be observed on the Eymir metadiabase dikes, and this is evidenced by the HFSE patterns of these samples similar to N-MORB, but slightly more depleted and associated with a pronounced negative Nb anomaly. Although island arc display highly variable REE patterns, it is quite common to see relatively flat patterns in back-arc systems (e.g. Gribble et al., 1996). Therefore, the relatively flat REE patterns shown by the Eymir metadiabases are consistent with a back-arc origin. The absence of true N-NORB signatures coupled with the involvement of subduction components as reflected by trace element and isotope chemistry indicates that the Eymir back-arc system has not reached the mature stage where the seafloor spreading mainly operates the

extensional process. Instead, it rather appears to have remained in the initial rifting stage.

In the next section, I compare the geochemical findings as inferred by this thesis with the published geochemical data, and combine them with the geological and petrographical evidences to shed light into the geodynamic evolution of the Palaeotethyan Karakaya units, and their final incorporation in an accretionary prism during Late Triassic time.

5.8. Geodynamic Evolution of the Karakaya Complex and Its Significance for the Palaeotethyan Events

It is indisputably accepted that there have been a number of seaways (whether of small or gigantic size) that separate the continental fragments from each other during the geodynamic evolution of the earth. Of these oceanic seaways, collectively named the "Tethys", the one that is believed to have existed between Middle Palaeozoic and Early Mesozoic is known as the "Palaeotethys" (e.g. Şengör and Yılmaz, 1981; Şengör et al., 1984). The Karakaya Complex is of critical importance to understand the fate of this oceanic realm, since it holds records of the closure that occurred as a result of the collision between Laurasian and Gondwanan-derived plates.

Even though a number of models have been put forward regarding the geodynamic evolution of the Karakaya Complex, these arguments actually revolves around two main ideas, namely the rift model and subduction/accretion model (see also Okay and Göncüoğlu, 2004). The rift model, which was originally proposed by Bingöl et al. (1973), argues that the Karakaya Units have been generated upon a basement (or basin) in response to extensional regime installed in Early Triassic. This idea, though modified in terms of several aspects, has been followed by a number of researchers (Koçyigit, 1987; Altıner and Koçyiğit, 1993; Genç and Yılmaz, 1995; Göncüoğlu et al., 2000) and they generally tried to explain the opening of the basin via back-arc spreading (Şengör and Yılmaz, 1981). The geochemical character of the mafic rocks within the

Karakaya Complex, however, reveal that they are dominantly of OIB-like magmas derived from an enriched mantle source (Çapan and Floyd, 1985; Pickett and Robertson, 2004; Sayıt and Göncüoğlu, 2009a). There are various studies that favor the presence of oceanic-related structures, such as, a seamount (s), an oceanic island (s), an oceanic plateau, or a large igneous province (Çapan and Floyd, 1985; Pickett and Robertson, 1996, 2004; Okay, 2000; Genç, 2004; Sayıt and Göncüoğlu, 2009a). Compared with the widespread presence of OIB-type magmas, the mafic rocks characterized by BABB signatures, though not so extensive, are found in the Küre and Ankara regions (Ustaömer and Robertson, 1994; Sayıt and Göncüoğlu, 2009a).

Even though the subduction-accretion models appear to be more suitable for the genesis of Karakaya basaltic magmas compared to the rift model, they also reflect contradictory interpretations within themselves. Tekeli (1981), the forerunner of the subduction-accretion hypothesis, proposes that the magmatic rocks represent the products of arc-related setting and stated that these rocks together with the other rock lithologies have been incorporated into an accretionary prism, forming a tectonic mélange. Okay et al. (1996) also suggests a similar idea, arguing that the Lower Karakaya Complex (their Nilüfer Unit) was formed in an ensimatic forearc-intraarc basin. Below, in the light of the results obtained by this thesis presented above in detail, the geodynamic evolution of the Karakaya Complex and the related Palaeotethyan events will be discussed on a tectonomagmatic framework.

There is no doubt that the age of the Karakaya Complex in NW Anatolia is clearly of pre-Liassic. The mélange units of the Karakaya Complex are unconformably overlain by Early Jurassic clastics thus limiting the uppermost age of the complex to latest Triassic (Koçyiğit, 1987; Altıner et al., 1991; Okay et al., 1991; Koçyiğit et al., 1991). This age is apparently younger than the Early Triassic age proposed initially by Bingöl et al. (1973). This is probably due to that they did not regard the overlying sequence as the part of the Karakaya

Complex, although they were aware of the fact that the cover sequence was of the Middle-Late Triassic.

The latest Triassic age also marks the age of the common deformation phase that has resulted from the so-called "Cimmeride Orogeny". The trace of this orogenic event is evidenced by the presence of Nilüfer-type metabasic rocks bearing high pressure overprints. The most widespread of those rocks is observed as HP-greenschists (Okay et al., 1991; Sayıt and Göncüoğlu, 2009a) as also indicated by this study. The Ar-Ar phengite ages of the eclogites and blueschist metabasites from the Nilüfer Unit are found to be Latest Triassic (Okay and Monie, 1997; Okay et al., 2002), thus consistent with the geological results. Furthermore, the Late Triassic age as indicated by a number of studies (e.g. Leven and Okay, 1996; Okay and Altıner, 2004) also confirms that the regional deformation observed in the Karakaya Complex (consequently, the Sakarya Composite Terrane) is restricted to the latest Triassic interval.

The lowermost limits that define the age of an oceanic realm on which the Karakaya related units have been associated; however, is a matter of debate. This problem mainly results from the reason how the Karakaya-related entities have been interpreted in the Palaeotethyan framework. The continental-rift model (e.g. Bingöl et al., 1973, Şengör and Yılmaz, 1981, Koçyiğit, 1987, Altıner and Koçyiğit, 1993, Genç and Yılmaz, 1995) interprets the lithologies of the Karakaya Complex as the result of opening of an E-W trending basin on the northern margin of the Tauride-Anatolide Platform via back-arc spreading. This tectonic model was developed primarily to explain the presence of exotic limestone blocks as well as volcano-sedimentary assemblages composed mainly of mafic lavas interbedded with limestone and chert, greywackes and arkosic sandstones (Bingöl et al., 1973). However, in this case, the product is a small basin which does not reflect the main ocean, namely the Palaeotethys. Thus, this thought has led those workers to think a separate Karakaya ocean or basin that was isolated from the Palaeotethys. Consequently, the defenders of this idea suggest a Late Permian-Late Triassic period for the lifetime of this basin.

However, the presence of pelagic sediments of Late Carboniferous age (Okay and Mostler, 1994) requires the existence of a deep basin as old as Carboniferous. This is also supported by the Late Permian metamorphism age of the Nilüfer Unit reported by Topuz et al. (2004). Their work suggests that the subduction process was still ongoing in Late Permian, therefore indicating existence of a deep basin before that time.

The other line of thought, which relates the generation of the Karakaya Complex to a subduction/accretion prism, appears to be more appropriate solution. In this alternative, some of the Karakaya-related assemblages are regarded to be purely oceanic, such as seamount or oceanic plateau, and they, at the final stage, are incorporated to an accretionary prism during latest Triassic together with the other assemblages that derive from continental sources. Therefore, in the subduction/accretion model, initially put forward by Tekeli (1981), some of the tectonostratigraphic units should, at least, have developed on, or characterize the Palaeotethys itself. Such a model can explain the presence of pelagic lithologies which are of Late Carboniferous age, and the Late Permian metamorphic ages.

Initially put forward by Tekeli (1981), the subduction/accretion model itself, however, is a highly debated subject. The scenarios include seamount(s), oceanic island(s), and/or an oceanic plateau (Capan and Floyd, 1985; Pickett and Robertson, 1996, 2004; Okay, 2000; Genç, 2004; Sayıt and Göncüoğlu, 2009a) to be accreted during the closure of Palaeotethys. However, Okay et al. (1996), similar to Tekeli (1981), argued that the basaltic rocks were generated in an arc-related setting, and they were formed in an ensimatic forearc-intraarc basin. The paucity of SSZ-type mafic rocks relative to abundant E-MORB and OIB-type magmas within the Nilüfer Unit, however, suggest that this tectonic setting is not suitable for the genesis of these mafic lavas. The Eymir metadiabases and the Küre metabasalts, which bear SSZ-type signatures, on the other hand, are products of different magmatic event, and they will be discussed in later paragraphs.

An oceanic plateau origin, which is initally proposed by Okay (2000) and followed by Genç (2004) in his own terms, is not supported by the geochemical data obtained by this study. Oceanic plateaus are largely made up of basaltic rocks of tholeiitic character (e.g. Mahoney et al., 1993; Frey et al., 2000) as opposed to the alkaline character dominating the Nilüfer Unit (Capan and Floyd, 1985; Pickett and Robertson, 1996, 2004; Sayıt and Göncüoğlu, 2009a). The Kerguelen Plateau, for example, is composed of tholeiitic basalts covering more than 85% of the unit (e.g. Condie, 2001). In addition, oceanic plateaus are characterized by largely flat REE patterns (e.g. Floyd, 1989; Mahoney et al., 1993), which contrast with the OIB and E-MORB assemblages defining the redefined Nilüfer Unit that displays variable enrichment in LREE relative to HREE (Figure 4.2), and nearly flat N-MORB normalized incompatible trace element patterns.

In terms of the rift model, there is no compelling geological or geochemical evidence to support the suggestion that the Nilüfer basalts were emplaced in a continental rift setting (Pickett and Robertson, 1996, 2004; Okay et al., 1996; Sayıt and Göncüoğlu, 2009a). Within the Nilüfer Unit, there is no field evidence of continental crustal material in primary contact with these OIB- and E-MORB-type basalts. It is also significant in this context that the investigated basaltic samples characterizing the Nilüfer Unit display little or no crustal contamination as displayed by their geochemistry. Furthermore, a back-arc basin opened on a continental basement does not also seem to be a plausible model for the geodynamic evolution of the Nilüfer Unit, as the basaltic rocks lack any geochemical signature which can be attributed to a subduction-modified mantle (e.g. Ferrar Magmatic Province, Hergt et al., 1991). Hence, rift models with the involvement of continental crust do not appear to be suitable for the genesis of Nilüfer-type basalts considered in this study.

The Middle-Late Triassic (Anisian-Carnian) E-MORB- and OIB-like magmatism (without crustal involvement) suggests that oceanic islands and/or seamounts have formed on oceanic crust during this time interval (Sayıt and Göncüoğlu,

2009a). Although a seamount origin was previously proposed by Pickett and Robertson (1996, 2004) for the Nilüfer Unit, their interpretation was restricted only to the Nilüfer-type assemblages suggested by Okay et al. (1991) in NW Anatolia. Therefore, this study differs considerably from those of Pickett and Robertson in terms of both extent and terminology. Çapan and Floyd (1985) also proposed a seamount origin; however their study also remained very local compared to what has been suggested by this study.

The petrological model proposed by Sayıt and Göncüoğlu (2009a) suggests that the seamounts were formed nearby the Palaeotethyan spreading ridge in association with a mantle plume. According to their model, the OIB-like magmatism results from the partial melts directly derived from the mantle plume. The E-MORB-type melts, on the other hand, are the products of the melt-mixing that has occurred as a result of mixing of enriched plume derived melts coming from garnet-stability field with the depleted spinel-facies melts. According to this model, the depleted spinel-facies melts were derived from an N-MORB source, i.e. depleted asthenospheric mantle upwelling through the mid-ocean ridge. The enriched character of the OIB-type melts is confirmed,here as indicated clearly by isotope geochemistry (Figure 4.23). The presence of a depleted source for the generation of E-MORB-type melts as previously suggested by Sayıt and Göncüoğlu (2009a), however, is not confirmed by the current study (see Chapter 4), since the geochemistry of the E-MORB-type metabasic rocks reflects enriched isotopic signatures (Figure 4.23), suggesting that the source of the E-MORB-type melts should also have been an enriched source. This indicates that the magmatism creating these seamounts should have occurred away from a spreading center (if any). Therefore, the main mechanism that generates both type of melts (E-MORB and OIB) was probably the plume itself.

5.9. The Geodynamic Model Proposed by This Study

As displayed by the geochemical and geological evidences presented by this study as well as the previous studies, the redefined Nilüfer Unit characterizes

seamounts and ocean islands that were formed on the Palaeotethyan oceanic crust in association of a mantle plume. After explaining the possible tectonic setting of the Nilüfer Unit, the important questions are: what was the relation of these oceanic islands with the other oceanic assemblages, and how were they incorporated into a sedimentary mélange with continent-derived rocks (i.e. Paleozoic platform carbonates, arkosic sandstones and greywackes?

Among the ocean-derived lithologies in close relation to the Palaeotethyan oceanic lithosphere, the ones characterizing oceanic islands is now well-constrained on the basis of this study as well as many published works (e.g. Pickett and Robertson, 2004; Sayıt and Göncüoğlu, 2009a). These assemblages mainly include metabasalts bearing dominantly alkaline OIB signatures and their derivatives (e.g. pillow breccias, hyaloclastites) primarily associated with pelagic and neritic limestones as well as chert and mudstones. Although these oceanic-island-type assemblages are ubiquitously found, the metabasic rocks with N-MORB signatures, reflecting the Palaeotethyan oceanic crust itself, have not been revealed so far from the central and western sectors of the Karakaya Complex.

In contrast to the Nilüfer-type assemblages which include no terrigenous sediments, the Eymir Unit is composed largely of metaclastics that indicate an origin of a continental basement. These lithologies actually have misled the workers in interpreting the Karakaya Complex. This is mainly due to the fact that the mélange character of the Karakaya assemblages has been obscured. In most of the places, these clastic lithologies form the matrix that envelops the metabasaltic (the Nilüfer Unit) and limestone blocks. These clastics commonly appear as of Late Triassic age, while in a few places significantly older ages has also been reported.

Occurrence of the Na-amphibole-bearing metabasic rocks in the Nilüfer Unit suggest that these lithologies should have buried deep inside the subduction zone in relatively cold conditions. This evidence, together with the oceanic-island character of these metabasic rocks, is indicative of a subduction/accretion prism,

where the fragments of oceanic islands have been incorporated and chaotically mixed with the continental-derived lithologies.

In order to understand the geodynamic evolution of the study area between Late Palaeozoic and the latest Triassic, the well-constrained findings requires the following criteria to be taken into account:

1. The Karakaya Complex represents a subduction/accretion complex formed as a result of the subduction of the Palaeotethyan oceanic lithosphere.

2. The formation age of the complex is the Late Triassic, while its metamorphism age is the latest Triassic.

3. The oceanic lithologies incorporated into the accretionary prism represent oceanic islands and their platforms, and they are of Middle-Late Triassic age.

4. Within the accretionary material, there exist lithologies derived from continental and/or arc crust, and from a carbonate platform of Devonian-Permian age.

5. The Karakaya Complex rests upon a Late Palaeozoic continental crust fragment that belongs to the Sakarya Composite Terrane. The contact between them appears to be mostly tectonic, though primary stratigraphic relationships with some clastic units have also been reported.

6. At the end of Permian (Chanxingian), it appears that an OIB-type volcanic activity started at the northern margin of the Sakarya continental crust or on an oceanic basin (the Palaeotethys) to the north of that margin. This age constitutes the oldest age that has been proven to reflect the age of volcanism.

7. For the Palaeozoic reconstruction, it is more appropriate to start with the end of Permian, since there is no much data regarding that time interval.

Though highly speculative, it can be suggested that during Early Carboniferous, the southward subduction of the Palaeotethyan oceanic slab resulted in arc-type

magmatism producing the Söğüt-type assemblages and associated granitoid bodies (e.g. Yılmaz, 1981; Göncüoğlu et al., 2000) on the northern margin of the Tauride-Anatolide Platform (Figure 5.1). At the same time interval, a back-arc rift also developed to the south of the Söğüt arc (Göncüoğlu et al., 2007). This continental back-arc rift, however, could not pass into advance stages, and remained as a failed (aborted) rift as indicated by the absence of pelagic assemblages. In this chain of events, it must be noted that the Palaeotethys, representing the main ocean, is located to the north of the Sakarya Terrane. It can be further argued that the southerly-dipping subduction may also have resulted in the formation of the Küre-type oceanic crust on the Palaeotethys.

If the rift model (the first alternative) is integrated into the subduction/accretion model (the second alternative), a geodynamic model as the following can be proposed. During Late Permian, the continued subduction of the Palaeotethyan oceanic slab resulted in rifting of the northern margin of the Tauride-Anatolide Platform. This rift basin (will be called the Karakaya Rift Basin on the basis of this study), was opened on the assemblages represented by a Söğüt-type arc basement and an overlying carbonate platform of Tauride-Anatolide character. Alternatively, this rift basin may have been opened in response to a mantle plume rising beneath the Palaeotethyan lithosphere. However, in this case, one would expect a highly voluminous magmatism, such as the Oligocene flood volcanism in Yemen (Baker et al., 1996) or Parana-Etendeka flood volcanism (Peate, 1997). Thus, the first option, namely a back-arc rift-type opening, seems more applicable. The Karakaya rift basin became gradually deepened to the end of Permian, as reflected by the Changxingian cherts alternating with arkosic sandstones. While deeping during Early-Middle Triassic, the Permian and Carboniferous limestone blocks of varying sizes were incorporated within the sediments as a result of the gravity slides.
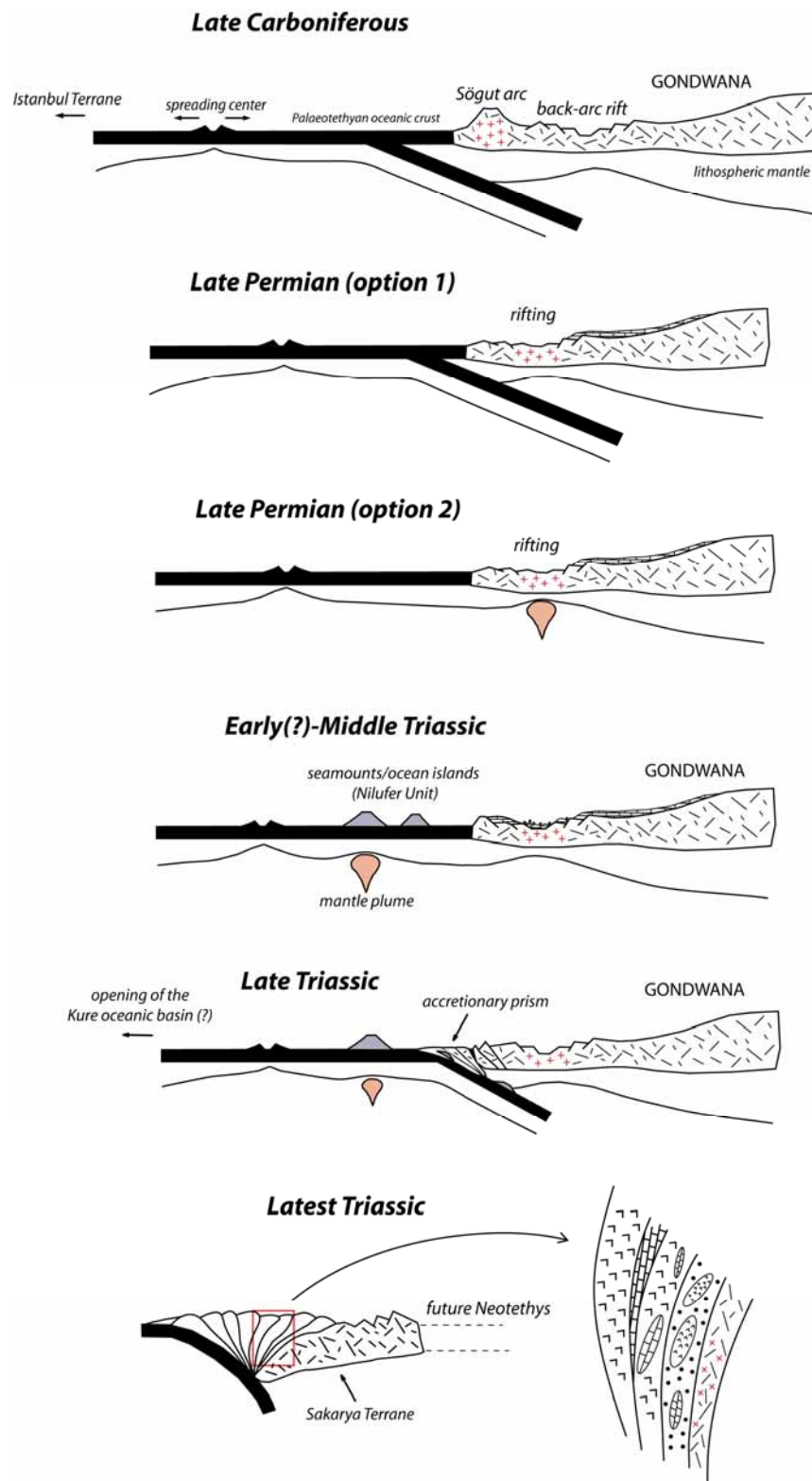
Figure 5.1. Geodynamic model for the evolution of the Karakaya Complex proposed by this study, integrating both rift- and subduction/accretion-related processes.

During Early?-Middle Triassic, the oceanic spreading brought the Palaeotethyan oceanic lithosphere over the mantle plume, resulting in mainly alkaline OIB-like magmatism with enriched geochemical signatures. These seamounts created in response to this mantle-plume related magmatism probably grew up to the sea-level or exceeded, and become oceanic islands that sit on the oceanic crust, as indicated by the Anisian neritic limestones interbedded with the metabasalts. In the deeper parts, the deep sea sediments (pelagic limestones, mudstones, cherts) have also been deposited synchronously with metabasalts along the flanks of the oceanic islands. The seamount/ocean island generation continued until early-Late Triassic as indicated by the Ladinian?-Carnian cherts interbedded with metabasalts in NW Anatolia (Sayıt and Göncüoğlu, 2009a). During the Late Triassic, with the ongoing subduction, the oceanic islands started to have been incorporated to the accretionary prism in front of the northern margin of the Tauride-Anatolide platform. The area of subduction/accretion was probably away from the forearc region where the active margin volcanism took place, and represented by a thin accreted mélange (Closs, 1984). The evidence for this comes from the intra-oceanic character of the metadiabase dikes cutting across the subduction/accretion prism. Here, the oceanic islands were sliced and mixed with material that derived from the Gondwanan carbonate platform and the Karakaya rift basin. Some of the slices with ocean island material in the subduction-accretion prism should have been deeply buried through the subducting slab as displayed by the development of Na-amphibole found in the Nilüfer metabasaltic rocks. In the deeper subducted slices, some of these metabasic rocks also experienced amphibolite and eclogite facies metamorphism (Topuz et al., 2004; Okay and Monie, 1997; Okay et al., 2002). During accretion, some small piggy-back-type basins were formed on top of the prism, and both shallow and deep sedimentation took place in these places. These small basins were the places where the Late Triassic clastics were deposited along with the Late Triassic cherts and limestones. Some of these clastics were later also incorporated with the metabasaltic rocks and buried to the deeper levels within the prism. At the end, with the closure of the Palaeotethys, the resulting picture is

a tectonic mélange characterized by pieces of dissimilar origin. This tectonic mélange includes in some parts fragments of oceanic islands chaotically mixed with the continental-derived clastics, while in some places comprises pieces of continental rift and its carbonate platform and associated sediments.

The fate of the Küre basin is behind the scope of this study but is worth to speculate. Most of the studies regard the Küre Basin as a small continental back-arc basin that has advanced into the mature oceanic stage (e.g. Ustaömer and Robertson 1994; Kozur et al., 2000; Stampfli and Borel, 2002; Moix et al., 2008), and they treat the Karakaya and Küre assemblages as representive of different basins. Okay et al. (2006), on the other hand, argue that there is no continental sliver observed which separates the Karakaya and Küre lithologies in the field; thus they assume that both were parts of the same ocean, namely the Palaeotethys. As indicated by their SSZ-type affinities (Ustaömer and Robertson, 1994), the Küre ophiolites are markedly different than the Nilüfer-type metabasic rocks which are dominantly of OIB-type trace element signatures (Figure 4.2). This striking difference shows that the Küre metabasalts should have represented a different type of tectonic setting. The intra-oceanic geochemical nature of the Küre extrusives away from any continent-derived effects suggests that it was probably characterizing an oceanic back-arc basin (e.g. today's the Mariana Trough, the Manus Basin, or the East-Scotia Ridge; Gribble et al., 1998; Sinton et al., 2003; Livermore, 2003) that had opened on the Palaeotethyan oceanic crust. Thus, in this study the Küre basin is treated as a remnant of the Palaeotethyan oceanic crust. In this respect, this interpretation is consistent with that of Okay et al. (2006).

The SSZ-type Eymir metadiabase dikes geochemically evaluated in detail are another matter of debate. In this study, the Eymir diabases are interpreted as the post-accretionary dikes intruding the Karakaya complex during closure of the Palaeotethys in latest Triassic. In the absence of any age constraints, these metadiabases are regarded as pre-Liassic because of the following reasons. First, based on the geological studies performed by Akyürek et al. (1984, 1996),

154

nowhere these metadiabase dikes appear to have intruded into rock assemblages which are younger than Triassic. Second, if they were the products of a younger closure event, i.e. Neotethys, they should have cross-cut a thick pile of the SCT including the basement, the Karakaya Complex and the overlying Mesozoic cover. In this case, it would be expected that the dikes should display continental contamination to some extent. However, no studied metadiabase samples show such a signature, therefore suggesting that these dikes should be probably of pre-Liassic and represent the magmatism related to the termination of the Palaeotethys.

CHAPTER 6

CONCLUSIONS

The Karakaya Complex is represented by a tectonic mélange that is composed of several rock assemblages of diverse origin which were chaotically mixed with each other during the latest Triassic as a result of the demise of the Palaeotethys. Among these mélange units, the Nilüfer Unit of Okay et al. (1991), which constitutes a part of pre-Liassic basement of the Sakarya Composite Terrane, is redefined and reevaluated in this study. The redefined Nilüfer Unit is represented by metabasic assemblages bearing OIB- and E-MORB-type signatures, which are interbedded with shallow- and deep-sea lithologies including neritic and pelagic limestones as well as mudstones and cherts. The Nilüfer-type assemblages can be traced along a wide region within the Karakaya Complex, extending from Central to NW Anatolia. To what extent the metabasic rocks cropping out in the eastern part of the complex can be evaluated within the definition of the redefined Nilüfer Unit; however, is a matter of debate.

The Nilüfer Unit is characterized entirely by ocean-derived assemblages; no continental detritus is included. The presence of HP-greenschist facies metabasic rocks (as reflected by the presence of Na-amphibole) suggests that the Nilüfer-type assemblages has been transported to deep levels through a subduction zone in relatively cold conditions. The presence of Na-amphibole is not only restricted to the foliated (schistose) varieties, but also found in the non-foliated lithologies. However, whether schistose or not, all metabasic lithologies within the Nilüfer Unit show the same geochemical signature, namely E-MORB- and OIB-type.

On the basis of the detailed trace element chemistry performed in this study, the Tepeköy Metamorphics, which were previously interpreted as an intra-oceanic arc by Göncüoğlu et al. (2000), are found to be of OIB- and E-MORB-type geochemical signatures, thus making them as a part of the Nilüfer Unit.

The Middle-Late Triassic age acquired from the neritic and pelagic limestones interbedded with the metabasalts in the Hacılar area is consistent with the previously suggested time interval for the generation of the Nilüfer Unit.

Regarding the Ankara region, it is not appropriate to separate the Karakaya units as "less" or "more" metamorphic. It is clearly shown by this study that the assemblages previously regarded as "less metamorphic" in the Ankara region do actually bear the traces of high pressure metamorphism. The intensity of deformation and degree of metamorphism is observed to change within short distances.

The Eymir Unit, which is the other redefined unit in this study, comprises variably deformed and metamorphosed clastic lithologies. The Eymir Unit constitutes the matrix material in which the variable-sized blocks of the metabasic rocks (the Nilüfer Unit) and limestones are embedded. The Eymir metaclastics are intruded by metadiabase dikes that display intra-oceanic SSZ-type characteristics. The Carnian age finding obtained from the radiolarians in a chert layer alternating with the metaclastics of the Eymir Unit indicates the presence of piggy-back-type basins formed on top of the accretionary prism during the closure of the Palaeotethys.

No paleontological or absolute age has been acquired regarding the age of the Eymir metadiabases. However, in the light of regional geological observations and non-contaminated geochemical nature of these dikes suggest that they are probably of pre-Liassic and represent the post-accretionary magmatism during the latest Triassic.

The Nilüfer metabasic assemblages have OIB- and E-MORB-type trace element signatures, whereas the Eymir metadibases are markedly different, displaying intra-oceanic SSZ-type signatures. As demonstrated by trace and isotope geochemistry, both Nilüfer and Eymir metabasic rocks show no evidence of contamination by continental crust. The absence of crustal contamination, but cross-cutting the metaclastic lithologies indicate that these dikes have probably intruded into a thin accreted mélange in front of the main accretionary prism.

The Nilüfer-type metabasic rocks, including both OIB- and E-MORB-type, are found to have been derived from a heterogeneous mantle source carrying enriched isotopic signatures (FOZO, HIMU, and EMII). The SSZ-type Eymir metadiabases, on the other hand, requires a depleted mantle source which has been modified by of slab-derived fluids and sediment melts.

This study proposes a geodynamic model integrating both rift and subduction/accretion models. As a working hypothesis, I suggest here that during latest Permian, the southward subduction of the Palaeotethys led to rifting on the northern margin of the Gondwana, forming a basin as represented by the rift succession observed in the Geyve region (Göncüoğlu et al., 2000, 2004). The Nilüfer Unit, representing the seamount(s) and oceanic island(s), was generated during Early(?)-Middle Triassic, while the plume affected the Palaeotethyan oceanic lithosphere, giving way to the E-MORB/OIB-type plume-related magmatism. During the latest Triassic, closure of the Palaeotethys resulted in incorporation of seamounts/oceanic islands and rift-related assemblages that became further associated with clastic material derived from peripheral forearc region of the accretionary prism. At the end, this chaotic amalgamation created what is known as the Karakaya Complex.

In order to provide further constraints on the geodynamic evolution of the Karakaya Complex, more studies are needed on the northern and eastern parts of the complex, especially regarding the geochemical characteristics of the

metabasic rocks cropping out in these regions. These geochemical findings, of course, should be supported by any paleontological or absolute age dating.

REFERENCES

Adamia, S., Bayraktutan, S., and Lordkipanidge, M., 1995. Structural correlations and Phanerozoic evolution of the Causasus-Eastern Pontides. In: Erler, A., Ercan, T., Bingöl, E., and Örcen, E. (eds.), Geology of the Black Sea Region. MTA Publications, 69-75.

Akyürek, B., and Soysal, Y., 1983. Biga Yarımadası Güneyinin (Savaştepe-Kırkağaç-Bergama-Ayvalık) temel jeoloji özellikleri. Maden Tetkik ve Arama Enstitüsü Dergisi, 95/96, 1-13.

Akyürek, B., Bilginer, E., Dağer, Z., and Sunu, O., 1979a. Hacılar (K. Çubuk-Ankara) bölgesinde Alt Triyas'ın varlığı. Türkiye Jeoloji Kurumu Bülteni, 22/2, 169-174.

Akyürek, B., Bilginer, E., Çatal, E., Dağer, Z., Soysal, Y., and Sunu, O., 1979b. Eldivan-Şabanözü (Çankırı) dolayında ofiyolit yerleşimine ilişkin bulgular. JMO yayınları, S.9, Ankara.

Akyürek, B., Bilginer, E., Akbaş, B., Hepşen, N., Pehlivan, Ş., Sunu, O., Soysal, Y., Dağer, Z., Çatal, E., Sözeri, B., Yıldırım, H., and Hakyemez, Y., 1982. Ankara-Elmadağ-Kalecik dolayının jeolojisi. Maden Tetkik ve Arama Enstitüsü, Rapor No : 7298 (unpublished).

Akyürek, B., Bilginer, E., Akbaş, B., Hepşen, N., Pehlivan, Ş., Sunu, O., Soysal, Y., Dağer, Z., Çatal, E., Sözeri, B., Yıldırım, H., and Hakyemez, Y., 1984. Basic geological features of Ankara-Elmadağ-Kalecik region. Jeoloji Mühendisliği, 20, 31-46 (In Turkish with English abstract).

Akyürek, B., Duru, M., Sütçü, Y.F., Papak, İ. Şaroğlu, F., Pehlivan, N., Gönenç, O., Granit, S., and Yaşar, T., 1996. Ankara ilinin çevre jeolojisi ve doğal kaynaklar projesi (1994 yılı Jeoloji grubu çalışmaları). Maden Tetkik ve Arama Enstitüsü, Rapor No: 9961 (unpublished).

Akyürek, B., Duru, M., Sütçü, Y.F., Papak, İ. Şaroğlu, F., Pehlivan, N., Gönenç, O., Granit, S., and Yaşar, T., 1997. 1/100000 ölçekli açınsama nitelikli Türkiye Jeoloji Haritaları Serisi, Ankara-F15 paftası: MTA yayınları, Ankara.

Albarède, F., Telouk, P., Blichert-Toft, J., Boyet, M., Agranier, A., and Nelson, B., 2004. Precise and accurate isotopic measurements using multiple-collector ICPMS. Geochimica et Cosmochimica Acta, 68, 2725-2744.

Altıner, D., and Koçyiğit, A., 1993. Third remark on the geology of the Karakaya basin. An Anisian megablock in northern central Anatolia: micropaleontologic, stratigraphic and tectonic implications for the rifting stage of Karakaya basin, Turkey. Revue de Palaeobiologie, 12, 1-17.

Baker, J.A., Thirlwall, M.F., and Menzies, M.A., 1996. Sr-Nd-Pb isotopic and trace element evidence for crustal contamination of plume-derived flood basalts: Oligocene flood volcanism in western Yemen. Geochimica et Cosmochimica Acta, 60, 2559-2581.

Batman, B., 1977. Haymana kuzeyinin jeolojik evrimi ve yöredeki melanjın incelenmesi: Doçentlik Tezi, 172 pp, Yerbilimleri Enst. Beytepe, Ankara.

Bedard, J.H., 1994. A procedure for calculating the equilibrium distribution of trace elements among the minerals of cumulate rocks, and the concentration of trace elements in the coexisting liquids. Chemical Geology, 118, 143-153.

Bilchert-Toft, J., Chauvel, C., and Albarède, F., 1997. Separation of Hf and Lu for high-precision isotope analysis of rock samples by magnetic sector-multiple collector ICP-MS. Contributions to Mineralogy and Petrology, 127, 248-260.

Bingöl, E., Akyürek, B., and Korkmazer, B., 1973. The geology of the Biga Peninsula and some features of the Karakaya Formation. Proceedings of the 50th Anniversary of the Turkish Republic Earth Science Congress. Mineral Research and Exploration Institute of Turkey (MTA) Publications, 70-77 (in Turkish with English abstract).

Brenan, J.M., Shaw, H.F., Ryerson, F.J., and Phinney, D.L., 1995. Mineral-aqueous fluid partitioning of trace elements at 900°C and 2.0 Gpa: Constraints on the trace element chemistry of mantle and deep crustal fluids. Geochimica et Cosmochimica Acta, 59, 3331-3350.

Chaffey, D. J., Cliff, R.A., and Wilson, B.M., 1989. Characterization of the St. Helena magma source. In: Saunders, A.D., and Norry, M.J. (eds.), Magmatism in the Ocean Basins. Geological Society, London, Special Publications, 42, 257-276.

Chauvel, C., Hofmann, A.W., and Vidal, P., 1992. HIMU-EM: The French Polynesia connection. Earth and Planateray Science Letters, 110, 99-119.

Cheatham, M., Sangrey, W.F., and White, W.M., 1993. Sources of error in external calibration ICP-MS analysis of geological samples and improved nonlinear drift correction procedure. Spectrochimica Acta, 48B, E487-E506.

Class, C., Miller, D.M., Goldstein, S.L., and Langmuir, C.H., 2000. Distinguishing melt and fluid subduction components in Umnak Volcanics, Aletuian Arc. Geochemistry Geophysics Geosystems, 1, 1999GC000010.

Closs, M., 1984. Flow melanges and the structural evolution of accretionary wedges. In: Raymond, L.A. (ed.), Melanges: Their nature, origin, and significance: Geological Society of America, Special Paper, 198, 71-79.

Coleman, R.G., and Lanphere, M.A., 1971. Distribution and age of high-grade blueschists, associated eclogites, and amphibolites from Oregon and California. Geological Society of America Bulletin, 82, 2397-2412.

Condie, K.C., 2001. Mantle Plumes and Their Record in Earth History. Cambridge University Press, 306 pp.

Çapan, U.Z., and Floyd, P.A., 1985. Geochemical and petrographic features of metabasalts within units of Ankara melange, Turkey. Ofioliti, 10, 3-18.

De Astis, G., La Volpe, L., Peccerillo, A., and Civetta, L., 1997. Volcanological and petrological evolution of Vulcano island (Aeolian Arc, southern Tyrrhenian Sea). Journal of Geophysical Research, 102, 8021-8050.

Dönmez, M., Akçay, A.E., Kara, H., Yergök, A.F., and Esentürk, K., 2008. 1/100000 ölçekli açınsama nitelikli Türkiye Jeoloji Haritaları Serisi, Kırşehir-I30 paftası: MTA yayınları, Ankara.

Dupre, B., and Allegre, C.J., 1983. Pb-Sr isotope variation in Indian Ocean basalts and mixing phenomena. Nature, 303, 142-146.

Ellam, R.M., and Cox, K.G., 1989. A Proterozoic lithospheric source for Karoo magmatism: evidence from the Nuanetsi picrites. Earth and Planetary Science Letters, 92, 207-218.

Elliott, T., Plank, T., Zindler, A., White, W., and Bourdon, B., 1997. Element transport from slab to volcanic front at the Mariana arc. Journal of Geophysical Research, 102, 14991-15019.

Erk, A.S., 1977. Ankara civarında Genç Paleozoyiğin Kulm fliş formasyonu. Maden Tetkik ve Arama Dergisi, 88, 73-94.

Erol, O., 1956. Ankara güneydoğusundaki Elma Dağı ve çevresinin jeolojisi ve jeomorfolojisi üzerinde bir araştırma. MTA yayınları, Seri. D, 9, Ankara.

Faure, G., 2001. Origin of Igneous Rocks: The Isotopic evidence. New York, Springer-Verlag, 496 pp.

Fitton, J.G., Saunders, A.G., Norry, M.J., Hardarson, B.S., Taylor, R.N., 1997. Thermal and chemical structure of the Iceland plume. Earth and Planetary Science Letters 153, 197-208.

Floyd, P.A., 1989. Geochemical features of intaplate oceanic plateau basalts. In: Saunders A.D., Norry, M.J. (eds.), Magmatism in the Ocean Basins. Geological Society, London, Special Publications, 42, 215-230.

Floyd, P.A., and Winchester, J.A., 1978. Identification and discrimination of altered and metamorphosed volcanic rocks using immobile elements. Chemical Geology, 21, 291-306.

Fretzdorff, S., Livermore, R.A., Devey, C.W, Leat, P.T., and Stoffers, P., 2002. Petrogenesis of the Back-arc East Scotia Ridge, South Atlantic Ocean. Journal of Petrology, 43, 1435-1467.

Frey, F.A., Green, D.H., and Roy, S.D., 1978. Integrated models of basalt petrogenesis: a study of quartz tholeiites to olivine melilitites from Southeastern Australia utilizing geochemical and experimental petrological data. Journal of Petrology, 19, 463-513.

Frey, F.A., Coffin, M.F., Wallace, P.J., et al. 2000. Origin and evolution of a submarine large igneous province: the Kerguelen Plateau and Broken Ridge, southern Indian Ocean. Earth and Planetary Science Letters, 176, 73-89.

Furman, T., Bryce, J.G., Karson, J., and Iotti, A., 2004. East African Rift System (EARS) plume structure: insights from Quaternary mafic lavas of Turkana, Kenya. Journal of Petrology, 45, 1069-1088.

Genç, Ş., 1987. Geology of the region between Uludağ and the İznik lake. IGCP Project No 5. Guide book for the field excursion along Western Anatolia, Turkey, 19-25.

Genç, Ş.C., 2004. A Triassic large igneous province in the Pontides, northern Turkey: geochemical data for its tectonic setting. Journal of Asian Earth Sciences, 22, 503-516.

Genç, Ş.C., and Yılmaz, Y., 1995. Evolution of the Triassic continental margin, northwest Anatolia. Tectonophysics, 243, 193-207.

Gibson, S.A., Thompson, R.N., Day, J.A., Humpris, S.E., and Dickin, A.P., 2005. Melt-generation processes associated with the Tristan mantle plume: Constraints on the origin of EM-1. Earth and Planetary Science Letters, 237, 744-767.

Gill, J.B., 1981. Orogenic Andesites and Plate Tectonics. New York, Springer-Verlag, 390 pp.

Göncüoğlu, M.C., Erendil, M., Tekeli, O., Aksay, A., Kuşçu, İ., and Ürgün, B., 1987. Geology of the Armutlu Peninsula. IGCP Project No 5, Guide Book. Field Excursion along Western Anatolia, 12-18.

Göncüoğlu, M.C., Turhan, N., Şentürk, K., Uysal, Ş., Özcan, A., and Işık, A., 1996. Geological characteristics of the structural units in Central Sakarya between Nallıhan and Sarıcakaya. Mineral Research and Exploration Institute of Turkey (MTA) Report, No. 10 094 (In Turkish).

Göncüoğlu, M.C., Dirik, K., and Kozlu, H., 1997. Pre-Alpine and Alpine Terranes in Turkey: explanatory notes to the terrane map of Turkey. Annales Geologique de Pays Hellenique, 37, 515-536.

Göncüoğlu, M.C., Turhan, N., Şentürk, K., Özcan, A., and Uysal, Ş. 2000. A geotraverse across NW Turkey: tectonic units of the Central Sakarya region and their tectonic evolution. In: Bozkurt, E., Winchester, J., Piper, J.A. (eds.), Tectonics and magmatism in Turkey and the Surrounding Area. Geological Society, London, Special Publications, 173, 139-161.

Göncüoğlu, M.C., Kuwahara, K., Tekin, K.U., and Turhan, N., 2004. Upper Permian (Changxingian) radiolarian cherts within the clastic successions of the "Karakaya Complex" in NW Anatolia. Turkish Journal of Earth Sciences, 13, 201-213.

Göncüoğlu, M.C., Çapkınoğlu, Ş., Gürsu, S., Noble, P., Turhan, N., Tekin, U.K., Okuyucu, C., and Göncüoğlu, Y., 2007. The Mississippian in the Central and Eastern Taurides (Turkey): constraints on the tectonic setting of the Tauride-Anatolide Platform. Geologica Carpathica, 58, 427-442.

Green, T.H., 1995. Significance of Nb/Ta as an indicator of geochemical processes in the crust-mantle system. Chemical Geology 120. 347-359.

Greenly, E., 1919. The geology of Anglesey: Great Britain Geological Survey Memoir, 1, 980.

Gribble, R.F., Stern, R.J., Newman, S., Bloomer, S.H., and O'Hearn, T., 1998. Chemical and isotopic composition of lavas from the northern Mariana Trough; implications for magma genesis in back-arc basins. Journal of Petrology, 39, 125-154.

Haase, K.M., Stoffers, P., and Garbe-Schönberg, C.D., 1997. The petrogenetic evolution of lavas from Easter Island and neighbouring seamounts, near-ridge hotspot volcanoes in the SE Pacific. Journal of Petrology 38, 785-813.

Hanan, B., and Schilling, J.-G., 1989. Depleted Iceland mantle plume geochemical signature: Artifact of multi-component mixing? Geochemistry, Geophysics, Geosystems, 1, doi:10.1029/19999GC000009.

Hart, S.R., 1984. A large-scale isotope anomaly in the Southern Hemisphere mantle. Nature, 309, 753-757.

Hart, S.R., and Davis, K.E., 1978. Nickel partitioning between olivine and silicate melt. Earth and Planetary Science Letters, 40, 203-219.

Hart, S.R., Hauri, E.H., Oschmann, L.A., and Whitehead, J.A., 1992. Mantle plumes and entrainment: isotopic evidence. Science, 256, 517-520.

Hart, W.K., Wolde, G.C., Walter, R.C., and Mertzman, S.A., 1989. Basaltic volcanism in Ethiopia: constraints on continental rifting and mantle interactions. Journal of Geophysical Research 94, 7731-7748.

Hawkesworth, C.J., Gallagher, K., Kelly, S., Mantovani, M., Peate, D.W., Regelous, M., and Rogers, N.W., 1992. Parana magmatism and the opening of South Atlantic. In: Storey, B.C., Alabaster, T., Pankhurst, R.J. (eds.), Magmatism and the Causes of Continental Break-up. Geological Society, London, Special Publications, 68, 221-240.

Hawkesworth, K., Gallagher, K., Hergt, J.M., and McDermott, F., 1993. Mantle and slab contributions in arc magmas. Annual Review of Earth and Planetary Science, 21, 175-204.

Hergt, J.M., Peate, D.W., and Hawkesworth, C.J., 1991. The petrogenesis of Mesozoic Gondwana low-Ti flood basalts. Earth and Planetary Science Letters, 105, 134-148.

Hochstaedter, A., Gill, J., Peters, R., Broughton, P., Holden, P., and Taylor, B., 2001. Across-arc geochemical trends in the Izu-Bonin arc: contributions from the subducting slab. Geochemistry Geophysics Geosystems, 2, 2000GC000105.

Hofmann, A.W., 1988. Chemical differentiation of the Earth: the relationship between mantle, continental crust, and oceanic crust. Earth and Planetary Science Letters, 90, 297-314.

Hofmann, A.W., Jochum, K.P., Seufert, M., and White, W.M., 1986. Nb and Pb in oceanic basalts: new constraints on mantle evolution. Earth and Planetary Science Letters, 79, 33-45.

Hsü, K.J., 1968. Principles of melanges and their bearing on the Franciscan-Knoxville Paradox. Geological Society of America Bulletin, 79, 1063-1074.

Ionov, D.A., and Hofmann, A.W., 1995. Nb-Ta-rich mantle amphiboles and micas: Implications for subduction-related metasomatic trace element fractionations. Earth and Planetary Science Letters, 131, 341-356.

Jacobsen, S.B., and Wasserburg, G.J., 1984. Sm-Nd isotopic evolution of chondrites and achondrites, II. Earth and Planetary Science Letters, 67, 137-150.

Johnson, K.T.M., 1998. Experimental determination of partition coefficients for rare earth and high-field-strength elements between clinopyroxene, garnet, and basaltic melt at high pressures. Contributions to Mineralogy and Petrology, 133, 60-68.

Johnson, K.T.M., Dick, H.J.B., and Schimizu, N., 1990. Melting in the oceanic upper mantle: an ion microprobe study of diopsides in abyssal peridotites. Journal of Geophysical Research, 95, 2661-2678.

Kaya, O., 1991. Stratigraphy of the Pre-Jurassic sedimentary rocks of the western parts of Turkey; type area study and tectonic considerations. type area study and tectonic considerations. Newsletter for Stratigraphy, 23, 123-140.

Kaya, O., and Mostler, H., 1992. A Middle Triassic age for low-grade greenschist facies metamorphic sequence in Bergama (İzmir), western Turkey: the first paleontological age assignment and structural-stratigraphic implications. Newsletter for Stratigraphy, 26, 1-17.

Kaya, O., Wiedmann, J., and Kozur, H., 1986. Preliminary report on the stratigraphy, age and structure of the so-called Late Paleozoic and/or Triassic "mélange or "suture zone complex" of northwestern and western Turkey. Yerbilimleri, 13, 1-16.

Kaya, O., Kozur, H., Sadeddin, W., and Helvacı, H., 2001. Late Norian conodont age for a metacarbonate unit in NW Anatolia, Turkey. Geobios, 34, 527-532.

Kelemen, P.B., Shimizu, N., and Dunn, T., 1993. Relative depletion of niobium in some arc magmas and the continental crust: partitioning of K, Nb, La and Ce during melt/rock reaction in the upper mantle. Earth and Planetary Science Letters, 120, 111-134.

Klein, E.M., Langmuir, C.L., and Staudigel, H., 1991. Geochemistry of basalts from the Southeast Indian Ridge, 115°E-138°E. Journal of Geophysical Research, 96, 2089-2107.

Koçyiğit, A., 1987. Tectono-stratigraphy of the Hasanoglan (Ankara) region: evolution of the Karakaya orogen. Yerbilimleri, 14, 269-293 (In Turkish with English abstract).

Koçyiğit, A., 1991a. First remark on the geology of Karakaya basin. Karakaya Orogen and pre-Jurassic nappes in eastern Pontides, Turkey. Geologica Romana, 27, 3-11.

Koçyiğit, A., 1991b. An example of an accretionary forearc basin from northern Central Anatolia and its implications for the history of subduction of Neo-Tethys in Turkey. Geological Society of America Bulletin, 103, 22-36.

Koçyiğit, A., 1992. Southward-vergent imbricate thrust zone in Yuvaköy: A record of the latest compressional event related to the collisional tectonic regime in Ankara-Erzincan Suture zone, TAPG Bull 4/I, 111-118.

Koçyiğit, A., and Tokay, M., 1985. Çatalçam (Zevker)-Erzincan arasında Kuzey Anadolu Fay Kuşağı'nın sismo-tektonik incelemesi: Fay Kuşağı'nın tektono-stratigrafisi, sistematiği ve Neotektonik özellikleri. Bayındırlık ve İskan Bakanlığı, Teknik Araş. Ve Uyg. Gn. Müd., Proje Kod no: 82-04-08-00-02, 101 pp (unpublished).

Koçyiğit, A., and Lünel, A.T., 1987. Geology and tectonic setting of Alcı region, Ankara. METU Journal of Pure and Applied Sciences, 20, 35-57.

Koçyiğit, A., Kaymakçı, N., Rojay, B., Özcan, E., Dirik, K., and Özçelik, Y., 1991. İnegöl-Bilecik-Bozüyük arasında kalan alanın jeolojik etüdü. Orta Dogu Teknik Üniversitesi-Türkiye Petrolleri Anonim Ortaklıgı projesi raporu, no: 90-03-09-01-05 (unpublished).

Kostopoulos, D.K., 1991. Melting of the shallow upper mantle: a new perspective. Journal of Petrology, 32, 671-699.

Kozur, H., 1997. Pelagic Permian and Triassic of the western Tethys and its paleogeographic and stratigraphic significance. Abstracts, XLVIII. Berg- und Hüttenmannischer Tag, Technische Universitat Bergakademie Freiberg, 21-25.

Kozur, H., Aydın, M., Demir, O., Yakar, H., Göncüoğlu, M.C., and Kuru, F., 2000. New stratigraphic and palaeogeographic results from the Palaeozoic and early Mesozoic of the Middle Pontides (northern Turkey) in the Azdavay, Devrekani, Küre and Inebolu areas: Implications for the Carboniferous-Early Cretaceous geodynamic evolution and some related remarks to the Karakaya oceanic rift basin. Geologica Croatica, 53, 209-268.

Leven, E.Ja., and Okay, A.I., 1996. Foraminifera from the exotic Permo-Carboniferous limestone blocks in the Karakaya Complex, northwest Turkey. Rivista Italiana Paleontologia e Stratigrafia, 102, 139-174.

Livermore, R., 2003. Back-arc spreading and mantle flow in the East Scotia Sea. In: Larter, R.D., and Leat, P.T. (eds.), Intra-Oceanic Subduction Systems: Tectonic and Magmatic Processes. Geological Society, London, Special Publications, 219, 315-331.

Mahoney, J.J., Storey, M., Duncan, R.A., Spencer, K.J., and Pringle, M., 1993. Geochemistry and geochronology of Leg 130 basement lavas: nature and origin of the Ontong Java Plateau. In: Berger WH, Kroenke LW, Mayer LA et al. Proc ODP Sci Results 130, College Station TX (Ocean Drilling Program), 3-22.

McKenzie, D., and O'Nions, R. K., 1991. Partial melt distributions from inversion of rare earth element concentrations. Journal of Petrology, 32, 1021-1091.

Moix, P., Beccaletto, L., Kozur, H.W., Hochard, C., Rosselet, F., and Stampfli, G.M., 2008. A new classification of the Turkish terranes and sutures and its implication for the paleotectonic history of the region. Tectonophysics, 451, 7-39.

Norman, M.D., and Garcia, M.O., 1999. Primitive magmas and source characteristics of the Hawaiian plume: petrology and geochemistry of shield picrites. Earth and Planetary Science Letters, 168, 27-44.

Norman, T., 1973. On the structure of the Ankara melange. Proceedings of the 50th Anniversary of the Turkish Republic Earth Science Congress. Mineral Research and Exploration Institute of Turkey (MTA) Publications, 77-94 (in Turkish with English abstract).

Okay, A.İ., 1989. Tectonic units in the Pontides, northern Turkey. In: Sengör, A.M.C. (ed.), Tectonic Evolution of the Tethyan Region. Kluwer Academic Publishers, USA, 109-116.

Okay, A.İ., 2000. Was the Late Triassic orogeny in Turkey caused by the collision of an oceanic plateau? In: Bozkurt, E., Winchester, J., Piper, J.A. (Eds.), Tectonics and magmatism in Turkey and the Surrounding Area. Geological Society, London, Special Publications, 173, 139-161.

Okay, A.İ., and Monie, 1997. Early Mesozoic subduction in the Eastern Mediterranean: Evidence from Triassic eclogite in nortwest Turkey. Geology, 25, 595-598.

Okay, A.I., and Tüysüz, O., 1999. Tethyan sutures of northern Turkey. In: Durand, B., Jolivet, L., Horvath, F., and Seranne, M. (eds.), The Mediterranean Basins: Tertiary Extension within the Alpine Orogen. Geological Society, London, Special Publications, 156, 475-515.

Okay, A.İ., and Altıner, D., 2004. Uppermost Triassic limestone in the Karakaya Complex-stratigraphic and tectonic significance. Turkish Journal of Earth Sciences, 13, 187-199.

Okay, A.İ., and Göncüoğlu, M.C., 2004. The Karakaya Complex: A review of data and concepts. Turkish Journal of Earth Sciences, 13, 77-95.

Okay, A.İ., Siyako, M, and Bürkan, B.A., 1991. Geology and tectonic evolution of the Biga Peninsula, northwest Turkey. Bulletin of Technical University of Istanbul, 44, 191-256.

Okay, A.İ., Satır, M., Maluski, H., Siyako, M., Monie, P., Metzger, R., and Akyüz, S., 1996. Paleo- and Neo-Tethyan events in northwest Turkey: geological and geochronological constraints. In: Yin, A., Harrison, M. (Eds.), Tectonics of Asia. Cambridge University Press, 420-441.

Okay, A.İ., Monod, O., and Monie, P., 2002. Triassic blueschists and eclogites from northwest Turkey: vestiges of the Paleo-Tethyan subduction. Lithos, 64, 155-178.

Okay, A.I., Satır, M., and Siebel, W., 2006. Pre-Alpide Palaeozoic and Mesozoic orogenic events in the Eastern Mediterranean region. In: Gee, D.G., and Stephenson, R.A. (eds.), European Lithosphere Dynamics. Geological Society, London, Memoirs, 32, 389-405.

Önder, F., and Göncüoğlu, M.C., 1989. Armutlu yarımadasında (Batı Pontidler) Üst Triyas konodontları. Maden Tetkik ve Arama Dergisi, 109, 147-152.

Özgül, L., 1993. Tectono-stratigraphy of the İmrahor (Ankara) region. B. Sc. Research Project, Middle East Technical University, 47 pp, Ankara.

Patchett, P.J., 1983. Importance of the Lu-Hf isotopic system in studies of planetary chronology and chemical evolution. Geochimica et Cosmochimica Acta, 47. 81-91.

Patchett, P.J., and Tatsumoto, M., 1980. Hafnium isotope variations in oceanic basalts. Geophysical Research Letters, 7, 1077-1080.

Pearce, J.A., 1975. Basalt geochemistry used to investigate past tectonic environments on Cyprus. Tectonophysics, 25, 41-67.

Pearce, J.A., 1983. The role of sub-continental lithosphere in magma genesis at active continental margins. In: Hawkesworth, C.J., and Norry, M.J. (eds.), Continental basalts and mantle xenoliths, 230-249. Nantwich: Shiva.

Pearce, J.A., and Cann, J.R., 1973. Tectonic setting of basic volcanic rocks determined using trace element analysis. Earth and Planetary Science Letters, 19, 290-300.

Pearce, J.A., and Norry, M., 1979. Petrogenetic implications of Ti, Zr, Y and Nb variations in volcanic rocks. Contributions to Mineralogy and Petrology, 69, 33-47.

Pearce, J.A., and Parkinson, I.J., 1993. Trace element models for mantle melting: application to volcanic arc petrogenesis. In: Prichard H.M., Alabaster T., Harris N.B.W., and Neary C. R., (eds.), Magmatic Processes and Plate Tectonics. Geological Society, London, Special Publications, 76, 373-403.

Pearce, J.A., Peate, D.W., 1995. Tectonic implications of the composition of volcanic arc magmas. Annual Review of Earth and Planetary Sciences 23, 251-285.

Pearce, J.A., and Stern, R.J., 2006. Origin of back-arc basin magmas: trace element and isotope perspectives. In: Christie, D.M., Fisher, C.R., Lee, S.-M., and Givens, S. (eds.), Back-Arc Spreading Systems: Geological, Biological, Chemical, and Physical Interactions, AGU, Geophysical Monographs, 166, 63-86.

Pearce, J.A., Baker, P.E., Harvey, P.K., and Luff, I.W., 1995. Geochemical evidence for subduction fluxes, mantle melting and fractional crystallization beneath the South Sandwich Island Arc. Journal of Petrology, 36, 1073-1109.

Pearce, J.A., Kempton, P.D., Nowell, G.M., Noble, S.R., 1999. Hf-Nd element and isotope perspective on the nature and provenance of mantle and subduction components in arc-basin systems: examples from the western Pacific. Journal of Petrology, 40, 1579-1611.

Pearce, J.A., Stern, R.J., Bloomer, S.H., and Fryer, P., 2005. Geochemical mapping of the Mariana Arc-Basin System: implications for the nature and distribution of subduction components. Geochemistry Geophysics Geosystems, 6, 2004GC000895.

Pearce, J.A., Kempton, P.D., and Gill, J.B., 2007. Hf-Nd evidence for the origin and distribution of mantle domains in the SW Pacific. Earth and Planetary Science Letters, 260, 98-114.

Peate, D.W., 1997. The Parana-Etendeka Province. In: Mahoney, J.J., and Coffin, M. (eds.), Large Igneous Provinces: Continental, Oceanic, and Planetary Flood Volcanism. AGU, Geophysical Monographs 100, 217-245.

171

Peate D.W., and Pearce, J.A., 1998. Causes of spatial compositional variations in Mariana arc lavas: Trace element evidence. The Island Arc, 7, 479-495.

Peate, D.W., Hawkesworth, C.J., and Mantovani, M.S.M., 1992. Chemical stratigraphy of the Parana lavas (South America): classification of magma types and their spatial distribution. Bulletin of Volcanology, 55, 119-139.

Pickett, E.A., and Robertson, A.H.F., 1996. Formation of the Late Paleozoic-Early Mesozoic Karakaya complex and related ophiolites in northwestern Turkey by Palaeotethyan subduction-accretion. Journal of the Geology Society, London, 153, 995-1009.

Pickett, E.A., and Robertson, A.H.F., 2004. Significance of the volcanogenic Nilüfer unit and related components of the Triassic Karakaya Complex for Tethyan Subduction/Accretion Processes in NW Turkey. Turkish Journal of Earth Sciences, 13, 97-143.

Plank, T., and Langmuir, C.H., 1993. Tracing trace elements from sediment input to volcanic output at subduction zones. Nature, 362, 739-743.

Plank, T., and Langmuir, C.H., 1998. The chemical composition of subducting sediment and its consequences for the crust and mantle. Chemical Geology, 145, 325-394.

Raymond, L.A., 1984. Classification of melanges. In: Raymond, L.A. (ed.), Melanges: Their nature, origin, and significance: Geological Society of America, Special Paper, 198, 7-20.

Rhodes, J.M., 1995. The 1852 and 1968 Mauna Loa picrite eruptions: clues to parental magma compositions and the magmatic plumbing system. AGU, Geophysical Monographs, 92, 241-262.

Robertson, A.H.F., 2002. Overview of the genesis and emplacement of Mesozoic ophiolites in the Eastern Mediterranean Tethyan region. Lithos, 65, 1-67.

Robertson, A.H.F., Ustaömer, T., Pickett, E., Collins, A., Andrew, T., and Dixon, J.E., 2004. Testing models of Late Palaeozoic-Early Mesozoic orogeny in Western Turkey: support for an evolving open-Tethys model. Journal of the Geology Society, London, 161, 501-511.

Rojay, B., and Göncüoğlu, M.C., 1997. Tectonic setting of some pre-Liassic low grade metamorphics in northern Anatolia. Yerbilimleri, 19, 109-118.

Saha, A., Basu, A.R., Wakabayashi, J., and Wortman, G.L., 2005. Geochemical evidence for a subducted infant arc in Franciscan high-grade-metamorphic tectonic blocks. Geological Society of America Bulletin, 117, 1318-1335.

Salters, V.J.M., and Hart, S.R., 1991. The mantle sources of ocean ridges, islands and arcs: the Hf-isotope connection. Earth and Planetary Science Letters, 104, 364-380.

Salters, V.J.M., and White, W.M., 1998. Hf constraints on mantle evolution. Chemical Geology, 145, 447-460.

Sayıt, K., and Göncüoğlu, M.C., 2009a. Geochemistry of mafic rocks of the Karakaya Complex, Turkey: Evidence for plume-involvement in the extensional oceanic regime during Middle-Late Triassic. International Journal of Earth Sciences, 98, 367-385.

Sayıt, K., and Göncüoğlu, M.C., 2009b. Geochemical characteristics of the basic volcanic rocks within the Karakaya Complex: A review. Yerbilimleri, 30, 181-191.

Sayıt K., Göncüoglu, M.C., and Furman, T., 2008. E-MORB- and OIB-Type Metabasalts From The Karakaya Complex: Trace Element Evidence For Melting Across The Spinel-Garnet Transition. Eos Transactions AGU, 89(53), Fall Meeting Supplement, Abstract V43B-2163.

Sayıt, K., Göncüoğlu, M.C., and Furman, T., 2009. Relict Seamounts within the Palaeotethyan Karakaya Complex, Turkey. Eos Transactions AGU, 90(52), Fall Meeting Supplement, Abstract V51C-1706.

Schilling, J.-G., Hanan, B.B., McCully, B., Kingsley, R.H., and Fontignie, D., 1994. Influence of the Sierra Leone mantle plume on the equatorial Mid-Atlantic Ridge: A Nd-Sr-Pb isotopic study. Journal of Geophysical Research, 99, 12005-12028.

Shaw, D.M., 1970. Trace element fractionation during anatexis. Geochimica at Cosmochimica Acta, 34, 237-243.

Sinton, J.M., Ford, L.L., Chappell, B., and McCulloch, M.T., 2003. Magma genesis and mantle heterogeneity in the Manus Back-Arc Basin, Papua New Guinea. Journal of Petrology, 44, 159-195.

Stampfli, G.M., 2000. Tethyan oceans. In: Bozkurt, E., Winchester, J., Piper, J.A. (eds.), Tectonics and magmatism in Turkey and the Surrounding Area. Geological Society, London, Special Publications, 173, 1-23.

Stampfli, G.M., Mosar, J., Favre, P., Pillevuit, A., and Vannay, J.-C., 2001. Permo-Mesozoic evolution of the western Tethyan realm: the Neotethys/East-Mediterranean connection. In: Ziegler, P.A., Cavazza, W., Robertson, A.H.F., and Crasquin-Soleau, S. (eds.), PeriTethys Memoir 6: Peritethyan Rift/wrench Basins and Passive Margins, IGCP 369. Memoirs du Museum National d'Historie Naturelle, 186, 51-108.

Stampfli, G.M., and Borel, G.D., 2002. A plate tectonic model for the Paleozoic and Mesozoic constrained by dynamic plate boundaries and restored synthetic oceanic isochrons. Earth and Planetary Science Letters, 196, 17-33.

Staudigel, H., Davies, G.R., Hart, S.R., Marchant, K.M., and Smith, B.M., 1995. Large scale isotopic Sr, Nd and O isotopic anatomy of altered oceanic crust: DSDP/ODP sites 417/418. Earth and Planateray Science Letters, 130, 169-185.

Stern, R.J., Kohut, E., Bloomer, S.H., Leybourne, M., Fouch, M., and Vervoort, J., 2006. Subduction factory processes beneath the Guguan cross-chain, Mariana Arc: no role for sediments, are serpentinites important? Contributions to Mineralogy and Petrology, 151, 202-221.

Stracke, A., Hofmann, A.W., and Hart, S.R., 2005. FOZO, HIMU, and the rest of the mantle zoo. Geochemistry Geophysics Geosystems, 6, Q05007, doi: 10.1029/2004GC000824.

Su, Y., and Langmuir, C.H., 2003. Global MORB chemistry compilation at the segment scale, PhD Thesis, Department of Earth and Environmental Sciences, Columbia University.

Sun, S.S., and McDonough, W.F., 1989. Chemical and isotopic systematics of oceanic basalts: implications for mantle composition and processes. In: Saunders, A.D., and Norry, M.J., (eds) Magmatism in the Ocean Basins. Geological Society, London, Special Publications, 42, 313-345.

Şengör, A.M.C., 2003. The repeated discovery of melanges and its implications for the possibility and the role of objective evidence in the scientific enterprise. Geological Society of America, Special Paper, 373, 385-445.

Şengör, A.M.C., and Yılmaz, Y., 1981. Tethyan Evolution of Turkey: a plate tectonics approach. Tectonophysics, 75, 181-241.

Şengör, A.M.C., Yılmaz, Y., and Ketin, İ., 1980. Remnants of a pre-Late Jurassic ocean in northern Turkey: Fragments of Permian-Triassic Paleo-Tethys. Geological Society of America Bulletin, 91, 599-609.

Şengör, A.M.C., Yılmaz, Y., and Sungurlu, O., 1984. Tectonics of the Mediterranean Cimmerides: nature and evolution of the western termination of Paleo-Tethys. In: Dixon, J.E., Robertson, A.H.F. (eds.), The Geological Evolution of the Eastern Mediterranean. Geological Society, London, Special Publications, 17, 77-112.

Taylor, S.R., and McLennan, S.M., 1995. The geochemical evolution of continental crust. Reviews of Geophysics, 33, 241-265.

Tekeli, O., 1981. Subduction complex of pre-Jurassic age, northern Anatolia, Turkey. Geology, 9, 68-72.

Thirlwall, M.F., 2002. Multicollector ICP-MS analysis of Pb isotopes using a ^{207}Pb-^{204}Pb double spike demonstrates up to 400 ppm/amu systematic errors in Tl-normalization. Chemical Geology, 184, 255-279.

Todt, W., Cliff, R.A., Hanser, A., and Hofmann, A.W., 1996. Evaluation of a 202Pb-205Pb double spike for high precision lead isotope analysis. In: Basu, A., and Hart, S. (eds.) Earth Processes: Reading the Isotopic Code. American Geophysical Union, 429-437.

Topuz, G., Altherr, R., Satır, M., and Schwarz, W.H., 2004. Low-grade metamorphic rocks from the Pulur complex, NE Turkey: implications for the pre-Liassic evolution of Eastern Pontides. International Journal of Earth Sciences, 93, 72-91.

Turhan, N., Okuyucu, C., and Göncüoğlu, M.C., 2004. Autochthonous Upper Permian (Midian) carbonates in the Western Sakarya Composite Terrane, Geyve Area, Turkey: Preliminary data. Turkish Journal of Earth Sciences, 13, 215-229.

Türkecan, A., and Yurtsever, A., 2002. 1/500000 ölçekli Türkiye Jeoloji Haritaları, İstanbul paftası, MTA yayınları, Ankara.

Ustaömer, T., and Robertson, A.H.F., 1994. Late Paleozoic marginal basin and subduction-accretion: the Paleotethyan Küre Complex, Central Pontides, northern Turkey. Journal of the Geology Society, London, 151, 291-305.

Ustaömer, T., and Robertson, A.H.F., 1999. Geochemical evidence used to test alternative plate tectonic models for the pre-Upper Jurassic (Palaeotethyan) units in the Central Pontides, N Turkey. Geological Journal, 34, 25-53.

Ünalan, G., Yüksel, V., Tekeli, T., Gönenç, O., Seyirt, Z., and Hüseyin, S., 1976. Haymana-Polatlı yöresinin (GB Ankara) Üst Kretase-Alt Tersiyer stratigrafisi ve paleocoğrafik evrimi. TJK Bülteni, 19/2, 159-176.

Weaver, B.L., Wood, D.A., Tarney, J., and Joron, J.L., 1987. Geochemistry of ocean island basalts from the South Atlantic: Ascension, Bouvet, St. Helena, Gough and Tristan da Cunha. In: Fitton, J.G., and Upton, B.G.J. (eds) Alkaline Igneous Rocks. Geological Society, London, Special Publications, 30, 253-267.

Weaver, B.L., Wood, D.A., Tarney, J., and Joron, J.L., 1986. Role of subducted sediment in the genesis of ocean-island basalts: Geochemical evidence from South Atlantic Ocean islands. Geology, 14, 275-278.

White, W. M., Albarède, F., and Télouk, P., 2000. High-precision analysis of Pb isotope ratios by multi-collector ICP-MS. Chemical Geology, 167, 257-270.

Wiedmann, J., Kozur, H., and Kaya, O., 1992. Faunas and age significance of the pre-Jurassic turbidite-olistostrome unit in the western parts of Turkey. Newsletter for Stratigraphy, 26, 133-144.

Winchester, J.A., and Floyd, P.A., 1977. Geochemical discrimination of different magma series and their differentiation products using immobile elements. Chemical Geology, 20, 325-343.

Wood, D.A., Gibson, I.L., and Thompson, R.N., 1976. Elemental mobility during zeolite facies metamorphism of the Tertiary basalts of eastern Iceland. Contributions to Mineralogy and Petrology, 55, 241-254.

Woodhead, J., Eggins, S., and Gamble, J., 1993. High field strength and transition element systematics in island arc and back-arc basin basalts: evidence for multi-phase melt extraction and a depleted mantle wedge. Earth and Planetary Science Letters, 114, 491-504.

Woodhead, J.D., Eggins, S.M., and Johnson, R.W., 1998. Magma genesis in the New Britain Island Arc: further insights into melting and mass transfer processes. Journal of Petrology, 39, 1641-1668.

Woodhead, J.D., Hergt, J.M., Davidson, J.P., and Eggins, S.M., 2001. Hafnium isotope evidence for "conservative" element mobility during subduction zone processes. Earth and Planetary Science Letters, 192, 331-346.

Workman, R.K., and Hart, S.R., 2005. Major and trace element composition of the depleted MORB mantle (DMM). Earth and Planetary Science Letters, 231, 53-72.

Workman, R.K., Hart, S.R., Jackson, M., Regelous, M., Farley, K.A., Blusztajn, J., Kurz, M., and Staudigel, H., 2004. Recycled metasomatized lithosphere as the origin of the Enriched Mantle II (EM2) end-member: Evidence from the Samoan Volcanic Chain. Geochemistry Geophysics Geosystems, 5, Q04008, doi: 10.1029/2003GC000623.

Yalınız, M.K., and Göncüoğlu, M.C., 2002. Geochemistry and petrology of "Nilüfer-type" metabasic rocks of eastern Kozak Massif, NW Turkey. 1. International Symposium of Istanbul Technical University, The Faculty of Mines on Earth Sciences and Engineering, Istanbul, Abstracts, pp 158.

Yılmaz, Y., 1981. Sakarya kıtası güney kenarının tektonik evrimi. İstanbul Yerbilimleri, 1, 33-52.

Yılmaz, Y., Serdar, H.S., Genç C., Yiğitbaş, E., Gürer Ö.F., Elmas, A., Yıldırım, M., Bozcu, M., and Gürpınar, O., 1997. The Geology and Evolution of the Tokat Massif, South Central Pontides, Turkey. International Geology Review, 39, 365-382.

Zindler, A., and Hart, S., 1986. Chemical Geodynamics. Annual Review of Earth and Planetary Science, 14, 493-571.

APPENDIX A

INFORMATION REGARDING THE STUDY AREAS

In Central Anatolia, the first part of the study area is located in İmrahor village; 5 km southeast of Ankara. This area covers an area of approximately 4 km^2 and it is included in the Ankara I29-b2 and I29-b3 quadrangles of 1:25000 topographic map of Turkey lying between the coordinates of 39°52'00'' - 39°53'30'' N latitudes and 32°52'30'' - 32°55'00'' E longitudes. The main hills in the study area are Çanakcı Hill in the north and Kocakaya Hill in the south.

The second part comprises Üreğil, Zerdalitepe and Kusunlar, which are located about 9 km and 11 km southeast of Ankara, respectively. This part covers an area of approximately 14 km^2 and it is included in the Ankara I29-b2 quadrangles of 1:25000 topographic map of Turkey lying between the coordinates of 39°52'30'' - 39°55'30'' N latitudes and 32°55'30'' - 33°00'00'' E longitudes. The main hills in the study area are Yumru Hill to the west, Tarla Hill in the south and Hanyeri Hill in the west.

The third part of the study area consists of Bayındır, Ortaköy, Gökçeyurt and Lalahan; located about 10 km and 13 km east of, and 16 and 19 km east of Ankara, respectively. This study area covers approximately 25 km^2 and it is included in the Ankara I29-b2 and Kırşehir I30-a1 quadrangles of 1:25000 topographic maps of Turkey lying between the coordinates of 39°54'30'' - 39°58'30'' N latitudes and 33°00'00'' - 33°07'30'' E longitudes. The highest peaks in the study area are the Mıhlı and Yaylabaşı Hills in the west, the Yayla Hill to the north and the Deliömer Hill in the east.

The fourth part of the study area includes Hasanoğlan, Kavaklı, Doğanoluk, Çardakbağı, and Bozca, which are located about 10 km, 16 km, 19 km, 21 km and 30 km northeast of Ankara, respectively. This study area covers approximately 30 km^2 and it is included in the Ankara H30-d3 and H30-d4 quadrangles of 1:25000 topographic map of Turkey lying between the coordinates of 40°00'00'' - 40°05'30'' N latitudes and 33°05'00'' - 33°14'00'' E longitudes. The main hills in the study area are Yenibağ Hill in the southwest, Gölbaşı and Keçikıran Hills to the east and Dedekaya Hill in the southeast.

The fifth part comprises Hacılar (Çubuk) which is located 24 km southwest of Ankara. This study area covers about 2 km^2, and included in the Ankara I29-a3 quadrangles of 1:25000 topographic map of Turkey lying between the coordinates of 39°45'55'' - 39°46'13'' N latitudes and 32°42'30'' - 32°43'00'' E longitudes. The highest peak in the area is the Hacılar Hill in the west.

The sixth part of the study area comprises Eymir and Karataş, located 13 km and 15 km southwest of Ankara. It covers an area of approximately 25 km^2 and it is included in the Ankara I29-b4 quadrangles of 1:25000 topographic map of Turkey lying between the coordinates of 39°47'00'' - 39°51'00'' N latitudes and 32°48'30'' - 32°52'30'' E longitudes. The highest peaks are Taşlık Hill in the southwest and Tandıroğlu Hill in the north.

The final part of the study area in Central Anatolia includes Hacılar (Çubuk) which is located 55 km northeast of Ankara. It occupies an area of approximately 3 km^2 and it is included in the Ankara H30-a1 quadrangles of 1:25000 topographic map of Turkey lying between the coordinates of 40°25'00'' - 40°26'00'' N latitudes and 33°02'00'' - 33°03'30'' E longitudes. The main hills in the study area are Beytaşı Hill in the north, Taşlıkıran Hill in the west, and Alanbaşı Hill in the south.

In the Central Sakarya region, the studied region includes Karaçobanpınarı, Alpagut, Laçin and Emremsultan. It covers an area of approximately 700 km^2 and it is included in the Ankara H25-c3,c4, H25-d3,d4, H26-c3,c4, H26-d3,d4 quadrangles of 1:25000 topographic map of Turkey lying between the coordinates

of 40°00'30'' - 40°10'30'' N latitudes and 30°23'30'' - 31°24'30'' E longitudes. The highest peaks are the Dededoruğu Hill to the west, Top Hill in the near-central part and Çalkaya Hill to the east.

In NW Anatolia, the first part of the study area consists of Sipali, Bahçecik, and Subaşı, which are located 43 km, 57 km and 50 km northeast-southeast of Bursa. It occupies an area of approximately 20 km^2, and it is included in the Bursa H23-d2 quadrangles of 1:25000 topographic map of Turkey lying between the coordinates of 40°05'30'' - 40°13'40'' N latitudes and 29°34'30'' - 29°45'00'' E longitudes. Main hills in the study area are Asarlık Hill to the southeast, Kocadüz Hill in the south and Kaplıkaya Hill to the north. The second part the study area is around Nilüfer Valley (the Doğancı Dam) which is located 12 km southwest of Bursa. It occupies an area of approximately 15 km^2, and it is included in the Bursa H21-c2,c3 quadrangles of 1:25000 topographic map of Turkey lying between the coordinates of 40°03'30'' - 40°09'30'' N latitudes and 28°56'00'' - 28°59'30'' E longitudes. Main hills in the study area are Akbaba Hill to the north, Babasultan Hill in the west, and Pırnallıkaya Hill to the south.

GEOCHEMICAL DATA

	Eymir metadiabase dikes												
	BO-2	**DO-11B**	**DO-12**	**DO-13**	**DO-18A**	**DO-23**	**DO-24**	**DO-9B**	**EY-4**	**EY-5**	**EY-9**	**HS-78**	**BU-8**
SiO_2	53.65	52.68	53.39	54.91	53.83	52.05	54.78	55.07	52.43	54.56	54.78	51.48	44.02
Al_2O_3	15.87	14.83	14.70	14.86	14.64	15.72	15.15	14.77	16.11	15.29	15.13	16.40	15.68
Fe_2O_3	11.35	14.12	13.01	13.00	13.41	9.88	12.84	13.01	11.20	13.42	13.47	8.42	9.45
MgO	5.90	4.80	4.20	4.20	4.40	7.30	4.10	4.10	7.10	4.00	3.90	8.30	5.26
CaO	8.95	7.42	7.75	7.42	8.34	10.35	7.38	7.30	7.68	7.61	7.31	9.83	15.36
Na_2O	3.17	3.09	3.14	3.34	3.13	2.89	3.34	3.42	3.23	3.27	3.41	3.06	2.44
K_2O	0.99	1.27	0.50	0.64	0.22	0.70	0.45	0.39	0.83	0.15	0.54	1.45	0.18
TiO_2	1.23	1.67	1.36	1.38	1.06	0.93	1.35	1.39	1.04	1.31	1.35	0.68	1.47
P_2O_5	0.13	0.10	0.11	0.13	0.11	0.08	0.12	0.12	0.09	0.11	0.10	0.06	0.13
MnO	0.19	0.24	0.21	0.21	0.22	0.17	0.21	0.22	0.20	0.23	0.22	0.16	0.13
Cr_2O_3													0.047
LOI	1.9	2.3	2.4	1.8	2.1	2.7	1.9	3.0	3.4	2.8	1.3	2.6	5.6
Ba	111	631	105	122	35	277	88	145	311	78	217	184	39
Hf	2.2	1.9	2.2	2.2	2.1	1.7	2.3	2.2	1.8	2.2	1.9	1.3	2.3
Nb	2.1	1.6	1.9	2.1	1.8	1.3	2.0	2.1	1.4	1.6	1.6	1.0	5.5
Rb	19.3	17.5	9.0	12.5	2.3	12.7	10.4	7.8	13.1	2.0	7.0	26.1	2.3
Sr	361	389	378	377	275	413	434	504	570	207	337	421	213
Ta	0.15	0.12	0.14	0.16	0.14	0.11	0.14	0.15	0.11	0.12	0.13	0.08	0.4
Th	0.71	0.56	0.70	0.70	0.54	0.33	0.74	0.70	0.36	0.52	0.43	0.32	0.50
U	0.18	0.18	0.21	0.19	0.16	0.12	0.25	0.21	0.12	0.33	0.18	0.10	0.20
V	314	503	426	415	453	252	400	411	285	387	391	215	299
Zr	78	62	72	69	70	62	77	67	63	70	62	50	85
Y	27.5	25.3	29.8	31.1	28.3	22.9	31.4	29.6	23.9	28.4	27.9	16.5	24.4
Pb	1.6	1.8	3.1	2.1	1.3	1.3	2.1	1.7	1.4	2.1	2.2	0.9	0.2
Sc	39.4	40.8	35.4	35.9	43.8	41.5	34.9	34.5	42.0	35.0	35.5	41.0	39.0
Co	51	50	49	56	53	51	52	47	48	45	51	50	33
Ni	25	6	5	4	3	45	4	8	15	2	4	49	48
Cr	68	12	10	10	9	137	10	16	28	8	10	141	
La	4.74	3.60	4.07	4.73	4.06	2.88	4.59	4.27	3.11	3.44	3.44	2.29	5.10
Ce	12.83	9.72	11.34	12.42	11.01	8.69	12.43	11.79	9.10	9.81	9.79	6.50	14.30
Pr	2.01	1.44	1.75	1.90	1.68	1.34	1.93	1.82	1.42	1.54	1.57	0.96	2.13
Nd	9.80	7.46	8.82	9.38	8.29	7.05	9.63	9.23	7.35	8.02	8.04	5.18	10.80
Sm	3.04	2.48	2.98	3.13	2.73	2.37	3.16	3.01	2.50	2.74	2.74	1.73	3.37
Eu	1.08	1.09	1.10	1.14	0.99	0.91	1.15	1.10	0.99	1.04	1.06	0.71	1.27
Gd	3.95	3.38	4.01	4.20	3.69	3.23	4.22	4.10	3.34	3.80	3.78	2.29	3.95
Tb	0.69	0.63	0.73	0.77	0.68	0.57	0.77	0.75	0.62	0.69	0.69	0.41	0.74
Dy	4.72	4.28	4.94	5.13	4.59	3.84	5.21	5.07	4.01	4.76	4.81	2.88	4.36
Ho	0.98	0.89	1.03	1.07	0.97	0.82	1.10	1.04	0.87	0.99	1.00	0.60	0.94
Er	2.72	2.54	3.04	2.98	2.63	2.20	3.17	2.96	2.39	2.85	2.93	1.66	2.52
Tm													0.37
Yb	2.68	2.47	2.95	2.99	2.66	2.19	3.09	2.92	2.32	2.80	2.82	1.66	2.45
Lu	0.42	0.40	0.46	0.47	0.43	0.35	0.49	0.46	0.38	0.45	0.43	0.26	0.36

						Nilufer metabasic rocks							
	CHC-2	**GK-1**	**GK-3**	**GK-6**	**HC-2**	**HS-03**	**HS-43B**	**HS-44**	**HS-46**	**HS-61**	**HS-62A**	**HS-62B**	**HS-62C**
SiO_2	48.23	49.16	44.78	43.15	49.53	47.55	41.77	46.68	51.93	44.15	50.18	44.55	44.00
Al_2O_3	11.56	13.34	12.83	9.80	11.53	12.98	17.85	14.01	12.20	10.71	4.21	4.96	5.84
Fe_2O_3	12.04	10.50	13.01	8.59	9.39	8.41	13.27	13.73	11.11	10.06	9.42	14.47	12.59
MgO	10.73	7.53	8.81	4.20	7.23	7.33	4.04	8.13	7.25	7.51	22.31	29.08	19.19
CaO	5.97	11.98	16.20	15.90	15.74	7.72	8.55	3.76	6.30	13.90	10.63	5.25	9.94
Na_2O	3.22	2.70	2.27	4.72	3.62	4.72	2.02	2.46	3.91	3.43	0.43	0.16	0.26
K_2O	0.47	2.72	1.12	1.39	0.38	0.15	2.48	2.17	1.76	0.51	0.29		0.09
TiO_2	2.21	1.80	1.13	1.43	1.99	2.62	3.87	3.09	2.14	2.00	0.74	0.97	1.25
P_2O_5	0.31	0.31	0.10	0.25	0.30	0.35	0.49	0.45	0.24	0.30	0.13	0.11	0.20
MnO	0.18	0.15	0.17	0.16	0.15	0.08	0.12	0.31	0.17	0.14	0.14	0.21	0.14
Cr_2O_3	0.084			0.043		0.014	b.d.	0.016	0.047	0.112			0.331
LOI	4.6	4.20	7.20	10.1	11.50	7.8	5.1	4.8	2.5	6.8	3.10	8.3	5.6
Ba	46	201	192	100	59	48	769	280	173	142	22	162	18
Hf	4.7	3.8	1.5	3.3	3.4	5.1	6.5	6.0	3.8	4.3	1.4	1.4	2.7
Nb	26.3	39.1	4.8	32.1	17.5	25.9	60.6	53.6	24.3	41.7	16.6	17.0	25.6
Rb	9.3	27.9	18.6	20.4	1.1	2.1	48.4	51.2	39.2	12.0	1.1	5.7	1.3
Sr	70	379	400	160	284	266	1439	178	596	396	52	51	98
Ta	1.5	2.28	0.31	2	1.09	1.7	3.7	3.2	1.4	2.5	0.96	1.31	1.5
Th	2.50	3.44	0.41	3.60	1.67	2.00	4.90	5.10	2.40	3.80	1.02	1.60	2.50
U	0.70	0.61	0.12	1.30	2.30	0.60	1.40	1.20	0.70	1.00	0.14	0.45	0.50
V	226	266	206	175	238	284	261	289	210	266	95	124	167
Zr	152	142	49	119	134	166	259	226	139	145	49	37	89
Y	20.9	24.9	16.1	19.6	23.7	17.3	27.9	22.6	19.5	20.4	7.3	13.0	12.8
Pb	2.5	13.9	1.1	2.2	1.2	1.0	1.2	1.1	1.0	0.7	1.9	0.5	1.2
Sc	27.0	24.3	23.0	22.0	25.3	29.0	14.0	26.0	28.0	43.0	20.2	23.0	29.0
Co	52	44	75	42	55	38	47	42	48	46	68	104	81
Ni	232	97	428	75	124	73	40	59	79	86	800	1387	623
Cr		171	582		192						1262	1269	
La	21.10	27.62	4.04	23.70	14.58	16.90	42.90	39.00	18.40	34.30	4.44	11.60	11.50
Ce	42.70	53.08	10.17	48.30	32.64	39.90	90.00	86.90	43.00	69.80	14.26	25.95	30.20
Pr	6.05	6.49	1.42	5.48	4.51	5.24	10.94	10.28	5.45	7.92	2.20	3.19	4.00
Nd	25.10	24.04	6.89	21.80	18.80	23.30	43.90	39.90	23.90	30.80	9.14	12.59	16.20
Sm	5.59	5.02	2.16	4.08	4.48	5.20	8.05	7.69	5.09	5.40	1.98	2.79	3.37
Eu	1.80	1.58	0.82	1.30	1.44	1.59	2.63	2.38	1.60	1.67	0.57	0.58	0.99
Gd	5.12	5.01	2.79	3.92	4.78	4.51	7.00	6.57	4.73	4.77	1.85	2.75	2.92
Tb	0.82	0.80	0.49	0.65	0.79	0.76	1.08	0.99	0.76	0.77	0.28	0.44	0.47
Dy	4.07	4.77	3.08	3.53	4.60	3.81	5.40	4.86	3.94	3.82	1.56	2.57	2.49
Ho	0.81	0.91	0.59	0.67	0.85	0.71	0.99	0.84	0.75	0.74	0.27	0.46	0.49
Er	1.91	2.46	1.52	1.79	2.11	1.84	2.63	2.08	1.94	1.83	0.63	1.20	1.23
Tm	0.26		0.27			0.25	0.37	0.28	0.26	0.28			0.17
Yb	1.66	2.17	1.34	1.66	1.77	1.50	2.21	1.63	1.59	1.69	0.57	1.00	0.98
Lu	0.23	0.33	0.20	0.25	0.26	0.21	0.31	0.23	0.23	0.24	0.08	0.14	0.15

Nilufer metabasic rocks

	HS-63	HS-64	HS-76A	HS-76B	HS-87	HS-88	HS-89	HS-90	HS-91	IM-8A	IM-8B	IM-9A	IM-9B
SiO_2	45.22	44.33	47.17	48.96	43.89	46.52	45.53	47.18	40.36	40.43	51.57	43.62	47.83
Al_2O_3	17.30	11.48	12.29	10.46	5.20	11.47	6.15	8.83	12.37	8.52	10.35	13.52	10.82
Fe_2O_3	12.19	9.85	11.92	8.86	11.51	10.39	11.78	9.95	10.11	12.01	9.69	12.46	7.85
MgO	4.32	8.37	9.25	4.47	20.31	7.91	21.27	9.79	5.42	9.84	7.09	9.34	4.04
CaO	8.91	13.94	8.51	11.89	10.19	17.28	11.71	19.73	13.87	12.31	6.93	5.92	11.10
Na_2O	4.21	3.08	3.19	4.69	0.28	3.24	0.22	1.98	4.04	0.54	3.64	3.04	5.85
K_2O	0.76	0.56	0.57	0.34	0.09	0.67	0.17	0.47	0.25	0.07	0.34	0.09	0.07
TiO_2	2.99	1.80	2.16	1.69	1.20	2.13	1.25	1.75	2.10	1.93	2.10	3.46	2.30
P_2O_5	0.62	0.26	0.29	0.22	0.19	0.33	0.17	0.18	0.46	0.35	0.33	0.16	0.43
MnO	0.18	0.14	0.25	0.28	0.14	0.17	0.15	0.15	0.15	0.10	0.05	0.07	0.09
Cr_2O_3	0.003	0.072	0.048	0.018	0.248				0.061	0.076	0.017	0.085	0.02
LOI	2.9	5.7	3.9	7.9	6.2	5.40	4.30	4.40	10.5	13.7	7.8	8.1	9.5
Ba	291	215	62	36	20	260	29	97	58	102	130	22	20
Hf	5.6	3.2	4.4	3.7	2.5	3.7	1.8	1.9	4.7	4.1	4.2	7.0	4.4
Nb	72.0	29.9	26.9	21.8	22.7	43.2	23.3	25.4	51.8	38.2	41.2	68.7	42.8
Rb	16.5	11.0	12.9	7.5	0.4	6.3	0.8	2.9	5.6	1.9	7.6	2.3	1.4
Sr	802	408	1159	420	90	484	48	270	152	314	144	112	407
Ta	4.3	1.7	1.7	1.3	1.4	2.63	1.43	1.56	3	2.4	2.4	4.4	2.8
Th	7.00	2.90	2.60	2.70	1.90	3.82	2.02	2.16	5.50	4.30	4.80	6.90	4.00
U	1.40	0.80	0.60	1.10	0.50	2.65	0.39	0.77	2.10	0.90	1.00	1.40	1.00
V	216	242	236	165	143	263	172	272	216	148	239	276	251
Zr	212	114	150	128	85	120	60	53	186	141	130	260	159
Y	28.5	17.3	21.8	17.3	11.5	21.6	12.5	16.7	21.8	17.1	15.7	18.3	18.5
Pb	1.0	0.8	2.0	1.6	0.3	2.7	0.5	2.6	1.1	2.4	1.4	0.5	1.4
Sc	12.0	30.0	28.0	20.0	29.0	34.9	45.9	53.0	21.0	22.0	22.0	44.0	23.0
Co	27	46	48	36	66	62	91	61	44	50	43	53	28
Ni	16	175	124	59	548	269	734	253	136	196	66	204	50
Cr						668	1918	766					
La	51.10	23.90	21.50	17.70	12.00	31.41	10.37	18.86	41.90	35.50	28.30	44.90	22.50
Ce	103.60	48.80	47.70	42.40	31.40	62.60	27.60	38.89	82.20	70.90	57.80	101.10	57.10
Pr	11.73	5.73	6.06	4.95	3.98	7.72	3.80	4.90	8.95	7.28	6.04	10.42	6.76
Nd	43.20	21.90	25.30	20.10	15.70	28.07	15.04	18.69	33.40	29.60	24.00	39.30	29.90
Sm	8.09	4.40	5.64	4.29	3.29	5.58	3.18	4.06	6.15	6.20	4.60	7.80	5.80
Eu	2.45	1.37	1.74	1.36	0.90	1.75	1.00	1.28	1.72	1.82	1.78	2.45	2.22
Gd	7.12	3.99	5.03	3.99	2.68	5.26	2.91	4.03	5.05	5.39	3.90	5.95	5.33
Tb	1.11	0.66	0.85	0.66	0.45	0.81	0.46	0.63	0.81	0.78	0.71	0.95	0.85
Dy	5.52	3.39	4.24	3.41	2.46	4.48	2.54	3.40	4.14	3.36	3.55	4.76	3.91
Ho	1.02	0.63	0.76	0.62	0.41	0.79	0.46	0.62	0.78	0.66	0.64	0.80	0.74
Er	2.80	1.73	2.12	1.71	1.19	1.96	1.18	1.56	2.02	1.59	1.67	1.84	1.88
Tm	0.37	0.23	0.28	0.24	0.16				0.29	0.19	0.18	0.23	0.22
Yb	2.30	1.57	1.76	1.49	1.02	1.47	0.92	1.12	1.86	1.19	1.20	1.45	1.38
Lu	0.32	0.21	0.25	0.20	0.13	0.21	0.12	0.14	0.25	0.18	0.21	0.16	0.20

Nilufer metabasic rocks

	IM-24	IM-28	KD-16	KD-19	LL-4	NIL-3	NIL-4	NIL-7	NIL-12	OR-28	OR-29	OR-33	OR-43
SiO_2	46.91	46.60	47.63	45.31	41.65	44.67	46.75	45.93	47.25	46.43	49.58	49.51	43.76
Al_2O_3	14.35	15.43	9.61	11.53	10.06	11.55	12.97	14.43	10.76	13.28	13.38	14.21	11.25
Fe_2O_3	13.39	12.49	9.25	10.56	13.91	11.47	11.65	12.64	13.75	12.85	12.50	12.74	11.98
MgO	12.37	9.06	4.37	4.98	10.15	12.83	7.74	7.66	14.81	8.39	5.67	8.88	15.89
CaO	7.23	11.94	13.90	15.18	12.00	6.40	9.68	7.77	7.58	9.72	11.75	8.57	6.91
Na_2O	3.08	2.75	4.41	3.27	2.05	2.82	3.52	3.61	2.25	3.16	4.57	2.96	1.32
K_2O	0.24	0.33	1.99	1.39	0.35	0.15	0.49	0.50	0.30	0.60	0.42	1.01	0.39
TiO_2	1.77	1.42	1.34	1.62	2.50	1.64	1.79	2.35	1.90	2.24	2.12	1.43	1.63
P_2O_5	0.25	0.09	0.36	0.22	0.37	0.20	0.18	0.28	0.25	0.25	0.24	0.15	0.16
MnO	0.21	0.17	0.12	0.13	0.16	0.15	0.16	0.17	0.19	0.17	0.13	0.17	0.16
Cr_2O_3			0.049	0.016	0.155	0.101	0.049	0.043		0.05			0.148
LOI	4.50	4.40	6.7	5.4	6.2	7.6	4.7	4.3	3.70	2.5	4.20	3.90	5.9
Ba	99	55	225	434	85	23	78	84	24	107	57	120	32
Hf	2.9	2.0	2.6	3.3	4.6	3.3	3.3	4.8	1.6	4.3	3.4	2.0	2.8
Nb	35.3	6.0	29.9	14.1	36.8	20.0	13.8	22.9	17.4	20.5	20.5	7.8	13.2
Rb	2.2	3.2	15.6	7.4	7.7	2.5	7.6	8.0	1.0	9.6	5.0	21.8	9.6
Sr	197	170	160	774	610	165	353	492	45	246	221	118	99
Ta	2.09	0.37	1.7	1	2.3	1.2	0.9	1.3	1.15	1.3	1.28	0.52	0.9
Th	3.11	0.30	3.60	1.20	3.50	1.40	1.30	2.20	1.43	2.00	1.60	0.65	1.30
U	0.70	0.08	1.20	0.40	1.00	0.50	0.40	0.60	0.37	0.50	0.29	0.25	0.40
V	244	269	196	300	255	210	251	249	184	289	278	234	222
Zr	98	64	114	107	165	113	119	166	45	152	92	59	104
Y	23.4	18.5	18.6	19.8	19.3	17.0	21.5	25.3	15.1	24.1	22.5	18.6	17.3
Pb	1.7	0.7	1.7	0.8	0.6	0.5	0.3	0.4	0.7	0.4	1.5	0.5	0.3
Sc	27.5	37.9	23.0	29.0	34.0	26.0	28.0	26.0	22.2	35.0	30.8	26.6	29.0
Co	65	56	33	37	82	62	46	50	85	54	66	75	70
Ni	295	118	33	27	306	235	102	121	764	171	184	449	462
Cr	363	254							1110		283	559	
La	21.97	4.27	23.20	10.70	25.10	15.20	12.70	19.20	14.22	15.00	15.21	5.94	10.60
Ce	45.59	11.40	46.00	25.50	56.20	32.90	30.10	42.50	33.76	36.70	35.35	14.76	25.50
Pr	5.70	1.68	5.14	3.43	6.98	4.31	4.06	5.65	4.72	4.93	4.97	2.14	3.32
Nd	21.65	8.53	20.60	14.30	28.60	17.90	17.30	24.90	19.56	21.80	20.79	9.92	15.10
Sm	4.65	2.65	4.03	3.77	6.06	3.81	4.40	6.13	4.47	5.00	5.10	2.92	3.66
Eu	1.50	1.03	1.23	1.25	1.79	1.32	1.44	2.01	1.30	1.53	1.62	0.94	1.19
Gd	4.84	3.27	3.89	3.99	5.49	3.89	4.60	6.24	4.35	5.13	5.18	3.38	3.86
Tb	0.78	0.55	0.63	0.67	0.86	0.64	0.75	0.99	0.67	0.87	0.83	0.58	0.63
Dy	4.63	3.50	3.43	3.49	4.02	3.21	3.88	5.23	3.62	4.88	4.77	3.71	3.54
Ho	0.88	0.67	0.68	0.73	0.75	0.64	0.79	0.96	0.61	0.91	0.85	0.72	0.67
Er	2.24	1.79	1.80	2.08	1.82	1.74	2.17	2.46	1.34	2.44	2.14	1.80	1.81
Tm			0.25	0.28	0.24	0.24	0.29	0.33		0.35			0.25
Yb	1.94	1.62	1.59	1.68	1.34	1.38	1.76	2.00	0.99	2.12	1.73	1.54	1.54
Lu	0.29	0.23	0.23	0.26	0.18	0.21	0.26	0.27	0.09	0.30	0.24	0.21	0.22

					Nilufer metabasic rocks						
	OR-44	**OR-47**	**OR-48**	**OR-49**	**OR-58**	**OR-75**	**OR-79**	**OR-89**	**OR-98**	**OR-104**	**OR-116**
SiO$_2$	46.54	48.16	48.71	45.43	51.42	50.54	49.60	49.52	46.97	49.03	49.66
Al$_2$O$_3$	10.82	11.48	13.00	9.01	14.05	13.86	12.57	11.30	12.44	16.69	13.96
Fe$_2$O$_3$	11.05	12.23	11.92	11.11	11.33	10.46	11.02	11.06	12.85	10.95	11.84
MgO	14.33	10.65	11.67	16.58	6.55	6.18	6.81	9.09	13.54	8.89	8.71
CaO	7.48	12.29	8.56	9.67	8.60	11.72	8.72	14.53	9.54	9.64	9.59
Na$_2$O	2.12	3.33	2.52	0.81	4.59	5.02	4.23	3.11	2.09	3.51	4.28
K$_2$O	0.26	0.21	1.50	0.17	1.67	0.47	0.51	0.14	0.07	0.57	0.39
TiO$_2$	1.63	1.59	1.89	1.76	1.84	2.17	2.16	0.97	1.56	1.15	1.45
P$_2$O$_5$	0.17	0.17	0.23	0.18	0.25	0.42	0.34	0.11	0.23	0.13	0.14
MnO	0.14	0.17	0.17	0.15	0.15	0.16	0.13	0.16	0.22	0.16	0.18
Cr$_2$O$_3$	0.134			0.154			0.037				
LOI	4.9	6.30	3.20	4.9	2.70	6.10	3.6	7.60	4.70	4.20	4.60
Ba	42	63	821	34	220	97	120	32	34	333	32
Hf	3.1	2.6	3.3	3.3	2.7	4.4	4.6	1.4	2.6	1.1	1.8
Nb	13.1	13.2	17.7	14.2	23.5	53.3	25.7	12.4	31.3	9.3	8.4
Rb	4.0	2.6	20.4	2.5	23.3	4.3	5.0	1.2	1.5	5.5	2.8
Sr	58	205	168	30	131	162	175	353	135	535	150
Ta	0.9	0.82	1.08	0.9	1.39	3.07	1.7	0.71	1.86	0.58	0.55
Th	1.10	1.08	1.37	1.80	2.01	5.08	2.50	1.02	2.68	0.62	0.61
U	0.30	0.33	0.33	0.30	0.48	0.91	0.60	0.22	0.58	0.14	0.28
V	227	219	270	242	271	239	227	192	230	190	219
Zr	105	92	111	115	84	181	164	48	93	38	51
Y	18.4	18.1	24.0	18.5	20.5	28.8	22.0	14.2	20.3	15.6	16.7
Pb	0.2	0.6	0.9	2.2	1.3	2.1	0.6	2.3	1.4	0.6	0.7
Sc	29.0	27.1	33.6	31.0	30.2	21.1	30.0	27.7	26.0	22.7	24.3
Co	61	74	73	66	86	45	41	95	64	54	84
Ni	379	590	336	416	74	78	80	840	371	206	436
Cr		1025	639		114	93		987	502	507	508
La	9.80	10.51	13.20	10.40	17.82	33.62	19.10	9.08	19.22	6.62	5.50
Ce	24.90	24.21	31.77	24.90	36.75	66.64	42.90	18.33	38.12	15.32	14.37
Pr	3.20	3.33	4.47	3.44	4.63	8.05	5.38	2.28	4.63	2.09	2.13
Nd	14.20	14.02	18.62	16.20	17.61	29.11	24.00	9.29	17.31	9.08	9.59
Sm	3.65	3.66	4.58	3.70	4.16	5.81	5.31	2.28	3.74	2.41	2.78
Eu	1.06	1.23	1.49	1.16	1.38	1.64	1.70	0.80	1.33	0.91	0.92
Gd	3.75	3.85	5.01	3.89	4.47	5.66	5.23	2.60	4.04	2.87	3.32
Tb	0.65	0.61	0.81	0.66	0.71	0.92	0.83	0.43	0.66	0.49	0.56
Dy	3.72	3.72	4.73	3.76	4.22	5.32	4.57	2.79	3.93	2.96	3.38
Ho	0.68	0.70	0.88	0.70	0.77	1.01	0.85	0.55	0.74	0.58	0.63
Er	1.82	1.73	2.17	1.88	1.95	2.67	2.19	1.40	1.91	1.49	1.59
Tm	0.25			0.25			0.31				
Yb	1.67	1.48	1.85	1.55	1.60	2.45	1.89	1.18	1.59	1.31	1.40
Lu	0.23	0.22	0.28	0.22	0.23	0.37	0.26	0.18	0.23	0.19	0.19

	SK-7-013	SC-7-45	SC-7-50	SC-7-84	SC-7-91	SC-7-92	SK-7-116G	SK-7-117D	SC-8-142	SC-8-143
SiO₂	46.84	38.13	39.52	46.60	45.45	38.26	45.19	45.53	43.82	44.33
Al₂O₃	13.04	5.76	4.07	13.51	5.00	5.22	10.26	11.86	15.61	15.07
Fe₂O₃	11.82	11.03	13.17	14.87	11.36	13.90	12.14	12.18	11.59	10.20
MgO	7.57	20.16	27.55	6.32	21.84	26.99	14.33	12.87	5.69	6.42
CaO	7.31	11.70	3.34	8.68	8.01	3.14	5.53	7.70	12.08	10.39
Na₂O	2.54	0.10	0.07	3.81	0.14	0.06	1.18	2.10	2.50	3.92
K₂O	3.08	0.03	0.05	0.49	0.03	0.03	0.10	0.36	1.38	0.86
TiO₂	2.90	0.76	0.78	2.83	1.14	0.93	1.92	1.53	1.90	1.71
P₂O₅	0.35	0.09	0.08	0.24	0.17	0.07	0.21	0.16	0.23	0.19
MnO	0.11	0.14	0.15	0.12	0.18	0.13	0.14	0.16	0.13	0.13
Cr₂O₃	0.031	0.191	0.317	0.01	0.253	0.35	0.221	0.139	0.045	0.028
LOI	3.9	11.3	10.1	2.2	5.9	10.1	8.3	5	4.7	6.5
Ba	880	8	14	117	6	113	26	96	138	95
Hf	5.3	1.3	1.4	5.4	1.9	1.7	3.3	2.4	3.6	3.6
Nb	31.5	6.5	4.4	33.3	9.0	6.1	18.4	12.5	25.7	23.3
Rb	57.5	0.6	2.6	8.3	0.5	0.8	1.9	6.4	25.3	15.8
Sr	670	355	16	256	14	28	113	232	309	266
Ta	2	0.5	0.4	2	0.7	0.5	1.1	0.7	1.6	1.5
Th	2.80	0.30	0.40	2.80	0.80	0.80	1.40	1.30	2.30	1.80
U	0.70	0.20	0.30	0.70	0.20	0.30	0.50	0.40	0.30	0.30
V	299	123	113	323	116	138	228	221	267	263
Zr	199	51	49	207	75	61	117	93	147	124
Y	23.5	7.8	9.0	29.5	9.0	12.7	14.4	16.6	25.8	24.4
Pb	2.1	0.7	0.9	0.7	0.6	0.6	1.6	0.7	0.6	1.1
Sc	27.0	14.0	14.0	32.0	21.0	17.0	28.0	32.0	31.0	32.0
Co	48	92	109	55	71	128	76	64	47	40
Ni	100	831	1330	19	715	1516	468	284	72	40
Cr										
La	23.70	2.90	4.10	25.60	8.30	5.20	14.20	10.50	19.80	17.00
Ce	56.90	7.70	10.20	57.40	18.70	14.00	33.20	23.50	42.50	37.20
Pr	7.34	1.30	1.39	7.23	2.23	2.01	4.33	3.16	5.40	4.72
Nd	32.70	7.20	5.70	30.50	8.30	9.10	19.20	14.70	22.60	20.40
Sm	6.61	1.82	1.71	6.78	1.92	2.63	4.05	3.20	4.85	4.36
Eu	2.33	0.61	0.52	2.23	0.38	0.81	1.17	1.13	1.58	1.49
Gd	6.09	1.82	1.90	6.87	2.13	2.83	3.65	3.48	4.92	4.72
Tb	0.97	0.30	0.32	1.09	0.34	0.50	0.63	0.61	0.82	0.78
Dy	5.35	1.54	1.97	5.88	1.89	2.63	3.15	3.42	4.73	4.47
Ho	0.85	0.30	0.34	1.09	0.32	0.49	0.56	0.62	0.90	0.88
Er	2.32	0.79	0.97	2.84	0.89	1.35	1.59	1.58	2.51	2.39
Tm	0.31	0.11	0.13	0.39	0.12	0.17	0.21	0.24	0.39	0.37
Yb	1.70	0.63	0.71	2.42	0.73	0.94	1.24	1.44	2.21	2.15
Lu	0.25	0.09	0.09	0.33	0.11	0.13	0.18	0.22	0.33	0.33

	SC-8-144	SC-8-146	SC-8-163	SC-8-166	SC-8-203	SC-8-205	SC-8-209	SC-8-211	SC-8-212
					Nilufer metabasic rocks				
SiO_2	43.68	47.91	49.53	49.44	41.81	42.30	38.88	45.01	46.59
Al_2O_3	16.89	13.12	10.93	14.09	3.37	11.65	4.54	4.15	4.13
Fe_2O_3	11.85	12.20	11.34	11.32	15.38	9.05	12.47	13.86	12.52
MgO	4.39	6.35	11.11	7.90	21.68	11.38	27.67	24.89	25.87
CaO	14.21	9.79	6.56	9.00	7.03	13.03	3.71	2.01	1.88
Na_2O	2.42	4.05	3.98	3.84	0.09	1.58	0.09	0.02	0.02
K_2O	0.64	0.34	0.73	0.40	0.05	0.95	0.22	0.02	0.02
TiO_2	2.16	3.16	1.80	1.02	1.09	1.28	0.66	0.88	0.84
P_2O_5	0.17	0.39	0.24	0.08	0.10	0.11	0.08	0.10	0.08
MnO	0.11	0.14	0.15	0.15	0.11	0.11	0.15	0.08	0.12
Cr_2O_3	0.05	0.023	0.103	0.01	0.359	0.12	0.305	0.373	0.348
LOI	3.1	2.2	3.1	2.5	8.2	8	10.5	7.9	6.9
Ba	61	159	75	116	22	299	27	11	8
Hf	4.0	6.2	3.3	1.5	2.0	3.0	1.0	1.2	1.0
Nb	25.9	47.6	21.7	11.1	9.7	13.4	5.2	7.2	6.2
Rb	9.5	6.8	23.4	5.2	5.6	31.3	6.6	0.9	0.9
Sr	314	283	172	207	25	375	95	14	10
Ta	1.8	3.1	1.4	0.7	0.6	0.8	0.3	0.5	0.4
Th	2.20	4.80	1.90	0.90	0.60	1.70	0.40	0.50	0.50
U	0.40	0.90	0.50	0.20	0.10	0.50	b.d.	0.20	0.10
V	282	299	252	419	113	192	97	109	95
Zr	161	223	131	45	66	95	39	51	46
Y	30.3	26.3	19.2	16.2	7.7	15.8	7.7	8.9	7.0
Pb	0.6	0.5	0.6	0.3	0.4	0.7	0.6	0.8	0.5
Sc	36.0	31.0	28.0	40.0	25.0	26.0	14.0	14.0	12.0
Co	39	45	55	45	148	54	113	128	114
Ni	25	30	203	38	1739	139	1438	906	751
Cr									
La	22.30	33.50	17.50	8.40	5.40	11.50	4.00	5.30	4.50
Ce	49.20	74.60	38.90	18.20	15.40	25.30	9.60	13.80	11.10
Pr	6.24	9.02	4.93	2.28	2.24	3.25	1.29	2.03	1.60
Nd	26.20	38.00	20.40	9.10	10.00	14.30	5.60	9.30	7.70
Sm	5.62	7.70	4.49	2.16	2.50	3.13	1.39	2.05	1.75
Eu	1.90	2.39	1.52	0.83	0.82	1.29	0.48	0.74	0.60
Gd	5.93	6.86	4.23	2.47	2.21	3.26	1.44	2.13	1.69
Tb	0.99	1.03	0.68	0.46	0.37	0.54	0.26	0.35	0.28
Dy	5.52	5.45	3.95	2.80	1.98	3.00	1.62	1.80	1.65
Ho	1.08	0.96	0.74	0.56	0.32	0.57	0.28	0.34	0.29
Er	2.98	2.48	2.01	1.70	0.79	1.53	0.74	0.83	0.74
Tm	0.44	0.34	0.28	0.27	0.11	0.22	0.12	0.11	0.08
Yb	2.70	1.92	1.60	1.62	0.67	1.44	0.67	0.63	0.50
Lu	0.40	0.25	0.23	0.24	0.11	0.19	0.09	0.08	0.07

	Nilufer metabasic rocks						
	SK-7-119G	**SN-7-62**	**SN-7-209**	**SN-7-210**	**SS-7-180**	**SS-7-295**	**ZT-3**
SiO$_2$	38.60	46.85	47.47	45.68	45.09	38.07	47.63
Al$_2$O$_3$	4.43	8.79	15.02	13.10	9.52	4.25	13.46
Fe$_2$O$_3$	13.09	11.17	15.07	17.40	12.72	14.49	11.09
MgO	28.53	12.42	3.38	4.08	9.37	28.56	9.61
CaO	3.01	13.15	7.58	6.83	11.57	2.24	9.31
Na$_2$O	0.11	1.47	3.10	3.26	2.72	0.04	2.92
K$_2$O	0.13	0.15	0.32	0.08	0.58	0.03	1.50
TiO$_2$	0.56	2.04	3.37	4.34	4.44	0.77	2.31
P$_2$O$_5$	0.06	0.21	0.32	0.38	0.43	0.10	0.34
MnO	0.13	0.15	0.15	0.17	0.17	0.16	0.19
Cr$_2$O$_3$	0.332	0.181	0.007	0.008	0.067	0.296	
LOI	10.3	3	3.9	4.4	2.9	10.2	5.20
Ba	15	38	111	43	130	12	146
Hf	1.2	3.8	4.3	5.7	8.5	1.4	2.3
Nb	3.9	19.4	26.6	35.9	43.2	6.1	19.6
Rb	3.7	3.2	5.5	1.9	9.7	1.2	26.5
Sr	37	565	577	233	167	18	173
Ta	0.3	1.4	1.8	2.4	2.8	0.3	1.27
Th	0.30	1.70	1.80	3.00	3.40	0.70	1.18
U	0.10	0.40	0.70	0.90	0.80	0.20	0.46
V	96	256	315	403	352	94	250
Zr	40	132	172	226	288	49	65
Y	6.5	16.8	21.0	26.3	31.6	9.0	22.1
Pb	0.5	1.0	0.8	0.7	0.4	0.2	1.4
Sc	14.0	39.0	24.0	30.0	53.0	16.0	23.6
Co	123	60	49	59	67	116	87
Ni	1539	146	91	67	143	1595	253
Cr							557
La	3.30	14.30	18.40	23.50	30.20	4.70	13.12
Ce	8.30	37.70	47.30	58.50	74.40	12.10	32.74
Pr	1.09	4.54	5.94	7.27	9.84	1.67	4.64
Nd	5.90	19.70	26.00	33.30	44.10	7.00	19.83
Sm	1.25	4.50	5.95	7.09	9.28	1.80	4.89
Eu	0.43	1.56	2.10	2.42	2.63	0.56	1.62
Gd	1.29	4.29	5.56	6.63	8.57	1.95	5.15
Tb	0.22	0.72	0.88	1.09	1.34	0.35	0.80
Dy	1.28	3.86	4.69	5.85	6.96	1.93	4.70
Ho	0.23	0.63	0.78	1.01	1.29	0.38	0.84
Er	0.70	1.56	1.99	2.64	3.17	0.98	2.07
Tm	0.10	0.22	0.31	0.37	0.47	0.15	
Yb	0.61	1.29	1.54	2.15	2.77	0.78	1.58
Lu	0.08	0.17	0.24	0.30	0.41	0.13	0.22

Sample	87Sr/86Sr	143Nd/144Nd	206Pb/204Pb	207Pb/204Pb	208Pb/204Pb	176Hf/177Hf
HS-90	0.704954	0.512602	19.69571	15.65350	39.64464	0.282757
HS-89	0.704005	0.512599	22.86195	15.80866	43.87959	0.282742
OR-48	0.706616	0.512799	20.03410	15.68426	40.32440	0.282872
NIL-12	0.704325	0.512787	21.96910	15.72339	42.13540	0.282866
IM-24	0.705960	0.512730	19.51829	15.67110	39.76361	0.282890
OR-33	0.706450	0.512844	20.23954	15.67043	40.13334	0.282917
OR-58	0.706123	0.512602	19.54273	15.66982	40.31832	0.282781
OR-98	0.705791	0.512728	19.65318	15.67723	39.96658	0.282889
BO-2	0.706177	0.512863	18.61207	15.60882	38.62269	0.283067
DO-23	0.707487	0.512927	18.54118	15.60675	38.53567	0.283092
HS-78	0.707010	0.512914	18.66847	15.59940	38.58774	0.283088
IM-28	0.704138	0.512953	19.26480	15.55535	38.89504	0.282969
OR-29	0.704936	0.512775	19.46882	15.65043	39.94491	0.282865
OR-104	0.705031	0.512819	19.07333	15.59752	39.28391	0.282937
OR-116	0.705108	0.512838	19.89312	15.65190	39.52045	0.282910
ZT-3	0.705941	0.512794	19.51036	15.63199	39.36183	0.282900

NIL-12   0.704325   0.512787   21.96910   15.72339   42.13540

CURRICULUM VITAE

PERSONAL INFORMATION

Surname, Name: Sayıt, Kaan
Nationality: Turkish (TC)
Date and Place of Birth: 14 December 1981, Ankara
Marital Status: Single
Phone: +90312 2105735
Fax: +90312 2105750
e-mail: ksayit@metu.edu.tr

EDUCATION

Degree	Institution	Year of Graduation
MS	METU Geological Engineering	2005
BS	METU Geological Engineering	2003
High School	Ankara Cumhuriyet High School	1998

WORK EXPERIENCE

Year	Place	Enrollment
2010	Aegir Ridge, North Atlantic Ocean	Shipboard Scientist
2009	San Diego State University	Project Member
2007-2008	Pennsylvania State University	Research Scholar
2004-present	METU Geological Engineering	Teaching Assistant

FOREIGN LANGUAGES

Fluent English

PUBLICATIONS

1. Sayıt, K., Göncüoğlu, M.C. and Furman, T. Petrological reconstruction of Triassic seamounts/oceanic islands within the Palaeotethys: Geochemical implications from the Karakaya Subduction/Accretion Complex, Northern Turkey (in review, submitted to Lithos).

2. Catlos, E.J., Sayıt, K., Sivasubramanian, P., and Dubey, C.S., 2010. Geochemical and geochronological data from charnockites and anorthosites from India's Kodaikanal-Palani Massif, Southern Granulite Terrain, India. (accepted, submitted to Bose volume titled "Topics in Igneous Petrology: a tribute to Prof. Mihir K. Bose" to be published by Springer)

3. Göncüoğlu, M.C., Sayıt, K., and Tekin, U.K. 2010. Oceanization of the northern Neotethys: Geochemical evidence from ophiolitic melange basalts within the İzmir-Ankara suture belt, NW Turkey. Lithos, 116, 175-187.

4. Sayıt, K. and Göncüoğlu, M.C., 2009. Geochemical characteristics of the basic volcanic rocks within the Karakaya Complex: A review. Yerbilimleri, 30, 181-191 (In Turkish with English abstract).

5. Sayıt, K. and Göncüoğlu, M.C., 2009. Geochemistry of mafic rocks of the Karakaya Complex, Turkey: Evidence for plume-involvement in the extensional oceanic regime during Middle-Late Triassic. International Journal of Earth Sciences, 98, 367-385.